Microtubule plus end binding proteins and nuclear movements in the *Saccharomyces cerevisiae* life cycle

Jeffrey Nathan Molk

A dissertation submitted to the faculty of the University of North Carolina at Chapel Hill in partial fulfillment of the requirements for the degree of Doctor of Philosophy in the Department of Biology.

Chapel Hill
2006

Approved by:

Advisor: Professor K. Bloom

Advisor: Professor E. D. Salmon

Reader: Associate Professor R. Cheney

Reader: Associate Professor R. Duronio

Reader: Associate Professor J. Kieber

ABSTRACT

JEFFREY NATHAN MOLK: Microtubule plus end binding proteins and nuclear movements in the *Saccharomyces cerevisiae* life cycle

(Under the direction of Dr. Kerry Bloom and Dr. E. D. Salmon)

Microtubules (MTs) are required for nuclear movements and chromosome segregation. MTs are polymers of tubulin protein with a defined polarity – the minus end is associated with the microtubule organizing center (MTOC) whereas the plus end probes the cellular environment. Additional proteins associated with the plus end act as adaptors between the MT and binding sites that facilitate nuclear and chromosome movements. The budding yeast *Saccharomyces cerevisiae* was used as a model system to examine two questions: (1) During mitotic spindle elongation, how does the cell ensure each daughter inherits a single MTOC? To investigate this, Mitotic Exit Network (MEN) proteins were analyzed in living cells. I find that, after anaphase onset, the MEN activator Tem1p accumulates persistently on the MTOC that enters the daughter cell. In contrast, the abundance of the MEN inhibitor Bub2p decreases during anaphase. This suggests that after anaphase onset, the presence of one MTOC in the daughter cell persistently signals mitotic exit. (2) By what mechanism do plus end binding proteins link oppositely oriented MT arrays? In the budding yeast mating pathway, the translocation of haploid nuclei toward each other is known as nuclear congression. I find nuclear congression is driven by MT plus end interactions. The plus end binding proteins Kar3p and Bik1p are required for efficient MT-

MT interactions. Additionally, I find that during mitosis in vegetative cells, Kar3p and Bik1p are part of a family of plus end binding proteins that are required for anti-parallel MT interactions. Taken together, these data suggest a specific subset of plus end binding proteins function similarly during mating and mitosis on oppositely oriented MT arrays.

ACKNOWLEDGEMENTS

With so many to thank, it is difficult to express my appreciation to all of the people who have helped me in my time at the University of North Carolina. First and foremost, I would like to thank my advisors, Dr. Kerry Bloom and Dr. E.D. (Ted) Salmon, for their willingness to let me work in their laboratories; for their patience in teaching me both the techniques involved in pursuing a research problem as well as pushing me to think broadly about scientific problems; for allowing me to independently pursue subjects that fit my interests; and for their guidance through the years.

Among the UNC faculty, I would like to thank my committee members, Dr. Richard Cheney, Dr. Bob Duronio, and Dr. Joe Kieber for their helpful advice and comments on my work. Dr. Elaine Yeh has been a great scientific resource over the years. I would like to thank her for our discussions about budding yeast and the support she has offered. I offer my deepest gratitude to Dr. Bob Goldstein who has not only supported my research but also aided greatly in the search for a postdoctoral advisor and has allowed me to begin exploring the biology of worms with the members of his laboratory. Additionally, I would like to thank Dr. Jeff Dangl for his kindness and advice; Dr. John Pringle (Stanford University) and his close friend, Dr. Danny Lew (Duke University), for teaching me about cell polarity and expanding my knowledge of yeast; Dr. Pat Brennwald, a wonderful collaborator; and Dr. Bill

Kier who not only teaches a fabulous biomechanics class, but who has always had a smile and words of encouragement over the years.

Laboratories do not function without lab technicians and I have been lucky enough to work with Jennifer Sims and Julian Haase in the Bloom lab and David Hoffman, Ben Moree, and Brian Manning in the Salmon lab. I thank them, and all of the undergraduates who they have worked with, for ensuring I had the reagents necessary to perform my experiments, for their technical advice, and for other support they have offered.

From my time in the Bloom lab, I would like to thank Dr. Dale Beach, Dr. Ajit Joglekar, Dr. K. Mythreye, Dr. Le Paliulis, Dr. Chad Pearson, Dr. Doug Thrower, and Dr. Leana Topper for their patient training and advice. From the Salmon lab, I would like to acknowledge Moa Biftu, Dr. Lisa Cameron, Dr. Julie Canman, Dr. Daniela Cimini, Dr. Jennifer DeLuca, Emily Farrar, Dr. Jay Gatlin, Jenny Hickey, Dr. Sonia Grego, Dr. Bonnie Howell, Dr. Paul Maddox, Ryan O'Quinn, and Xiaohu Wan for their friendship, instruction, and advice.

A number of graduate students at UNC have been critical for my sanity. I would like to acknowledge Emily Fisher, Willow Gabriel, Andy Gerschutz, David Hubert, Jan LaRocque, Nick Kappas, Jacob Sawyer, Minna Roh, and Jenn To. Dr. Jean-Claude Labbe, Dr. Gidi Shemer, and Dr. Dan Marston have also been great colleagues. Special thanks go to Nate Dudley and Erin McCarthy for their friendship, training, and advice. I would also like to thank those that I have collaborated with in various projects over the years: Dr. Trisha Davis, Dr. David Odde, Dr. David Pellman, and Dr. Scott Schuyler. I would like to especially acknowledge Melissa Gardner for not only her hard work and the productivity of our collaborations, but for her friendship as well.

Finally, it is impossible to have any success in life without the support of your friends. Dr. Chia-wei Tsai and Dr. Vincent Klink served as my initial mentors at the University of Maryland and have been good friends throughout my graduate experience, offering me council, advice, and wisdom, for which I am eternally grateful. Seagrumn Gilbert, Ben Moree, Jennifer Sims, and Cory Sims have been great friends who have seen me through graduate school. Kaitlin, Nana, Dominic, and Troy Morelli have become my family in North Carolina and I am indebted to their support. David Bouck stands out as the best scientific colleague I have had at UNC. My scientific achievements would not have been nearly as complete without his patience, inquisitive nature, and willingness to let me talk his ear off. I would like to thank David for his kindness and friendship. Phil Kominski, who needs to work on returning phone calls, may not understand what I work on or why I do it, but he and his wife, Elizabeth Kominski, have always supported and encouraged me and for that I thank them.

I would like to thank Dr. Stephen Wolniak, from the University of Maryland. Without Steve's Zoology 411 class, I would never have been excited by biology or pursued a career in science. Without Steve's kindness in letting me join his lab as an undergraduate, I would never have had the framework to think correctly about how to do "good science" or the confidence to make mistakes and recover from them. And, without Steve's friendship, I never would have made it through graduate school.

I thank my family, especially my grandparents, Gladys and Jim Cox, for their support.

Finally, this work is dedicated to my parents, Kathy Molk and Dr. Martin Molk. I cannot really express it, so how about this: thanks for always picking up the phone.

TABLE OF CONTENTS

LIST OF TABLES

LIST OF ILLUSTRATIONS

LIST OF ABBREVIATIONS AND SYMBOLS

Δ - Gene deletion

μm – Micrometer (micron)

AU – Arbitrary units

CEN - Centromere

CFP – Cyan fluorescent protein

Chr III – Chromosome III

DIC – Differential interference contrast

dMA – Daughter inherited mitotic apparatus

DNA- Deoxyribonucleic acid

dSPB – Daughter inherited spindle pole body

FRAP – Fluorescence recovery after photobleaching

GAL - Galactose

GAP – Guanine-activating protein

GDP – Guanosine diphosphate

GEF – Guanine nucleotide exchange factor

GFP – Green fluorescent protein

3xGFP – Three tandem copies of green fluorescent protein

GTP – Guanosine triphosphate

HB – Hygromycin B

ipMT – Interpolar microtubule

Kan – Kanamycin (G418) resistance

KLP – Kinesin-like protein

kMT – Kinetochore microtubule

MAPs – Microtubule associated proteins

MEN – Mitotic exit network

mMA – Mother inherited mitotic apparatus

MTs – Microtubules

MTOC – Microtubule organizing center

ms - Milliseconds

min - Minutes

mSPB – Mother inherited spindle pole body

nm – Nanometer

nkMT – Non-kinetochore microtubule

OD – Optical density

PCR – Polymerase chain reaction

RFP – Red fluorescent protein

s - Seconds

SPBs – Spindle pole bodies

YPD – Yeast peptone, dextrose

CHAPTER 1: GENERAL INTRODUCTION

Overview

Microtubules (MTs) are polarized filaments that are required for cell division and fertilization in eukaryotes. The physical segregation of the chromosomes during cell division depends on the formation and function of the mitotic spindle (Figure 1.1A). The mitotic spindle is formed from MTs that are organized into a fusiform array. Within the spindle, MTs interact with chromosomes or other MTs during mitosis. In fungi, MTs can position the nucleus along the division axis. Additionally, MTs are required to bring two haploid nuclei together for fusion, or karyogamy, in the early stages of development. How MTs function during an organism's life cycle remains an important problem in cell biology.

Cytological descriptions of cell division have existed for over 100 years (Wilson, 1896). After replication of the DNA and the microtubule organizing center (MTOC), or spindle pole, mitosis begins in prophase when chromosomes condense and spindle poles separate. In prometaphase, the bipolar mitotic spindle takes shape and chromosomes attach to MTs via the kinetochore. The kinetochore is a multi-subunit protein complex that assembles on the centromere sequences of DNA. Proteins that bind the ends of MTs are critical for both spindle assembly and kinetochore-MT (kMT) attachments. The kinetochore of each sister chromatid attaches to MTs nucleated from opposite spindle poles, resulting in biorientation. When all of the sister chromatids have biorientated and aligned at the equator of the bipolar spindle, the cell is in metaphase. At anaphase onset, sister chromatids split. The individual chromosomes move to the spindle poles by MT depolymerization (anaphase A),

whereas the spindle poles move apart by MT-MT sliding and polymerization (anaphase B). At telophase the central spindle disassembles and chromosomes begin to decondense as the cell prepares to enter interphase. Interphase cells can either divide again or enter the mating pathway.

Cellular proliferation requires MTOCs, MTs, and MT associated proteins (MAPs) act coordinately to construct a functional cytoskeleton as organisms develop. Aberrant spindle function can cause cells to inherit improper chromosome numbers, a defect known as aneuploidy (Kops et al., 2005). Aneuploidy is a common phenotype of solid tumors in humans (Kops et al., 2005). Great attention has been paid to the role defective kMT attachments play in aneuploidy (Cimini and Degrassi, 2005). However, it was recognized in the late 19th and early 20th centuries that the presence of extra MTOCs resulted in multi-polar mitoses, chromosome segregation defects, and abnormal cell clusters, or tumors (Boveri, 1902). Currently, multiple MTOCs are recognized as a characteristic of most cancer cells (Nigg, 2002). In breast cancer cells, an increase in MTOC size is correlated with chromosome instability and aneuploidy (Lingle et al., 2002). Therefore, in addition to ensuring that kMT attachments are correctly established, the cell must monitor the number and size of the MTOC each daughter inherits to prevent genome instability. By examining MTOC inheritance and MT function, new mechanisms of cell division can be elucidated that may have relevance to tumorigenesis.

In this introduction, MT function in mitotic nuclear movements, chromosome segregation, and diploid formation are reviewed. The work that follows focuses on two major questions in cell biology: (1) During mitotic spindle elongation, how does the cell ensure each daughter inherits a single MTOC? (2) By what mechanism do plus end binding

proteins link oppositely oriented MT arrays? I have used the model organism *Saccharomyces cerevisiae* to investigate nuclear migration and MT plus end binding protein function. The following chapters will focus on monitoring nuclear movements during mitosis to ensure one spindle pole is inherited by the daughter (Chapter 2); the interaction of MT plus ends during mating (Chapter 3); the dynamics of mitosis when two mitotic spindles form in the same cell (Chapter 4); and the function of MT plus end binding proteins during mitotic spindle assembly (Chapter 5). Finally, I summarize the conclusions from this work and highlight future directions for this research (Chapter 6).

MT Structure

Microtubules were first identified using polarized light and electron microscopy as fine filaments that constituted the mitotic spindle (Inoue, 1953; Ledbetter and Porter, 1963). The isolation of the mitotic apparatus, and then individual MTs, allowed a biochemical characterization of the spindle (Mazia and Dan, 1952; Weisenberg, 1972; Weisenberg and Rosenfeld, 1975). MTs are polar structures that form when the protein tubulin self-assembles (Figure 1.1B) (Mohri, 1968). Though there are multiple tubulin isoforms, generally 4 nm alpha-tubulin and beta-tubulin forms 8 nm heterodimers; the dimers polymerize into linear protofilaments (Amos and Klug, 1974; Kirschner et al., 1974). Protofilament numbers can vary between organisms, but generally 13 protofilaments associate in vivo to form a single MT that is approximately 24 nm in diameter (Amos and Klug, 1974; Chalfie and Thomson, 1982; Mandelkow and Mandelkow, 1985; Tilney et al., 1973). MTs originate from microtubule organizing centers (MTOCs), a term that commonly refers to MT nucleating sites, such as centrosomes or spindle pole bodies (SPBs), but can

also include MT capture sites like kinetochores (Euteneuer and McIntosh, 1981; Pickett-Heaps, 1969). Centrosomes nucleate MTs at the pericentriolar material and help constrain protofilament numbers to 13 per MT (Evans et al., 1985; Gould and Borisy, 1977; Snyder and McIntosh, 1975). In lower eukaryotes, SPBs nucleate MTs from a plaque structure on the inner or outer face of the spindle pole (O'Toole et al., 1999; Peterson and Ris, 1976; Winey et al., 1995). Tubulin dimers that are not incorporated into MTs are freely diffusible and form a dynamic cellular protein pool (Inoue and Sato, 1967; Salmon et al., 1984b).

Polymerizing MT ends are blunt, whereas depolymerizing protofilaments often peel away from the MT in a "ram's horn" configuration (Kirschner et al., 1974; Mandelkow and Mandelkow, 1985; Mandelkow et al., 1991). The configuration of the ends during growth and shortening could govern protein association with the MT. The plus end of a MT is defined as the site where the net addition of tubulin occurs, whereas there is a net loss of dimers at the minus end (Bergen and Borisy, 1980; Binder et al., 1975; Summers and Kirschner, 1979). The MT plus end grows into the cytoplasm to interact with the kinetochore, organelles, the cell cortex, or other MTs; the minus end associates with the MTOC (Euteneuer and McIntosh, 1980; Euteneuer and McIntosh, 1981; Heidemann and McIntosh, 1980; Mitchison and Kirschner, 1985a). MT ends that are polymerizing or depolymerizing can interact persistently with attachment sites, resulting in force generation and intracellular motility (Dogterom et al., 2005).

MT Dynamics and Force Generation

MT dynamics and MAPs are required for force generation during cell division. MTs must search the cytoplasm for attachment sites and, once attached, generate sufficient forces

to move nuclei or chromosomes. MTs are labile structures that are sensitive to cell cycle regulation, pH, temperature, pressure, calcium concentrations, and pharmacological agents (Harris, 1962; Inoue and Sato, 1967; Kiehart, 1981; Salmon, 1975; Salmon and Segall, 1980; Saxton et al., 1984; Tilney and Porter, 1967). Observations that the spindle is a labile structure led to Inoue's hypothesis that MTs exist in dynamic equilibrium with tubulin subunits in the cytoplasm (Inoue and Sato, 1967). Inoue proposed that spindle fibers are composed of parallel arrays of thin filaments formed by globular protein molecules that reversibly associate. The contraction and elongation of the spindle fibers could provide the force to move chromosomes in mitosis. The equilibrium was suggested to be temperature sensitive with polymers disassociating at low temperatures and associating at high temperatures. Since protein synthesis is not required for MT recovery after depolymerization, Inoue concluded that a large protein pool exists to form the filaments when subunit addition is favored.

Dynamic equilibrium was confounded by the nucleotide binding state of tubulin. MTs bind GTP or GDP, and the hydrolysis of GTP induces MT depolymerization (Weisenberg and Deery, 1976). If MTs are at equilibrium, then disassembly should be favored, a condition that is not compatible with spindle formation (Kirschner and Mitchison, 1986). Therefore, Kirschner and Mitchison proposed the dynamic instability model for MT self-assembly. A main principle of dynamic instability is that MTs exist in steady state as GTP is hydrolyzed. An exchangeable GTP binding site is found at the MT plus end (Mitchison, 1993). A GTP cap at the plus end could govern the assembly and disassembly of the MT. The GTP cap size is likely small, consisting of only the first few tubulin dimers at the plus end (Drechsel and Kirschner, 1994; Walker et al., 1991). Having phases of growth,

when the GTP cap is present, and shortening, when GDP is bound, with small transition frequencies in between each phase was proposed to result in dynamic instability. In vivo studies verified these predictions. MTs nucleated from the centrosome spend most of their time in slow growth with infrequent transitions to rapid shortening (Cassimeris et al., 1988; Horio and Hotani, 1986; Mitchison and Kirschner, 1984; Sammak and Borisy, 1988; Walker et al., 1988). The transition of MTs from growth to shortening was referred to as catastrophe, whereas rescue occurred when MTs quickly switch from shortening to growth (Walker et al., 1988). Further, dynamic instability proposed that factors such as MAPs could stabilize spindle MTs by capping the plus end. While in other models the structure of the plus end, and not the GTP cap, regulates MT polymerization and depolymerization (Hyman and Karsenti, 1996), dynamic instability appears to govern MT behavior in living cells.

During mitosis, MTs can attach to the kinetochore; provide structural integrity to the spindle as non-kinetochore MTs (nkMTs), of which a subset form the central spindle or interpolar MTs (ipMTs); or they can be astral MTs that grow away from the spindle into the cytoplasm (McDonald et al., 1992; McIntosh et al., 1985; Snyder and McIntosh, 1975). Subpopulations of MTs display different dynamic properties. For example, kMTs are more stable than nkMTs during mitosis (Mitchison et al., 1986; Mitchison and Kirschner, 1985b; Snyder and McIntosh, 1975; Wadsworth and Salmon, 1986a). Tubulin in MTs exchanges with the cytoplasmic pool to accommodate changes in length (Maddox et al., 2000; Salmon et al., 1984a). Using photoactived or photobleached tubulin, fluorescence was seen to move poleward during metaphase and anaphase as dimers were lost from the minus end (Gorbsky et al., 1987; Gorbsky et al., 1988; Mitchison, 1989; Mitchison and Salmon, 1992). This suggests the kinetochore is a site of force generation. In metazoan cells, free polymerizing

nkMT plus ends function in part as a polar ejection force and push objects away from the spindle poles (Rieder et al., 1986). Interestingly, MT polymerization and depolymerization occurs solely at the plus end in budding yeast (Maddox et al., 2000; Tanaka et al., 2005).

Direct examples of MT-dependent force generation are abundant in studies of kinetochore function. Using purified chromosomes, MT plus ends preferentially bound kinetochores (Huitorel and Kirschner, 1988). In vivo, astral MTs could capture unattached kinetochores and induce chromosome movement toward the spindle pole (Nicklas et al., 1979). Monooriented chromosomes or prometaphase chromosomes captured by a single MT led to "tugging" on the kinetochore followed by rapid poleward acceleration without detaching from the MT (Alexander and Rieder, 1991; Bajer, 1982; Coue et al., 1991; McNeill and Berns, 1981; Rieder and Alexander, 1990). Once the kinetochore binds the plus end, MTs remain attached during polymerization and depolymerization, driving chromosome movements (Hyman and Mitchison, 1990; Koshland et al., 1988). In prometaphase and metaphase, bi-oriented sister kinetochores moved through an abrupt, coordinated switching mechanism called directional instability in which multiple kMTs synchronously polymerize or depolymerize (Pearson et al., 2001; Skibbens et al., 1993). During anaphase, tubulin addition and the sliding of MTs past one another is a force generating process that drives spindle elongation (Leslie and Pickett-Heaps, 1983; Masuda and Cande, 1987). MTs can also interact with cytoplasmic membranes or cortical sites without detaching during dynamic instability to provide organelle motility (Maddox et al., 1999; Waterman-Storer et al., 1995). Thus, dynamic MTs are critical for the intracellular movements that occur during cell division.

Budding Yeast Cell Cycle

Mitosis

The budding yeast *Saccharomyces cerevisiae* is a model genetic organism for studying MT function and MTOC inheritance in vivo. In these cells, the formation of a bud in late G1 or early S phase specifies the axis upon which chromosomes are segregated. Budding yeast have a closed mitosis in which the nuclear envelope does not break down during division. Therefore, the nucleus must be positioned along the mother-bud axis by the cytoskeleton so that all 16 haploid chromosomes are segregated correctly. A limited number of MTs, initially observed as filaments inside the nucleus, comprise the mitotic spindle (Peterson and Ris, 1976; Robinow and Marak, 1966). MTs nucleated at the SPB inner plaque attach to kinetochores or interact with oppositely oriented MTs to form the central spindle. One nuclear MT attaches to each kinetochore for a total of 16 kMTs while four ipMTs form the central spindle (Figure 1.2A) (O'Toole et al., 1999; Peterson and Ris, 1976; Winey et al., 1995).

The outer plaques of the SPBs nucleate MTs that will function exclusively in the cytoplasm (King et al., 1982; Peterson and Ris, 1976). Approximately three cytoplasmic MTs are nucleated from each SPB (Figure 1.2A) (Adams and Pringle, 1984; Kilmartin and Adams, 1984; King et al., 1982). The SPB from the previous division nucleates the MTs that orient toward the bud (Pereira et al., 2001). Nuclear movement to the bud neck and the subsequent penetration of the nucleus into the bud depends on cytoplasmic MTs (Figure 1.2B) (Huffaker et al., 1988; Jacobs et al., 1988; Palmer et al., 1989; Robinow and Marak, 1966; Sullivan and Huffaker, 1992). The movement of the spindle to the bud neck is referred to as spindle orientation. Following spindle orientation, anaphase begins and the penetration

of the nucleus into the bud neck is known as nuclear migration. However, spindle elongation does not require cytoplasmic MTs in budding yeast (Huffaker et al., 1988; Palmer et al., 1992). The ability of MTs to search the bud neck and bud cortex is critical because dampening MT dynamics impairs the ability of the spindle to orient properly (Adames and Cooper, 2000; Gupta et al., 2002; Kosco et al., 2001). Cytoplasmic MTs grow and shrink but rarely pause, sweeping and sliding along the cortex to generate the forces for nuclear migration (Adames and Cooper, 2000; Carminati and Stearns, 1997; Yeh et al., 2000).

The cell has established a series of checkpoints that delay cell cycle progression to correct errors that may arise during division (Hartwell and Weinert, 1989). One checkpoint monitors the movement of the nucleus into the bud (Bloecher et al., 2000; Yeh et al., 1995). Nuclear migration is monitored by the Mitotic Exit Network (MEN), a pathway that delays cyclin destruction and spindle breakdown when the mitotic apparatus is mal-positioned (Bardin et al., 2000; Bloecher et al., 2000). Tem1p is a small, *ras*-like protein that is proposed to signal mitotic exit when bound to GTP (Bardin et al., 2000; Shirayama et al., 1994b). Bub2p is a checkpoint protein that delays mitotic exit by inhibiting Tem1p activation (Bardin et al., 2000; Fesquet et al., 1999; Hoyt et al., 1991; Ro et al., 2002). In the MEN pathway, activation of Tem1p leads to the localization of the Cdc15p and Dbf2p/Mob1p kinases (Asakawa et al., 2001; Lee et al., 2001). The result of MEN activation is the maintenance of Cdc14p release from the nucleolus during anaphase. Cytoplasmic Cdc14p triggers the proteolysis of substrates to drive cells back into interphase (Jaspersen et al., 1999; Juang et al., 1997). Thus, cytoplasmic MTs help guide one SPB into the bud to ensure each cell inherits a single MTOC.

Mating

In the mating pathway, cytoplasmic MTs are required for movement of oppositely oriented haploid nuclei toward each other prior to nuclear fusion, or karyogamy (Figure 1.2B). This migration is termed nuclear congression in *Saccharomyces cerevisiae* and pronuclear migration in *Caenorhabditis elegans* and mammalian systems (Gonczy et al., 1999; Payne et al., 2003; Rose, 1996). In budding yeast, haploid cells are either mating type **a** or α. Mixing opposite mating type haploids induces a signal transduction cascade that commits both cells to the mating pathway (Cross et al., 1988; Haber, 1998; Rose, 1991). Entry into the mating pathway is followed by polarity axis establishment and mating projection, or shmoo, formation. Cytoplasmic MTs are guided to the shmoo tip cortex, orienting the nucleus to the site of cell fusion (Miller et al., 1999). Once oriented, MTs are anchored to the shmoo tip and MT growth and shortening results in nuclear oscillations (Maddox et al., 1999). After cell fusion, MTs draw both nuclei together. The movement of haploid nuclei toward each other is known as nuclear congression. A number of karyogamy mutants have been isolated that are defective in nuclear congression and result in two nuclei within the heterokaryon that is formed (Conde and Fink, 1976a; Kurihara et al., 1994; Polaina and Conde, 1982). Many of the proteins required for karyogamy are MAPs that have critical functions during mitosis.

Microtubule Associated Proteins

MAPs function to promote the polymerization or depolymerization of MTs, attach MTs to cellular components, and transport proteins along the MT lattice (Figure 1.1B). The first isolated MAPs were required for the in vitro polymerization of tubulin (Murphy and

Borisy, 1975; Weingarten et al., 1975). Tubulin polymerized with MAPs display dynamic instability in which catastrophe was decreased and rescue was increased (Pryer et al., 1992). Early studies demonstrated granules could move in MT containing axopodia (Tilney and Porter, 1967) or in giant squid axons (Allen et al., 1982). This transport was facilitated by MT motor proteins, a set of specialized MAPs that localize to sites that include the mitotic spindle (Scholey et al., 1985; Vale et al., 1985a; Vale et al., 1985b). Non-motor MAPs also exist and localize to specific sites along the MT by binding to newly polymerized or depolymerized ends, by motor transport, or by phosphorylation that targets these proteins to the correct sites (Akhmanova and Hoogenraad, 2005). MAPs have distinct functions in the cytoplasm and in the nucleus during the *S. cerevisiae* life cycle. Motor proteins act at the cortex to generate sliding forces, attach MTs to cortical sites or kinetochores during growth and shortening, and to transport proteins along the lattice (Adames and Cooper, 2000; Carvalho et al., 2004; Maddox et al., 2003b; Maekawa et al., 2003; Tanaka et al., 2005). Non-motor MAPs often regulate MT stability and function in nuclear movements or kinetochore-MT attachments (Berlin et al., 1990; McAinsh et al., 2003; Miller et al., 1998).

Motor Protein MAPs

In budding yeast, the kinesin-like protein (KLP) Kar3p functions in the cytoplasm and nucleus during mating and mitosis. Kar3p, a member of the kinesin 14 family, was originally isolated as a protein required for nuclear congression (Meluh and Rose, 1990; Polaina and Conde, 1982). Kar3p localizes to cytoplasmic MTs in the shmoo tip and enriches at the plus ends of depolymerizing MTs to maintain the attachment to the shmoo tip (Maddox et al., 2003b; Meluh and Rose, 1990). Cik1p targets Kar3p to MT plus ends during

nuclear congression (Barrett et al., 2000; Manning et al., 1999; Page et al., 1994; Page and Snyder, 1992). Additionally, Kar3p limits the length and number of cytoplasmic MTs nucleated from the SPB during mitosis (Huyett et al., 1998; Saunders et al., 1997a). Kar3p may function redundantly with other motors during nuclear migration, or Kar3p could act at the mother cell cortex to reposition mal-oriented spindles (Cottingham et al., 1999; Cottingham and Hoyt, 1997; DeZwaan et al., 1997; Hoepfner et al., 2002).

Three additional motor proteins are required for nuclear movements during mitosis in budding yeast. The cytoplasmic dynein heavy chain Dhc1p/Dyn1p associates with MTs and provides the pulling force for nuclear migration into the bud (Adames and Cooper, 2000; Eshel et al., 1993; Kahana et al., 1995; Shaw et al., 1997b; Yeh et al., 1995). Kip3p is a KLP with MT depolymerase activity that functions in the spindle orientation pathway (Cottingham et al., 1999; DeZwaan et al., 1997; Miller et al., 1998). Kip2p is a KLP that has been liked to both the spindle orientation and nuclear migration pathways (Carvalho et al., 2004; Maekawa et al., 2003; Miller et al., 1998).

Inside the nucleus, motor proteins function at the kinetochore and on ipMTs. In the absence of Kar3p, cells exhibit at G2/M delay with large buds and short mitotic spindles (Meluh and Rose, 1990; Saunders and Hoyt, 1992). Early in vitro and biochemical studies suggested Kar3p functioned in minus end directed motility and MT depolymerization at the kinetochore (Endow et al., 1994; Middleton and Carbon, 1994; Saunders et al., 1997a; Saunders et al., 1997b). Currently, Kar3p is thought to function at the kinetochore to transport chromosomes prior to biorientation (Jones et al., 1999; Sorger et al., 1994; Tanaka et al., 2005; Zeng et al., 1999). Kar3p along ipMTs was also hypothesized to act as an inward force during spindle assembly (Saunders and Hoyt, 1992). The outward force that

opposes Kar3p was proposed to originate from Cin8p and Kip1p, kinesin 5 proteins that slide anti-parallel ipMTs apart during spindle formation (Kapitein et al., 2005; Roof et al., 1992; Saunders and Hoyt, 1992). Removing the inward force by deleting *KAR3* should make spindles longer due to unrestrained Cin8p/Kip1p activity. Paradoxically, spindles are shorter in the absence of Kar3p (Zeng et al., 1999). Therefore, the role of Kar3p in spindle assembly remains unclear.

Non-motor MAPs

During spindle orientation and nuclear migration, non-motor MAPs function at cytoplasmic MT plus ends. Spindle orientation is accomplished by guiding MTs along the actin network that polarizes toward the bud neck and bud tip (Ayscough et al., 1997; Palmer et al., 1992; Theesfeld et al., 1999). Bim1p, the EB1 homolog in budding yeast, is a MT binding protein that is required for spindle orientation after bud emergence. Bim1p associates with Kar9p, the putative Adenomatous Polyposis Coli homolog, to guide MT plus ends along the actin network (Hwang et al., 2003; Korinek et al., 2000; Lee et al., 2000). Bim1p preferentially localizes to growing MT plus ends in the cytoplasm (Maddox et al., 2003b). Bik1p, the CLIP-170 ortholog, acts in dynein dependent nuclear migration (Carvalho et al., 2004; Sheeman et al., 2003). Bik1p and Kar9p are also required for nuclear congression during mating (Berlin et al., 1990; Kurihara et al., 1994). Therefore, non-motor MAPs are critical for accomplishing nuclear movements.

Within the nucleus, a series of non-motor MAPs also play essential roles in chromosome segregation. Greater than 60 proteins comprise the yeast kinetochore and many of these proteins, like Nuf2p and Bim1p, either directly or indirectly interact with the MT

plus end to make kMT attachments or monitor chromosome alignment (McAinsh et al., 2003). Additionally, non-motor MAPs interact with the central spindle MTs to regulate mitosis. Slk19p, isolated in a synthetic lethal screen with *kar3Δ* cells, is required to stabilize the central spindle during anaphase in addition to functioning at the kinetochore (Sullivan et al., 2001; Zeng et al., 1999). Similarly, Ase1p, a MT binding protein, Bim1p, and Bik1p participate in anaphase spindle elongation (Pellman et al., 1995; Schuyler et al., 2003). Therefore, MAPs function in nuclear positioning, chromosome segregation, and anaphase spindle integrity during mitosis.

Nuclear migration and plus end binding protein function in vivo

A number of questions surround the molecular mechanisms that govern nuclear migration and plus end binding proteins. How does the cell sense nuclear migration has been completed to ensure one MTOC is inherited by the daughter cell? How do oppositely oriented MT arrays locate each other and function in a coordinated fashion? Are MT-MT interactions required for cell division?

Each question focuses on dynamic process that requires an analysis of individual cells over time. Using live cell fluorescence microscopy techniques, nuclear migration and plus end function can be analyzed. To determine how one SPB is inherited by the daughter cell, I examined MEN components and found the activation of mitotic exit was correlated with SPB penetration of the bud neck (Chapter 2). Once the SPB entered the bud, MEN activators persistently accumulated on the SPB (Chapter 2). To understand the mechanism whereby oppositely oriented MT plus ends interact, I examined nuclear congression after induction of the mating pathway. I found nuclear congression was driven by MT plus end interactions

(Chapter 3). Kar3p and Bik1p were required for the efficient association of the plus ends before karyogamy (Chapter 3). When nuclear congression failed, a mitotic division followed with two spindles in the same cell. In these heterokaryons, I showed anaphase onset was asynchronous but spindle breakdown was coordinated after one SPB entered the bud (Chapter 4). This suggests mitotic exit is initiated by a global signal that ensures one SPB is inherited by the daughter cell. Finally, to investigate MT plus end interactions during mitosis, I examined spindle assembly in vegetative cells. I found that Kar3p is part of a family of plus end binding proteins that are required to resist mechanical stress on the spindle during mitosis (Chapter 5).

Figures

Figure 1.1: Spindle structure in higher eukaryotes and schematic of MT dynamics.

Bipolar spindle formation in eukaryotes requires dynamic MTs. (A) Late prometaphase in a newt lung epithelial cell (Bar, 2 μm). Spindle MTs, nucleated from the MTOCs, form a bipolar arrangement that results in congression of chromosomes to the metaphase plate. In this cell, one pair of sister chromatids is found on the periphery of the spindle, awaiting transport to the metaphase plate. (B) Characteristics of MT dynamic instability. Alpha- and beta-tubulin (green circles) dimerize and, during polymerization (upper diagram), incorporate preferentially to the plus end of the MT. Gamma-tubulin (red circles) is present at the minus end and associates with the MTOC (blue square). Other proteins, including signaling proteins, can localize to the MT minus end (cyan circles). A subset of plus end binding proteins will associate with the MT during phases of growth (purple circles). During depolymerization (lower diagram), the plus end assumes the “ram’s head” configuration as tubulin dimers are lost. A second subset of plus end binding proteins can localize preferentially to shortening MTs (pink circles). The transition from growth to shortening is known as catastrophe; the transition from shortening to growth is known as rescue.

A.

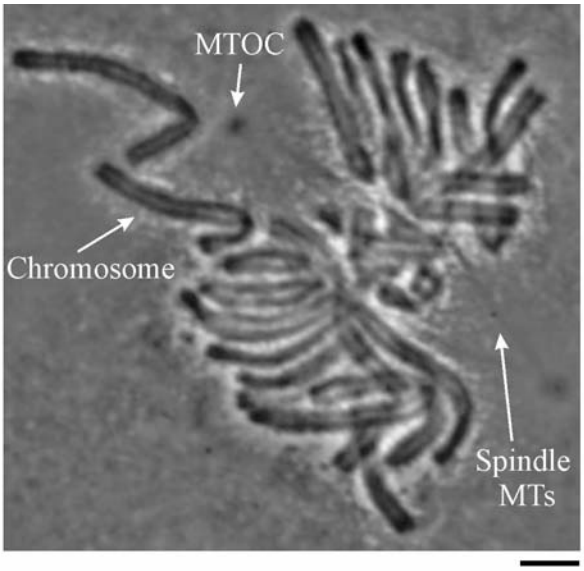
MTOC
Chromosome
Spindle
MTs

B.

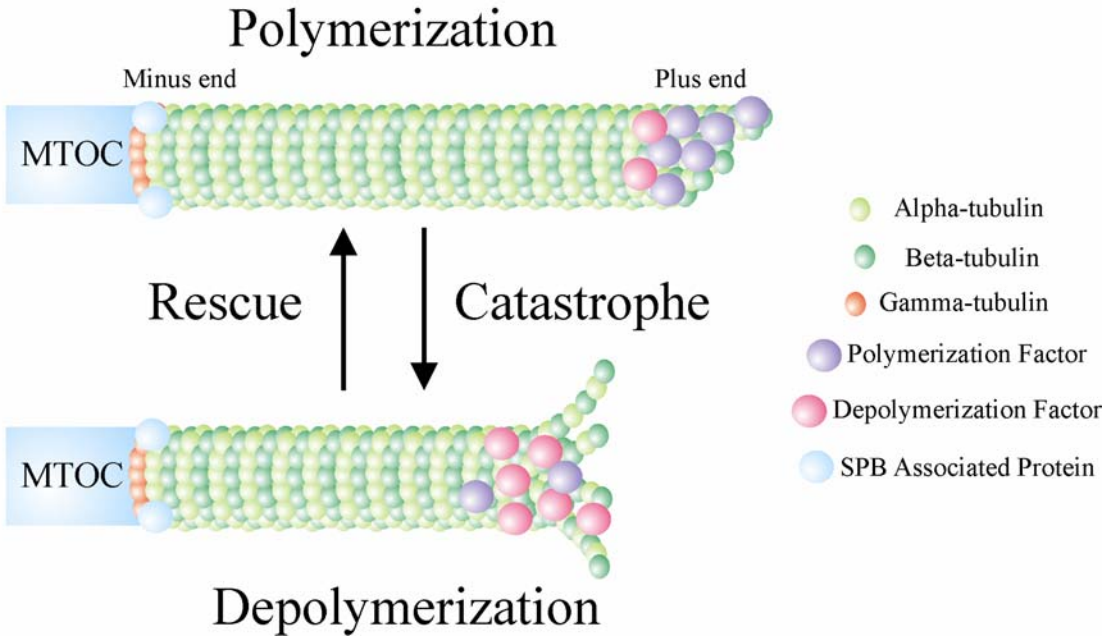
Polymerization
Minus end
Plus end
MTOC
Rescue
Catastrophe
MTOC
Depolymerization
Alpha-tubulin
Beta-tubulin
Gamma-tubulin
Polymerization Factor
Depolymerization Factor
SPB Associated Protein

Figure 1.2: Spindle structure and nuclear movements in *Saccharomyces cerevisiae*.

MTs function inside the nuclear envelope for chromosome segregation as well as in the cytoplasm to facilitate nuclear movements. (A) Budding yeast preanaphase mitotic spindle structure. Within the nucleus (gray circle), 16 kMTs (yellow lines) are nucleated from each SPB (red circles) to form kinetochore clusters on either side of the spindle equator. Four ipMTs (green lines) from each SPB grow out toward the opposite spindle pole. Bipolar spindle assembly results in ~1.5 μm mitotic apparatus. Two to five cytoplasmic MTs (cyan lines) are nucleated from the SPB to perform nuclear movements in the cell. (B) Unbudded cells can undergo two types of nuclear movements. After bud formation during mitosis (left), cytoplasmic MTs orient the spindle to the bud neck (nucleus – large gray circle; SPBs – small gray circles; MTs – green lines). Anaphase onset leads to dynein-dependent migration of the nucleus, segregating a set of chromosomes and one SPB to both cells. However, if cells enter the mating pathway (right), MTs interact with the actin network to orient the nucleus along the polarity axis (actin cables – red lines; actin patches – red circles). Once oriented, MT plus ends attach to the shmoo tip. MT dynamic instability results in nuclear oscillations after shmoo tip attachment. Once cells fuse, oppositely oriented MTs interact and nuclear congression occurs.

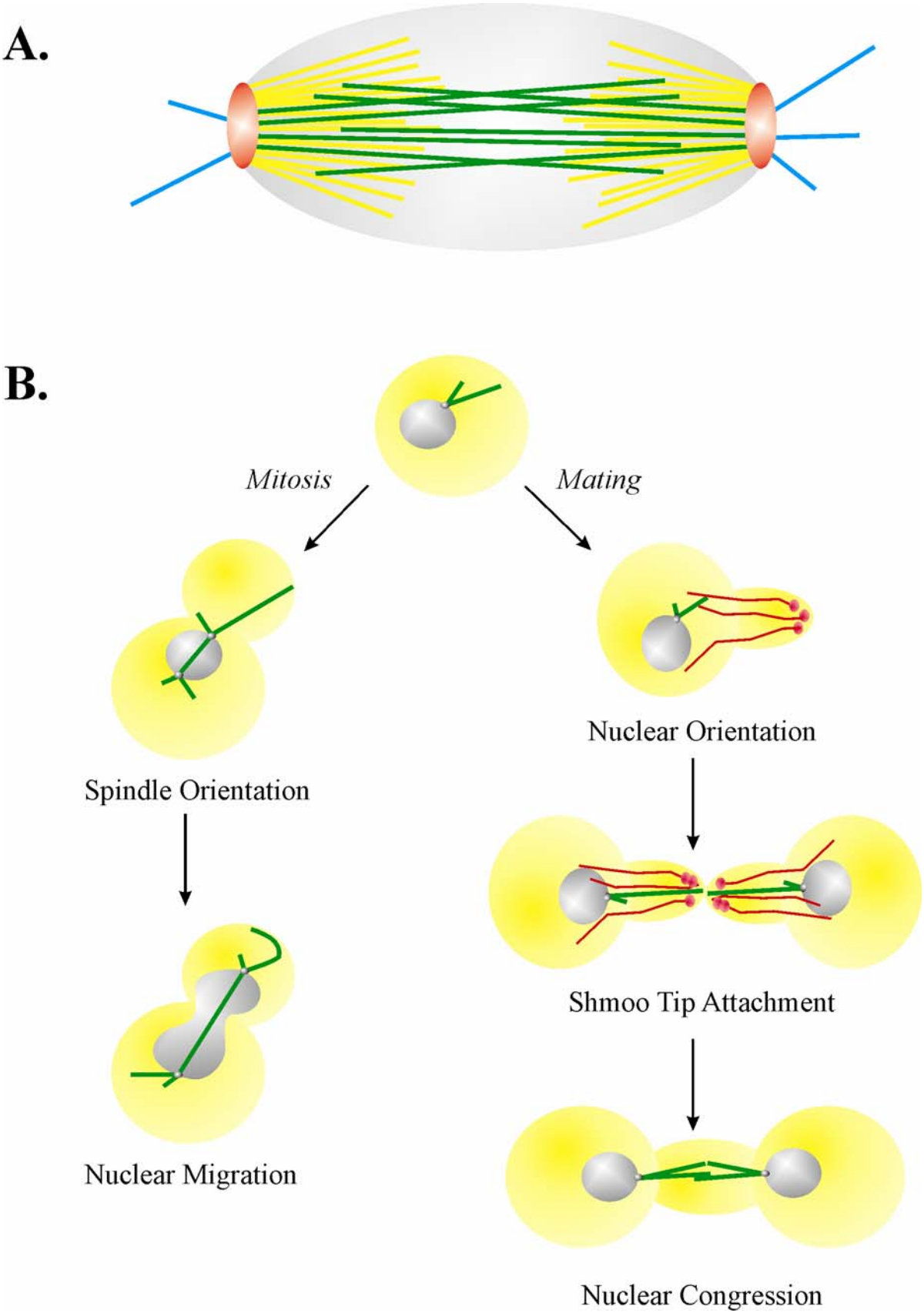
A.
B.
Mitosis
Mating
Spindle Orientation
Nuclear Migration
Nuclear Orientation
Shmoo Tip Attachment
Nuclear Congression

CHAPTER 2: THE DIFFERENTIAL ROLES OF BUDDING YEAST Tem1p, Cdc15p, AND Bub2p PROTEIN DYNAMICS IN MITOTIC EXIT

Contributing Authors: Jeffrey N. Molk, Scott C. Schuyler, Jenny Y. Liu, James G. Evans, E. D. Salmon, David Pellman, and Kerry Bloom

Abstract

In the budding yeast *Saccharomyces cerevisiae* the mitotic spindle must be positioned along the mother-bud axis to activate the Mitotic Exit Network (MEN) in anaphase. To examine MEN proteins during mitotic exit, we imaged the MEN activators Tem1p and Cdc15p and the MEN regulator Bub2p *in vivo*. Quantitative live cell fluorescence microscopy demonstrated the spindle pole body that segregated into the daughter cell (dSPB) signaled mitotic exit upon penetration into the bud. Activation of mitotic exit was associated with an increased abundance of Tem1p-GFP and the localization of Cdc15p-GFP on the dSPB. In contrast, Bub2p-GFP fluorescence intensity decreased in mid-to-late anaphase on the dSPB. Therefore, MEN protein localization fluctuates to switch from Bub2p inhibition of mitotic exit to Cdc15p activation of mitotic exit. The mechanism that elevates Tem1p-GFP abundance in anaphase is specific to dSPB penetration into the bud and Dhc1p and Lte1p promote Tem1p-GFP localization. Finally, Fluorescence Recovery After Photobleaching (FRAP) measurements revealed Tem1p-GFP is dynamic at the dSPB in late anaphase. These data suggest spindle pole penetration into the bud activates mitotic exit, resulting in Tem1p and Cdc15p persistence at the dSPB to initiate the MEN signal cascade.

Introduction

In the budding yeast *Saccharomyces cerevisiae* initiation of mitotic exit follows nuclear segregation into the bud. Before anaphase onset cytoplasmic microtubules align the nucleus, containing the mitotic spindle, along the mother-bud axis with one microtubule organizing center, called the spindle pole body (SPB), proximal to the bud neck (Byers and Goetsch, 1975; Kilmartin and Adams, 1984; Robinow and Marak, 1966). The SPB from the previous division segregates to the daughter bud (dSPB) in >95% of cells (Pereira et al., 2001). Microtubule motor proteins, such as Dhc1p, Kip2p, and Kip3p, individually contribute to the specific orientation of the spindle along the mother-bud axis (Li et al., 1993; Miller et al., 1998; Yeh et al., 1995; Yeh et al., 2000). Time-lapse microscopy has demonstrated anaphase spindle elongation in the mother cell results in a mitotic exit delay until the nucleus repositions along the mother-bud axis (Bardin et al., 2000; Bloecher et al., 2000; Daum et al., 2000; Pereira et al., 2000; Yeh et al., 1995). Thus, a spindle position checkpoint exists to monitor the orientation of the mitotic spindle, ensuring faithful nuclear segregation (Hoyt, 2000).

The spindle position checkpoint includes the Bub2p and Bfa1p two component Guanine Activating Protein (GAP) complex that inhibits mitotic progression (Alexandru et al., 1999; Bloecher et al., 2000; Fesquet et al., 1999; Li, 1999). Bub2p and Bfa1p localize to both SPBs but preferentially accumulate on the dSPB when spindles are repositioning along the mother-bud axis (Fraschini et al., 1999; Pereira et al., 2000; Pereira et al., 2001). A major target of Bub2p/Bfa1p is the Mitotic Exit Network (MEN), a signal transduction cascade that includes a guanine nucleotide binding protein, Tem1p, and protein kinases such as Cdc15p. Tem1p, Cdc15p, and other MEN proteins asymmetrically localize to the spindle poles

(Bardin and Amon, 2001; McCollum and Gould, 2001). The Bub2p/Bfa1p GAP complex is proposed to inhibit the MEN in preanaphase through specific interactions with Tem1p at the dSPB (Geymonat et al., 2002; Ro et al., 2002). After spindle elongation into the bud, Tem1p may be activated by the putative Guanine Exchange Factor (GEF) Lte1p at the bud cell cortex to promote Cdc15p localization to the dSPB, beginning the MEN signal cascade (Bardin et al., 2000; Pereira et al., 2000). In the absence of Bub2p, Tem1p does not localize to the dSPB until late anaphase and Cdc15p localizes before anaphase resulting in inappropriate mitotic exit if spindle abnormalities exist (Hoyt et al., 1991; Pereira et al., 2000; Visintin and Amon, 2001). These data suggest Bub2p influences the localization of upstream MEN components at the dSPB.

The asymmetric localization of MEN components has lead to a spatial separation mechanism for MEN function (Bardin et al., 2000; Pereira et al., 2000). If the spindle is not positioned along the mother-bud axis the dSPB will not enter the bud and mitotic exit will be delayed by Bub2p-Bfa1p GAP inactivation of Tem1p. Entry of the dSPB into the bud places Tem1p in the same compartment as Lte1p to activate mitotic exit. However, Lte1p GEF activity is required for Lte1p localization at the bud cortex but is not essential for mitotic exit (Yoshida et al., 2003). Furthermore, Lte1p is not required for mitotic exit at physiological temperatures (Adames et al., 2001; Shirayama et al., 1994a). A second mechanism for mitotic exit may involve negative regulation by cytoplasmic microtubules (Adames et al., 2001). In this model, mitotic exit proceeds only when cytoplasmic microtubule connections with the bud neck are lost. The spatial separation and cytoplasmic microtubule models are not mutually exclusive and it is possible that both dSPB penetration into the bud and loss of cytoplasmic microtubules at the bud neck are required for cells to exit mitosis.

Models for mitotic exit have not incorporated either the spatial or the temporal regulation of MEN protein localization in living cells. Is there an event associated with spindle elongation, such as dSPB penetration into the bud or dSPB contact with the distal bud cortex, that correlates with mitotic exit? If so, how do the early MEN components Tem1p and Cdc15p localize in response to the initiating event for mitotic exit? Does the MEN inhibitor Bub2p alter its localization on the dSPB during mitotic exit? Do MEN proteins such as Tem1p exchange with the cytoplasmic protein pool? Finally, can Lte1p or regulators of spindle positioning affect the localization of Tem1p on the dSPB?

To investigate these questions, we have used quantitative live cell imaging of fluorescence fusion proteins and measurements of Fluorescence Recovery After Photobleaching (FRAP). The initiating signal for mitotic exit is dSPB penetration into the bud. Additionally, Tem1p-GFP and Cdc15p-GFP persistently accumulate on the dSPB upon bud neck penetration while Bub2p-GFP fluorescence intensity declines in mid-to-late anaphase. Tem1p-GFP on the dSPB is dynamic in late anaphase indicating the accumulation of Tem1p during anaphase does not result in tight binding to the dSPB. The major increase in Tem1p-GFP fluorescence on the dSPB occurs specifically in the bud compartment and Tem1p-GFP abundance is promoted by the minus-end microtubule motor protein dynein (Dhc1p) and Lte1p. Thus, activation of mitotic exit causes a change in MEN protein abundance and persistence upon dSPB penetration of the bud that drives the progression to interphase.

Materials and Methods

Media and strain construction

Media and genetic techniques are described elsewhere (Rose and Broach, 1990). Geneticin (Life Technologies, Invitrogen Co., Carlsbad, CA) or hygromycin B (CellGro Co., Herndon, VA) was used at a concentration of 0.2 or 0.4 μM in YPD. α-factor (Research Genetics, Invitrogen Co., Carlsbad, CA) was used at a final concentration of 10 μg/ml. PCR primer sequences are listed in Table 2.S1 and *S. cerevisiae* strains used in this study are listed in Table 2.1.

A wild-type strain expressing GFP-Tub1p (PY 2370) was mated with an *ase1Δ* strain (PY 1973) to generate PY 3446 (Lee et al., 1999; Sikorski and Hieter, 1989; Tirnauer et al., 1999). pB1594 integrated three tandem copies of GFP at the 3' end of the *LTE1* coding region (Lte1p-3xGFP). The growth of this strain was tested at 14°C and 37°C, and it was similar to wild-type (Figure 2.S1A). The Lte1p-3xGFP construct complemented the cold sensitivity of *lte1Δ* and *ase1Δ lte1Δ* synthetic lethality at 37°C (Figure 2.S1A and 2.S1B).

Fusion of GFP to the 3' ends of *TEM1, BUB2,* and *CDC15* was constructed by PCR fragment-mediated transformation using the pFA6::*GFP-KANMX* template (Wach et al., 1994). The resulting strains exhibited wild-type growth rates indicating neither Tem1p nor Cdc15p function were compromised (Figure 2.S2A). Similarly, none of the strains were benomyl sensitive suggesting the spindle position checkpoint was not abrogated (Figure 2.S2B). Gene disruptions were made using PCR fragment-mediated transformation conferring antibiotic resistance (Goldstein and McCusker, 1999; Longtine et al., 1998; Wach et al., 1994). All integrations were confirmed by PCR. Cyan Fluorescence Protein (CFP)-

Tub1p plasmid, derived from pAFS125 (Straight et al., 1997), was linearized with *StuI* before transformation.

Timing of mitotic exit image acquisition and data analysis

Liquid log phase *ASE1* and *ase1Δ* strains expressing GFP-Tub1p were treated with α-factor for two hours at 30°C (90% shmoos), released into fresh medium, washed, and imaged 40 to 50 minutes later as detailed in Tirnauer et al. (1999). Time-lapse movies were made at 25°C by acquiring alternating differential interference contrast (DIC) and epi-fluorescence images in 17 Z-planes of 0.3-μm steps (2 x 2 binning) every 2 min. Six hundred-millisecond fluorescence exposure times were used with seven-eighths of the excitation light attenuated by a neutral density filter. DIC exposures were for 30 ms. Fluorescence Z-series from each time point were merged and analyzed as a single projection superimposed on the corresponding DIC image. All image manipulations and measurements were made using Openlab Software v3.0.2 (Improvision, Lexington, MA).

The first image after clear spindle penetration into the bud was designated as t = 0 min for measuring mitotic exit events. This criterion results in a number of instances where the spindle pole is within the bud volume at t = 0 min. Thus, the resolution of our imaging is 2 min. A cortical interaction was scored when the spindle pole body was ≤0.5 μm from the side of the bud cortex in either a stationary position or a brushing-sweeping motion in two consecutive images. Cells where cortical contact may have occurred at the top or bottom of the cell were omitted. Spindle elongation rates were determined by linear regression of two to four time points from a 1.5-2 μm to a 4-6 μm bipolar spindle for the fast phase of spindle elongation and two to eight time points from a 4-6 μm to a 8-12 μm spindle for the slow phase of spindle elongation. Septation was scored as the rotation of the daughter and mother

cells relative to one another in DIC images (Bi et al., 1998; Yeh et al., 1995). Measurements were exported to Microsoft Excel (Microsoft Co., Seattle, WA) and statistical comparisons were made using Statview (SAS Institute Inc., Cary, NC) and Kaleidagraph 3.0.4 (Abelbeck Software, Reading, PA).

Native level Lte1p-3xGFP localization

Midlogarithmically growing Lte1p-3xGFP-expressing cells mixed with wild-type untransformed cells were imaged by acquiring 80 plane Z-stacks at 0.2-μm steps (1 x 1 binning) with 2-s epi-fluorescence exposures and 30-ms transillumination exposures. Images were deconvolved using 500 iterations an Accelerated-Maximum-Likelihood-Estimation restoration algorithm optimized for low light imaging in Huygens2 (Scientific Volume Imaging, Hilversum, Netherlands). Autofluorescence was subtracted using the nearby untransformed wild-type cells. The data were rendered using the "Simulated Fluorescence Process" algorithm within Imaris3 (Bitplane, Zurich, Switzerland).

Live cell analysis of MEN fluorescence fusion proteins

Midlogarithmic phase cells expressing Tem1p-GFP, Bub2p-GFP, Cdc15p-GFP, and CFP-Tub1p were imaged as described elsewhere at ~22°C (Maddox et al., 2000; Shaw et al., 1997a). Image processing was performed with MetaMorph software (Universal Imaging Co., West Chester, PA). Three- or five-plane Z-series at 0.75-μm steps (2 x 2 binning) were acquired every two minutes with 400-ms epi-fluorescence exposures and a single 100-ms DIC exposure (1 x 1 binning). For two color imaging, the yellow fluorescence protein (YFP) epi-fluorescence exposure time was 500 ms and the CFP epi-fluorescence exposure time was 350 ms.

MEN fluorescence fusion protein image analysis

Three-dimensional stacks of Tem1p-GFP, Bub2p-GFP, Cdc15p-GFP, or CFP-Tub1p time-lapse movies were compiled into a single maximum projection for each time point (Shaw et al., 1997a). Fluorescence intensity measurements were made by placing a 35-40 pixel^2 circle around a Tem1p-GFP or Bub2p-GFP signal and the integrated intensity was recorded to a linked Microsoft Excel spreadsheet. The mSPB fluorescence intensities of Tem1p-GFP are overestimates because cells with no mSPB fluorescence were not measured. Background fluorescence was subtracted by placing the same measurement circle in three different nearby intracellular regions without a Tem1p-GFP or Bub2p-GFP signal and the three measurements were averaged to give a single data point for each time interval. Three-dimensional static images, where a single five-plane Z-series at 0.75-μm steps was acquired, were not compiled; the brightest signal from the five planes was used to generate the single data point. To determine the stage of mitosis, bud size and position of the SPB relative to the bud neck were used. A signal proximal to the bud neck was scored as preanaphase; a signal moving towards the daughter cortex or in between the bud neck and daughter cell cortex were scored as anaphase spindle elongation; a signal directly adjacent to the daughter cell cortex was scored as late anaphase. Student's two-tailed *t* test was used for all statistical analysis and $p < 0.01$ was considered significant.

For Tem1p-GFP fluorescence intensity measurements during anaphase, 9 living cells were imaged as above (no binning) and three-plane Z-series were compiled. Each dSPB was measured for fluorescence intensity and distance from the Tem1p-GFP signal to the center of the bud neck using Track Points in MetaMorph. All measurements were averaged and at

least two measurements were used for each time point. Spindle length was recorded using the linear calibrated distance between two Tem1p-GFP foci. Anaphase onset was marked at *t* = 0 min and any time prior to anaphase onset was denoted as a negative value (i.e. *t* = -8 min). Single Bub2p-GFP cells were analyzed similarly using 2 x 2 binned images of compiled five-plane Z-series.

FRAP of Tem1p-GFP

FRAP experiments were performed as detailed elsewhere (Kosco et al., 2001; Maddox et al., 2000). Cells were photobleached with a 35-ms laser pulse. For Tem1p-GFP a single focal plane with a 400-ms epi-fluorescence exposure time was obtained for three data points prior to photobleaching and 10 data points after photobleaching at 3-s intervals followed by 10 data points obtained at 10-s intervals and then four to six data points at 30-s intervals. Thus, each recovery was measured for ~270 s. Aperiodic DIC images (100-ms exposure time) were acquired for each experiment as well. Recovery was not significantly altered by photobleaching due to image acquisition for up to 30 frames acquired in unbleached cells (our unpublished results). A 5 x 5 pixel box was used to make fluorescence intensity measurements. Intracellular background was subtracted according to the methods above and three measurements were averaged for each data point. Dividing the dSPB fluorescence intensity measured immediately after photobleaching by the fluorescence intensity prior to photobleaching indicated an average of 4% of Tem1p-GFP remained unbleached at the dSPB before recovery (our unpublished results).

Fluorescence recovery, or the loss of bleached fluorescence at the dSPB, was initially analyzed by assuming a single rate constant as follows (Salmon et al., 1984a; Saxton et al., 1984; Wadsworth and Salmon, 1986b):

$$F_\infty - F(t) = [F_\infty - F(0)]\, e^{-kt}, \qquad (1)$$

where F_∞ is the average intensity of the bleached region after maximum recovery, $F(t)$ is the fluorescence intensity at each time point (t = 0 s was immediately after photobleaching), $F(0)$ is the fluorescence intensity at t = 0 s, k is the rate constant for exponential decay, and t is time. The natural logarithm of the quantity on the left side of the following equation derived from (Eq. 1):

$$\frac{F_\infty - F(t)}{F_\infty - F(0)} = e^{-kt}, \qquad (2)$$

was plotted vs. time for analysis. A single straight line on this logarithmic plot predicts a single rate constant but the two slopes for Tem1p-GFP indicated a fast recovery fraction and a slow recovery fraction. To analyze the biphasic nature of bleached subunit disassociation, the data from Eq. 2 that generated the logarithmic plot were exported to SigmaPlot 8.0 (SPSS Science, Chicago, IL) and analyzed using the Exponential Decay function (Double, 4 Parameter) for two rate constants that follows from the formula:

$$\frac{F_\infty - F(t)}{F_\infty - F(0)} = f_f * (e^{-kf\,t}) + f_s * (e^{-ks\,t}), \qquad (3)$$

where the fast phase and slow phase rate constant (k_f and k_s), and the fraction of recovery due to the fast and slow phases (f_f and f_s) were calculated. Using these rate constants and recovery values we generated a best-fit biphasic recovery curve for the theoretical association of unbleached subunits to the dSPB with the formula:

$$F(t) = F(0) + f_f * (F_\infty - F(0)) * (1-e^{-kf\Delta t}) + f_s * (F_\infty - F(0)) * (1-e^{-ks\Delta t}) , \qquad (4)$$

where $\Delta t = t - t_0$. The best-fit data for single and biphasic recovery were plotted separately with the experimental data for comparison.

To determine the fraction of Tem1p-GFP that recovers to the dSPB within the imaging interval we calculated the fluorescence recovery ratio, *R* (Howell et al., 2000):

$$R = \frac{F_\infty - F(0)}{F_{pre*} - F(0)} \qquad (5)$$

The fluorescence intensity prior to photobleaching (F_{pre*}) was determined by multiplying each of the three fluorescence intensity measurements prior to photobleaching ($F(t)_{pre}$) by the ratio of total cellular fluorescence intensity immediately after photobleaching ($F_{c\text{-}post}$) to the total cellular fluorescence intensity immediately prior to photobleaching ($F_{c\text{-}pre}$):

$$F(t)_{pre\text{-}corr} = F(t)_{pre} * \frac{F_{c\text{-}post}}{F_{c\text{-}pre}} \qquad (6)$$

The three corrected fluorescence intensity values ($F(t)_{pre\text{-}corr}$) were averaged to a single prebleach data point (F_{pre*}) used in Eq. 5. This will correct for the fraction of Tem1p-GFP fluorophore in the total protein pool destroyed by the laser pulse during photobleaching and averaged 20% in each experiment.

Results

Spindle pole body passage through the bud neck signals mitotic exit

A connection between spindle morphology during anaphase and mitotic exit has not been established. We analyzed wild-type cells expressing GFP-Tub1p to determine if there is an event associated with spindle elongation that correlates with mitotic exit (Figure 2.1A and 2.1B). The average time from dSPB passage through the bud neck to contact with the distal bud cortex was 6 min (Figure 2.2A) and the mean interval from dSPB-cortical contact to septation was 16 min (Figure 2.2B). The time from dSPB penetration into the bud to septation was 22 min (Figure 2.2C), demonstrating a strict temporal link between dSPB entry into the bud, completion of mitotic exit, and septation.

dSPB penetration into the bud is coincident with spindle elongation. Using *ase1Δ* cells that exhibit premature spindle breakdown in early anaphase (Pellman et al., 1995; Schuyler et al., 2003), we tested if there is a requirement for a stable anaphase spindle to signal mitotic exit. The behavior of spindle poles in *ase1Δ* mutants was similar to wild-type cells (Figure 2.1C and 2.1D). The mean intervals between dSPB entry into the bud and cortical contact, cortical contact and septation, and entry into the bud and septation were indistinguishable in *ase1Δ* cells when compared to wild-type (Figure 2.2A - 2.2C; wild-type: n = 56, *ase1Δ*: n = 50). Thus, dSPB penetration into the bud signals mitotic exit.

To test whether dSPB penetration into the bud compartment or direct contact between the dSPB and the bud cortex distal from the bud neck signals mitotic exit, we determined if there was a significant correlation between dSPB entry into the bud, distal cortical contact, and septation. If there is a direct correlation between the timing of any two of these events, the slope of the best-fit line should equal 1; if the events are not correlated the slope will be

0. The timing of dSPB entry into the bud to the first contact with the distal bud cell cortex does not correlate with the timing of dSPB entry into the bud to septation (0.086 +/- 0.212, Figure 2.2D). Therefore septation does not correlate with dSPB-distal cortical contact.

Since the interval between dSPB entry into the bud and septation is essentially invariant (Figure 2.2C), a longer interval from dSPB penetration into the bud to distal cortical contact predicts a shorter interval between distal cortical contact and septation or a negative correlation. The timing of dSPB entry of the bud to distal cortical contact vs. the timing of distal cortical contact to septation was negatively correlated (–0.914 +/- 0.212, Figure 2.2E). Therefore, dSPB entry into the bud triggers septation. Moreover, the total amount of time the dSPB spends in contact with the daughter cell cortex as a percentage of the total time the dSPB spends within the bud does not predict the timing of septation (0.000 +/- 0.066, Figure 2.2F). Similarly, *ase1Δ* cells showed neither a relationship between the time of initial dSPB-distal cortical contact and septation (0.192 +/- 0.219, Figure 2.2G) nor between the percentage of time the dSPB contacted the cell cortex and septation (-0.005 +/- 0.093, Figure 2.2H). Together these data provide strong evidence that dSPB penetration into the bud, and not dSPB-distal cortical contact or stable anaphase spindle elongation, triggers mitotic exit.

Tem1p-GFP distribution changes during spindle positioning and spindle elongation

The accumulation of Tem1p on the dSPB during mitosis could link spindle alignment and dSPB passage into the bud with activation of the MEN. To examine the localization and dynamics of Tem1p, GFP was fused to the 3' end of the endogenous *TEM1* locus. In cells where the spindle has not aligned along the mother-bud axis Tem1p-GFP often localized preferentially to one SPB that subsequently positioned on the mother side of the bud neck (Figure 2.3A). This asymmetric accumulation was usually maintained until anaphase onset.

However, in a small fraction of cells, both SPB were labeled equally with Tem1p-GFP in preanaphase (Figure 2.3B, 0 min). Anaphase onset in all wild-type Tem1p-GFP expressing cells resulted in a fluorescence intensity increase on the dSPB in the bud (Figure 2.3B). After spindle breakdown Tem1p-GFP was lost from the dSPB and was not detected at any other structure in the cell (our unpublished results). Tem1p-GFP on the mSPB localized at least transiently in >80% of living cells during spindle alignment and/or spindle elongation, indicating Tem1p localizes to both SPBs before and during mitotic exit activation.

To quantitate the levels of Tem1p-GFP on spindle poles in wild-type cells, we measured the fluorescence intensity of Tem1p-GFP during mitosis for cells imaged in three dimensions in the population and over time (see Table 2.2 for summary of all fluorescence intensity measurements). On average Tem1p-GFP was more intense on the dSPB, indicating Tem1p-GFP preferentially accumulated on the SPBs that entered the daughter cell during mitosis (Figure 2.4A). In addition, Tem1p-GFP increased in fluorescence intensity on dSPBs as spindles elongated (Figure 2.4A). By late anaphase Tem1p-GFP was two times as intense on the dSPB, a significant difference from preanaphase cells ($p < 1 \times 10^{-6}$). Tem1p-GFP did not significantly increase on the mSPB from preanaphase to late anaphase ($p > 0.10$). As a control, we measured the structural SPB component Spc29p and found Spc29p-GFP does not double in fluorescence intensity on either SPB during mitosis ($p > 0.05$). Recording individual cells progressing through mitosis demonstrated that the increase in Tem1p-GFP fluorescence intensity closely followed dSPB penetration into the daughter cell (Figure 2.4B). The fluorescence signal peaked in late anaphase when the spindle reached maximum elongation. The mSPB Tem1p-GFP signal was variable during spindle elongation and did not display a consistent localization pattern preventing analysis similar to the dSPB.

The increase in Tem1p-GFP on the dSPB during spindle elongation could be due to spindle pole penetration into the bud or could be a consequence of anaphase onset. To distinguish between these possibilities, we deleted the dynein heavy chain (*DHC1*) resulting in a fraction of cells where the spindle does not align along the mother-bud axis and anaphase spindle elongation occurs entirely within the mother cell (Li et al., 1993; Yeh et al., 1995). In *dhc1Δ* mutants where the spindle was elongated within the mother cell, Tem1p-GFP labeled both SPBs and did not display the increased asymmetric fluorescence intensity characteristic of wild-type spindle elongation (Figure 2.3C). Together, these data suggest as anaphase proceeds Tem1p accumulates and persists at the dSPB upon penetration into the daughter cell.

Cdc15p localization coincides with spindle elongation in anaphase

If the MEN is activated when Tem1p-GFP fluorescence increases, then the downstream protein kinase Cdc15p should accumulate at the dSPB upon penetration into the bud. We constructed a strain expressing Cdc15p-GFP as well as CFP-Tub1p to determine the accumulation of Cdc15p at the dSPB relative to spindle elongation into the bud. Cdc15p-GFP accumulated at the dSPB 4 min after anaphase onset when the dSPB began to penetrate the bud neck (Figure 2.5B, 4 min). The mSPB was not labeled with Cdc15p-GFP during early anaphase, indicating the initial localization of Cdc15p-GFP is specific for penetration of the bud. As anaphase proceeded, Cdc15p-GFP continued to accumulate on the dSPB and also localized to the mSPB (Figure 2.5B, 16 min and 24 min). Therefore, the timing of Cdc15p localization to the dSPB coincided both with the increase in Tem1p accumulation after anaphase onset and dSPB penetration into the bud.

Bub2p-GFP decreases on the dSPB during late anaphase

When the MEN is activated, does the localization of Bub2p change in living cells? In wild-type cells both Tem1p-GFP and Cdc15p-GFP increase in fluorescence intensity on the dSPB during anaphase (Figures 2.3 and 2.5). To determine if Bub2p localization is altered during anaphase, GFP was fused to the C-terminus of Bub2p. Bub2p-GFP increased in fluorescence intensity on the dSPB during anaphase spindle elongation and then decreased in fluorescence intensity in late anaphase (Figure 2.6A). Bub2p-GFP fluorescence intensity on the mSPB was lost soon after anaphase onset (Figure 2.6A). Measuring the fluorescence intensity of Bub2p-GFP in individual cells during spindle elongation demonstrated Bub2p-GFP levels decreased from the dSPB in either midanaphase (Figure 2.6B) or when the spindle pole reached the distal daughter cell cortex in late anaphase (Figure 2.6C). The quantitative fluorescence intensity measurements of Tem1p-GFP, Spc29p-GFP, and Bub2p-GFP are plotted in Figure 2.6D for direct comparison of these probes. From these quantitative data, we conclude Bub2p is lost from the dSPB in mid-to-late anaphase when Tem1p localization becomes most abundant.

Compartmentalization of Lte1p is restricted to the daughter cell cortex

The inhibitory activity of the spindle position checkpoint on Tem1p may be counteracted by Lte1p once the dSPB segregates into the bud (Bardin et al., 2000; Pereira et al., 2000). The increase in Tem1p at the dSPB in the bud could result from an interaction between Tem1p and a large fraction of Lte1p in the bud cytosol that activates mitotic exit. Alternatively, the majority of Lte1p could localize to the bud cortex predicting Tem1p-Lte1p

interactions rely on dynamic protein exchange in the cytoplasm. To determine the localization of the MEN activator Lte1p in more detail, we introduced three tandem copies of GFP at the C-terminus of Lte1p (Lte1p-3xGFP). Lte1p-3xGFP was characterized in wild-type cells by deconvolution microscopy and three-dimensional reconstruction (Figure 2.7). Three-dimensional lateral projections of 23 cells showed that all of the detectable Lte1p-3xGFP is unevenly distributed to the periphery of the cell adjacent to the plasma membrane (our unpublished results). Since the majority of Lte1p localizes to the bud cortex, Tem1p-Lte1p interactions must be dynamic if Lte1p affects Tem1p localization at the dSPB.

Characterization of Tem1p-GFP dynamics by FRAP

We examined Tem1p at the dSPB in more detail to understand the mechanisms that underlie Tem1p dynamics and accumulation during activation of mitotic exit. The increase in Tem1p-GFP at the dSPB in late anaphase as well as the localization of Lte1p to the bud cortex suggests Tem1p is dynamic and exchanges between the cytoplasm and spindle pole. Alternatively, Tem1p could bind tightly to the dSPB in late anaphase. To determine if Tem1p is dynamic, we photobleached Tem1p-GFP in late anaphase during mitotic exit and quantified Tem1p-GFP recovery to the dSPB (Figure 2.8A and 2.8B). Kinetic analysis of recovery indicated a fast and a slow phase to Tem1p-GFP recovery. An example of a single exponential and a biphasic fit to the experimental data is shown in Figure 2.8C and 2.8D. The fast fraction of Tem1p-GFP has an average half-recovery time ($t_{1/2}$) of 4.50 +/- 2.29 s (mean +/- SD) with 56.5% of the recovery to the dSPB due to the fast fraction (Table 2.3). The slow fraction of Tem1p-GFP had a $t_{1/2}$ of 133 +/- 85.5 s and 43.5% recovery to the dSPB

was contributed by the slow fraction (Table 2.3). The total recovery (*R*) of Tem1p-GFP to the dSPB was 61.2% over the 5-min imaging interval.

The high temporal resolution required to resolve the two kinetic phases of Tem1p-GFP limited image acquisition to single Z-planes. To determine if shifts in the Z-focal plane of the mitotic spindle or subtle photobleaching during image acquisition resulted in only ~61% fluorescence recovery to the dSPB, we photobleached cells and acquired a single five-plane Z-series at 5 and 10 min after the laser pulse. The calculated *R* value of Tem1p-GFP at the dSPB using this approach was 96% (n = 5) indicating that Tem1p at the dSPB exchanges nearly completely with the cytoplasmic pool within 10 min. Thus, Tem1p is dynamic at the dSPB in late anaphase.

Tem1p-GFP distribution responds to active spindle positioning

The dynamics of Tem1p at the dSPB may reflect the ability of Tem1p to respond to positional cues during spindle orientation. In wild-type cells Tem1p preferentially localizes to the dSPB as it positions along the mother-bud axis (Figure 2.3A). Tem1p persistence at the dSPB in anaphase, instead of just an increase in localization, may be the key to signaling mitotic exit. Oscillations of wild-type preanaphase spindles within the mother cell before spindle alignment and establishment of Tem1p-GFP asymmetry are rare. To examine Tem1p-GFP on spindle poles orienting along the mother-bud axis, we examined Tem1p-GFP in *kar9Δ* mutants defective in nuclear positioning (Miller and Rose, 1998). Tem1p-GFP transiently accumulated on either spindle pole in these mutants when the spindle was approximately parallel to the bud neck (Figure 2.9A). Preferential Tem1p-GFP distributions on a single SPB prior to anaphase were not sufficient for mitotic exit because the cell

remained arrested until the spindle reoriented along the mother-bud axis (Figure 2.9A). Further, passage of the spindle through the bud neck did not irreversibly increase Tem1p-GFP. The spindle could transiently enter the bud causing an increase of Tem1p-GFP on the dSPB and then move back into the mother cell resulting in decreased fluorescence intensity (Figure 2.9A, 34 min and 38 min). On spindle elongation, Tem1p-GFP accumulated on the SPB positioned in the daughter cell (Figure 2.9A, 62 min).

By designating the SPB that eventually enters the bud as the dSPB and the SPB that is retained in the mother cell as the mSPB, we plotted the change in Tem1p-GFP fluorescence intensity for each SPB as well as the distance from the SPB to the bud neck (Figure 2.9B, dSPB, and 2.9C, mSPB). The fluorescence intensity of the dSPB dramatically increased when penetration into the daughter cell occurred. Additionally, the dSPB appeared to stabilize in fluorescence intensity near the bud neck before penetration into the daughter cell, similar to the situation during wild-type spindle positioning in preanaphase. Finally, the persistence of Tem1p on the dSPB is a consequence of entry into the bud and presumably signals mitotic exit.

Lte1p is required for Tem1p-GFP localization during mitotic exit

How Lte1p at the bud cortex may regulate dynamic Tem1p in the cytoplasm is still unclear. The restriction of Lte1p to the bud during preanaphase and early anaphase could contribute to the specific accumulation of Tem1p on the dSPB upon penetration into the bud. To determine if Lte1p contributes to Tem1p-GFP localization during mitotic exit, we compared the fluorescence intensity of Tem1p-GFP on the dSPB in late anaphase between wild-type strains and *lte1Δ* cells (Figure 2.10A). As a control, we deleted *ASE1*. Deletion of

ASE1 results in a delay in anaphase onset (Schuyler et al., 2003) but does not change the timing of anaphase or mitotic exit (Figure 2.1 and 2.2), predicting Tem1p-GFP fluorescence intensity should not be different from wild-type levels. The fluorescence intensity of Tem1p-GFP in *ase1Δ* cells was not significantly different from wild-type cells, with the ratio of Tem1p-GFP fluorescence intensity in the mutant cells to Tem1p-GFP fluorescence intensity in wild type cells equaling 1.08:1.00 ($p > 0.10$). In contrast, Tem1p-GFP is significantly reduced in *lte1Δ* cells grown at 32°C (fluorescence intensity ratio 0.54:1.00; $p < 1 \times 10^{-7}$). Analysis of Bub2p-GFP on the dSPB in wild-type and *lte1Δ* cells grown at 32°C indicated there was no significant loss of Bub2p-GFP fluorescence intensity (our unpublished results). Thus, Tem1p localization to the dSPB is specifically promoted by Lte1p in vivo.

Microtubule motor proteins and Kar9p regulate Tem1p-GFP localization in late anaphase

Because Tem1p-GFP fluorescence intensity varies with spindle positioning (Figure 2.9), it is possible factors involved in nuclear orientation can also moderate the amount of Tem1p-GFP found on spindle poles. By analyzing Tem1p-GFP on the dSPB in late anaphase of properly positioned spindles we could determine the effect of spindle orientation factors on Tem1p-GFP abundance (Figure 2.10B). Deletion of the cytoplasmic dynein heavy chain (*DHC1*) significantly decreased Tem1p-GFP fluorescence intensity on the dSPB of properly elongated spindles in the bud (fluorescence intensity ratio = 0.63:1.00; $p < 1 \times 10^{-4}$). In *dhc1Δ* cells Bub2p-GFP fluorescence intensity was not altered significantly in any stage of the cell cycle (our unpublished results) indicating the loss of fluorescence is specific for Tem1p. Tem1p-GFP fluorescence intensity was reduced by deleting the microtubule motor protein *KIP2* (fluorescence intensity ratio = 0.72:1.00; $p < 0.013$) and spindle orientation

factor *KAR9* (fluorescence intensity ratio = 0.76:1.00; $p < 0.02$). In contrast, loss of Bud6p, a cortical protein involved in Kar9p-independent spindle orientation (Segal et al., 2002) had no effect on the accumulation of Tem1p-GFP at the dSPB in late anaphase (fluorescence intensity ratio = 1.00:1.00; $p > 0.10$). Finally, deletion of the microtubule motor protein *KIP3* resulted in increased Tem1p-GFP localization to the dSPB compared with wild-type controls in late anaphase (fluorescence intensity ratio = 1.43:1.00, $p < 0.01$). Thus, Dhc1p and other spindle orientation factors regulate Tem1p abundance and persistence in late anaphase.

Discussion

Using quantitative live cell microscopy we have investigated the dynamics of MEN proteins during mitotic exit. Passage of the spindle pole into the bud, and not contact with the distal bud cortex, signaled mitotic exit (Figures 2.1 and 2.2). Positioning of the dSPB at the bud neck and subsequent entry into the daughter cell resulted in the increased accumulation of Tem1p at the dSPB relative to the mSPB (Figures 2.3 and 2.4). These data indicate that Tem1p on the dSPB does not need to contact the distal bud cortex to either facilitate Tem1p accumulation on the dSPB or to activate mitotic exit. The increased Tem1p localization to the dSPB once in the bud could merely reflect a programmed increase in Tem1p protein levels that peak in telophase (Bardin et al., 2000) or SPB maturation during mitosis. Using mal-oriented spindles we showed that positioning along the mother-bud axis rather than the time spent in preanaphase or anaphase generates Tem1p-GFP asymmetry (Figure 2.3C and Figure 2.9). Additionally, increases in fluorescence intensity occurred when the spindle pole entered the daughter cell (Figure 2.3C and Figure 2.9). Thus, Tem1p localization responds to the spatial movement of the mitotic spindle and entry into the bud.

Determining the mechanism of Tem1p accumulation on the dSPB requires information about both the factors that regulate Tem1p localization and the dynamics of Tem1p. To understand the regulation of Tem1p-GFP abundance on the dSPB we examined Tem1p-GFP in *lte1Δ* cells. The majority of Lte1p localizes to the bud cortex and could promote Tem1p localization to the dSPB in the bud (Figure 2.7). In the absence of Lte1p the abundance of Tem1p is significantly diminished (Figure 2.10A). Importantly, this indicates that if a "threshold" level of Tem1p on the dSPB exists that must be surpassed before mitotic exit is activated, this threshold is low in *lte1Δ* mutants. Because dSPB penetration into the

bud results in activation of mitotic exit, Tem1p-Lte1p interactions either have to occur in the cytoplasm or Tem1p interacts with Lte1p at the bud cortex and then re-localizes to the dSPB. Because there is no evidence that Tem1p localizes to the bud cortex, most likely Tem1p and Lte1p interact in the cytoplasm, suggesting Lte1p may be dynamic and exchange between the bud cortex and the cytoplasmic protein pool. In support of this hypothesis, a cytoplasmic pool of Lte1p has been shown to exist during mitotic exit (Castillon et al., 2003). Lte1p has been linked with Ras function and the Lte1p GEF domain is not necessary for mitotic exit (Yoshida et al., 2003). Our data indicate that Lte1p may function to promote Tem1p localization at the dSPB. One possibility is that Tem1p localization is controlled by Lte1p independently of Lte1p GEF activity. Tem1p has a high rate of GDP release in vitro (Geymonat et al., 2002), suggesting the intrinsic nucleotide dynamics of Tem1p may not need to be supplemented by Lte1p GEF activity to drive mitotic exit. Lte1p could serve as a redundant mechanism at physiological temperatures to ensure Tem1p localizes to the dSPB in sufficient amounts to interact with Cdc15p for mitotic exit to occur.

To examine Tem1p dynamics and test if Tem1p is stable or exchanges with the cytoplasmic protein pool at the dSPB in late anaphase, we photobleached Tem1p-GFP. This analysis revealed two kinetic fractions of Tem1p at the dSPB in late anaphase (Figure 2.8 and Table 2.3). What are possible explanations for the biphasic recovery of Tem1p-GFP to the dSPB? Local diffusion of Tem1p to the dSPB may account for the fast phase and a second mechanism may account for the slow phase, perhaps interactions with different binding partners including Bub2p, Cdc15, or other proteins. The two fractions could reflect the nucleotide hydrolysis states of Tem1p during mitotic exit. Alternatively, the two phases may represent interactions with different subsets of proteins at the dSPB, such as Tem1p-Cdc15p

and Tem1p-Bub2p interactions, or transport of Tem1p by different microtubule motor proteins. Although the nature of the biphasic recovery remains unknown, our FRAP measurements demonstrate Tem1p at the dSPB rapidly exchanges with the cytoplasmic protein pool.

Tem1p protein exchange at the dSPB as well as the positional changes in Tem1p-GFP fluorescence intensity during spindle positioning (Figures 2.3 and 2.9) suggest that pulling or pushing forces could result in rapid changes in Tem1p abundance. In wild-type cells, microtubules from the mSPB probe the mother cell cortex rather than forming prolonged attachments that promote force generation (Figure 2.4) (Shaw et al., 1997b). The transient localization of Tem1p-GFP at the mSPB may reflect the lack of microtubule attachments that generate force in the mother cell. A prediction from our data is that there is greater net force on the dSPB during mitosis, especially in anaphase. Similarly, dynein generates a dominant force to move the nucleus through the bud neck (Yeh et al., 1995; Yeh et al., 2000) and Dhc1p is needed to concentrate Tem1p-GFP on the dSPB in late anaphase (Figure 2.10B). This suggests Tem1p localization depends on either microtubule dynamics, transport by microtubule motor proteins, or force generation. Because the plus-end motor Kip2p also decreases Tem1p-GFP at the dSPB, a more general defect in either nuclear migration or microtubule dynamics likely regulate Tem1p abundance at the dSPB. Deletion of *KIP3* results in an increase in Tem1p-GFP on the dSPB. This result could be an indirect effect due to a delay in the cell cycle in *kip3Δ* mutants (Straight et al., 1998), a phenotype we have seen in other mutants delayed in the cell cycle (our unpublished results). How do Dhc1p and Kip2p promote Tem1p abundance at the dSPB? One possibility is that both Dhc1p and Kip2p transport Tem1p in different directions along the microtubules. Alternatively, forces

or tension at the dSPB may be a general mechanism that regulates Tem1p accumulation. However, the molecular mechanism of Tem1p loss from the dSPB in *dhc1Δ* cells requires further study.

After the increased accumulation of Tem1p at dSPB upon penetration of the bud neck, Cdc15p initially accumulated on the dSPB and subsequently localized to both SPBs (Figure 2.5) whereas Bub2p decreased from spindle poles in mid-to-late anaphase (Figure 2.6). Coupling this data with our observations on Tem1p, we can envision a model for mitotic exit that integrates protein dynamics. In wild-type cells with properly positioned preanaphase spindles, Tem1p accumulation is antagonized by Bub2p at the dSPB. Bub2p inhibition prevents Tem1p and Cdc15p accumulation at the dSPB. Factors that promote Tem1p accumulation may include Dhc1p, Lte1p, tension or force, unknown accessory factors, and position relative to the bud. The positional dependence for Tem1p localization to the dSPB may also be due to a gradient of Tem1p in the GTP bound form that is found in the bud. On anaphase onset and dSPB penetration into the bud a switch is activated allowing Cdc15p to accumulate on the dSPB. Because Cdc15p is activated, Bub2p localization to the dSPB is not favored. A feedback loop could exist at this point, where Cdc15p promotes Tem1p accumulation to allow more Cdc15p accumulation at the dSPB, while Cdc15p prevents Bub2p binding to the dSPB. Tem1p and Cdc15p accumulate on the dSPB to signal mitotic exit, whereas Bub2p is either released from the dSPB or has its binding sites at the dSPB filled by the Tem1p-Cdc15p complex. The switch to persistent Tem1p-Cdc15p signaling allows mitotic exit to proceed.

In conclusion, we provide evidence that the accumulation of dynamic Tem1p as spindle poles pass the bud neck and a change in Bub2p distribution correlates with mitotic

exit. The dynamic nature of Tem1p allows it to respond quickly to changes within the cell, making Tem1p an ideal spatial sensor in vivo. The discovery of a protein intimately linked to both spindle positioning and activating mitotic exit will allow dissection of the connections between forces that position structures and cell signaling networks during the cell cycle.

Acknowledgements

Reproduced from *Molecular Biology of the Cell*, (2004, Volume 15, pages 1519 – 1532) by copyright permission of The American Society for Cell Biology. Part of this work was carried out at the W.M. Keck Foundation Imaging Facility at the Whitehead Institute. We are grateful to the Bloom, Salmon, and Pellman laboratories for helpful suggestions and critical evaluations of the manuscript. We thank Dale Beach, Jennifer DeLuca, Benjamin Glick, Ben Moree, John Pringle, Marisa Segal, and Jennifer Stemple for reagents, strains, and advice. J. N. M. thanks members of the Bloom and Salmon laboratories for patiently training him and Vincent Klink, Chia-wei Tsai, and Stephen Wolniak for years of instruction on how to do "good science." This work was supported by National Institutes of Health Grants GM61345-01 (D.P.), GM-24364 (E.D.S.), and GM-32238 (K.B.).

Tables and Figures

Strain name	Relevant Genotype	Source or Reference
L 4852	MAT**a** *ade2-100 leu2-3,-112 his3-l1,-15 trp1-1 ura3-1*	G. Fink[A]
PY 1973	MAT**a** *ade2-100 leu2-3,-112 his3-11,-15 trp1-1 ura3-1 ase1Δ::KAN^r*	Lee et al., 1999
PY 2370	MAT**a** *ade2-100 ade3 leu2-3, -112 his3-1,-15 trp1-1 ura3-1 TUB1::GFP-URA3*	Tirnauer et al., 1999
PY 3446	MAT**a** *ade2-100 leu2-3,-112 his3-11,-15 trp1-1 ura3-1 ase1Δ::KAN^r TUB1::GFP-URA3*	Schuyler et al., 2003
PY 3548	MAT**a** *ade2-100 leu2-3,-112 his3-11,-15 trp1-1 ura3-1 LTE1::3xGFP-URA3*	This Study
YEF 473A	MAT**a** *trp1Δ63 leu2Δ1 ura3-52 his3Δ200 lys2-801*	Bi and Pringle, 1998
KBY 9201	MAT**a** *trp1Δ63 leu2Δ1 ura3-52 his3Δ200 lys2-801 TEM1::GFP-KAN^r*	This Study
KBY 9202	MAT**a** *trp1Δ63 leu2Δ1 ura3-52 his3Δ200 lys2-801 CDC15::GFP-KAN^r*	This Study
KBY 9203	MAT**a** *trp1Δ63 leu2Δ1 ura3-52 his3Δ200 lys2-801 TEM1::GFP-HB^r*	This Study
KBY 9205	MAT**a** *trp1Δ63 leu2Δ1 ura3-52 his3Δ200 lys2-801 kar9Δ::HB^r TEM1::GFP-KAN^r*	This Study
KBY 9208	MAT**a** *trp1Δ63 leu2Δ1 ura3-52 his3Δ200 lys2-801 dhc1Δ::HIS3 TEM1::GFP-KAN^r*	This Study[B]
KBY 9209	MAT**a** *trp1Δ63 leu2Δ1 ura3-52 his3Δ200 lys2-801 SPC29::GFP-KAN^r*	This Study
KBY 9211	MAT**a** *trp1Δ63 leu2Δ1 ura3-52 his3Δ200 lys2-801 kip2Δ::KAN^r TEM1::GFP-HB^r*	This Study
KBY 9212	MAT**a** *trp1Δ63 leu2Δ1 ura3-52 his3Δ200 lys2-801 kip3Δ::KAN^r TEM1::GFP-HB^r*	This Study
KBY 9217	MAT**a** *trp1Δ63 leu2Δ1 ura3-52 his3Δ200 lys2-801 lte1Δ::HB^r TEM1::GFP-KAN^r*	This Study
KBY 9221	MAT**a** *trp1Δ63 leu2Δ1 ura3-52 his3Δ200 lys2-801 BUB2::GFP-KAN^r*	This Study
KBY 9225	MAT**a** *trp1Δ63 leu2Δ1 ura3-52 his3Δ200 lys2-801 bud6Δ::TRP1 TEM1::GFP-KAN^r*	This Study[C]
KBY 9228	MAT**a** *trp1Δ63 leu2Δ1 ura3-52 his3Δ200 lys2-801 CDC15::GFP-KAN^r TUB1::CFP-URA3*	This Study
KBY 9233	MAT**a** *trp1Δ63 leu2Δ1 ura3-52 his3Δ200 lys2-801 dhc1Δ::HIS3 BUB2::GFP-KAN^r*	This Study[B]
KBY 9234	MAT**a** *trp1Δ63 leu2Δ1 ura3-52 his3Δ200 lys2-801 lte1Δ::HB^r BUB2::GFP-KAN^r*	This Study
KBY 9248	MAT**a** *trp1Δ63 leu2Δ1 ura3-52 his3Δ200 lys2-801 ase1Δ::HB^r TEM1::GFP-KAN^r*	This Study

[A]Whitehead Institute, Cambridge, MA.
[B]Parent strain provided by J. Pringle, University of North Carolina, Chapel Hill, NC.
[C]Parent strain provided by D. Beach, University of North Carolina, Chapel Hill, NC.

Table 2.1: *S. cerevisiae* strains used in this chapter.

SPB Measured[A]	Genetic Background	Fluorescence Ratio[B]	p-value
		Spc29p-GFP	
dSPB (PA vs LA)[C]	wild-type	1 : 1.34	$p > 0.05$
mSPB (PA vs LA)	wild-type	1 : 1.03	$p > 0.10$
		Tem1p-GFP	
dSPB (PA vs LA)	wild-type	1 : 2.02	**$p < 10^{-6}$** [D]
mSPB (PA vs LA)	wild-type	1 : 1.41	$p < 0.05$
dSPB	*Δase1*	1.08 : 1	$p > 0.10$
dSPB	*Δlte1*	0.54 : 1	**$p < 10^{-7}$**
dSPB	*Δkar9*	0.76 : 1	$p < 0.02$
dSPB	*Δbud6*	1.00 : 1	$p > 0.10$
dSPB	*Δdhc1*	0.63 : 1	**$p < 10^{-4}$**
dSPB	*Δkip2*	0.72 : 1	$p < 0.02$
dSPB	*Δkip3*	1.43 : 1	**$p < 0.01$**
		Bub2p-GFP	
dSPB (PA vs LA)	wild-type	1.03 : 1	$p > 0.10$
dSPB (PA)	*Δlte1*	1.10 : 1	$p > 0.10$
dSPB (LA)	*Δlte1*	0.88 : 1	$p > 0.10$

[A]Late anaphase spindle pole measured unless noted.
[B]Mutant vs wild-type ratio reported unless indicated otherwise.
[C]PA = preanaphase spindle pole measured; LA = late anaphase spindle pole measured.
[D]Bold type denotes statistically significant difference ($p < 0.01$).

Table 2.2: Summary of fluorescence intensity measurements.

Fluorescence probe measured is in italics. Fluorescence intensity ratio is either the mutant fluorescence intensity divided by wild-type fluorescence intensity of the spindle pole or the dSPB to the mSPB in the background indicated. All statistical calculations were made using Student's two-tailed *t* test.

Probe	k_f	$t_{1/2f}$	f_f[A]	k_s	$t_{1/2s}$	f_s	R[B]
Tem1p-GFP	0.203	4.50	56.5	0.0103	133	43.5	62.1

[A]All fraction of recovery values are given as percentages (f x 100) of the total recovery *R*.
[B]*R* was corrected for the amount of Tem1p-GFP photobleached by the laser pulse (see MATERIALS AND METHODS).

Table 2.3: FRAP of Tem1p-GFP on the anaphase dSPB.

FRAP measurements of Tem1p-GFP. k_f - rate constant for fast or single phase; $t_{1/2f}$ – half recovery time of fast or single phase phase; f_f – recovery of fast phase corrected for the pool of Tem1p-GFP that is present in the cell after photobleaching; k_s – slow phase rate constant; $t_{1/2s}$ – half-recovery time for slow phase; f_s –slow phase of recovery corrected for photobleached Tem1p-GFP; R – total recovery to the photobleached region during the observation period. n = 6 for Tem1p-GFP FRAP measurements. See Maddox et al. (2000) and Materials for details on quantification.

Primer	Sequence
ASE1 5' KO	5'-TCTACTACAGTTATACCGCATATGAACCCTTCTTTAGCAACACCGTTGA CTGTGTCGACCATGGCAGCTGAAGCTTCGTACGC-3' (83mer)
ASE1 3' KO	5'-GAATGTTTAATTGAAATTTACCTTCTGGCGACATGGAAAGTTTATATAT GCTGTGCTCAGGTTCGCATAGGCCACTAGTGGATCTG-3' (86mer)
ASE1 5' CK	5'-GCAAAGATACGAACAAACGG-3' (20mer)
ASE1 3' CK	5'-TCCAGAGTCACGGTGCAATG-3' (20mer)
BUB2 5' GFP	5'- TATGACCTATTGGTAGACCACTTGACCGACCCAGACATATATATACCG GCACGGATCCCCGGGTTAATTAA-3' (71mer)
BUB2 3' GFP	5'- ACACATACAGACATATAAACGTTGTAGAATTAAACGATAAAATATAA GAATTCGAGCTCGTTTAAAC-3' (67mer)
BUB2 5' CK	5'- GCTGGGCGTCGGGTTCATCG-3' (20mer)
CDC15-GFP5'	5'-CCAAAGATAAAAGTGACGGCTTTTCCGTCCCCATTACAACATTTCAAAC AAGTAAAGGAGAAGAACT-3'(67mer)
CDC15-GFP3'	5'-CAGTATTGGAAGGTTCACAATTCTATATATAGTGTTAATGTAATGCTGAT GGCGGCGTTAGTATCG-3'(66mer)
CDC15-CHK5'	5'-GACGACGCAAAGACAGCAGC-3'(20mer)
KAR9-DELUP	5'-CCGCACGAATCTTTGTCTGTAACAGCCTTAAAGATTTCAGTAGCACTGCC GCATAGGCCACTAGTGGATCTG-3'(72mer)
KAR9-DELDN	5'-GGGGTTTTATCTAAACGCCCTTCTCTTGGTGAAAGTAACTGTGATAAGGC AGCTGAAGCTTCGTACGC-3'(68mer)
KIP2-5'	5'-TCAAGGCAAACATAGAACACTTGATAAAATTCTTACCATAATACCACCA TTGCAGCTGAAGCTTCGTACGC-3'(71mer)
KIP2-3'	5'-CAGAACAATCCGCACAAGGAAAAAAGCACCCGAGATCTGGGACCCTCAC CTAAGCATAGGCCACTAGTGGATCTG-3'(75mer)
KIP2UPCHK	5'-TAGGCTGCAGAGTTCA-3'(16mer)
KIP2DNCHK	5'-GCCTTTTATGCGCTGTCT-3'(18mer)
KIP3::KAN5'	5'-CATATTCCCTGATTGCATCGTTTATCTGATTATCATTTCATTGCATTCTTCA GCTGAAGCTTCGTACGC-3' (69mer)
KIP3::KAN3'	5'-GCGTTTAATGCTGGCGGAAAGAAGTTATATTCGATAGTTTACGTAGGATAG CATAGGCCACTAGTGGATCTG-3' (72mer)
KIP3-5'	5'-CTTGGCCAGAGACTTGGGCTG-3'(21mer)
KIP3-3'1	5'-CACTAGAATTACCCATCGTTTCAGG-3'(25mer)
LTE1 5' KO	5'-CCCTGAACCATGGAAATATTTAGCCAGAAAGATTACTACCCGACTCCATCC TCCAGCTGAAGCTTCGTACGC-3' (72mer)
LTE1 3' KO	5'- GGACGCAACCCACCAGTGGATTCACAGAGTTAAGTAGATTTCTTATTGTAG GCATAGGCCACTAGTGGATCTG-3' (73mer)
LTE1 5' CK	5'- GTACTCGTGTTATTCGCTCG-3' (20mer)
LTE1 3' CK	5'- ACATGTATGTATGCTCCATC-3' (20mer)
F-LTE1-3448	5'-GCCTCGAGGACGTGTCAGCTAATGTTG-3'(27mer)
R-LTE1-4503	5'-GCGGATCCGAGGTGGTGGTGGTTGTGGATAGTTCATTAATC-3'(41mer)
TEM1-GFP 5'	5'-AGCCCTCCTCGTCGCCCTCATCTAAGGCACCATCGCCGGGGTTAATACAAG TAAAGGAGAAGAACT-3'(67mer)
TEM1-GFP3'	5'-GATATTGTGGATGTACATACCTTCTATATCTCCTTAAAGCTATTGTGTAGCA TGGCGGCGTTAGTATCG-3'(69mer)
TEM1-CHK5'	5'-GGTGTATGGTGTATGGATG-3'(19mer)
TEM1-CHK3'	5'-GACGACGCAAAGACAGCAGC-3'(20mer)

Table 2.S1: Oligonucleotides used in this chapter.

Strain name[A]	Relevant Genotype	Source or Reference
PY 1746	MAT**a** *ade2-100 leu2-3,-112 his3-11,-15 trp1-1 ura3-1 ase1Δ::URA3*	This Study
PY 3410	MAT**a** *ade2-100 leu2-3,-112 his3-l1,-15 trp1-1 ura3-1 lte1Δ::KAN*^{r}	This Study
PY 3425	MAT**a** *ade2-100 leu2-3,-112 his3-l1,-15 trp1-1 ura3-1 ase1Δ::URA3 lte1Δ::KAN*^{r}	This Study
PY 4113	MAT**a** *ade2-100 leu2-3,-112 his3-11,-15 trp1-1 ura3-1 ase1Δ::URA3 LTE1::3xGFP-URA3*	This Study
KBY 9050	MAT**a** *trp1Δ63 leu2Δ1 ura3-52 his3Δ200 lys2-801 bub2Δ::URA3*	This Study

*Other strains used in supplementary studies listed in Table 2.1.

Table 2.S2: Strains used in supplementary figures for this chapter.

Figure 2.1: Spindle behavior and mitotic exit in wild-type and *ase1Δ* cells.

Time-lapse series of anaphase in haploid wild-type (A and B) and *ase1Δ* mutant (C and D) cells expressing a GFP-Tub1p (Bar, 2μm). (A) An example of an early contact event between the SPB and the distal bud cortex, relative to the mean value of the population, in a wild-type cell. Early spindle pole body-cortical contact (3.0 min, red arrow), septation (21.6 min, yellow arrow), and cell separation (43.7 min) from the time of spindle pole body entry into the bud (0.0 min). (B) An example of a late contact event between the SPB and the distal bud cortex, relative to the mean population value, in a wild-type cell. Late spindle pole body-cortical contact (9.7 min, red arrow), septation (21.8 min, yellow arrow), and cell separation (46.8 min) from the time of spindle pole body entry into the bud (0.0 min). (C) An example of an early contact event in an *ase1Δ* cell. Early spindle pole body-cortical contact (2.9 min, red arrow), septation (24.1 min, yellow arrow), and bud emergence (51.7 min) from the time of spindle pole body entry into the bud (0.0 min). (D) An example of a late contact event in an *ase1Δ* cell. Late spindle pole body-cortical contact (12.3 min, red arrow), septation (24.8 min, yellow arrow), and bud emergence (45.8 min) from the time of spindle pole body entry into the bud (0.0 min).

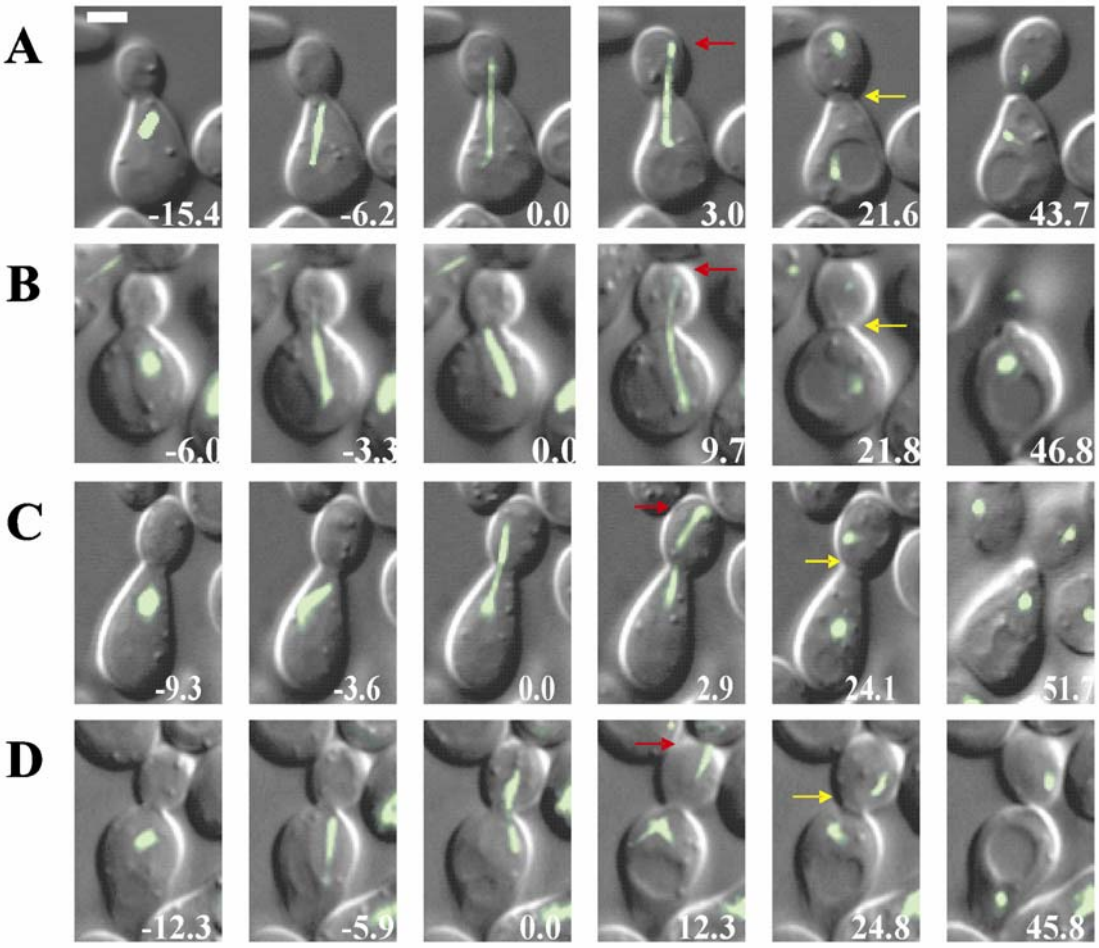
A
-15.4
-6.2
0.0
3.0
21.6
43.7
B
-6.0
-3.3
0.0
9.7
21.8
46.8
C
-9.3
-3.6
0.0
2.9
24.1
51.7
D
-12.3
-5.9
0.0
12.3
24.8
45.8

Figure 2.2: Quantification of mitotic spindle behavior in wild-type and *ase1Δ* cells.

The timing of mitotic exit correlates best with entry of the daughter spindle pole body into the bud and is not affected by premature spindle collapse. The box plots in A to C display the upper and lower quartiles as the boundaries of the box with the horizontal line inside the box denoting the median. The whiskers indicate the boundaries of the outliers which are represented by small circles and were defined by data greater than the quantity (upper quartile + [1.5*inter-quartile distance]) or less than (lower quartile- [1.5*inter-quartile distance]). wt denotes wild-type cells analyzed. n = 56 wt cells and 50 *ase1Δ* cells. (A) The time of spindle pole body entry into the bud to cortical contact is not different in an *ase1Δ* mutant compared to wild-type (p-value = 0.3408 < 0.9500). (B) The time of daughter cell cortical contact to septation is not different in an *ase1Δ* mutant compared to wild-type (p-value = 0.4408 < 0.9500). (C) The timing of spindle pole body entry into the bud to septation is not different in an *ase1Δ* mutant from wild-type (p-value = 0.8773 < 0.9500). (D) There is no correlation between spindle pole body contact with the bud cortex and the timing of the initiation of septation in wild-type cells (slope of 0.086 +/- 0.212; mean +/- SE). (E) There is negative correlation between the timing of spindle pole body contact with the bud cortex and the time between cortical contact and the initiation of septation in wild-type cells (slope of -0.914 +/- 0.212). (F) There is no correlation between the duration of the spindle pole body contact with the bud cortex and the initiation of septation in wild-type cells (slope of 0.000 +/- 0.066). (G) There is no correlation between spindle pole body contact with the bud cortex and the initiation of septation in *ase1Δ* cells (slope of 0.192 +/- 0.219). (H) There is no correlation between the duration of the spindle pole body contact with the bud cortex and the initiation of septation in *ase1Δ* cells (slope of -0.005 +/- 0.093).

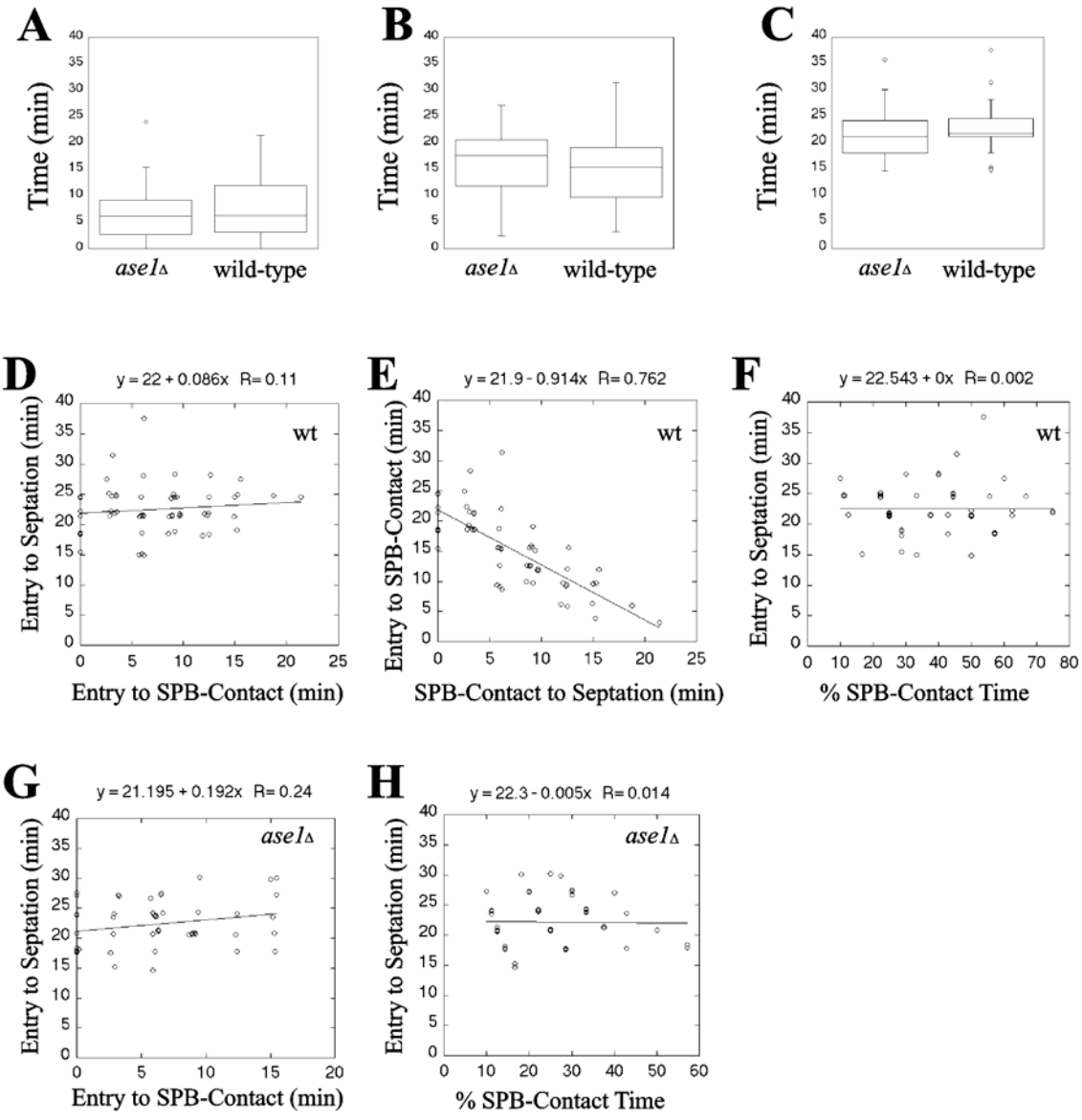
A
Time (min)
ase1Δ
wild-type
B
Time (min)
ase1Δ
wild-type
C
Time (min)
ase1Δ
wild-type
D
y = 22 + 0.086x R= 0.11
wt
Entry to Septation (min)
Entry to SPB-Contact (min)
E
y = 21.9 - 0.914x R= 0.762
wt
Entry to SPB-Contact (min)
SPB-Contact to Septation (min)
F
y = 22.543 + 0x R= 0.002
wt
Entry to Septation (min)
% SPB-Contact Time
G
y = 21.195 + 0.192x R= 0.24
ase1Δ
Entry to Septation (min)
Entry to SPB-Contact (min)
H
y = 22.3 - 0.005x R= 0.014
ase1Δ
Entry to Septation (min)
% SPB-Contact Time

Figure 2.3: Tem1p-GFP localization during spindle positioning and elongation.

Tem1p-GFP accumulates in response to spatial positioning during mitosis (Bar, 5 μm). (A) Cell undergoing spindle rotation before anaphase expressing Tem1p-GFP. Arrow indicates mSPB. (0 min) The mitotic spindle is oriented parallel to the bud neck and one SPB was preferentially labeled with Tem1p-GFP. (5 min) Spindle positioning altered Tem1p-GFP fluorescence intensity. (20 min) As spindle rotation is completed Tem1p-GFP clearly localized preferentially to the dSPB. (B) Tem1p-GFP localization during anaphase elongation of the mitotic spindle. Arrow denotes dSPB. (0 min) Tem1p-GFP labeled the mSPB at an apparent equal intensity to Tem1p-GFP on the dSPB. (14 min) On spindle elongation Tem1p-GFP was dim on the mSPB but intensely labeled the dSPB. (28 min) Tem1p-GFP appeared to increase in fluorescence intensity in late anaphase on the dSPB. (C) Three representative cells expressing Tem1p-GFP in *dhc1Δ* cells with elongated spindles in the mother cell.

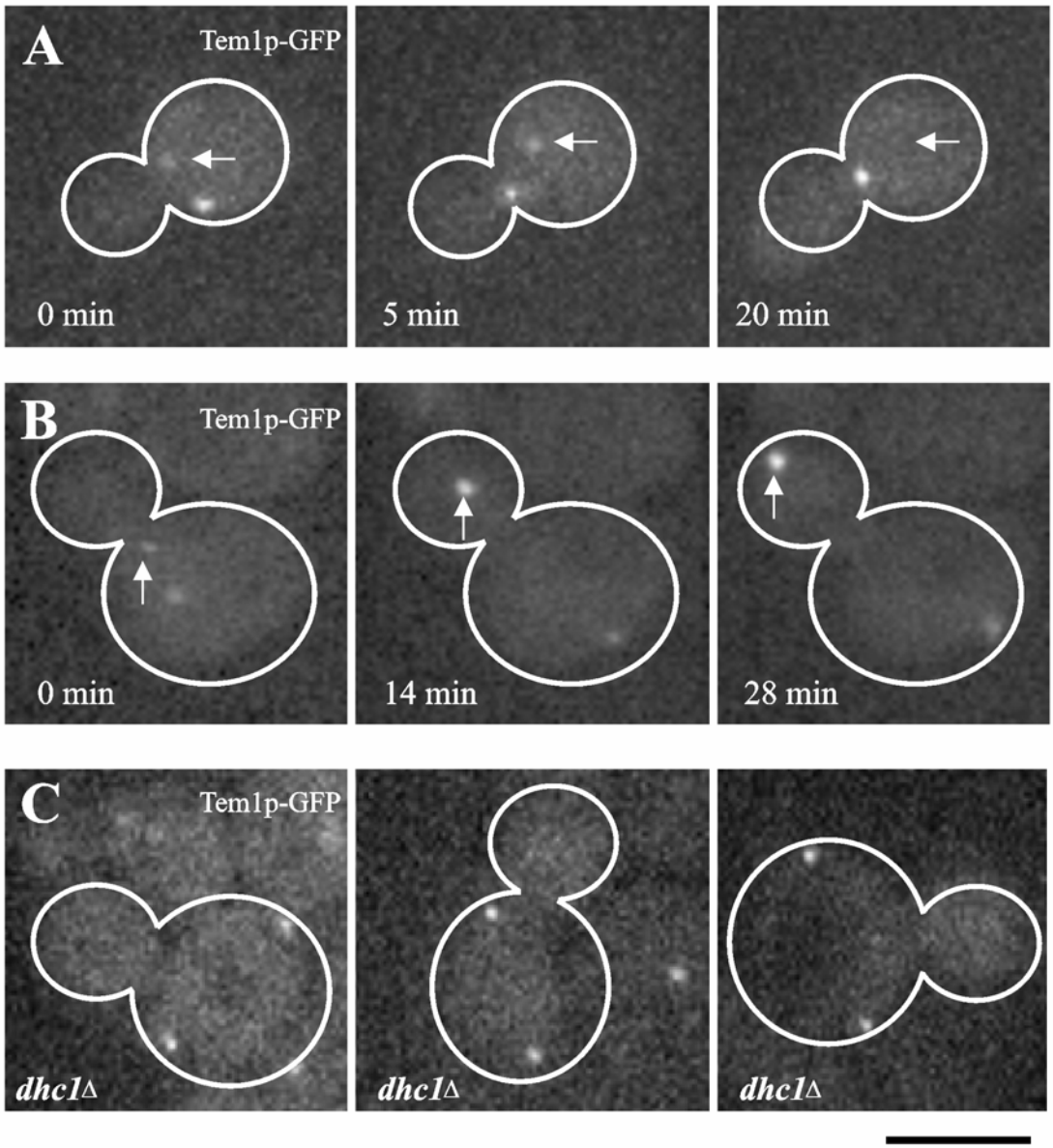
A
Tem1p-GFP
0 min
5 min
20 min
B
Tem1p-GFP
0 min
14 min
28 min
C
Tem1p-GFP
dhc1Δ
dhc1Δ
dhc1Δ

Figure 2.4: Quantification of Tem1p-GFP in living cells.

Fluorescence intensity measurements of Tem1p-GFP. (A) Fluorescence intensity measurements of Tem1p during mitosis. mSPB are overestimated as those cells with no mSPB focus were not accounted for. Error bars indicate SD for each measurement. dSPB (gray columns) n = 38 (preanaphase), 23 (spindle elongation), and 50 (late anaphase). mSPB (white columns) n = 20 (preanaphase), 27 (spindle elongation), and 39 (late anaphase). (B) Average distance and intensity measurements for Tem1p-GFP of nine cells during spindle elongation. Black squares, average relative Tem1p-GFP fluorescence intensity in arbitrary units (AU); gray triangles, average distance from the Tem1p-GFP focus to the center of the bud neck in microns. Spindle lengths based on distance from dSPB to transient mSPBs labeled with Tem1p-GFP: preanaphase, 1.99 μm; 0 – 10 min, 3.47 μm; 12 – 20 min, 5.14 μm; 22 – 30 min, 5.83 μm; and ≥32 min, 6.84 μm.

A

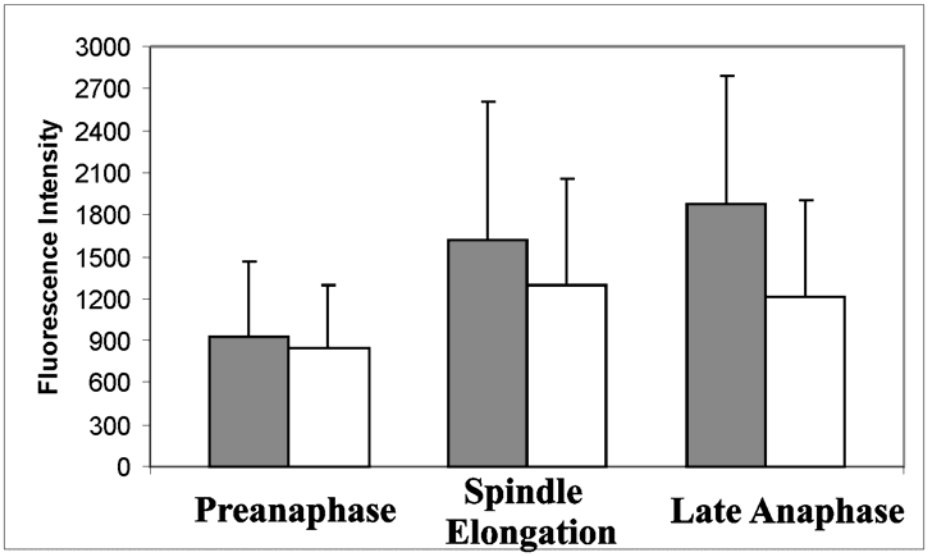
Fluorescence Intensity
3000
2700
2400
2100
1800
1500
1200
900
600
300
0
Preanaphase
Spindle Elongation
Late Anaphase

B

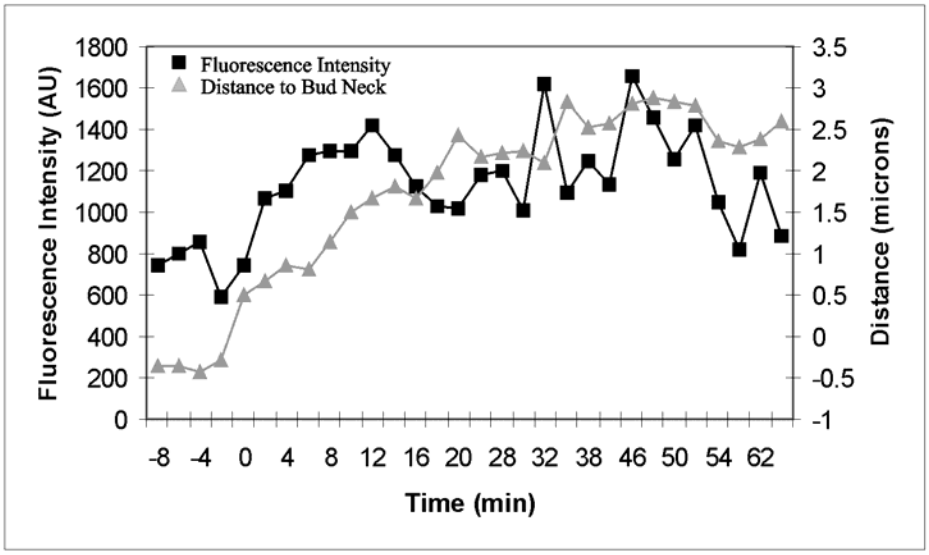
Fluorescence Intensity (AU)
Distance (microns)
Fluorescence Intensity
Distance to Bud Neck
1800
1600
1400
1200
1000
800
600
400
200
0
3.5
3
2.5
2
1.5
1
0.5
0
-0.5
-1
-8 -4 0 4 8 12 16 20 28 32 38 46 50 54 62
Time (min)

Figure 2.5: Cdc15p-GFP localization.

Live cell localization of Cdc15p-GFP during anaphase (Bar, 5μm). (A) Mitotic spindle elongation marked by CFP-Tub1p. The frame before spindle extension, visualized by CFP-Tub1p, was designated as the initial time point in this experiment. Penetration of the bud neck occurred at t = 4 min. (B) Cdc15p-GFP localization during anaphase spindle elongation. (0 min) Cdc15p-GFP does not localize to SPBs. (4 min) On mitotic spindle elongation Cdc15p-GFP accumulates on the dSPB. (16 min, 24 min) Accumulation of Cdc15p-GFP occurred on both SPBs in late anaphase.

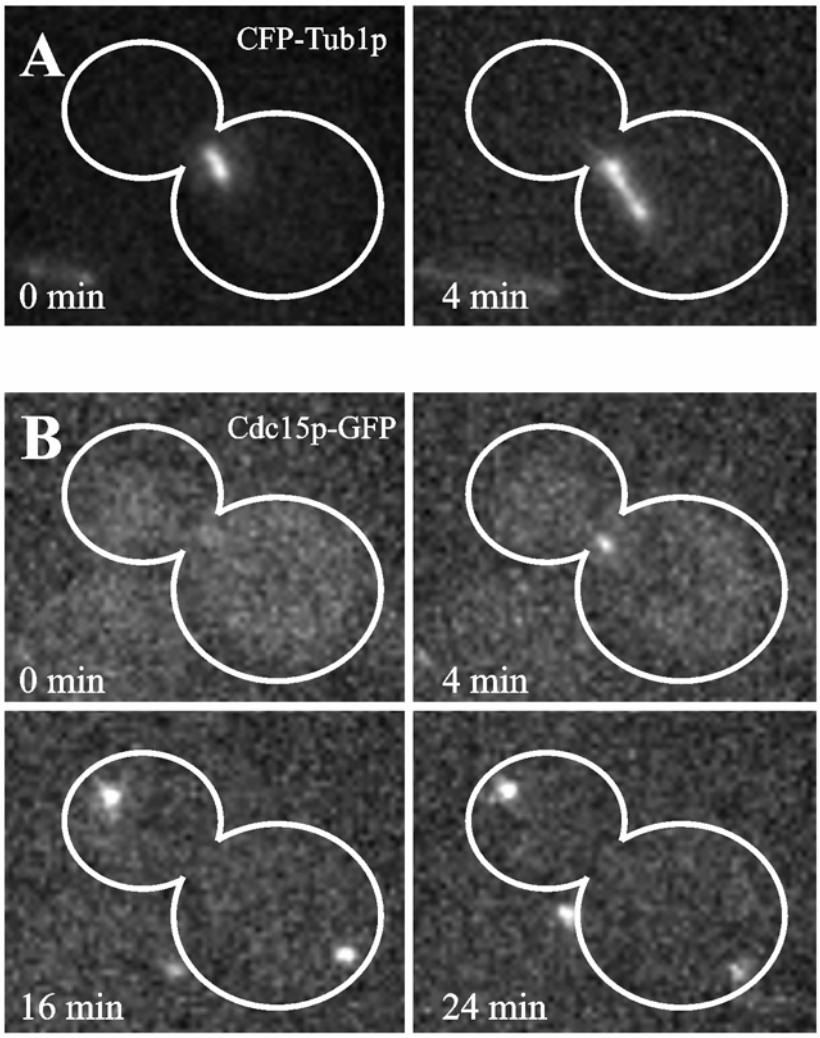
A
CFP-Tub1p
0 min
4 min
B
Cdc15p-GFP
0 min
4 min
16 min
24 min

Figure 2.6: Quantification of Bub2p-GFP fluorescence intensity.

Bub2p-GFP fluorescence intensity analysis. (A) Bub2p-GFP localization in living cells. DIC image is inset to fluorescence image (Bar, 5μm for fluorescence image). (0 min, 2 min) Bub2p-GFP localizes to both SPBs. (11 min, 16 min) Bub2p-GFP increases on the dSPB and is lost from the mSPB. (21 min, 25 min) Bub2p-GFP is lost from the dSPB. (B) Example of Bub2p-GFP fluorescence intensity decrease on the dSPB in midanaphase. Large gray arrow, spindle elongation; black arrow, maximum spindle extension. Black squares, fluorescence intensity in arbitrary units (AU); gray triangles, distance to bud neck in micrometers. (C) Example of Bub2p-GFP fluorescence intensity decrease on the dSPB in late anaphase. Large gray arrow, spindle elongation; black arrow, maximum spindle extension. Black squares, fluorescence intensity in arbitrary units (AU); gray triangles, distance to bud neck in microns. (D) Summary of Tem1p-GFP, Spc29p-GFP, and Bub2p-GFP quantitative measurements. Arbitrary fluorescence intensity scale is derived from the approximate fluorescence intensity of each probe as measured in the previous figures.

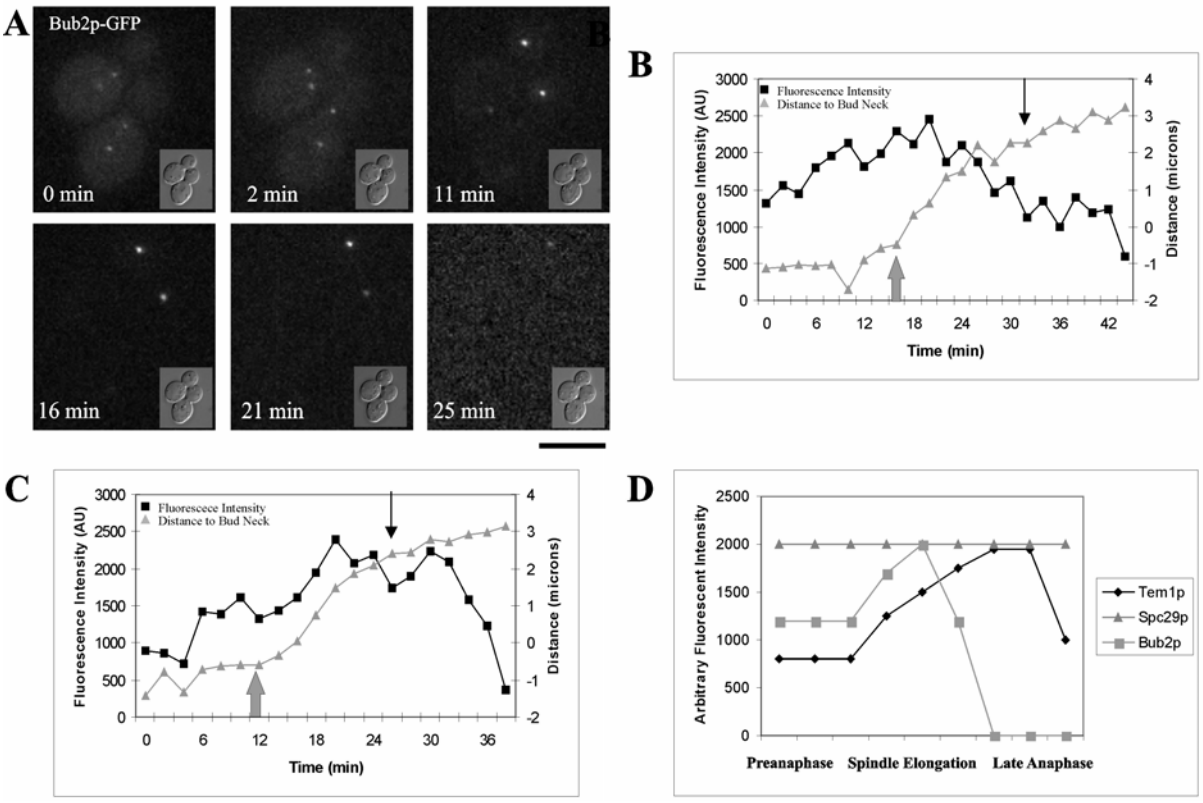
A
Bub2p-GFP
0 min
2 min
11 min
16 min
21 min
25 min
B
Fluorescence Intensity
Distance to Bud Neck
Fluorescence Intensity (AU)
Distance (microns)
Time (min)
C
Fluorescece Intensity
Distance to Bud Neck
Fluorescence Intensity (AU)
Distance (microns)
Time (min)
D
Arbitrary Fluorescent Intensity
Tem1p
Spc29p
Bub2p
Preanaphase
Spindle Elongation
Late Anaphase

Figure 2.7: Lte1p-3xGFP localization.

Native level Lte1p-3xGFP is localized to the daughter cell cortex. (A) An example of a deconvolved cell in two dimensions (Bar, 2μm). (B-D) Projections of the three-dimensional image show that all of the Lte1p-3xGFP is localized to the periphery of the cell next to the cortex and is not associated with any internal structure within the bud.

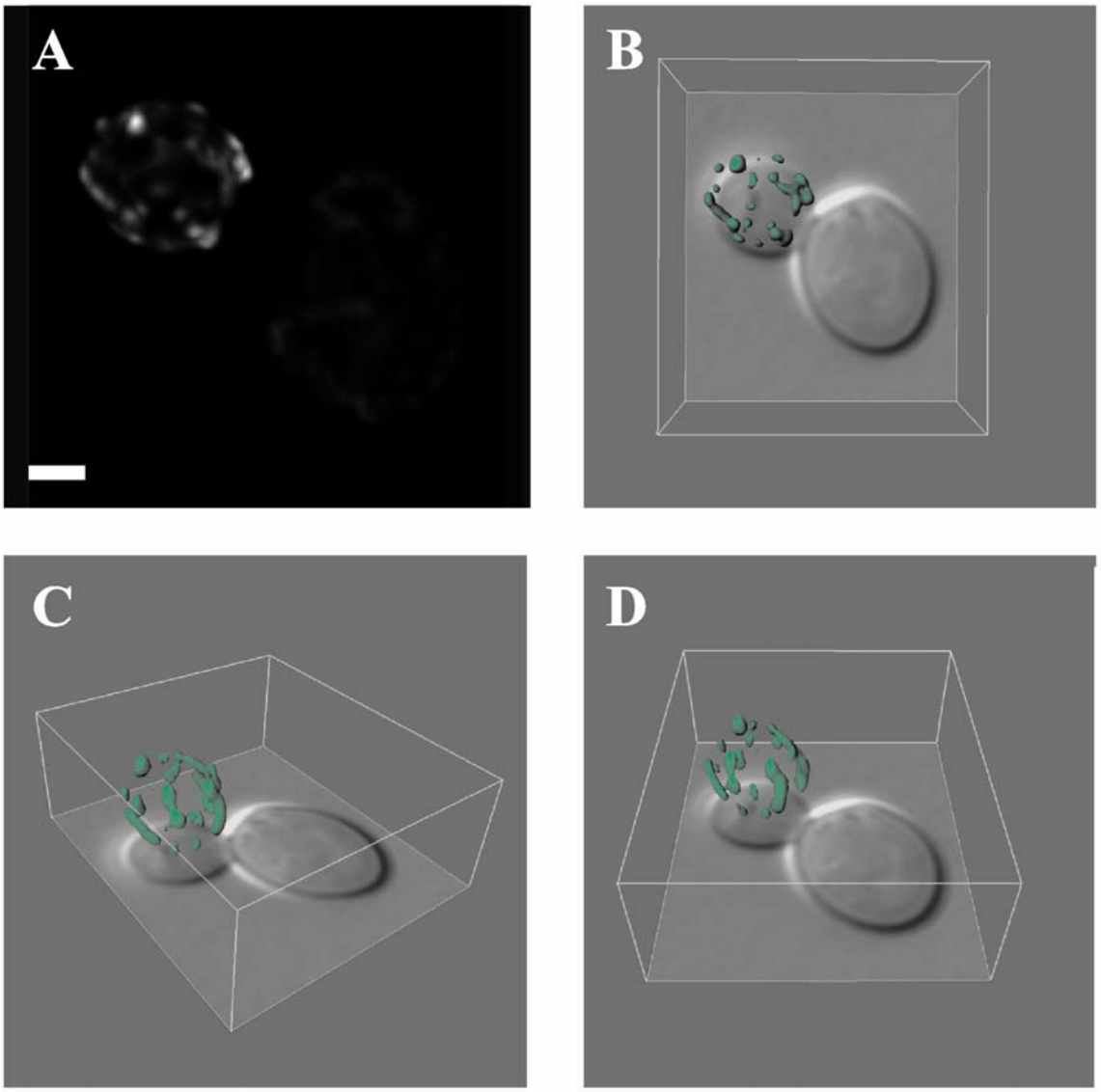
A
B
C
D

Figure 2.8: Tem1p-GFP fluorescence recovery after photobleaching.

FRAP of Tem1p-GFP in late anaphase. Fluorescence intensity is recorded in arbitrary units (AU). (A) Prebleach t = -3 s; time of photobleaching t = 0 s; recovery t = 160 s (Bar, 5 μm). (B) Quantified recovery of fluorescence for the same dSPB photobleached in A. (C) Comparison of experimental data (black squares) with single exponential best-fit data (gray triangles). (D) Comparison of experimental data (black squares) with biphasic exponential best fit data (gray triangles). See MATERIALS AND METHODS for details of analysis.

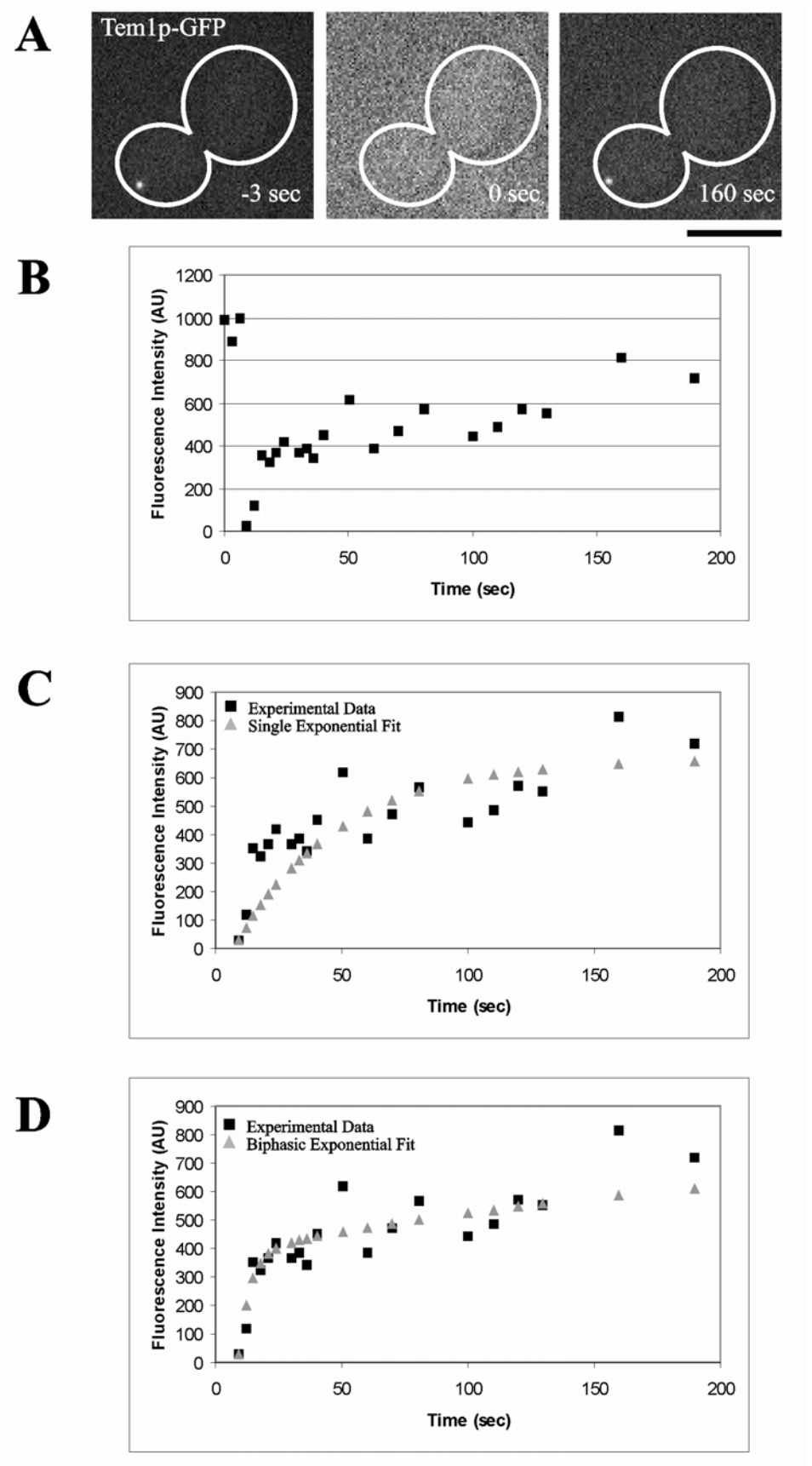
A
Tem1p-GFP
-3 sec
0 sec
160 sec
B
Fluorescence Intensity (AU)
Time (sec)
C
Experimental Data
Single Exponential Fit
Fluorescence Intensity (AU)
Time (sec)
D
Experimental Data
Biphasic Exponential Fit
Fluorescence Intensity (AU)
Time (sec)

Figure 2.9: Tem1p-GFP localization during spindle orientation.

Spindle reorientation results in accumulation of Tem1p-GFP on the SPB that enters the bud in *kar9Δ* mutants. (A) Selected frames from a movie showing changes in Tem1p-GFP fluorescence intensity during active reorientation of mitotic spindle. Arrow denotes SPB that will enter bud (Bar, 5 μm). (B) Quantified changes of Tem1p-GFP fluorescence in arbitrary units (AU; black squares) and distance from the bud neck in microns (gray triangles) for the dSPB in A. (C) Measured changes of Tem1p-GFP fluorescence in arbitrary units (AU; black squares) and distance from the bud neck in microns (gray triangles) for the mSPB from the cell in A. The line gap in distance data points correlates with images where no mSPB signal was detected; in these cases the fluorescence intensity was recorded as zero.

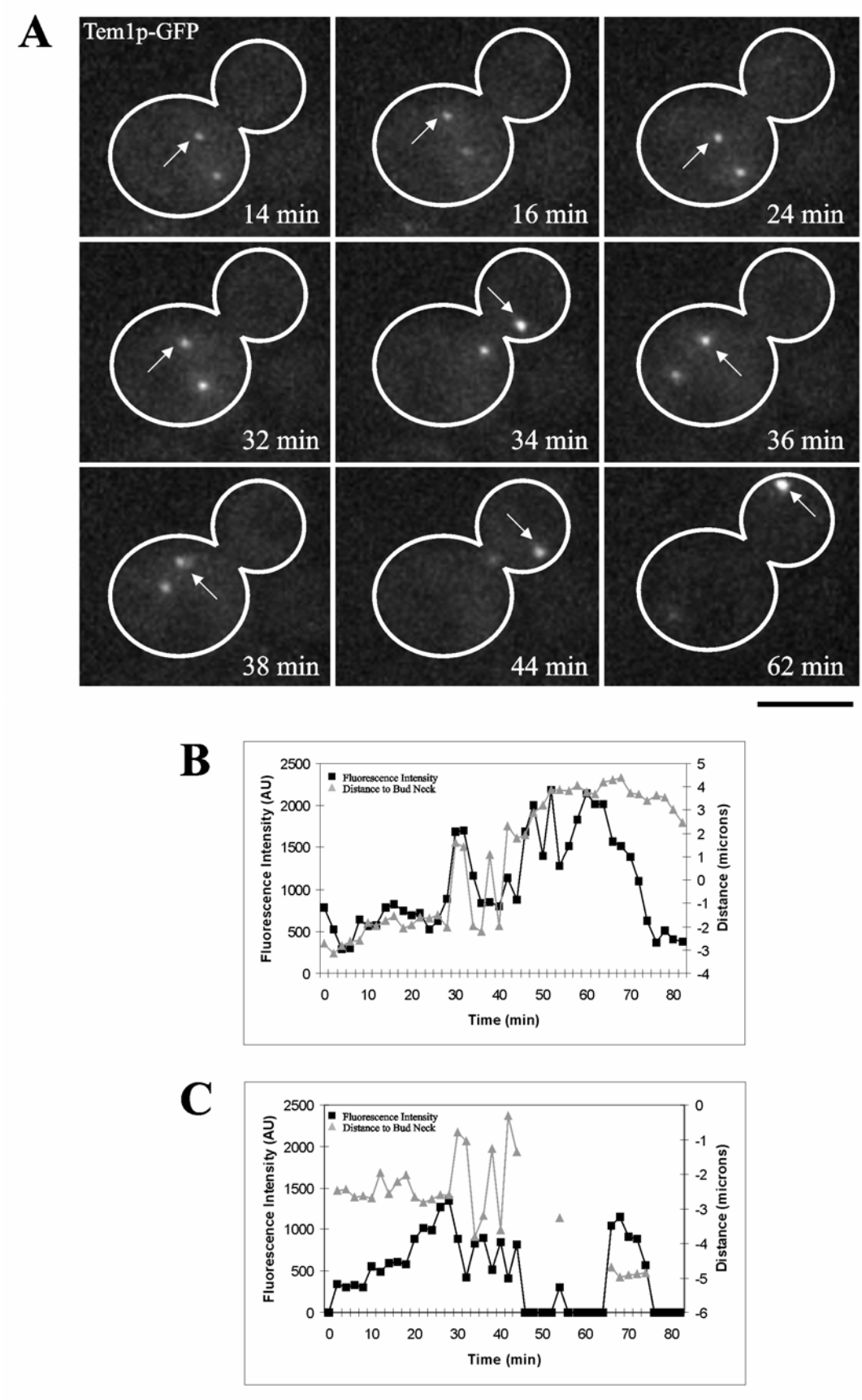
A
Tem1p-GFP
14 min
16 min
24 min
32 min
34 min
36 min
38 min
44 min
62 min
B
Fluorescence Intensity
Distance to Bud Neck
Fluorescence Intensity (AU)
Distance (microns)
Time (min)
C
Fluorescence Intensity
Distance to Bud Neck
Fluorescence Intensity (AU)
Distance (microns)
Time (min)

Figure 2.10: Tem1p-GFP fluorescence intensity in late anaphase.

Fluorescence ratio of Tem1p-GFP accumulation on the dSPB in late anaphase cells. (A) The fluorescence intensity on the dSPB of Tem1p-GFP in *ase1Δ* or *lte1Δ* mutants was divided by the fluorescence intensity of wild-type Tem1p-GFP in late anaphase to generate a fluorescence intensity ratio. Gray bar indicate non-significant differences from wild type; black bar indicates significant difference from wild-type. At least 25 individual cells were measured and averaged for each strain. (B) Tem1p-GFP fluorescence intensity ratio in spindle orientation factors and microtubule motor mutant cells. Gray bars indicate nonsignificant deviation from wild-type fluorescence intensity and black bars denote significant changes from wild-type fluorescence intensity. At least 25 individual cells were measured and averaged for each strain.

A

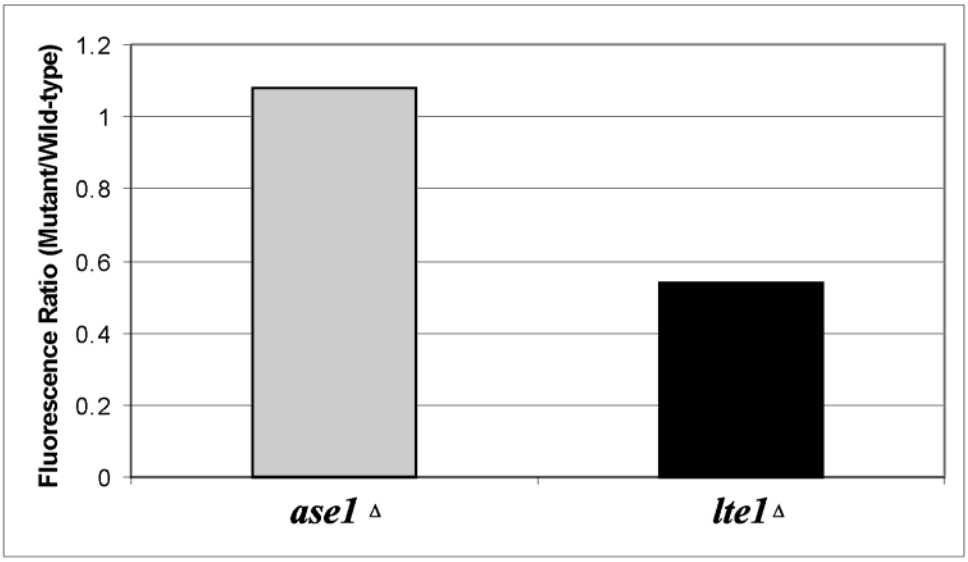
Fluorescence Ratio (Mutant/Wild-type)
1.2
1
0.8
0.6
0.4
0.2
0
ase1Δ
lte1Δ

B

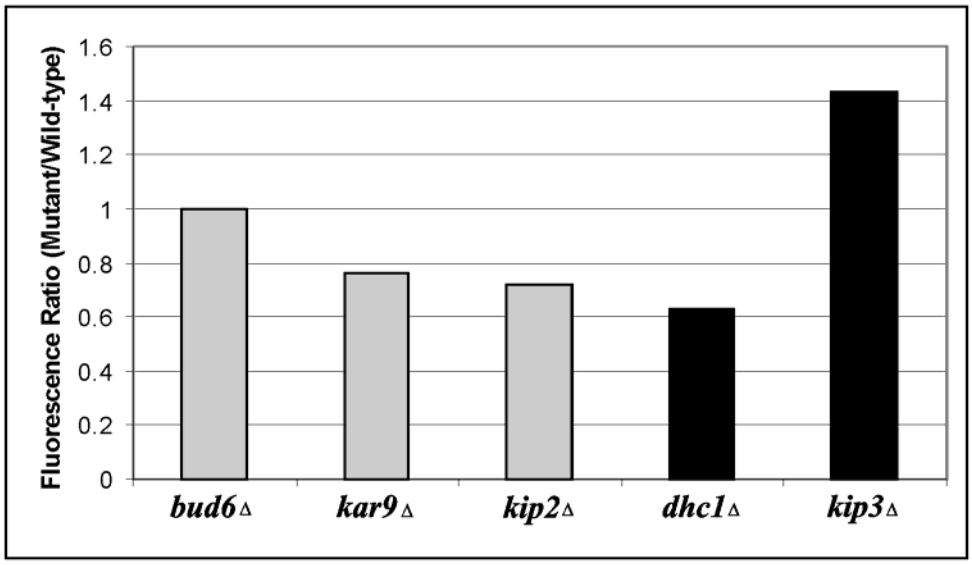
Fluorescence Ratio (Mutant/Wild-type)
1.6
1.4
1.2
1
0.8
0.6
0.4
0.2
0
bud6Δ
kar9Δ
kip2Δ
dhc1Δ
kip3Δ

Figure 2.S1: Lte1p-3xGFP function *in vivo*.

The Lte1p-3xGFP construct is functional. (A) Lte1p-3xGFP growth is similar to wild-type at 14°C, 30°C, and 37°C. *lte1Δ* cells are cold-sensitive and have a mild temperature sensitive phenotype. (B) Lte1p-3xGFP complements the *lte1Δ ase1Δ* synthetic lethality at 37°C.

A

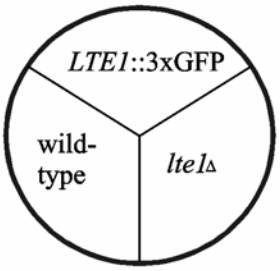

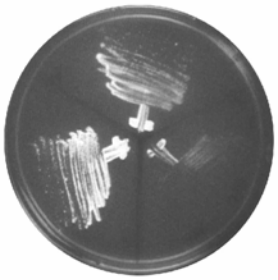

14 degrees

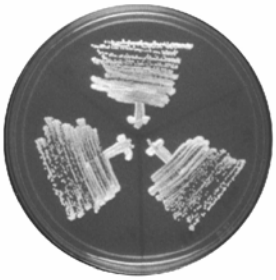

30 degrees

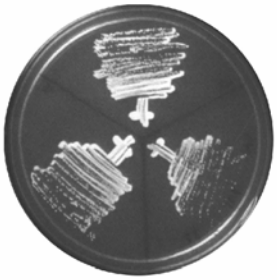

37 degrees

B

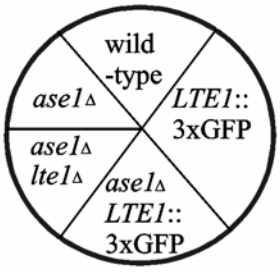

30 degrees

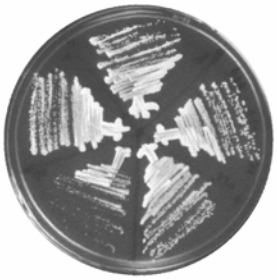

37 degrees

Figure 2.S2: Functional assessment of strains expressing MEN-GFP fusion proteins.

Strains expressing MEN fusion proteins are not growth compromised. (A) Growth curve for wild-type (YEF 473A), *bub2Δ* (KBY 9050), Tem1p-GFP (KBY 9201), Cdc15p-GFP (KBY 9202), Bub2p-GFP (KBY 9221). OD readings were taken at 660 nm every 90 minutes. *tem1* or *cdc15* mutants arrest as large budded cells predicting growth will not match wild-type if function is compromised. (B) Benomyl sensitivity for strains listed in A. Cells were maintained at 32°C for two days. If the spindle position checkpoint is compromised growth is inhibited on benomyl as seen for *bub2Δ* (KBY 9050).

A

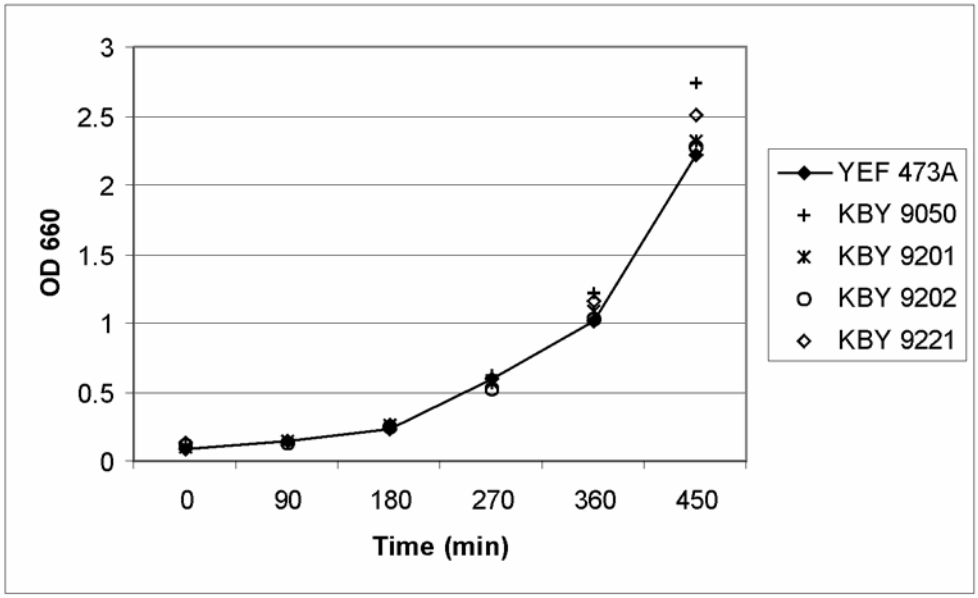
OD 660
3
2.5
2
1.5
1
0.5
0
0
90
180
270
360
450
Time (min)
YEF 473A
KBY 9050
KBY 9201
KBY 9202
KBY 9221

B

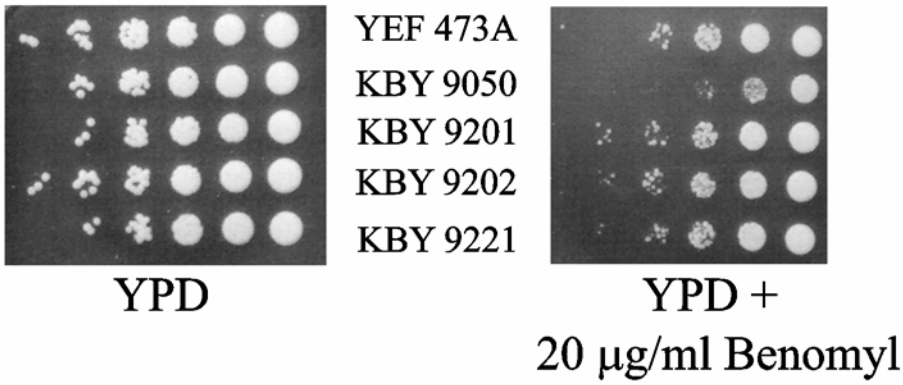
YEF 473A
KBY 9050
KBY 9201
KBY 9202
KBY 9221
YPD
YPD +
20 μg/ml Benomyl

CHAPTER 3: NUCLEAR CONGRESSION IS DRIVEN BY MICROTUBULE PLUS-END INTERACTIONS IN *S. cerevisiae*

Contributing Authors: Jeffrey N. Molk, E. D. Salmon, Kerry Bloom

Abstract

Nuclear movement before karyogamy in eukaryotes is known as pronuclear migration or nuclear congression in *Saccharomyces cerevisiae*. In this study, *S. cerevisiae* is used as a model system to study microtubule (MT)-dependent nuclear movements during mating. We find that nuclear congression occurs through the interaction of MT plus ends rather than sliding and extensive microtubule overlap. Furthermore, the orientation and attachment of MTs to the shmoo tip before cell wall breakdown is not required for nuclear congression. The microtubule plus end-binding proteins Kar3p, a class 14 COOH-terminal kinesin, and Bik1p, the CLIP-170 ortholog, localize to plus ends in the shmoo tip and initiate MT interactions and depolymerization after cell wall breakdown. These data support a model in which nuclear congression in budding yeast occurs by plus end MT capture and depolymerization, generating forces sufficient to move the nuclei through the cytoplasm. This is the first evidence that MT plus end interactions from oppositely oriented organizing centers can provide the force for organelle transport in vivo.

Introduction

Little is known about how microtubules (MTs) overlap and function in living cells to promote haploid nuclear fusion, or karyogamy. The budding yeast *Saccharomyces cerevisiae* provides a genetic model system to study nuclear congression, the process in which haploid nuclei are moved towards each other (Rose, 1996). MTs are nucleated from the spindle pole body (SPB), and plus ends elongate into the cytoplasm (Figure 3.1A) (Lin et al., 2001; Maddox et al., 2003b; Tirnauer et al., 1999). A MT plus end protein complex is formed to orient the nucleus and maintain the attachment of dynamic MT plus ends to the shmoo tip (Figure 3.1B) (Maddox et al., 1999; Maddox et al., 2003b; Miller and Rose, 1998). Attached MT plus ends switch between polymerization and depolymerization phases of dynamic instability, producing nuclear oscillations toward and away from the shmoo tip (Maddox et al., 1999). At the onset of cell fusion, MT plus ends from oppositely oriented mating cells are in proximity to one another (Figure 3.1C), ultimately facilitating MT-MT interactions. Nuclear oscillations cease after MT interactions are established and MTs switch into a persistent depolymerization state during nuclear congression (Maddox et al., 1999). Once MTs have drawn both nuclei into proximity, karyogamy can begin.

A number of proteins bind MT plus ends and are required for karyogamy. The minus end-directed MT motor protein Kar3p concentrates at plus ends and is required to maintain depolymerizing MTs at the shmoo tip in addition to functioning in nuclear congression (Maddox et al., 2003b; Meluh and Rose, 1990). Nuclear translocation and orientation to the shmoo tip before cell fusion are actin dependent. Kar9p associates with the MT plus end-binding protein Bim1p, the budding yeast EB1 homolog, and the type V myosin Myo2p to link MTs to the polarized actin cytoskeleton (Hwang et al., 2003). Bik1p, the human CLIP-

170 orthologue, binds MT plus ends to stabilize MT length and is critical for karyogamy (Berlin et al., 1990; Lin et al., 2001; Pellman et al., 1995). Both Bik1p and Kar9p are transported to the MT plus end by the kinesin-like protein Kip2p, but no role for Kip2p in karyogamy has been described (Carvalho et al., 2004; Maekawa et al., 2003; Miller et al., 1998).

The main hypothesis for nuclear congression in living cells is a "sliding cross-bridge" mechanism in which, after cell fusion, MTs from opposite SPBs are thought to elongate past each other, producing a bundle of overlapping MTs of opposite orientation (Figure 3.1D) (Rose, 1996). Kar3p, through its minus end-directed motility, is thought to cross-link the overlapping MTs and pull the SPBs together (Endow et al., 1994; Meluh and Rose, 1990; Polaina and Conde, 1982). In addition to sliding, the MTs are proposed to shorten as the SPBs come together. An unexplained puzzle in the sliding cross-bridge model is what coordinates MT depolymerization with sliding, because MT shortening occurs as the two SPBs and attached nuclei come together. The sliding cross-bridge model proposes that Kar3p depolymerizes MTs from the minus end at the spindle poles, although this was based on early in vitro studies (Endow et al., 1994; Rose, 1996). Thus far, fluorescent marks on MTs indicate that both polymerization and depolymerization occur solely at the plus ends (Maddox et al., 1999; Maddox et al., 2000; Tanaka et al., 2005). Additionally, a recent in vitro study demonstrated that Kar3p is a plus end MT depolymerase (Sproul et al., 2005). These data suggest proteins at the plus ends regulate polymerization and depolymerization and could both tether dynamic plus ends to the shmoo tip and perform nuclear congression. In the sliding cross-bridge model, plus ends should be found near the SPBs during nuclear congression.

An alternative model for nuclear congression arises from the proximity of plus end-binding proteins on MTs at the shmoo tip before cell fusion (Figure 3.1E). In the plus end model, linkage of MTs from opposite SPBs occurs when plus end complexes interact. MT depolymerization would provide the force to pull the nuclei together. This model predicts that plus end complexes remain concentrated at the site where MTs from oppositely oriented SPBs contacted each other after cell fusion.

To determine by what mechanism nuclear congression occurs, MTs and plus end-binding proteins were analyzed in living *S. cerevisiae* cells. Before nuclear congression, Kar3p, Bik1p, and Kip2p were required for the anchorage of MT plus ends to the shmoo tip. After cell fusion, MT plus ends interacted stochastically to drive nuclear congression. Bik1p and Kar3p localized to oppositely oriented MT plus ends that interacted near the site of cell fusion in wild-type cells. As nuclear congression occurred, the position of the plus ends were unchanged as SPBs moved inward. By analyzing karyogamy mutants, our data suggested that Kar3p was required to initiate MT plus end interactions, whereas Bik1p promoted persistent MT interactions during nuclear congression. Kar9p contributed to the fidelity of nuclear congression by guiding plus ends toward each other. These data support a model in which oppositely oriented MTs interact and depolymerize at their plus ends to draw opposing nuclei together in *S. cerevisiae*.

Materials and Methods

Media and strain construction

Media composition and genetic techniques are described elsewhere (Rose and Broach, 1990). Geneticin (Invitrogen) or hygromycin B (CellGro) were used at a concentration of 300 μg/mL. α-factor (Sigma-Aldrich) resuspended in distilled water was used at a final concentration of 8 μg/mL. 5-Fluoroorotic Acid (Toronto Research Chemicals) was used at a concentration of 1 g/L.

S. cerevisiae strains and plasmids used in this study are listed in Table 3.1. *kar3Δ* strains and the Bik1p-3xGFP plasmid were provided by D. Dawson (Tufts University, Boston, MA) and D. Pellman (Dana Farber Cancer Center, Boston, MA), respectively. Deletion of genes was performed using the pFA6::MX vectors (Longtine et al., 1998; Wach et al., 1994). GFP-Tub1p (Straight et al., 1997) and CFP-Tub1p (provided by M. Segal, University of Cambridge, Cambridge, UK) was linearized with *StuI* before transformation, whereas Bik1p-3xGFP was linearized with *NsiI* before integration (Carvalho et al., 2004).

Pheromone and mating assay growth conditions

Cells were grown to early to midexponential phase in YPD (yeast extract/peptone/glucose) or appropriate selective media at 32°C except for *kar3Δ* strains, which were grown at 25°C. All subsequent manipulations were performed at 32°C. For pheromone treatment, MATa cells were collected by centrifugation and resuspended in YPD supplemented with α-factor. Cells were incubated for 90-120 min, collected, and resuspended in distilled water before imaging.

For mating assays, MATa and MATα cells were grown to early to midexponential phase in YPD or the appropriate selective media. 500 μL of cells from each mating type were mixed, transferred into a 1-ml syringe, and collected on a 13-mm, 0.45-μm membrane (Millipore). The membrane was placed on a 60 x 15 mm YPD plate with the collected cells facing up for 60-120 min. Cells were resuspended by placing the filter paper into 500 μL of distilled water, vortexed to release the cells from the membrane, collected by centrifugation, and resuspended in distilled water before imaging. Cells were imaged on yeast complete media slabs supplemented with 25% gelatin. If cells were arrested with mating pheromone, the slabs were supplemented with 20 μg/mL α-factor.

Image acquisition and data analysis

All images were acquired using spinning disk confocal microscopy as previously described (Maddox et al., 2003a) except where noted. Wide-field images were acquired with a 100x NA 1.4 differential interference contrast objective on an upright microscope (Eclipse E-600; Nikon) or an inverted microscope (TE-2000; Nikon). Image acquisition was performed as previously described (Chapter 2). The epi-fluorescence exposure time (2 x 2 binning) was 300-400 ms, whereas the differential interference contrast exposure time was 100-250 ms. Five-plane Z-series of 0.50-μm steps were acquired every 7-120 s and compiled into a single maximum projection image for each time point.

Imaging processing and fluorescence intensity measurements were performed in MetaMorph software (Universal Imaging Corp.) as previously described (Chapter 2). γ adjustments for image presentation were performed in MetaMorph after data analysis was completed, and any brightness or contrast adjustments were performed in CorelDRAW 10

(Corel Co.). Nuclear orientation to the shmoo tip was scored as wild-type if the GFP-Tub1p-marked SPB was either within or near the base of the mating projection. Aberrant nuclear orientation was recorded when the SPB was in the half of the cell body distal from the shmoo tip. The amount of time GFP-Tub1p fluorescence extended from the SPB to the shmoo tip during time-lapse imaging was recorded as the degree of persistence. Images were calibrated before analysis, and distances were recorded from projections of compiled 5-plane Z-series using either the single line tool or the calipers tool in MetaMorph to a linked Microsoft Excel spreadsheet. Nuclear congression was scored as defective if SPBs were visibly separated in the fluorescence image >0.5 μm after cell fusion occurred in still images. Successful nuclear congression in living cells was noted when both SPBs migrated toward each other and associated persistently. Rarely, time-lapse videos did not record SPB fusion and bud formation, possibly introducing a slight overestimate in the percentage of successful nuclear congression.

Results

Kar3p and Bik1p are required for coupling dynamic MTs to the shmoo tip

Kar9p, Bik1p, and Kar3p are required for karyogamy after cell fusion (Berlin et al., 1990; Kurihara et al., 1994; Meluh and Rose, 1990). *kar3Δ* mutants have the most severe nuclear congression defect, followed by *bik1Δ* and *kar9Δ* cells (Figure 3.2). To test whether defective nuclear congression was preceded by a defect in nuclear orientation to the shmoo tip, GFP-Tub1p marked SPBs and MTs were examined. In wild-type cells, nuclear orientation occurred when the SPB was inside or near the base of the shmoo tip (Figure 3.3A and Table 3.S1). As expected, *kar9Δ* cells had a nuclear orientation defect (Miller and Rose, 1998), and the SPB was positioned in the cell body distal to the shmoo tip (Table 3.S1). However, nuclear orientation to the shmoo tip occurred in the absence of Bik1p and Kar3p (Figure 3.3 and Table 3.S1). Additionally, Kip2p was not required for nuclear orientation (Figure 3.3 and Table 3.S1). Therefore, the nuclear congression defects characterized for *kar3Δ* and *bik1Δ* mutants do not result from a general defect in nuclear orientation.

After nuclear orientation in wild-type cells, MTs remain attached to the shmoo tip (Maddox et al., 1999). The persistence of MT plus end attachment at the shmoo tip was measured by the percentage of time that continuous GFP-Tub1p fluorescence extended from the SPB to the shmoo tip in time-lapse records. In wild-type cells, the degree of persistence was 100%, indicating that the attachment of one or more MTs was continuously maintained at the shmoo tip (Figure 3.3A and Table 3.S1). The attachment was not persistent in *kar3Δ* cells when MTs switched to depolymerization (Figure 3.3B and Table 3.S1) (Maddox et al., 2003b; Miller and Rose, 1998). Similarly, the degree of persistence was reduced in *bik1Δ* and *kip2Δ* mutants (Figure 3.3C, 3.3D, and Table 3.S1). In these cells, detachment occurred

when MTs switched to depolymerization. Therefore, like Kar3p, Bik1p is required to maintain depolymerizing MT plus ends at the shmoo tip.

During mitosis, Bik1p localizes to both growing and shortening MT plus ends in the cytoplasm (Carvalho et al., 2004). In pheromone-treated cells, Bik1p-3xGFP localized predominately to MT plus ends in the shmoo tip and marked growing and shortening MT plus ends (Figure 3.4). The incorporation of new plus ends into the shmoo tip bundle could increase the fluorescence intensity over time (Figures 3.4B and 3.4C). Bik1p-3xGFP fluorescence intensity at the shmoo tip accumulated when the distance from the SPB to the shmoo tip decreased (Figure 3.4B). Conversely, the fluorescence intensity diminished when the SPB-shmoo tip distance increased (Figure 3.4C). This suggests that Bik1p may anchor shortening MT plus ends to the shmoo tip similarly to Kar3p (Maddox et al., 2003b).

Nuclear congression occurs when MT plus ends interact

A critical difference between the sliding cross-bridge and plus end models is the position of MT plus ends during nuclear congression. To determine the distribution of MT plus ends, we examined Bik1p-3xGFP or Kar3p-GFP during nuclear congression. In 82% of cells, these proteins localized as a focus in between both SPBs before and during nuclear congression (n = 23/28 cells). Using Bik1p-3xGFP to label plus ends, we acquired single plane images at 1-s intervals. Before nuclear congression, MT plus ends concentrated at the shmoo tips, and newly nucleated MTs could elongate and become incorporated into the shmoo tip bundle. Once shortening was activated, SPBs moved in toward the position of the initial plus end interactions (Figure 3.5A). The two sets of plus ends joined into a single Bik1p-3xGFP focus that persisted after nuclear congression began (Figure 3.5A, 286-391 s;

arrows). SPBs moved in toward the Bik1p-3xGFP focus at 1.08 +/- 0.72 μm/min (n = 6 cells), and nuclear congression could be completed in as little as 2 min. During nuclear congression, newly nucleated MTs could incorporate into or be released from the Bik1p-3xGFP focus but were not seen to cross over toward the other SPB. Kymographs demonstrated that the two SPBs moved in toward the site of plus end interactions during nuclear congression (n = 5 cells; Figure 3.5A, bottom).

To ensure Bik1p-3xGFP was labeling MT ends during nuclear congression, we mated GFP-Tub1p expressing cells with Bik1p-3xGFP cells (Figure 3.5B) and imaged them in three dimensions over time. A single Bik1p-3xGFP focus was observed at the site of MT tip interaction (Figure 3.5B, 30-90 s; arrows). Occasional spreading of the Bik1p-3xGFP signal from a distinct focus to a more diffuse localization along the MT was visible at later time points (Figure 3.5B, 117.5-167.5 s). The position of the Bik1p-3xGFP focus did not significantly change as SPBs moved inward (Figure 3.5B, bottom). Kar3p-GFP also localized as a single focus between the two SPBs in mating cells (Figure 3.S1). Thus, during nuclear congression, MT plus ends from opposing SPBs interact, and depolymerization drives the SPBs together for nuclear fusion.

If the plus end depolymerization model is the predominant mechanism for nuclear congression, then the zone of MT overlap should be small or undetectable (Figure 3.6A). Linescans of GFP-Tub1p during nuclear congression showed two peaks of fluorescence that corresponded to the SPBs with no detectable overlap zone (Figure 3.6B, left panels). Additionally, measurements of the fluorescence intensity before and during nuclear congression were analyzed (Figure 3.6C). If MTs slide past each other before nuclear congression, the fluorescence should be additive. However, after MT plus end interactions

occurred (Figure 3.6C, graph; arrow), the GFP-Tub1p fluorescence did not increase as SPBs moved inward (Figure 3.6C, graph).

As a positive control, MT overlap in the central spindle during anaphase of mitosis was analyzed. Line scans of the central spindle displayed three peaks: two representing SPBs (Figure 3.6B, graphs; arrows) and one at the midzone (Figure 3.6B, right panels). This demonstrates that overlap between one to two MTs (O'Toole et al., 1999) can be detected. The lack of MT overlap and the localization of Bik1p and Kar3p to a single focus indicate that plus end linkages are the predominant anchorage mechanism for nuclear congression.

Nuclear congression does not require prior nuclear orientation

The karyogamy defect in the nuclear orientation mutant *kar9Δ* is not as severe as other karyogamy mutants (Figure 3.2). One possible explanation is that in the absence of nuclear orientation, oppositely oriented MT plus ends use a stochastic search-and-capture mechanism to interact and promote nuclear congression. To test this hypothesis, *kar9Δ* cells with separated SPBs were examined following cell fusion (Figure 3.7). MTs were seen to grow and shrink in the cytoplasm (Figure 3.7, 3-7 min) and lateral MT interactions, which were visible in the same focal plane, did not move SPBs together (Figure 3.7, 7.5-13 min). In contrast, nuclear congression did occur when MT tips contacted each other (Figure 3.7, 17-18.5 min; n = 5/6 cells). Therefore, MT plus end interactions, but not orientation to the shmoo tip, are required for nuclear congression in *kar9Δ* cells.

Bik1p is required for persistent MT interactions during nuclear congression

Bik1p is required for the formation or stability of MTs in mating cells (Berlin et al., 1990) and is delivered to MT plus ends by Kip2p. Bik1p-3xGFP localized predominantly to the SPB in *kip2Δ* cells with diminished localization at presumptive MT plus ends (n = 117/118 cells; Figure 3.8A). The low level of Bik1p-3xGFP at plus ends in *kip2Δ* cells is not sufficient to promote persistent attachment of MTs to the shmoo tip (Table 3.S1). However, despite the shorter length of MTs, there is no mating defect in *kip2Δ* cells (Table 3.S2) (Miller et al., 1998). Thus, MT length is not the critical parameter for nuclear congression, and reduced levels of Bik1p on the plus ends appear sufficient to support karyogamy but not persistent attachment.

To ensure the delivery of Bik1p to the plus-end was specific to Kip2p, *kar3Δ* cells were also examined. Bik1p-3xGFP labeled both polymerizing and depolymerizing MT plus ends in the shmoo tip as well as the SPB of *kar3Δ* cells (Figure 3.8A), suggesting that the shmoo tip attachment and karyogamy defects observed in *kar3Δ* cells do not result from Bik1p mislocalization.

If MT length is not a critical factor governing nuclear congression, Bik1p could be required to promote persistent interactions between MTs. Alternatively, Bik1p could be a factor that directly links plus ends to promote nuclear congression. In *bik1Δ* mutants expressing GFP-Tub1p, MTs were short and rapidly depolymerized back to the SPBs, limiting the ability of oppositely oriented MTs to interact (Figure 3.S2). This phenotype resulted in a large fraction of cells (10/13 cells) that did not perform nuclear congression. In those cells where nuclear congression did occur, MTs appeared to interact without rapidly shortening back to the SPBs (Figure 3.8B). Despite the instability of MT interactions in

bik1Δ cells, the MTs could remain associated long enough to draw the opposing SPBs together (Figure 3.8B, 11 and 14 min). These data suggest that Bik1p promotes persistent MT-MT interactions or contributes to plus end linkage during nuclear congression.

Kar3p is required for microtubule plus end interactions during nuclear congression

Kar3p may be the key component in MT plus end interactions during nuclear congression. In bilateral crosses of *kar3Δ* mutants, the MTs were longer than in wild-type cells, and MTs did not interact to perform nuclear congression (Figure 3.9A). Unlike *kar9Δ* cells, MT plus ends passed each other without interacting in *kar3Δ* mutants (Figure 3.9A, 0-29 min). No MT plus end interactions were observed when *kar3Δ* strains expressing Bik1p-3xGFP crossed to GFP-Tub1p were imaged (Figure 3.S3), and nuclear congression was rarely seen in *kar3Δ* bilateral crosses (18/19 cells no congression). Thus, Kar3p is required to promote the persistent interaction of oppositely oriented MT plus ends during nuclear congression before the switch to coordinated MT depolymerization occurs.

kar3-1 cells contain a constitutive point mutation in *KAR3* that results in rigor binding of the motor head to the MT and generates a semidominant mating defect (Meluh and Rose, 1990; Polaina and Conde, 1982). In the sliding cross-bridge model, Kar3p should act along the length of MTs to promote MT interactions. kar3-1p localizes along the length of the MT instead of concentrating at the plus end (Maddox et al., 2003b; Meluh and Rose, 1990). If plus end interactions drive nuclear congression, failing to concentrate Kar3p at the plus ends may prevent nuclear congression from occurring. When *kar3-1* was the only source of Kar3p in the cell, MTs did not interact, and nuclear congression did not occur (8/8 cells no

congression; see Figure 3.9A for representative example). Therefore, rigor-bound Kar3p is not sufficient for nuclear congression.

In contrast, mating *kar3-1* cells to wild-type cells resulted in a single bridge of GFP-Tub1p fluorescence between the two SPBs in ~50% of cells (Figure 3.9B). The rigor-bound *kar3-1* prevented complete MT depolymerization in these cells but did not prevent the persistence of MT-MT interactions (10/11 cells with no congression). A single focus of plus ends, visualized by Bik1p-3xGFP, did not form between the two SPBs (n = 6 cells; Figure 3.9C). Bik1p-3xGFP redistributed from a single focus in the wild-type cell before cell fusion to a diffuse localization along the MTs as cross-linking occurred after cell fusion (Figure 3.9C, 3.5-5.5 min). This indicates that when kar3-1p bound to the MT lattice encounters Kar3p, interactions are no longer restricted to the plus end. Thus, Kar3p localization at the plus end initiates MT-MT interactions during nuclear congression.

Discussion

The sliding cross-bridge model for nuclear congression arose from the genetic and biochemical analysis of karyogamy (Rose, 1996). Considering recent data that demonstrates MTs assemble and disassemble from the plus end and that proteins localized to the plus ends play a critical role in nuclear migration during mitosis (Lee et al., 2003; Maddox et al., 2000; Sheeman et al., 2003), an examination of nuclear congression was warranted. Does nuclear congression occur by the sliding of oppositely oriented MTs or by force generation coupled to plus end depolymerization? Our data indicate that depolymerization of the MT plus end brings two haploid nuclei together to form a diploid cell in budding yeast. Rather than cross-linking along the length of oppositely oriented MTs, a complex comprised minimally of Bik1p and Kar3p localizes to MT plus ends originating from opposite SPBs. MT depolymerization, possibly coupled to the sliding of MT plus ends past one another over a short distance, allows both nuclei to move in toward the site of cell fusion before karyogamy. These results reveal a novel mechanism for nuclear congression in which plus end-binding proteins and MT-based motors drive nuclear fusion via persistent attachment of depolymerizing plus ends. The consequences of plus end depolymerization-based nuclear congression are considered below.

Nuclear orientation is required for the fidelity of nuclear congression

Nuclear orientation to the shmoo tip depends on an intact actin cytoskeleton that is responsible for polarized growth (Hasek et al., 1987). Kar9p links MT plus end to the actin network to guide the nucleus to the shmoo tip (Hwang et al., 2003). Loss of Kar9p results in severe nuclear orientation defects (Table 3.S1) (Miller and Rose, 1998). However, in these

cells, nuclear congression did occur in the instances where interactions between MT plus ends were observed (Figures 3.2 and 3.7). Conversely, for *kar3Δ* and *bik1Δ* cells, nuclear orientation did not confer success in congression (Figure 3.2). These data suggest Kar9p and the polarized actin network enhance the fidelity of nuclear congression by bringing MT tips into proximity upon cell wall breakdown, but they likely do not play a role in plus end interactions or MT shortening before karyogamy.

A consequence of nuclear orientation is the attachment of MTs to the shmoo tip (Maddox et al., 1999; Miller et al., 1999). In *kip2Δ* cells, attachment to the shmoo tip is reduced, but nuclear congression can occur (Figures 3.2 and 3.3) (Miller et al., 1998). Nuclear congression is reduced but successful in *kar9Δ* and *bik1Δ* cells that also have defective MT-shmoo tip attachments (Figures 3.2 and 3.3). Therefore, like nuclear orientation, MT attachment to the shmoo tip is not required for karyogamy, but attachment may enhance the probability of contact between oppositely oriented MT plus ends in mating cells.

Nuclear congression

The sliding cross-bridge model predicts that Kar3p will cross-link and slide MTs past one another while depolymerizing MT minus ends (Rose, 1996). This model is supported by: (1) the failure of MT-MT interactions to occur in fixed *kar3-102* cells that were interpreted to be defective in lateral MT associations (Meluh and Rose, 1990); (2) the MT depolymerase activity of Kar3p that was initially reported to occur at the minus end in vitro (Endow et al., 1994); and (3) that Kar3p could cross-link MTs along their length when associated with a second protein, Cik1p (Barrett et al., 2000). However, it has recently been

shown that Kar3p is targeted to MT plus ends and, in vitro, Kar3p-dependent MT depolymerization occurs at the plus ends (Maddox et al., 2003b; Sproul et al., 2005). In light of these facts, we reinvestigated nuclear congression and found MT plus ends associate and shorten to promote nuclear fusion. Both Kar3p-GFP and Bik1p-3xGFP localize to MT plus ends that appear to interact at a single site in between both SPBs before nuclear congression (Figures 3.5 and 3.S1). Additionally, no detectable overlap zone is present when MTs are imaged during nuclear congression (Figure 3.6). It should be noted that the spreading of the Bik1p-3xGFP signal during the later stages of nuclear congression could represent a small overlap zone where Kar3p-dependent sliding occurred (Figure 3.5). Finally, when rigor bound kar3-1p is distributed along the length of the MT, the concentration of plus ends between SPBs is disrupted (Figure 3.9C). Since MT dynamics are regulated at the plus end in both the shmoo tip (Maddox et al., 1999) and in mitotic cells (Maddox et al., 2000; Tanaka et al., 2005), we propose that MT plus end depolymerization provides the motive force to move both nuclei together.

What molecules are required for plus end interactions and MT depolymerization during nuclear congression? In the absence of Kar3p, MT plus ends did not interact to perform nuclear congression (Figures 3.9 and 3.S3). Therefore, Kar3p is required for the interaction of MT plus ends. In contrast, Bik1p is required to allow MTs to persistently interact during nuclear congression. In the absence of Bik1p, oppositely oriented MTs often do not contact each other as a result of their short length and rapid depolymerization (Figure 3.S2). We suggest that Bik1p stabilizes MTs to allow persistent cross-linking to occur or that Bik1p acts to directly maintain MT-MT interactions. In *kip2Δ* cells there is no mating defect, although MT length is similar to *bik1Δ* cells (Figure 3.2 and Table 3.S2), suggesting that

short MTs do not prevent nuclear congression. The low level of Bik1p that localizes to the MT plus ends is likely sufficient to promote nuclear congression in *kip2Δ* cells (Figure 3.8A). These data suggest that Kar3p links oppositely oriented MTs, whereas Bik1p may stabilize plus ends and/or promote plus end interactions.

MTs shorten after plus end interactions are established, indicating that depolymerization is favored over dynamic instability. Depolymerization could be triggered by Kar3p or Kip3p, a second motor protein that has MT depolymerase activity (Miller et al., 1998). *kip3Δ* cells did not have a mating defect (Table 3.S2) (Miller et al., 1998), so the contribution of Kip3p to nuclear congression in wild-type cells is likely minimal. One hypothesis is that Kar3p favors MT plus end depolymerization when bound to oppositely oriented MTs. The inhibition of MT shortening after cross-linking in *kar3-1* cells could reflect the role of Kar3p as the critical depolymerase during nuclear congression (Figure 3.9B and 3.9C). Alternatively, cell cycle regulation or structural changes in the MT could promote depolymerization.

How do Kar3p and Bik1p maintain plus end interactions and depolymerize oppositely oriented MT arrays? MT plus ends orient and remain proximal to each other after cell wall breakdown (Figure 3.10A and 3.10B). We propose that Kar3p-dependent motor activity cross-links oppositely oriented MT plus ends, initiating nuclear congression (Figure 3.10C and 3.10D). After the initial MT-MT interactions are established, Kar3p could slide antiparallel MTs over a short distance. Once cross-linked, coordinated depolymerization begins and Kar3p, along with Bik1p, maintains the association of shortening MT plus ends as the nuclei move inward (Figure 3.10E). Kar3p and Bik1p could be part of a protein "sleeve" similar to a proposal for kinetochore-MT interactions in higher eukaryotes (Hill, 1985)

around MT plus ends. Kar3p in the sleeve complex could then induce shortening of the MTs. Alternatively, the minus end motor activity of Kar3p could cross-link and attempt to slide the MTs past each other, generating forces on the plus ends that induce depolymerization. The spreading of Bik1p-3xGFP during nuclear congression could be due to sliding of plus ends past one another, generating a slight overlap zone (Figures 3.5 and 3.6). In this model, MT plus ends could interact directly at their tips or could have a small region of overlap.

Parallels to Pronuclear Migration

How does nuclear congression compare with metazoan fertilization? In higher eukaryotes, dynein-dependent pronuclear migration precedes karyogamy (Gonczy et al., 1999; Payne et al., 2003). In budding yeast, dynein has no role in nuclear congression (Table 3.S2). The plus end interaction mechanism of budding yeast could dominate the process as a result of the limited number of MTs nucleated at the SPB that must be stabilized to facilitate nuclear congression. During metazoan pronuclear migration, the relatively large number of MTs may promote MT-nuclear envelope interactions that favor dynein function. Could plus ends have a major function in pronuclear migration? Or is the plus end complex of nuclear congression more similar to the cross-linking of interpolar MTs in the central spindle mitosis? The analysis of nuclear congression in budding yeast should provide insight into MT plus end-based force generation in vivo.

Acknowledgements

Reproduced from *The Journal of Cell Biology* (2006, Volume 172, pages 27 – 39) by copyright permission of The Rockefeller University Press. We thank David Bouck, Bob Goldstein, Paul Maddox, Chad Pearson, Mark Rose, Jennifer Sims, and members of the Bloom and Salmon laboratories for assistance with microscopy, strains, reagents, critical readings of the manuscript, and advice. We are especially grateful to David Pellman for providing the Bik1p-3xGFP plasmid and Dean Dawson for supplying us with *kar3Δ* strains.

This work was funded by the Human Frontier Science Program grant RGP29/2003 (to E.D. Salmon) and the National Institutes of Health grants GM-24364 (to E.D. Salmon), GM-60678 (to E.D. Salmon), and GM-32238 (to K. Bloom).

Tables and Figures

Strain Name	Relevant Genotype	Source or Reference
DC 49-7.1 C	MAT**a** *ura3-52 trp1-289 leu2-3, 112 arg4Δ57*	D. Dawson[A]
DC 48-5.1 C	MATα *his3Δ1 ura3-52 trp1-289 arg4Δ42*	D. Dawson
TRS 108-5	MAT**a** *ura3-52 trp1-289 leu2-3, 112 arg4Δ57 kar3Δ::KAN^r* pMR820	D. Dawson
TRS 107-6	MATα *his3Δ1 ura3-52 trp1-289 arg4Δ42 kar3Δ::KAN^r* pMR820	D. Dawson
YEF 473A	MAT**a** *trp1Δ63 leu2Δ1 ura3-52 his3Δ200 lys2-801*	(Bi and Pringle, 1996)
YEF 473B	MATα *trp1Δ63 leu2Δ1 ura3-52 his3Δ200 lys2-801*	(Bi and Pringle, 1996)
GT1	MAT**a** *trp1Δ63 leu2Δ1 ura3-52 his3Δ200 lys2-801 GFP-TUB1::URA3*	(Maddox et al., 2000)
KBY 5026	MAT**a** *trp1Δ63 leu2Δ1 ura3-52 his3Δ200 lys2-801 kip3Δ::KAN^r GFP-TUB1::URA3*	J. Sims[B]
KBY 5049	MAT**a** *trp1Δ63 leu2Δ1 ura3-52 his3Δ200 lys2-801 kip2Δ::HB^r GFP-TUB1::URA3*	J. Sims
KBY 5058	MAT**a** *trp1Δ63 leu2Δ1 ura3-52 his3Δ200 lys2-801 kar9Δ::LEU2 GFP-TUB1::URA3*	J. Sims
KBY 9258	MATα *trp1Δ63 leu2Δ1 ura3-52 his3Δ200 lys2-801 GFP-TUB1::URA3*	This Study
KBY 9261	MAT**a** *trp1Δ63 leu2Δ1 ura3-52 his3Δ200 lys2-801 dhc1Δ::HIS3 GFP-TUB1::URA3*	This Study
KBY 9262	MATα *trp1Δ63 leu2Δ1 ura3-52 his3Δ200 lys2-801 dhc1Δ::HIS3 GFP-TUB1::URA3*	This Study
KBY 9291	MATα *trp1Δ63 leu2Δ1 ura3-52 his3Δ200 lys2-801 GFP-TUB1::URA3 kar9Δ::LEU2*	This Study
KBY 9293	MAT**a** *trp1Δ63 leu2Δ1 ura3-52 his3Δ200 lys2-801 kar3Δ::TRP1*	This Study
KBY 9313	MAT**a** *trp1Δ63 leu2Δ1 ura3-52 his3Δ200 lys2-801 kar3Δ::TRP1 GFP-TUB1::URA3*	This Study
KBY 9306	MAT**a** *trp1Δ63 leu2Δ1 ura3-52 his3Δ200 lys2-801 GFP-TUB1::URA3 bik1Δ::TRP1*	This Study
KBY 9308	MATα *trp1Δ63 leu2Δ1 ura3-52 his3Δ200 lys2-801 GFP-TUB1::URA3 bik1Δ::TRP1*	This Study
KBY 9311	MATα *trp1Δ63 leu2Δ1 ura3-52 his3Δ200 lys2-801 GFP-TUB1::URA3 kip2Δ::KAN^r*	This Study
KBY 9312	MATα *trp1Δ63 leu2Δ1 ura3-52 his3Δ200 lys2-801 GFP-TUB1::URA3 kip3Δ:: KAN^r*	This Study
KBY 9316	MAT**a** *trp1Δ63 leu2Δ1 ura3-52 his3Δ200 lys2-801 bik1Δ::TRP1*	This Study
KBY 9317	MATα *trp1Δ63 leu2Δ1 ura3-52 his3Δ200 lys2-801 bik1Δ::TRP1*	This Study
KBY 9318	MAT**a** *trp1Δ63 leu2Δ1 ura3-52 his3Δ200 lys2-801 BIK1::3xGFP-TRP1*	This Study
KBY 9319	MAT**a** *ura3-52 trp1-289 leu2-3, 112 arg4Δ57 kar3Δ::KAN^r BIK1::3xGFP-TRP1* pMR820	This Study
KBY 9320	MATα *his3Δ1 ura3-52 trp1-289 arg4Δ42 kar3Δ::KAN^r BIK1::3xGFP-TRP1* pMR820	This Study
KBY 9322	MAT**a** *ura3-52 trp1-289 leu2-3, 112 arg4Δ57 kar3Δ::KAN^r BIK1::3xGFP-TRP1*	This Study
KBY 9323	MATα *his3Δ1 ura3-52 trp1-289 arg4Δ42 kar3Δ::KAN^r BIK1::3xGFP-TRP1*	This Study
KBY 9324	MAT**a** *trp1Δ63 leu2Δ1 ura3-52 his3Δ200 lys2-801 kip2Δ::KAN^r BIK1::3xGFP-TRP1*	This Study
KBY 9325	MAT**a** *trp1Δ63 leu2Δ1 ura3-52 his3Δ200 lys2-801 BIK1::3xGFP-TRP1 CFP-TUB1::URA3*	This Study
KBY 9337	MATα *trp1Δ63 leu2Δ1 ura3-52 his3Δ200 lys2-801 BIK1::3xGFP-TRP1*	This Study

Plasmid Name	Relevant Genotype	Source or Reference
pMR820	*KAR3-URA3* (Amp^r)	(Meluh and Rose, 1990)
pAFS125	*GFP-TUB1-URA3* (Amp^r)	(Straight et al., 1997)
CFP-Tub1p	*CFP-TUB1-URA3* (Amp^r)	M. Segal[C]
Bik1p-3xGFP	*BIK1-3xGFP-TRP1* (Amp^r)	(Carvalho et al., 2004)

[A]Tufts University, Boston, MA [B]University of North Carolina, Chapel Hill, NC [C]University of Cambridge, Cambridge, UK

Table 3.1: *S. cerevisiae* strains used in this chapter.

Cell Type	Orient to Shmoo Tip	n	Degree of Persistence	Attach/Total Time (min)	n
Wild-type	98%	103	100%	200/200	10
kip2Δ	99%	105	40%	79.5/200	10
kar9Δ	55%	100	18%	31/180	9
bik1Δ	97%	105	12%	35.5/300	15
kar3Δ	95%	102	54%	107/200	10

Table 3.S1: Nuclear orientation and cytoplasmic MT attachment frequencies.

Successful nuclear orientation to the shmoo tip (Orient to Shmoo Tip) was scored when the SPB was inside or near the base of the shmoo tip. Defects in nuclear orientation to the shmoo tip were recorded when the SPB was in the half of the cell body distal to the shmoo tip. Degree of persistence was defined as the percentage of time MTs remained attached to the shmoo tip in time-lapse movies (Attach/Total Time).

Bilateral Cross	Normal Congression	Aberrant Congression	n
Wild-type x Wild-type	38 (100%)	0 (0%)	38
dhc1Δ x *dhc1Δ*	67 (100%)	0 (0%)	67
kip3Δ x *kip3Δ*	21 (100%)	0 (0%)	21
kip2Δ x *kip2Δ*	36 (100%)	0 (0%)	36
kar9Δ x *kar9Δ*	23 (59%)	16 (41%)	39
bik1Δ x *bik1Δ*	10 (23%)	33 (77%)	43
kar3Δ x *kar3Δ*	1 (1%)	85 (99%)	86

Table 3.S2: Frequency of nuclear congression defects in bilateral karyogamy mutants.

Nuclear congression was scored as normal when both SPBs were ≤0.5-μm from each other or there was only one focus of GFP-Tub1p fluorescence. Aberrant nuclear congression was recorded when both SPBs were clearly separated from each other after cell fusion had occurred.

Figure 3.1: Schematic of nuclear orientation, cytoplasmic microtubule attachment to the shmoo tip, and nuclear congression.

Nucleus is gray; SPB is black circle; MTs are black bars; actin filaments are gray cables; actin patches are small gray circles. (A) Nuclear orientation to the shmoo tip. MTs are guided along filamentous actin toward the shmoo tip. Kar9p, Bim1p, and Myo2p are required for nuclear orientation, but the contributions of Kar3p, Bik1p, and Kip2p are unknown. (B) MT attachment to the shmoo tip. MTs are tethered to the mating projection by Kar3p during depolymerization and Bim1p during polymerization. Bik1p and Kip2p function in MT attachment is unknown. (C) Before cell-cell fusion, MTs are maintained at the shmoo tip. (D) Sliding cross-bridge model for nuclear congression. Oppositely oriented MTs overlap and are cross-linked along their lengths, whereas depolymerization is induced at the spindle poles (Rose, 1996). (E) Plus end model for nuclear congression. MT plus ends cross-link and induce depolymerization to draw opposing nuclei together. In either the sliding cross-bridge or plus end models, the localization and/or function of Kar3p, Bik1p, Kip2p, and Kar9p during live cell nuclear congression is not known.

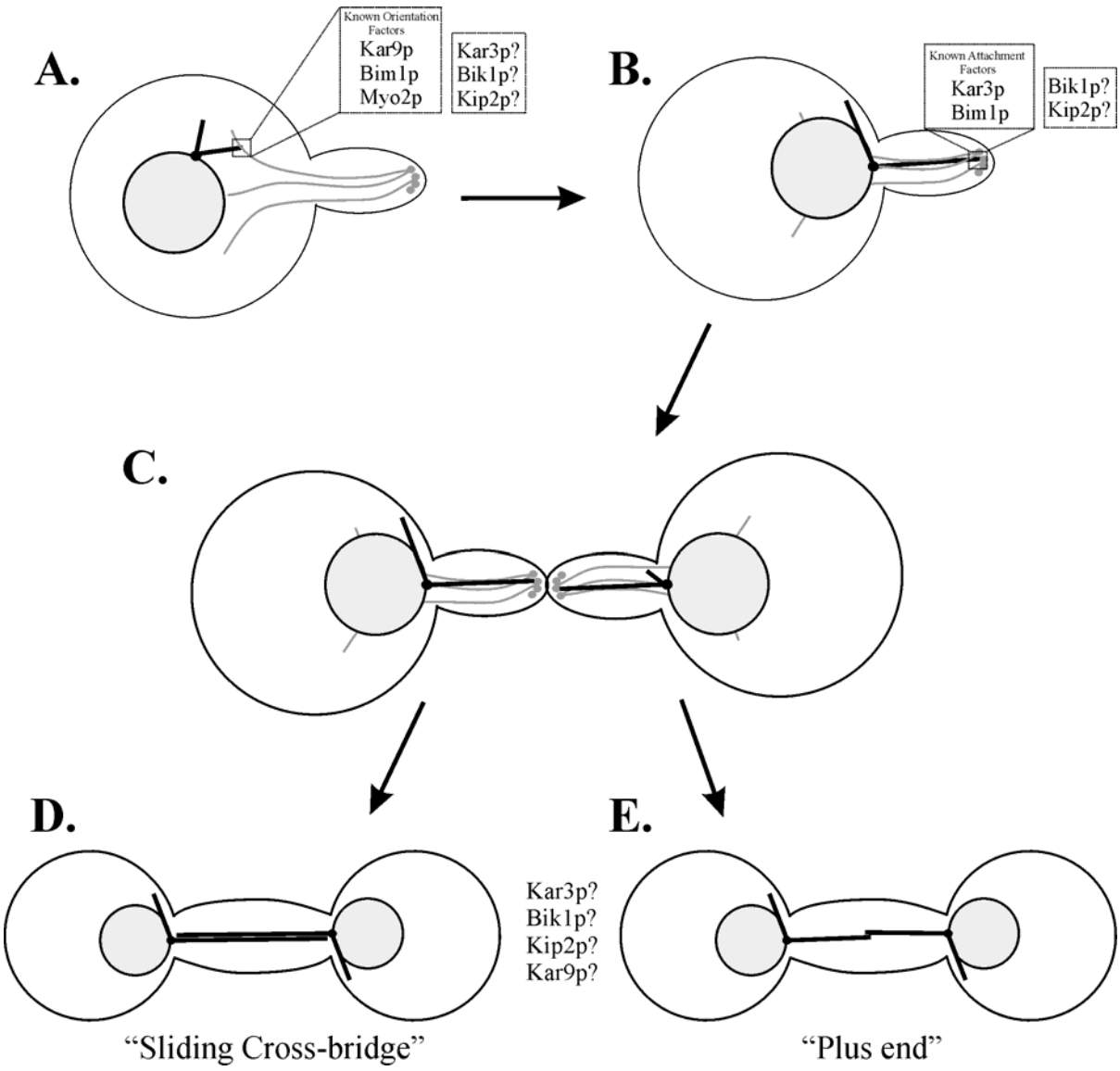
A.
Known Orientation Factors
Kar9p
Bim1p
Myo2p
Kar3p?
Bik1p?
Kip2p?
B.
Known Attachment Factors
Kar3p
Bim1p
Bik1p?
Kip2p?
C.
D.
E.
Kar3p?
Bik1p?
Kip2p?
Kar9p?
"Sliding Cross-bridge"
"Plus end"

Figure 3.2: Percentage of successful nuclear orientation, cytoplasmic MT attachment to the shmoo tip, and nuclear congression in karyogamy mutants.

Summary of measurements of the stages leading to karyogamy. Nuclear orientation, white bars; cytoplasmic MT attachment, gray bars; nuclear congression, black bars. Nuclear orientation was scored as successful if the SPB, marked by GFP-Tub1p, was positioned in or near the base of the shmoo tip. Cytoplasmic MT attachment to the shmoo tip was determined using the degree of persistence, or the amount of time MTs remained attached to the shmoo tip in consecutive frames during time-lapse imaging. Nuclear congression was scored as wild-type if both SPBs were fused into a single GFP-Tub1p focus or two closely associated foci (~0.5 μm). Nuclear orientation and cytoplasmic MT attachment in *dhc1Δ* and *kip3Δ* was not scored (ND; see Maddox et al., 2003b for relative measurements).

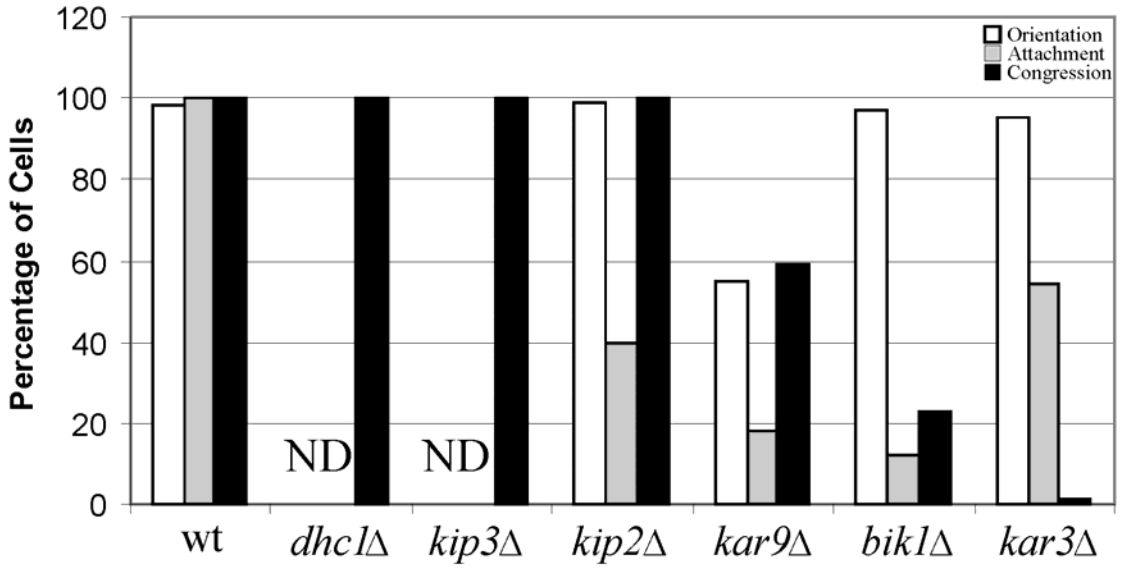
Percentage of Cells
120
100
80
60
40
20
0
Orientation
Attachment
Congression
ND
ND
wt
dhc1Δ
kip3Δ
kip2Δ
kar9Δ
bik1Δ
kar3Δ

Figure 3.3: Cytoplasmic MT attachment to the mating projection is not persistent in *kar3Δ*, *bik1Δ*, or *kip2Δ* cells.

Images of MT attachment to the shmoo tip. Arrowheads denote the positions of SPB, marked by GFP-Tub1p fluorescence, relative to shmoo tip. (A) Wild-type (wt) cells displayed persistent attachment of cytoplasmic MTs to the shmoo tip (0 min), whereas the SPB oscillates along the polarity axis of the cell (1.5, 3, and 8 min). (B) *kar3Δ* cells with cytoplasmic MT attachment to the shmoo tip (0 min) detached upon depolymerization (6.5 min) and regained attachments upon polymerization toward the mating projection (8.5 min). New attachments were lost during a second depolymerization event (10.5 min). (C) *bik1Δ* cells have short cytoplasmic MTs that were attached to the mating projection (0 min) and detached as depolymerization occurred (1 min). New attachments were gained and lost during the time-lapse (3 and 7.5 min). (D) *kip2Δ* cells with short cytoplasmic MT attachments to the shmoo tip (0 min) lost the attachment (1 min), regained it, and then lost the attachment (4.5 and 6 min). The GFP-Tub1p fluorescence in *kip2Δ* cells distal from the shmoo tip marked the SPB (wild-type SPB 1.87 μm from shmoo tip; *kip2Δ* SPB is 1.64 μm from shmoo tip; $p > 0.09$; $n = 20$ cells each). Bar, 2 μm.

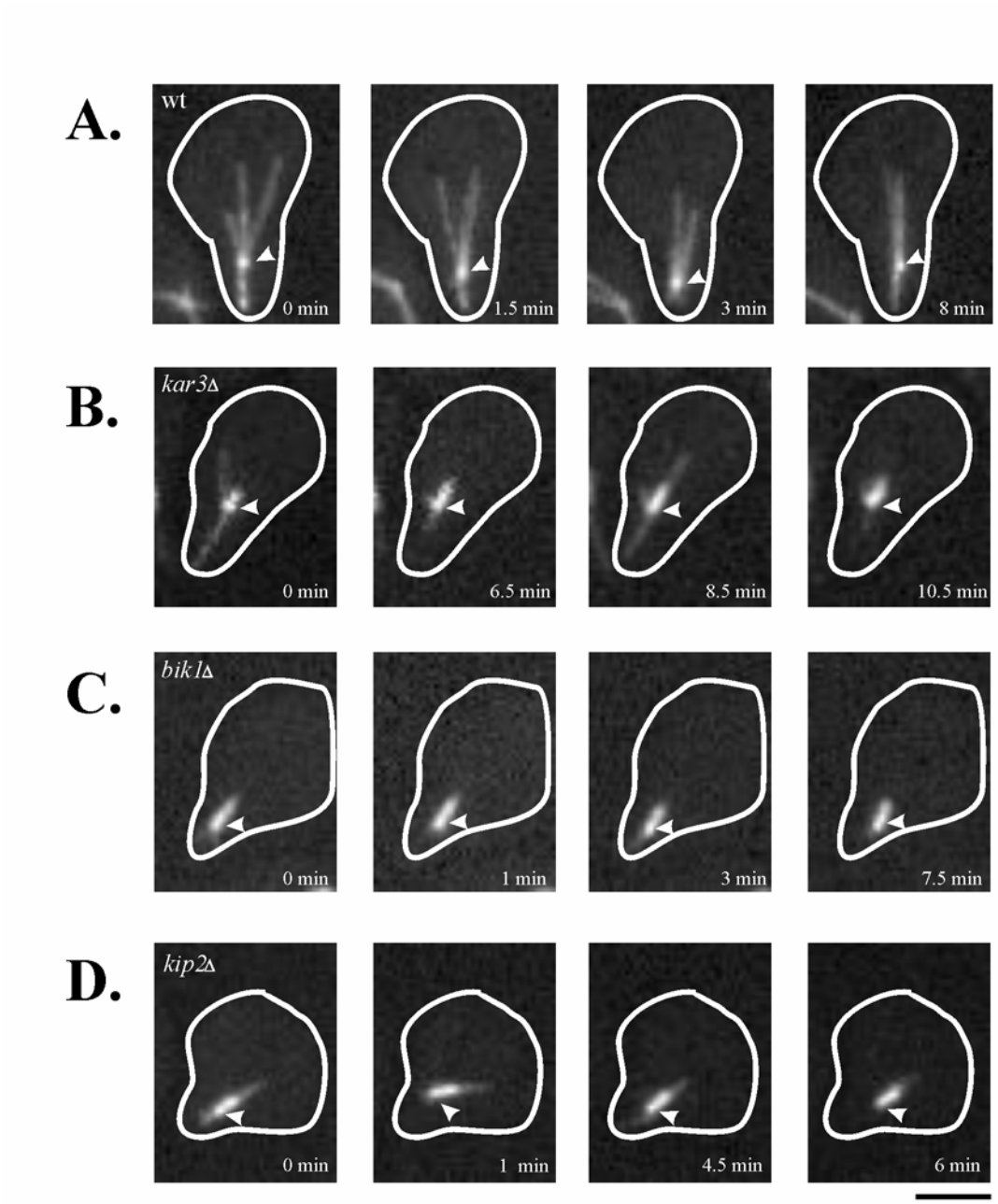
A.
wt
0 min
1.5 min
3 min
8 min
B.
kar3Δ
0 min
6.5 min
8.5 min
10.5 min
C.
bik1Δ
0 min
1 min
3 min
7.5 min
D.
kip2Δ
0 min
1 min
4.5 min
6 min

Figure 3.4: Bik1p-3xGFP localized to the shmoo tip and SPB in cells challenged with mating pheromone.

Bik1p-3xGFP localization in pheromone treated cells. (A) Bik1p-3xGFP colocalization with CFP-Tub1p by wide-field microscopy. Left panel is Bik1p-3xGFP; middle panel is CFP-Tub1p fluorescence; right panel is overlay of Bik1p-3xGFP in green and CFP-Tub1p in red. Bik1p localized to both the shmoo tip and SPB. (B) Bik1p-3xGFP localization in pheromone-treated cells. Top panel is a montage from time-lapse imaging of Bik1p-3xGFP. Single planes were acquired approximately every 3 s. Note the enrichment of Bik1p-3xGFP at the shmoo tip (facing up) during depolymerization. (B and C) Bottom panel is a plot of Bik1p-3xGFP fluorescence intensity (gray triangles) and distance from the SPB (black squares) to the shmoo tip over time. As the SPB moved toward the shmoo tip, Bik1p-3xGFP fluorescence on MT plus ends at the mating projection increased. (C) Bik1p-3xGFP localization in pheromone-treated cells. Top panel is time-lapse imaging of Bik1p-3xGFP localization in the mating projection. Five-plane Z-series were acquired every 30 s, and maximum projection images are presented. Asterisks denote Bik1p-3xGFP-marked MT plus ends that incorporate into the shmoo tip; arrow signifies Bik1p-3xGFP localization to newly nucleated MT plus end. Note Bik1p-3xGFP localization on nonshmoo tip MTs facing the cell body (149.6 s). Bik1p-3xGFP increased in fluorescence intensity as the SPB moved toward the shmoo tip and decreased in fluorescence intensity as the SPB-to-shmoo tip distance increased. Bars, 2 μm.

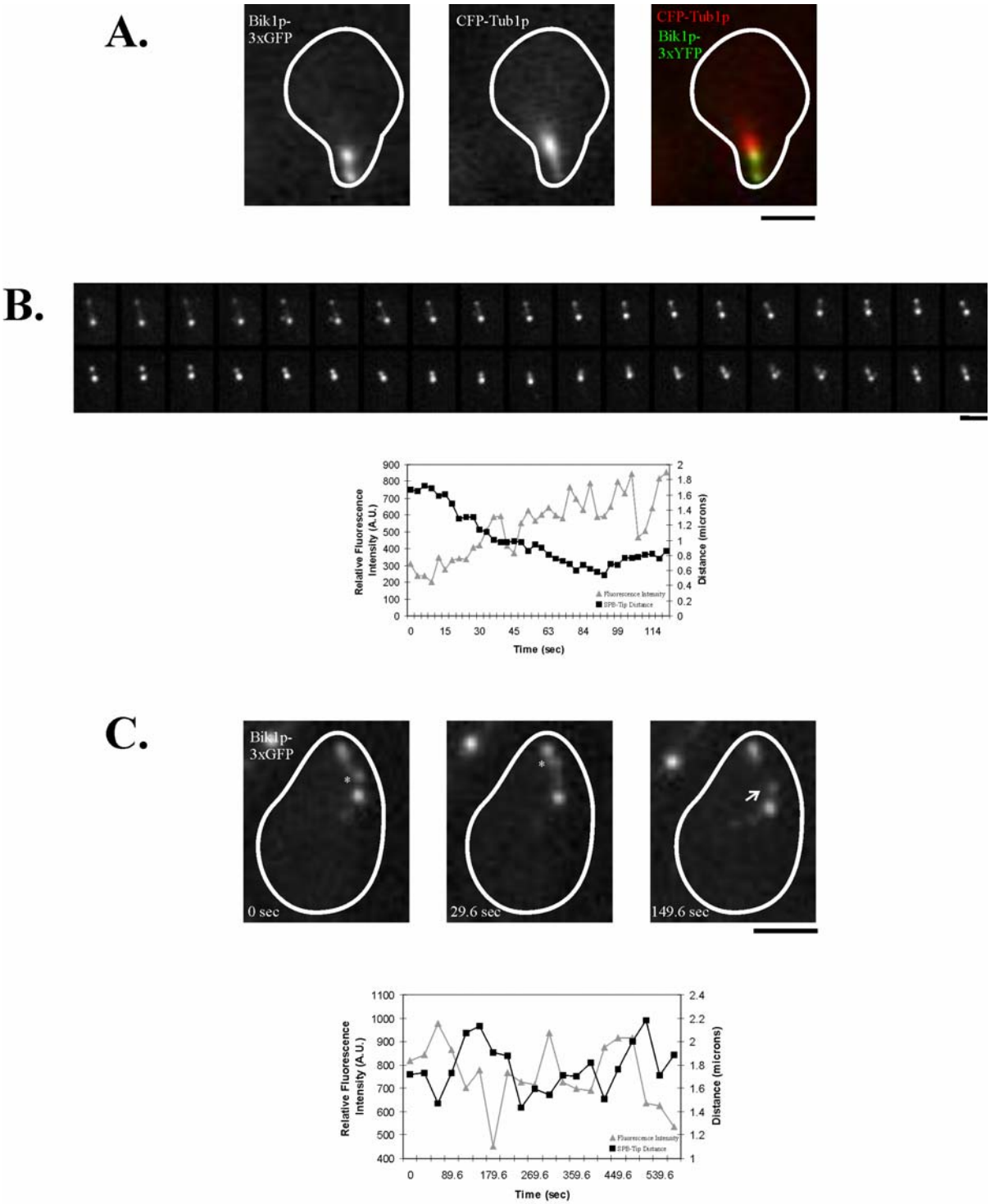
A.
Bik1p-
3xGFP
CFP-Tub1p
CFP-Tub1p
Bik1p-
3xYFP
B.
Relative Fluorescence Intensity (A.U.)
Distance (microns)
Fluorescence Intensity
SPB-Tip Distance
Time (sec)
C.
Bik1p-
3xGFP
0 sec
29.6 sec
149.6 sec
Relative Fluorescence Intensity (A.U.)
Distance (microns)
Fluorescence Intensity
SPB-Tip Distance
Time (sec)

Figure 3.5: Nuclear congression occurs by MT plus end cross-linking and depolymerization.

Nuclear congression in wild-type cells. (A) Top panel (14 s) shows cells of opposite mating types expressing Bik1p-3xGFP. Arrowheads denote SPBs (upper SPB, SPB_U, lower SPB, SPB_L). (175-178 s) Bik1p-3xGFP plus ends cross-link during nuclear congression. New MT plus ends could incorporate into the plus ends that cross-linked opposite MTs during nuclear congression. (286 s) Initial interactions between plus ends labeled with Bik1p-3xGFP, noted by arrow. (322-391 s) Nuclear congression occurred, and SPBs moved toward the site of initial plus end interactions. Arrows point to the site where MT plus ends that were nucleated from opposite SPBs interact. Bottom panel shows kymograph of nuclear congression. Time bar ~20 s (calibrated for 1-s intervals taken during the bulk of imaging). Asterisk denotes plus end Bik1p-3xGFP signal; arrow marks approximate time of plus end fusion. SPBs move inward to the region where plus ends interacted during nuclear congression. (B) Top panel (0 s) shows a cell expressing Bik1p-3xGFP (left) mated to a cell expressing GFP-Tub1p (right). (30 s) Oppositely oriented microtubules associated in a single Bik1p-3xGFP focus (arrows) in between the two SPBs (arrowheads; left SPB, SPB_L, right SPB, SPB_R). (45-75 s) MTs remain associated with the Bik1p-3xGFP focus as SPB position changed. (90-147.5 s) SPBs began to move toward each other as nuclear congression occurred. Note the stable position of the Bik1p-3xGFP focus as the SPBs moved inward. (157.5 and 167.5 s) The SPBs became one focus before nuclear fusion. Bottom panel shows kymograph of nuclear congression. Time bar ~90 s. Asterisk denotes Bik1p-3xGFP focus; arrow marks approximate time of plus end fusion. The SPBs move inward toward the Bik1p-3xGFP focus that maintained its position during nuclear congression. Bars, 2 μm.

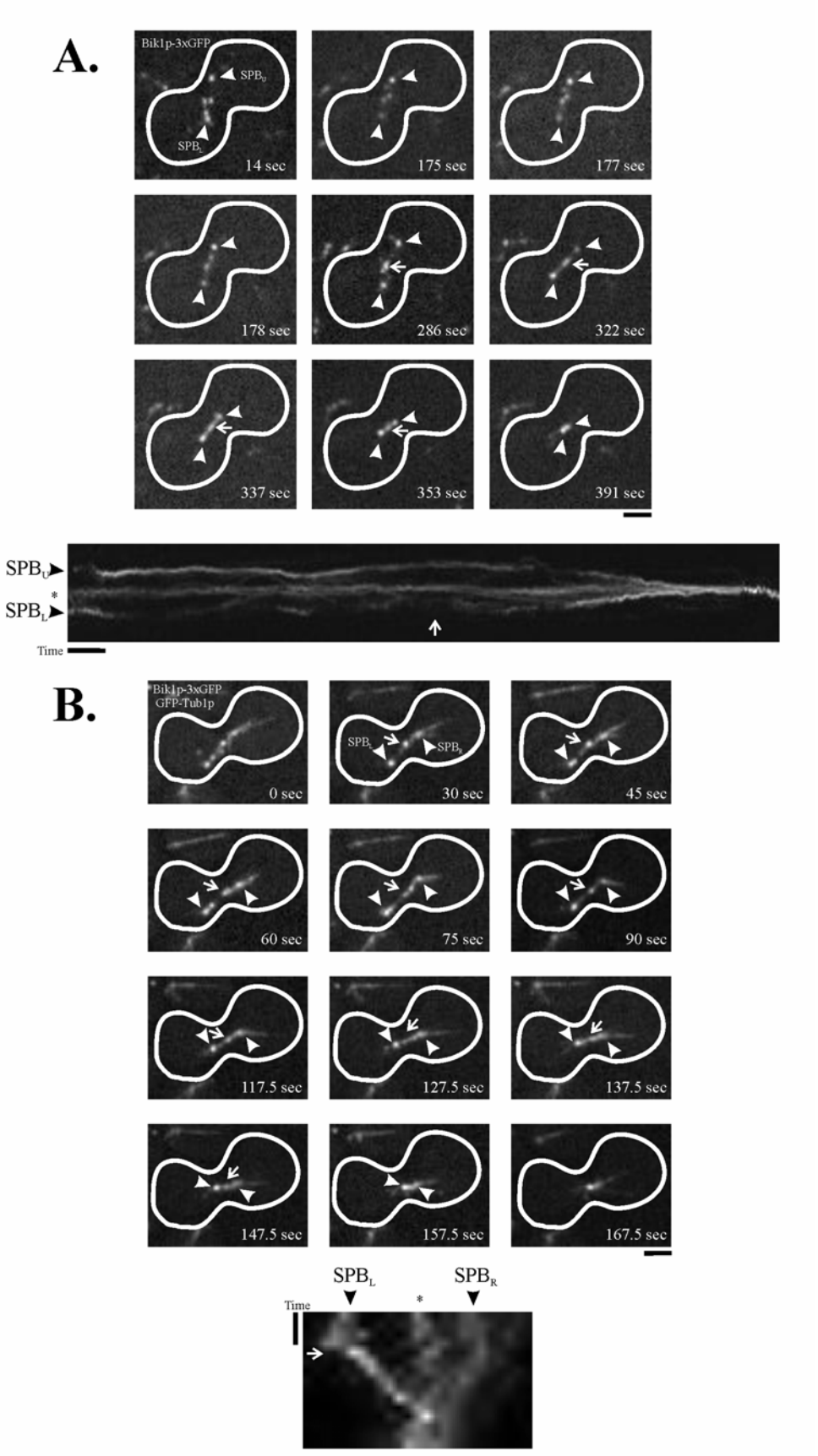
A.
Bik1p-3xGFP
SPB
SPB
14 sec
175 sec
177 sec
178 sec
286 sec
322 sec
337 sec
353 sec
391 sec
SPB
SPB
*
Time
B.
Bik1p-3xGFP
GFP-Tub1p
SPB
SPB
0 sec
30 sec
45 sec
60 sec
75 sec
90 sec
117.5 sec
127.5 sec
137.5 sec
147.5 sec
157.5 sec
167.5 sec
SPB
SPB
*
Time

Figure 3.6: GFP-Tub1p fluorescence intensity does not increase during nuclear congression.

(A) Montage of wild-type cells expressing GFP-Tub1p during nuclear congression. Nuclear congression begins at ~97 s, and both SPBs move in toward the region of initial plus end MT interactions. (B) Comparisons of MT overlap fluorescence during mating (left) and mitosis (right). Images are projections of five-plane Z-series. Arrows mark SPBs. From the time of initial MT interactions through the time-lapse images, mating cells show two major peaks of fluorescence at the SPBs. In contrast, mitotic cells have a third peak corresponding to overlapping MTs in the midzone (n = 5 cells each). (C) Top panels are descriptions of fluorescence intensity analysis for GFP-Tub1p cells during nuclear congression. Three non-overlapping 5 x 5 pixel boxes (left) were placed between, but not including, the two SPBs to record the integrated fluorescence intensity in the region before and after nuclear congression. Background was subtracted by moving the boxes to nearby regions in the cell without GFP-Tub1p fluorescence. As nuclear congression began the area became best fit by two boxes (middle) and then a single box (right). Bottom panel shows fluorescence intensity measurements. Arrow denotes the beginning of nuclear congression. The integrated fluorescence intensity from the top (blue), middle (pink), and bottom box (yellow) was plotted versus time. If sliding occurred, then the fluorescence intensity of the middle box and two outer boxes should equal the sum of the fluorescence intensity before MT cross-linking. The fluorescence before MT interactions occurred could fluctuate as newly nucleated MTs were incorporated into the MT bundle (0-90 s, yellow line). However, the fluorescence did not double in this region before or during nuclear congression after MT-MT interactions were established, suggesting that the sliding of MTs does not occur during nuclear congression. This result was seen in all cells imaged and analyzed (n = 5). Bars, 2 μm.

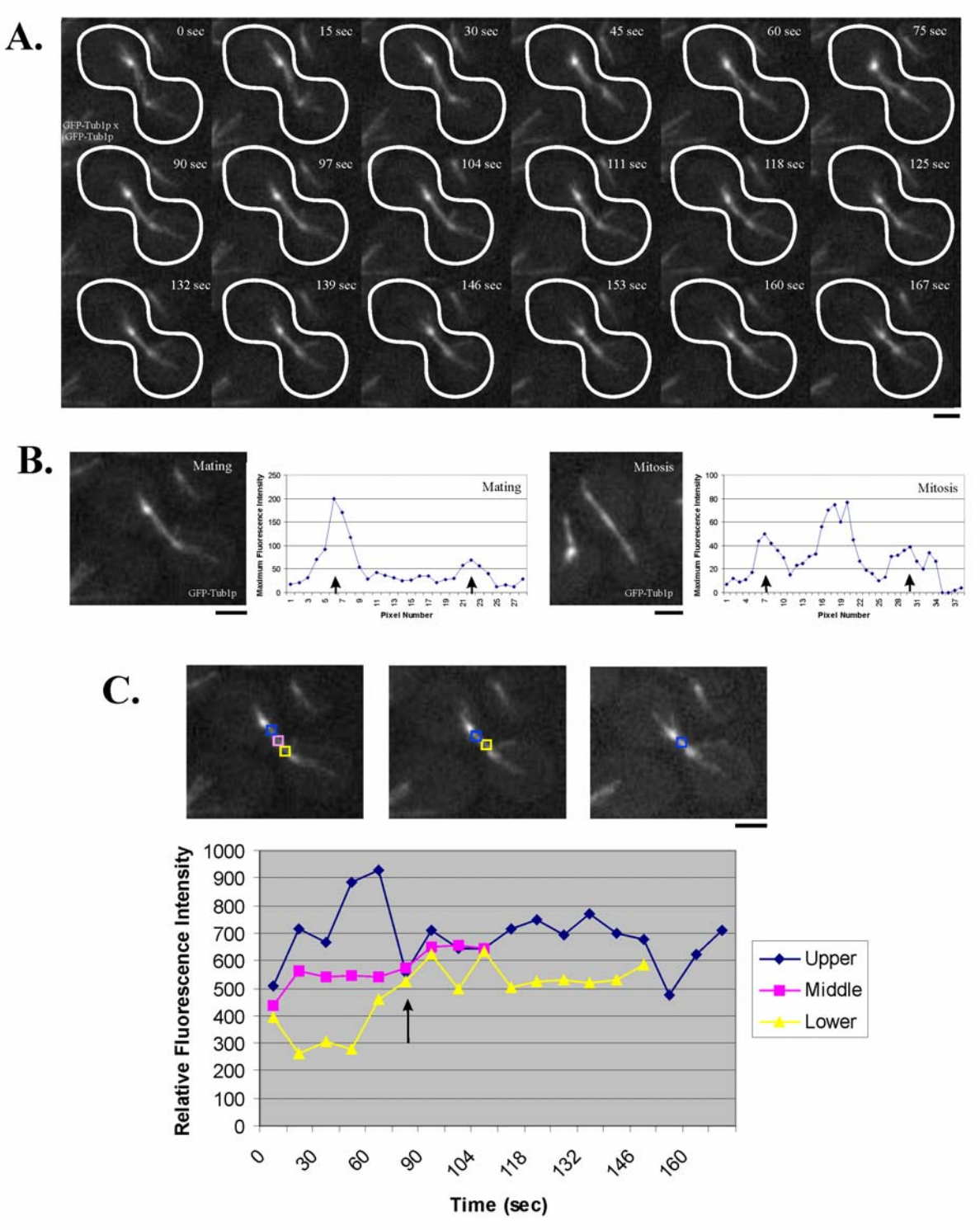
A.
0 sec
15 sec
30 sec
45 sec
60 sec
75 sec
GFP-Tub1p x
GFP-Tub1p
90 sec
97 sec
104 sec
111 sec
118 sec
125 sec
132 sec
139 sec
146 sec
153 sec
160 sec
167 sec
B.
Mating
GFP-Tub1p
Maximum Fluorescence Intensity
Pixel Number
Mitosis
C.
Relative Fluorescence Intensity
Time (sec)
Upper
Middle
Lower

Figure 3.7: Nuclear congression in *kar9Δ* cells.

Nuclear congression occurred in the absence of Kar9p. (0-8 min) SPBs motility as a result of MT-cortical interactions changed spindle pole position without resulting in nuclear congression. (8.5-12.5 min) An apparent lateral MT interaction did not result in nuclear congression. (13.5 and 17 min) SPBs were positioned to face each other, and MTs grew toward each other. (17.5 min) MTs interacted at the plus end to begin nuclear congression. (18-18.5 min) Nuclear congression was completed as both SPBs were drawn toward each other. Bar, 2 μm.

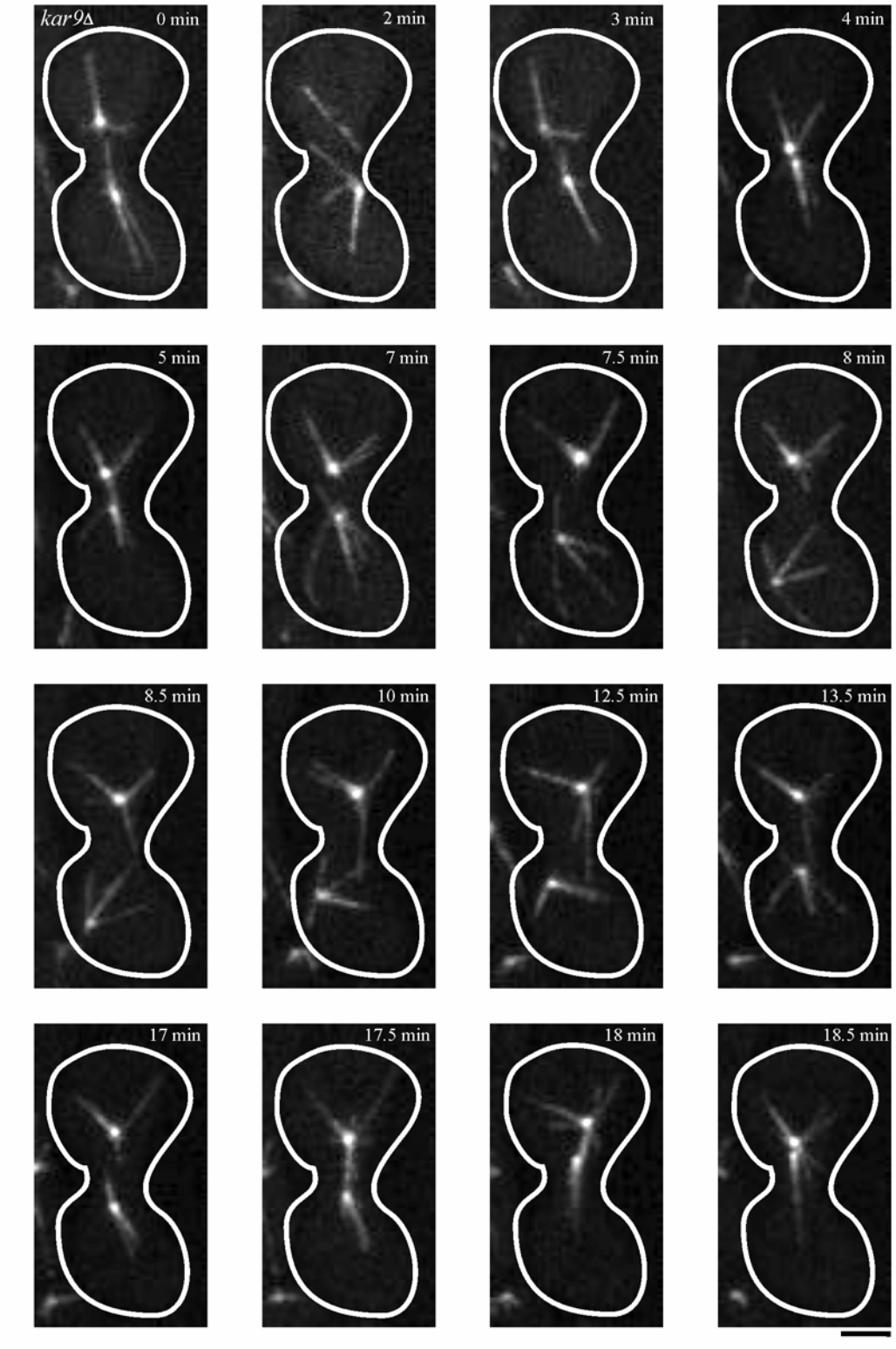
kar9Δ
0 min
2 min
3 min
4 min
5 min
7 min
7.5 min
8 min
8.5 min
10 min
12.5 min
13.5 min
17 min
17.5 min
18 min
18.5 min

Figure 3.8: Nuclear congression in *bik1Δ* cells.

Bik1p is required for persistent MT interactions during nuclear congression. (A) Bik1p-3xGFP localization in *kar3Δ* and *kip2Δ* cells. Left panel shows that in the absence of Kar3p, Bik1p-3xGFP localized to both growing and shortening MTs in the shmoo tip, a result of the *kar3Δ* attachment defect. Right panel shows that Bik1p-3xGFP localization on shmoo tip and nonshmoo tip MTs was reduced but still visible in *kip2Δ* cells. Arrowheads denote the positions of the SPBs. (B) Nuclear congression in *bik1Δ* cells expressing GFP-Tub1p. Separated SPBs close to the center of the cell body (0 min) nucleated short MTs (1 min) that were in proximity to each other (3-7 min). The increased fluorescence facing away from the site of cell fusion likely represents nuclear tubulin fluorescence. MTs from opposing spindle poles appeared to cross-link (9 min), although this linkage broke (10 min) and reformed (11 min) to ultimately allow nuclear congression (14 min). Bar, 2 μm.

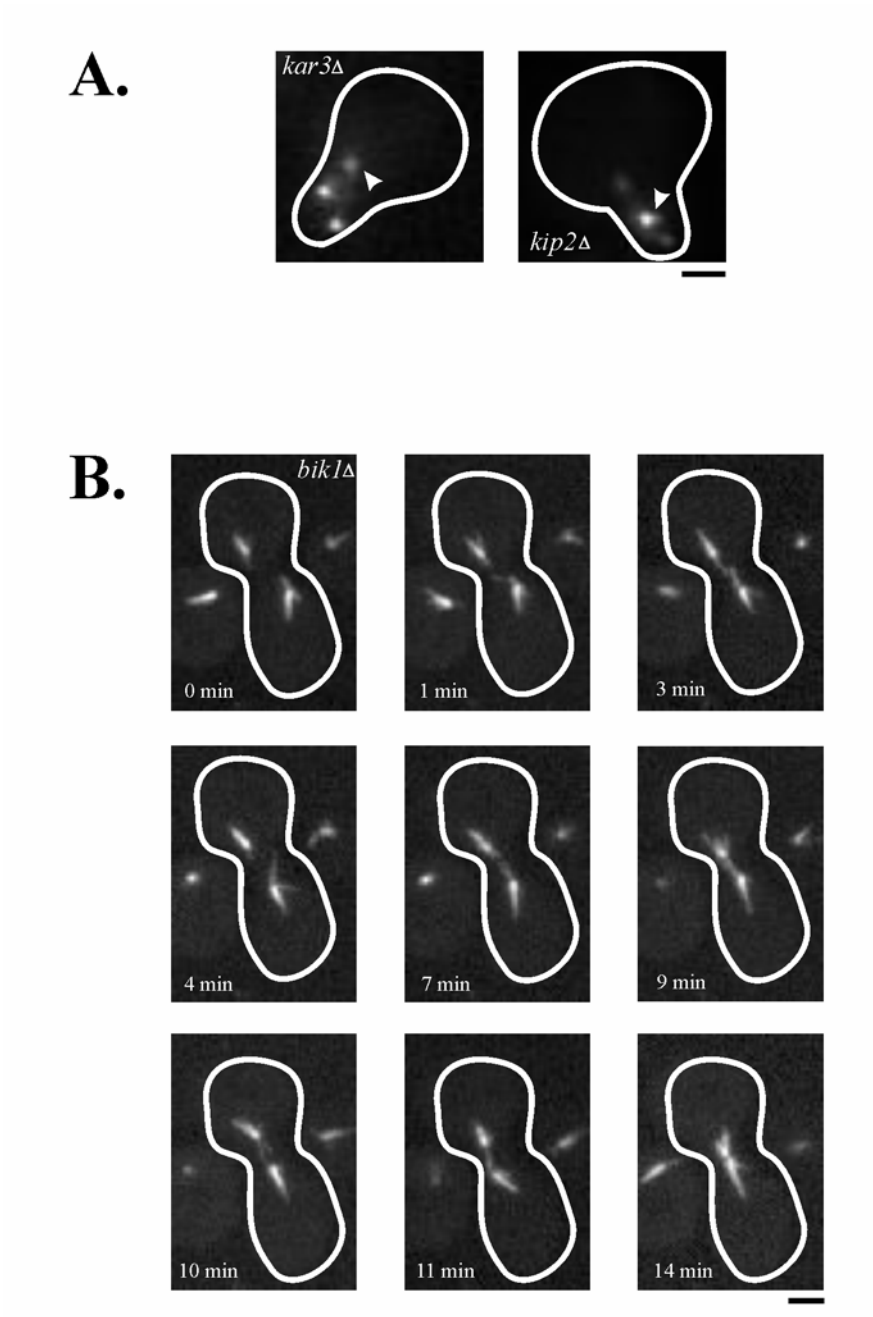
A.
kar3Δ
kip2Δ
B.
bik1Δ
0 min
1 min
3 min
4 min
7 min
9 min
10 min
11 min
14 min

Figure 3.9: Kar3p is required for plus end interactions during nuclear congression.

Kar3p is required to cross-link and shorten MTs. (A) MT behavior in bilateral *kar3Δ* crosses. (0-7 min) Long cytoplasmic MTs interacted with opposing MTs without resulting in nuclear congression. (11 and 15 min) SPBs were drawn together, but nuclear congression did not occur. (19-29 min) MTs appeared to interact at the plus end, but these interactions did not change SPB position or result in nuclear congression. (B) *kar3-1* mutants that were mated to wild-type cells resulted in cross-linked MTs that did not shorten. Arrowheads denote SPBs. (0-6 min) Two SPBs were separated by a GFP-Tub1p bridge of cross-linked MTs. (C) *kar3-1* cells expressing GFP-Tub1p mated to wild-type cells expressing Bik1p-3xGFP. Arrowheads denote SPBs. (0 min) Bik1p-3xGFP localizes to MT plus ends in the shmoo tip. (2 min) Initial MT-MT interactions occurred. (3.5 min) MTs are cross-linked without a strong Bik1p-3xGFP focus in between SPBs. (5.5-22 min) No Bik1p-3xGFP focus is present as MTs remain associated. Some movement of SPBs toward each other occurs over time. Bars, 2 μm.

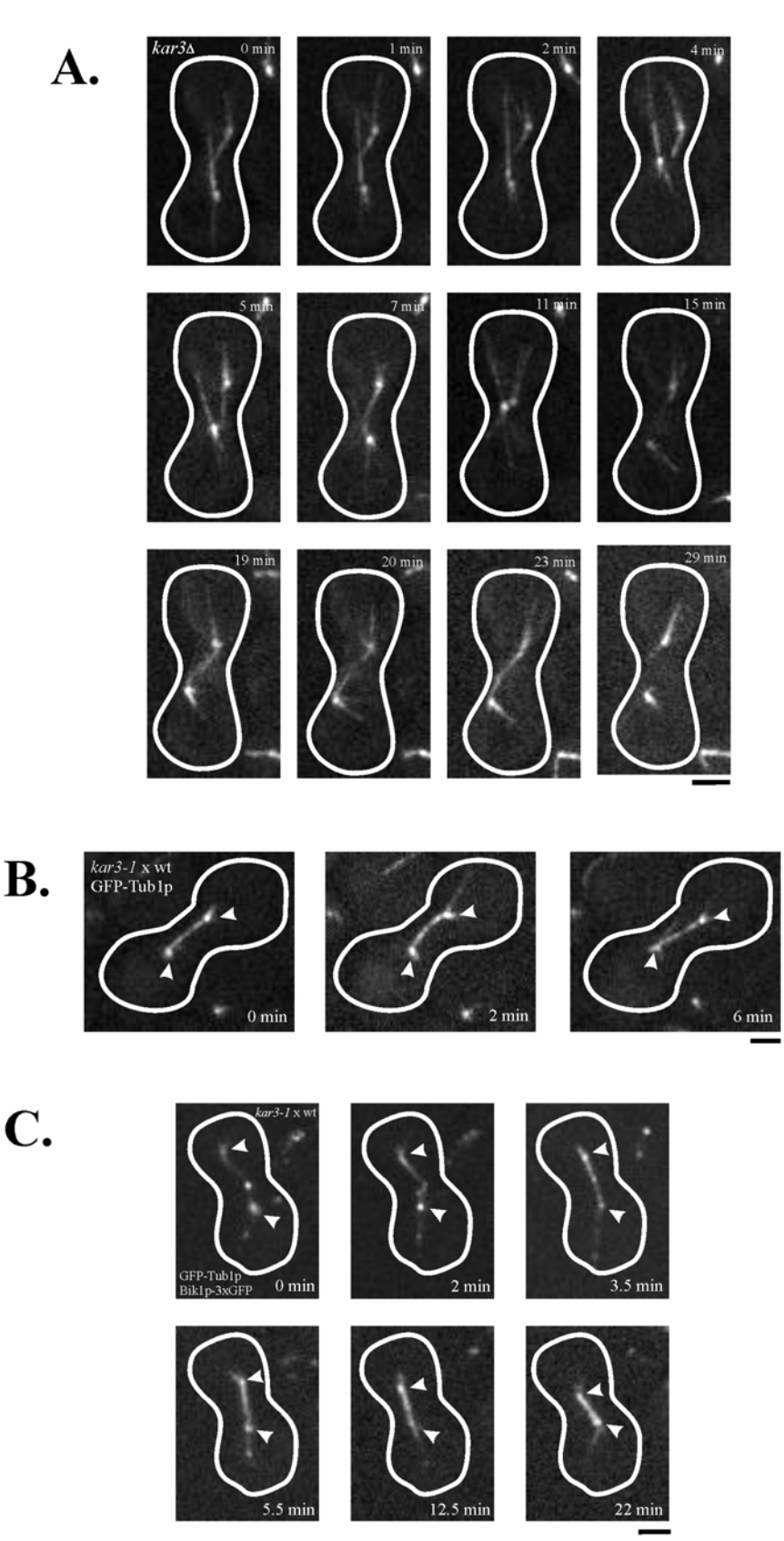
A.
kar3Δ
0 min
1 min
2 min
4 min
5 min
7 min
11 min
15 min
19 min
20 min
23 min
29 min
B.
kar3-1 x wt
GFP-Tub1p
0 min
2 min
6 min
C.
kar3-1 x wt
GFP-Tub1p
Bik1p-3xGFP
0 min
2 min
3.5 min
5.5 min
12.5 min
22 min

Figure 3.10: Model for nuclear congression in *S. cerevisiae*.

Nucleus is gray (black outline); SPB is black circle; MTs are black lines; Kar3p/Bik1p plus end complex is a small gray circle. (A and B) MTs previously attached to the shmoo tip probe the cytoplasm to find oppositely oriented MTs. (C) The plus ends of microtubules initiate interactions via Kar3p. (D) MT plus ends may slide past each other and cross-link, switching the MTs to a persistent depolymerization state. (E) SPBs move into the site of plus end interaction as MTs depolymerize, allowing nuclei to begin karyogamy.

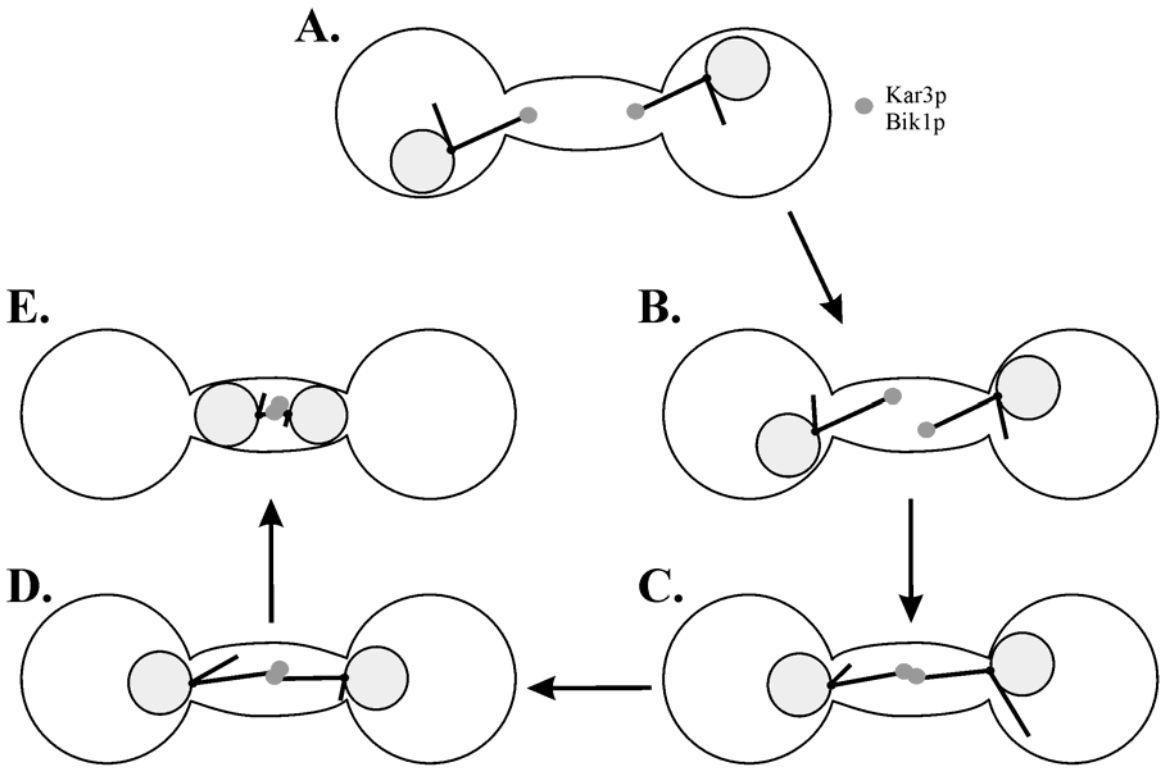
A.
Kar3p
Bik1p
B.
C.
D.
E.

Figure 3.S1: Kar3p-GFP localization during nuclear congression.

Kar3p-GFP localized to the MT plus ends during nuclear congression. SPBs marked by arrowheads; plus end capture site marked by asterisk. (0 s) Kar3p-GFP cells were crossed to GFP-Tub1p cells, resulting in labeling of MTs and plus ends. (15-30 s) Capture by opposite MT plus ends was visible. Note the asymmetric distance of SPBs from the capture site. (45-75 s) The left SPB overlapped with the plus end capture site and nucleated a cytoplasmic MT toward the opposite SPB. (90-135 s) Nuclear congression occurred as the right SPB moved toward the plus end cross-linking site where the other SPB was located. Bar, 2 μm.

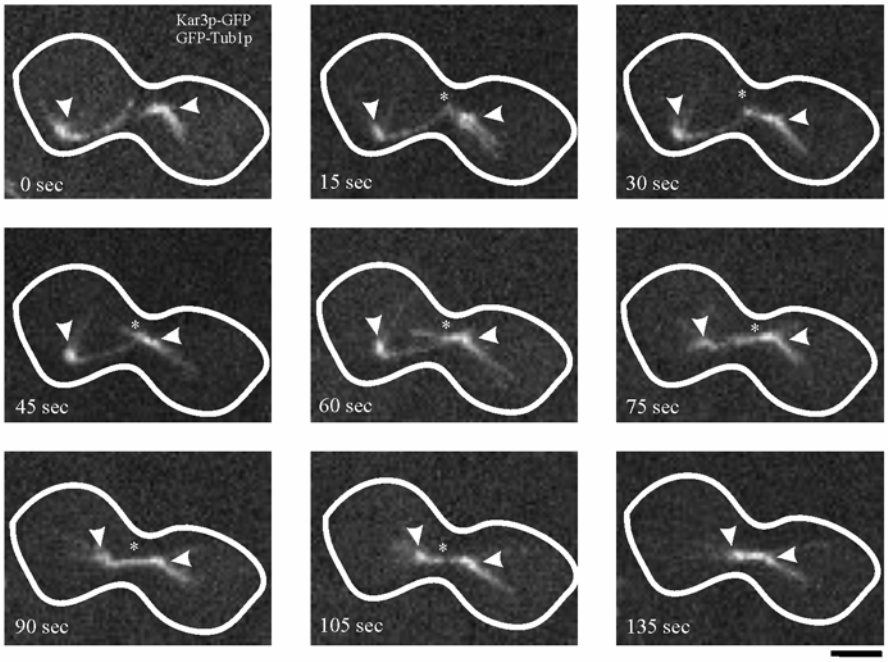
Kar3p-GFP
GFP-Tub1p
0 sec
15 sec
30 sec
45 sec
60 sec
75 sec
90 sec
105 sec
135 sec

Figure 3.S2: MTs rarely interact in *bik1Δ* cells.

Cytoplasmic MT behavior in bilateral *bik1Δ* crosses. GFP-Tub1p labeled MT behavior in *bik1Δ* cells. Two initially separated SPBs (0 min) nucleated MTs into the isthmus of the fused cells (1.5 and 2 min). The GFP-Tub1p fluorescence facing away from the site of cell fusion likely represents nuclear fluorescence. Rapid depolymerization of MTs contacting the isthmus between the cells often occurred (2.5-4 min). Bar, 2 μm.

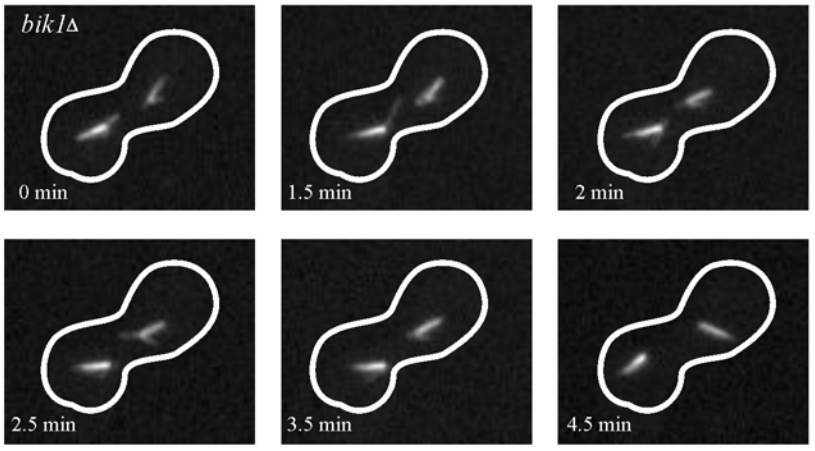
bik1Δ
0 min
1.5 min
2 min
2.5 min
3.5 min
4.5 min

Figure 3.S3: Nuclear congression failure in *kar3Δ* cells.

kar3Δ cells expressing GFP-Tub1p and Bik1p-3xGFP. Arrowheads denote SPB position. (0-0.5 min) Plus ends labeled with Bik1p-3xGFP came into proximity near the site of cell fusion. (1 min) The plus end connection was lost and both plus ends are labeled with Bik1p-3xGFP. Bar, 2 μm.

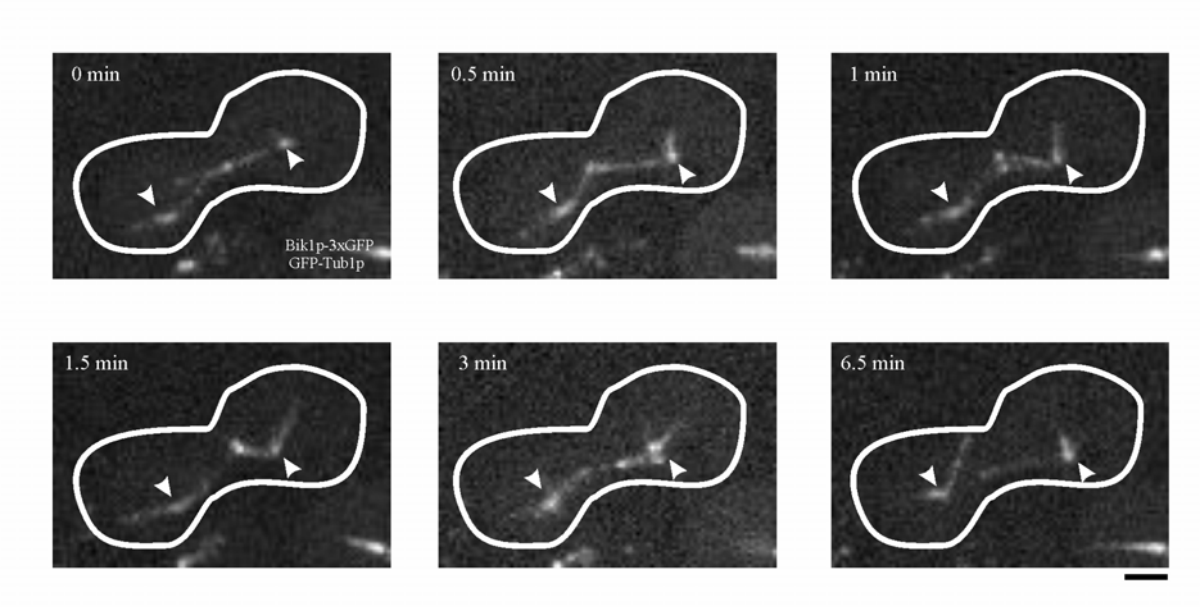
0 min
Bik1p-3xGFP
GFP-Tub1p
0.5 min
1 min
1.5 min
3 min
6.5 min

CHAPTER 4: SPINDLE DISASSEMBLY IS REGULATED GLOBALLY IN BUDDING YEAST

Contributing Authors: Jeffrey N. Molk, E. D. Salmon, and Kerry Bloom

Abstract

Genome instability occurs when >2 microtubule organizing centers are present in the same cell (Nigg, 2002; Sluder and Nordberg, 2004). How multi-spindle disassembly is regulated to ensure that spindle poles are segregated to both daughter cells remains unclear. Using karyogamy mutants in *Saccharomyces cerevisiae* to generate heterokaryons with two nuclei, we have tested if anaphase spindle elongation and disassembly dynamics are coordinated. In higher eukaryotes, the signal for anaphase onset is global and can override the spindle assembly checkpoint (Pinsky and Biggins, 2005; Rieder et al., 1995; Rieder et al., 1994). In contrast, spindle elongation proceeded autonomously in budding yeast heterokaryons. Though anaphase onset was autonomous, spindle disassembly was synchronous. This suggests spindle disassembly is regulated by a pancellular signal after anaphase onset. In support of this hypothesis, microtubule-based forces in the bud could pull the preanaphase nucleus into the daughter without activating spindle disassembly. We present a model where anaphase onset and the positioning of one SPB in the bud via cortical pulling forces activates mitotic exit in heterokaryons.

Introduction

The presence of multiple microtubule organizing centers is a characteristic of many cancers and can result in the formation of multiple spindles and chromosome instability (Nigg, 2002; Sluder and Nordberg, 2004). Therefore, it is of great interest to understand how cells with multiple spindles proceed through mitosis. In tissue culture cells, heterokaryons with two spindles can be formed by cell fusion and nuclei in different stages of the cell cycle will synchronize before mitosis begins (Johnson and Rao, 1970; Rao and Johnson, 1970). Once both nuclei have entered mitosis, the spindle checkpoint acts locally within each mitotic apparatus to ensure the chromosomes are bioriented before anaphase (Rieder et al., 1997). However, once one spindle satisfies the checkpoint and enters anaphase, the signal for anaphase onset is diffusive and global, overriding the checkpoint and ignoring unattached chromosomes in the second spindle (Rieder et al., 1997). The coordination between spindle disassembly was not analyzed in these studies. In *S. cerevisiae*, two spindle heterokaryons are formed in the mating pathway when nuclear fusion, or karyogamy, is defective (Conde and Fink, 1976b; Demeter et al., 2000). Specifically, mutants lacking Kar9p or Bik1p increase the frequency of two spindle heterokaryons by failing to efficiently move both nuclei together (Chapter 3) (Berlin et al., 1990; Miller and Rose, 1998). Previously, budding yeast heterokaryons were used to determine that the response to DNA damage locally inhibits anaphase onset in one nucleus but does not block the second spindle from elongating (Demeter et al., 2000). Here, we have used heterokaryons without DNA damage as a model system to study if the signals for anaphase onset and spindle disassembly are global.

Materials and Methods

Wild-type (GT1 and KBY 9258), *kar9Δ* (KBY 5058 and KBY 9291), and *bik1Δ* (KBY 9306 and KBY 9308) strains have been described previously (Chapter 3). Strain growth, mating assays, microscopy, image analysis, and image presentation were performed as previously described (Chapter 3). Multi-positional, five-plane Z-series were acquired every 1.5 - 3 min using a linearly encoded Ludl stage mounted on a Nikon TE-2000 stand (Chapter 3) controlled by MetaMorph 6.0. Therefore, the temporal resolution was limited to ~1.5 min. The positions of up to five image fields were memorized in MetaMorph and recorded as a single time-lapse stack file that was parsed into stack files for each image field using customized journals. Penetration of the bud was scored as the first image where the dSPB passed into the bud compartment. The image immediately prior to spindle elongation was designated as t = 0 min for quantitative analysis. In cells where nuclear transiting occurred, the image immediately prior to the first elongation of the spindle was designated as the time of penetration of the bud after anaphase onset. Spindle length measurements were made using the region tools in MetaMorph on calibrated image files and exported to a linked Microsoft Excel spreadsheet for analysis. At the time of spindle disassembly, the spindle length was recorded as 0 μm.

Results

Cells expressing GFP-Tub1p were mated and spindle dynamics were followed by time-lapse digital fluorescence microscopy. After karyogamy, wild-type cells form a single spindle that positioned at the bud neck and elongated into the zygotic bud during anaphase (Figure 4.1A and 4.1B). Anaphase onset was marked as the image frame that immediately preceded the elongation of the spindle (> 2 μm) (n = 11 cells; Figure 4.1B). Karyogamy mutants were analyzed to examine anaphase onset when two spindles were present. In 76% of *kar9Δ* and 82% of *bik1Δ* heterokaryons, one spindle entered anaphase 4.5 – 19 min before the second spindle (Table 4.1 and Figure 4.2). The mitotic apparatus inherited by the daughter cell (dMA) or the mitotic apparatus retained in the mother cell (mMA), could begin anaphase first. In 60% of *kar9Δ* cells, the dMA elongated an average of 4.5 min before the mMA (Figures 4.2A and 4.3). In 16% of *kar9Δ* heterokaryons, the mMA entered anaphase an average of 19 min before the dMA (Figure 4.2A). Similarly, the dMA elongated first in 50% of *bik1Δ* heterokaryons with the mMA entering anaphase 9 min later on average (Figure 4.2B). Elongation of the mMA first occurred in 32% of *bik1Δ* cells and resulted in an average lag of 19 min in anaphase onset of the dMA (Figure 4.2B). In all cells where the mMA elongated first, the dMA was pulled into the bud and could move rapidly between the mother and daughter, a phenomenon known as nuclear transiting. During nuclear transiting, the dMA remained in preanaphase for 4.5 – 34 min after the mMA entered anaphase (Figure 4.2). These data suggest anaphase onset is regulated locally within each nucleus in *S. cerevisiae* heterokaryons.

Following anaphase onset in wild-type cells, the daughter bound SPB (dSPB) enters the bud and activates the Mitotic Exit Network (MEN), ultimately triggering spindle

disassembly (Bosl and Li, 2005; D'Amours and Amon, 2004). Disassembly was scored when continuous GFP-Tub1p spindle fluorescence was lost in late anaphase. In wild-type mating cells after anaphase onset, the interval from dSPB penetration of the bud to spindle disassembly averaged 34 min (Table 4.2), similar to the timing of mitotic exit in vegetative cells (Chapter 2). Only one SPB was inherited by the bud (n = 11/11 cells). Spindle orientation defects in *kar9Δ* mutants resulted in nuclei positioned away from the bud neck in the mother cell (Figure 4.3A). The duration of anaphase was similar to wild-type cells, but after anaphase onset, there was a 4 min delay in penetration of the bud neck by the dSPB (data not shown). Thus, in *kar9Δ* heterokaryons, the interval from dSPB penetration of the bud neck to spindle disassembly was reduced to 27 min on average (Table 4.2). In *kar9Δ* cells, both spindles disassembled within 1 – 3 min of each other (Table 4.1). The mMA could be trapped at one end of the mother cell, resulting in a horseshoe-shaped spindle that disassembled shortly after the dMA (Figure 4.3B). The bud inherited a single SPB in 91% of *kar9Δ* mutants (n = 23 cells). In *bik1Δ* cells, the time from dSPB passage of the bud neck after anaphase onset to spindle disassembly averaged 25 min (Table 4.2). The difference in the disassembly of both spindles was 2 – 5 min (Table 4.1). The higher variation in *bik1Δ* heterokaryon spindle disassembly was related to premature breakdown. In *bik1Δ* cells, anaphase spindles would bend and buckle, resulting in the loss of GFP-Tub1p fluorescence as if the spindle was broken in the middle (Figure 4.4B; broken spindles – *bik1Δ* = 9/18 cells, *kar9Δ* = 0/16 cells). This suggests that, unlike wild-type and *kar9Δ*, spindles in *bik1Δ* cells do not tolerate bending. 70% of *bik1Δ* heterokaryons segregated one SPB into the bud (n = 27 cells). The average interval between spindle disassembly in heterokaryons was near the temporal resolution of our imaging and lower than the average interval for anaphase onset

between both spindles (1 – 5 min vs. 4.5 – 19 min). Therefore, spindle disassembly is initiated by a global signal in budding yeast.

The global signal for spindle disassembly in zygotes could be activated after anaphase onset as one SPB passes into the bud. Alternatively, mitotic exit may not require anaphase onset and could be activated upon the first passage of the SPB into the bud. To distinguish between these two possibilities, nuclear transiting was examined in zygotes. Nuclear transiting occurred at least once in 50% of wild-type (n = 12 cells), 52% of *kar9Δ,* and 62% of *bik1Δ* zygotes (Table 4.1). In heterokaryons, nuclear transiting was observed in all cells where the mMA elongated first (Table 4.1). When the mMA elongated first, there was a lag in anaphase onset of the dMA that was pulled into the bud (Figures 4.4B and 4.S1). This suggests that positioning of the preanaphase spindle in the bud may locally inhibit anaphase. However, if dSPB penetration into the bud is sufficient to activate mitotic exit, then spindles should disassemble ~30 min after the dMA passed into the daughter during nuclear transiting. In cells where nuclear transiting occurred, the time from the first passage of the dMA into the bud to spindle disassembly averaged 48 min for wild-type, 42 min for *kar9Δ*, and 52 min for *bik1Δ* (Table 4.2). Thus, the penetration of the dSPB into the bud only triggers mitotic exit after anaphase onset.

Discussion

Using heterokaryons, we have examined the timing of anaphase onset and mitotic apparatus disassembly during multi-spindle mitoses. Unlike metazoans, our data suggests anaphase onset is locally regulated in heterokaryons. This agrees with Demeter et al. (2000), who found that anaphase onset was locally inhibited after DNA damage in only one of the heterokaryon nuclei. Our results demonstrate that the preanaphase spindle can transit into the zygotic bud without activating mitotic exit (Figures 4.3 and 4.4). Thus, in addition to aberrant chromosome attachments in the nucleus, defects in spindle positioning may delay anaphase onset. Spindle disassembly, however, is initiated by a pancellular signal. The global signal for spindle disassembly is activated after anaphase onset once the dSPB penetrates into the bud (Figure 4.4 and Table 4.2).

Our observations support the following model for mitotic exit in heterokaryons (Figure 4.5). The entry into anaphase triggers spindle elongation and is coincident with dynein-dependent cortical pulling forces that position one SPB in the bud (Adames and Cooper, 2000; Yeh et al., 1995). Mitotic exit is activated when the dSPB enters the bud after anaphase onset (Table 4.2) (Chapter 2), resulting in the disassembly of both spindles coordinately. In vegetative cells, MEN activation allows Cdc14p to remain in the cytoplasm (D'Amours and Amon, 2004). The release of Cdc14p from both nuclei could act as the global trigger for mitotic exit. If the cortical pulling forces are uncoupled from anaphase onset, the dMA can transit into the bud. Nuclear transiting does not inhibit the mMA from entering anaphase. However, disassembly of both spindles does not occur until the dMA positions along the mother-bud axis and elongates. This suggests that the dMA may inhibit the mMA from exiting mitosis until both spindles enter anaphase. There are at least three

mechanisms that could result in dMA feedback on the mMA: 1) Anaphase onset of the dMA sends a positive signal to the mMA to activate mitotic exit. 2) There is a threshold of Cdc14p that must be released into the cytoplasm before mitotic exit can proceed. In this scheme, release of one half of the cellular Cdc14p by the mMA is insufficient to activate mitotic exit; 3) The mMA may transiently release Cdc14p but the inappropriate positioning of the dMA in the bud activates the spindle position checkpoint. Thus, Cdc14p will ultimately be retained in each nucleus until the dMA is positioned along the mother-bud axis and begins to elongate. In any case, the cell will ensure only one SPB is inherited by the daughter cell, avoiding subsequent multi-spindle divisions.

Acknowledgements

We thank David Bouck, Jay Gatlin, Erin McCarthy, and members of the Bloom and Salmon laboratories for advice, assistance, and critical readings of the manuscript. This work was funded by the Human Frontier Science Program grant RGP29/2003 (E.D.S.), and the National Institutes of Health grants GM-24364 (E.D.S.), GM-60678 (E.D.S.), and GM-32238 (K.B.).

Tables and Figures

Mating	AO[A]	AO Difference[B]	BD Difference[C]	NT[D]/n
kar9Δ x *kar9Δ*	Dau	4.5 +/- 3.7	1.5 +/- 1.6	8/15
	Sim	0	1.0 +/- 1.8	1/6
	Mom	19 +/- 15	3.3 +/- 4.2	4/4
bik1Δ x *bik1Δ*	Dau	8.9 +/- 10	4.9 +/- 4.6	7/17
	Sim	0	2.1 +/- 3.3	3/6
	Mom	19 +/- 7.0	5.6 +/- 4.8	11/11

p-value > 0.01 for all measurements when comparing *kar9Δ* versus *bik1Δ* cells.
[A]AO – Scoring for Anaphase Onset where the first spindle that elongated was inherited by the daughter (Dau), the mother (Mom), or both elongated simultaneously (Sim).
[B]AO Difference – The difference in the time (min) of anaphase onset between the two spindles.
[C]BD Difference – The interval (min) between disassembly of the two spindles.
[D]NT – Nuclear Transiting.

Table 4.1: Kinetics of anaphase in heterokaryons.

Karyogamy mutants expressing GFP-Tub1p were mated, allowed to bud, and then the followed by time-lapse fluorescence microscopy to determine the kinetics of anaphase.

Mating	Nuclear Transit to BD[A]	AO to BD[A]	n[B]
wt x wt	48 +/- 7.6	34 +/- 4.8	4/9
kar9Δ x *kar9Δ*	52 +/- 20	27 +/- 9.7	10/19
bik1Δ x *bik1Δ*	42 +/- 12	25 +/- 8.2	15/20

[A]Time reported in minutes
[B]n is number of observations for column one/column two

Table 4.2: Kinetics of mitotic exit in heterokaryons.

Figure 4.1: Spindle elongation in the first zygotic division of wild-type cells.

Spindle dynamics in the first zygotic division of budding yeast. (A) Schematic of the mating pathway. Cells that enter the mating pathway form shmoos and MTs (black lines) orient the nucleus (gray circle) to the shmoo tip. After cell fusion, haploid nuclei move together and perform karyogamy. Once a bud is formed, the mitotic spindle assembles (dark gray line) and is positioned at the bud neck. Anaphase spindle elongation results in dSPB penetration of the bud and spindle disassembly, resulting in one nucleus in the bud and one nucleus in the fused cell body, or mother cell. (B) *Upper panel*: Spindle positioning and elongation during the first zygotic division in wild-type cells expressing GFP-Tub1p imaged by confocal microscopy. Bud faces to lower right. Before anaphase, spindles rotated, allowing MTs from both SPBs to interact with the bud neck (-32 min – 0 min). After anaphase onset, the spindle elongated and MTs from the dSPB interacted with the bud cortex, resulting in bending of the spindle into a C-shape (0 min – 24 min, arrowheads). Disassembly resulted in the bud and mother each inheriting one SPB (30 min). Bar, 2 μm, DIC image bottom right. *Lower panel*: Plot of spindle length over time. Arrow marks anaphase onset.

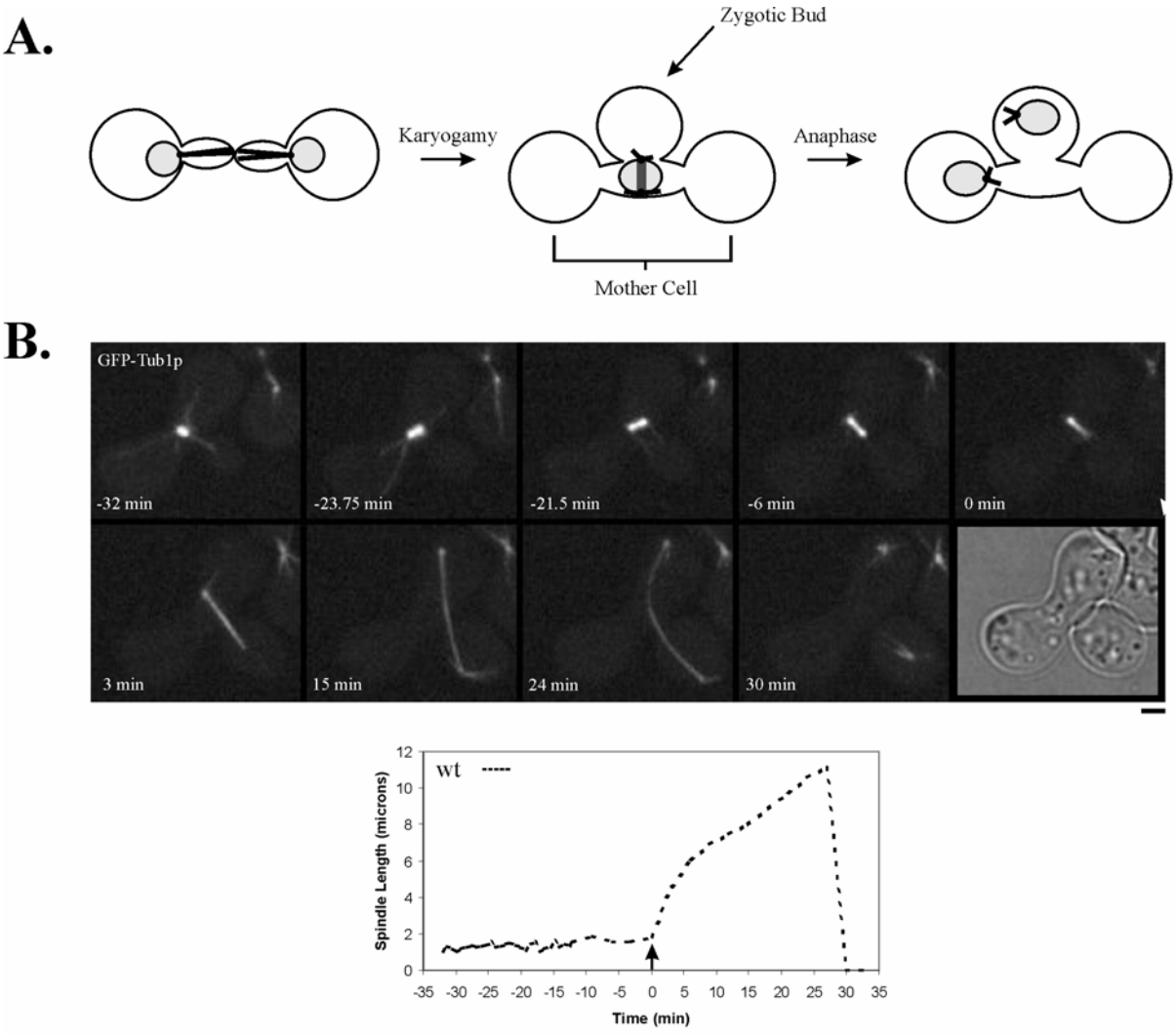
A.
Zygotic Bud
Karyogamy
Anaphase
Mother Cell
B.
GFP-Tub1p
-32 min
-23.75 min
-21.5 min
-6 min
0 min
3 min
15 min
24 min
30 min
wt
Spindle Length (microns)
Time (min)

Figure 4.2: Quantitative analysis of anaphase onset in heterokaryons.

Histograms of the difference in anaphase onset between two spindles. Difference was calculated as the time of second spindle elongation minus the time of first spindle elongation. Black bars – dMA data; gray bars, mMA data. (A) *kar9Δ* heterokaryons. (B) *bik1Δ* heterokaryons.

A.

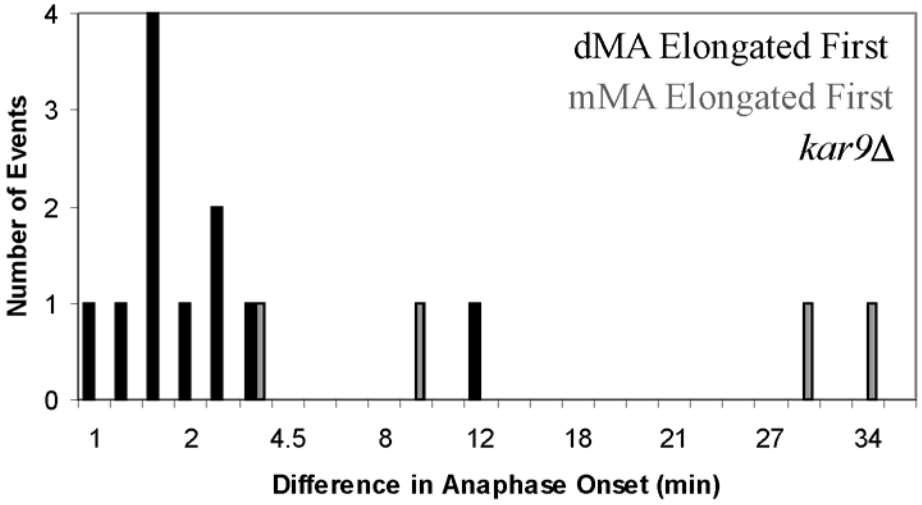
dMA Elongated First
mMA Elongated First
*kar9*Δ
Number of Events
0
1
2
3
4
1
2
4.5
8
12
18
21
27
34
Difference in Anaphase Onset (min)

B.

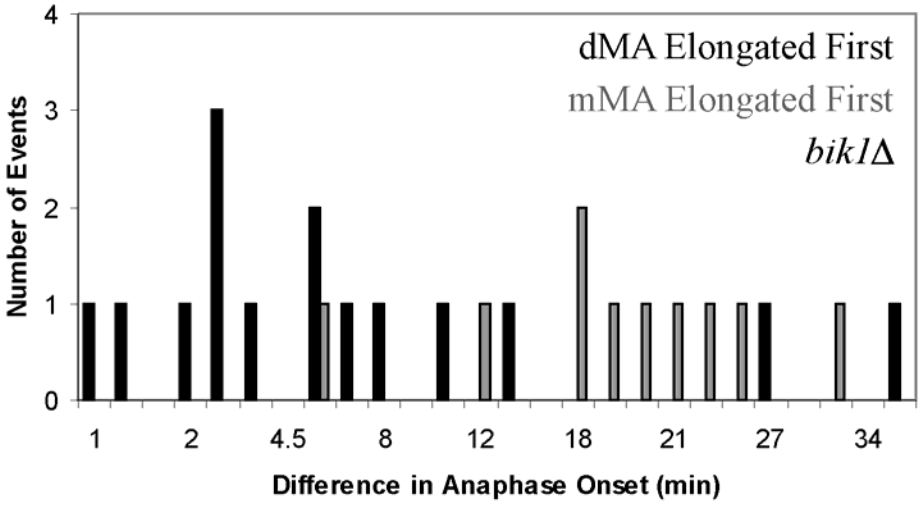
dMA Elongated First
mMA Elongated First
*bik1*Δ
Number of Events
0
1
2
3
4
1
2
4.5
8
12
18
21
27
34
Difference in Anaphase Onset (min)

Figure 4.3: Spindle dynamics in *kar9Δ* heterokaryons.

(A) Schematic of the *kar9Δ* karyogamy defect. Cells that enter the mating pathway form shmoos but cannot orient MTs (black lines) to the shmoo tip, resulting in defects in nuclear positioning (gray circle). After cell fusion, failed karyogamy results in each of the two haploid nuclei forming spindles (dark gray lines) that do not position at the bud neck. Anaphase spindle elongation results in the inheritance of one nucleus into the bud while three remain in the mother cell. (B) and (C) depict mitosis in *kar9Δ* heterokaryons expressing GFP-Tub1p that were imaged by wide-field microscopy. (B) *Upper panel*: The dMA positions at the bud neck and enters anaphase while the mMA is at the periphery of the cell (-4.5 min – 0 min). Once the mMA enters anaphase, it is trapped in the cell body, bending the spindle into a horseshoe shape (3 min – 21 min). *Lower panel*: Plot of spindle length over time. Black line – dMA; gray line – mMA; dashed black line – wild-type. Arrows denote anaphase onset of dMA (black) and mMA (gray). (C) *Upper panel*: Spindles initially position away from the bud neck (-16 min). The dMA exhibits nuclear transiting before spindle elongation (-14 min – 0 min). Anaphase spindle elongation and spindle disassembly results in the inheritance of one SPB by the bud (26 min). Bar, 2 μm, DIC image bottom right. *Lower panel*: Graph of spindle length over time. Black line – dMA; gray line – mMA; dashed black line – wild-type. Arrows denote anaphase onset of dMA (black) and mMA (gray). Black arrowheads mark nuclear transiting events when the dMA passed the bud neck and entered the bud. Multiple passes between the mother and bud were observed.

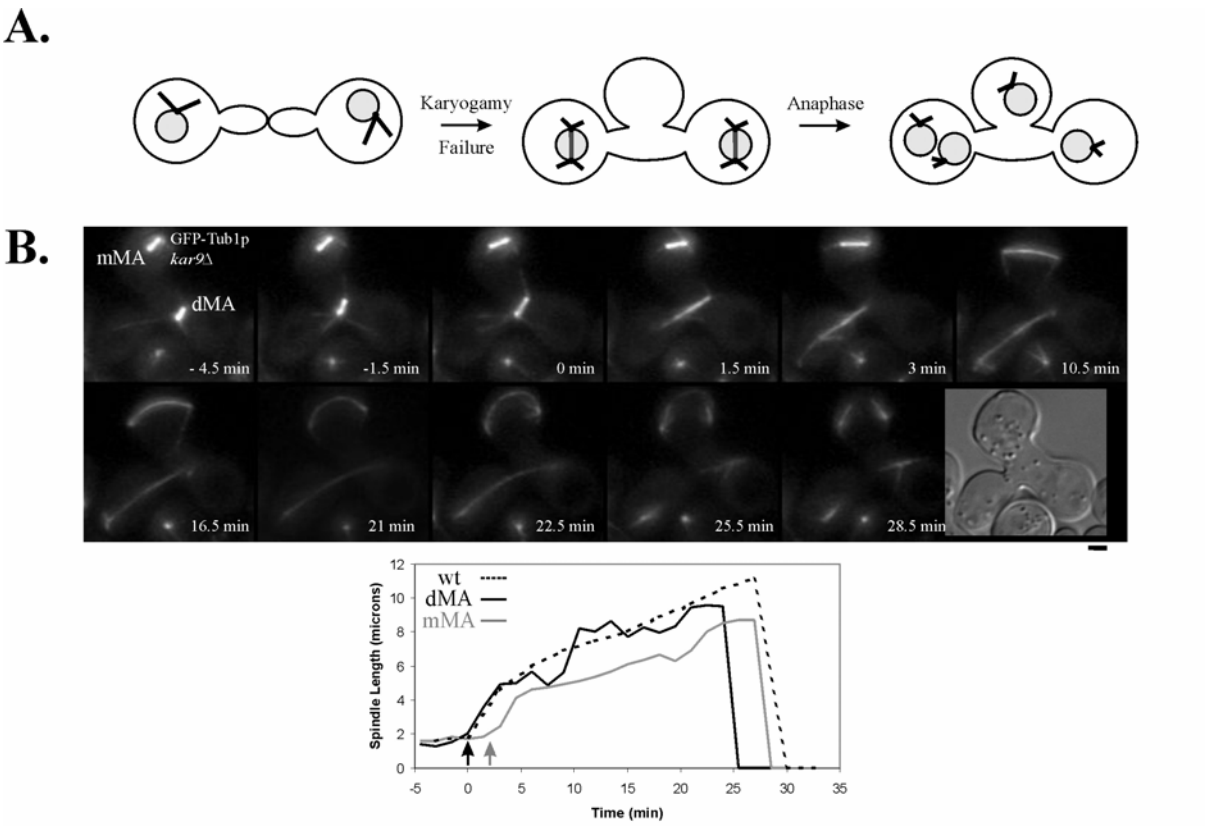
A.
Karyogamy
Failure
Anaphase
B.
mMA
GFP-Tub1p
kar9Δ
dMA
- 4.5 min
-1.5 min
0 min
1.5 min
3 min
10.5 min
16.5 min
21 min
22.5 min
25.5 min
28.5 min
wt
dMA
mMA
Spindle Length (microns)
Time (min)
C.
GFP-Tub1p
kar9Δ
dMA
mMA
-16 min
-14 min
-10 min
-6 min
-2 min
0 min
2 min
4 min
6 min
10 min
18 min
22 min
26 min
wt
dMA
mMA
Spindle Length (microns)
Time (min)

Figure 4.4: Spindle dynamics in *bik1Δ* heterokaryons.

(A) Schematic of the *bik1Δ* karyogamy defect. Cells induced to mate form shmoos and orient nuclei (gray circle) to the mating projection but do not make persistent MT (black lines) attachment to the shmoo tip. MTs are shorter than wild-type in *bik1Δ* heterokaryons. After cell fusion, karyogamy is defective because MT-MT interactions are rare, resulting in the formation of two haploid spindles (dark gray lines) that position at the bud neck. Anaphase spindle elongation results in the inheritance of one nucleus into the bud while three remain in the mother cell. (B) *Upper panel*: Confocal images of mitosis in *bik1Δ* heterokaryons. Spindles positioned at the bud neck (-20 min) and the dMA transited into the bud (-9 min). The dMA collapsed and reformed during preanaphase while the mMA entered anaphase (0 min – 30 min). The dMA entered anaphase but bending of the spindle induced disassembly before the mMA (31 min – 39 min). Bar, 2 μm, DIC image bottom right. *Lower panel*: Plot of spindle length over time. Black line – dMA; gray line – mMA; dashed black line – wild-type. Arrows denote anaphase onset of dMA (black) and mMA (gray). Note the long delay between anaphase onset of the dMA and the mMA.

A.

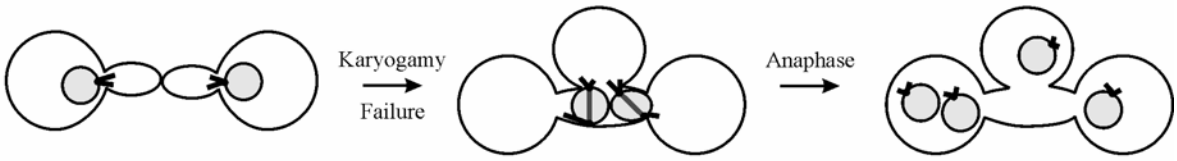
Karyogamy
Failure
Anaphase

B.

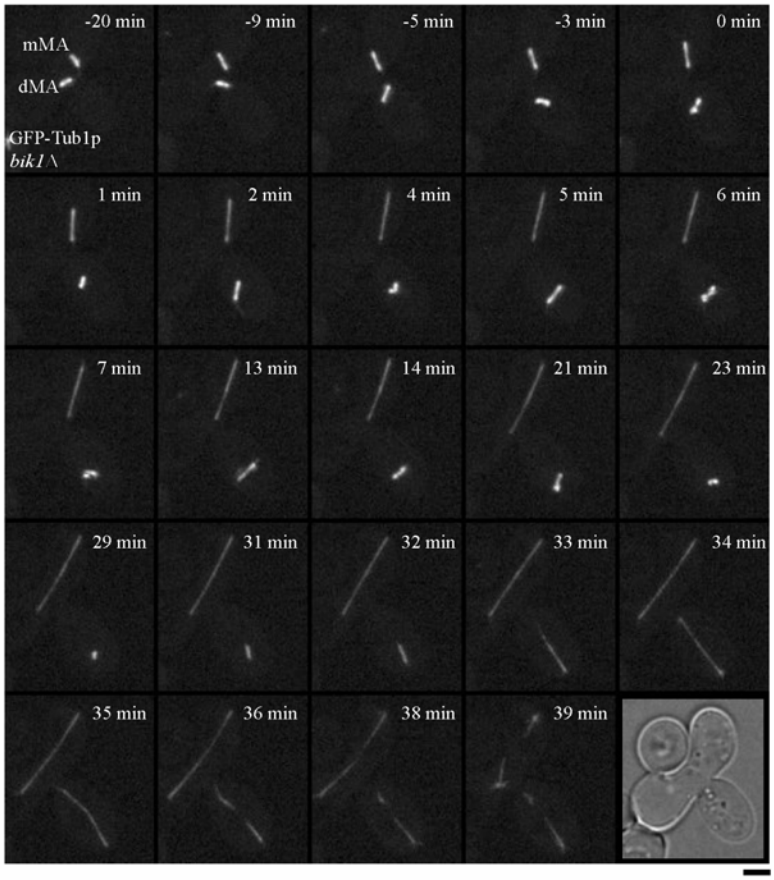
-20 min
-9 min
-5 min
-3 min
0 min
mMA
dMA
GFP-Tub1p
bik1Δ
1 min
2 min
4 min
5 min
6 min
7 min
13 min
14 min
21 min
23 min
29 min
31 min
32 min
33 min
34 min
35 min
36 min
38 min
39 min

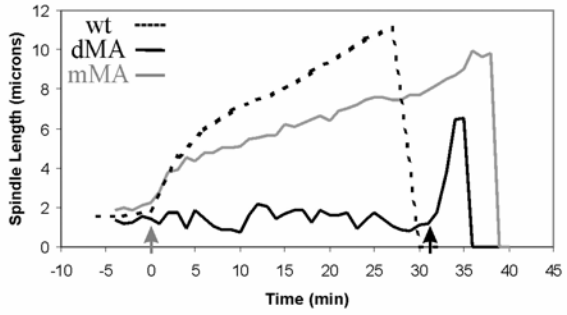
wt
dMA
mMA
Spindle Length (microns)
Time (min)
0
2
4
6
8
10
12
-10
-5
0
5
10
15
20
25
30
35
40
45

Figure 4.5: Model for spindle dynamics in heterokaryons.

SPBs – black circles; spindle MTs – gray line; cytoplasmic MTs – black line. In heterokaryons, anaphase onset is coincident with cytoplasmic MT sliding along the bud cortex (left) to drive one elongating spindle into the bud. This results in the inheritance of one SPB by the daughter cell. In contrast, when nuclear transiting occurs (right), cortical pulling forces move the dMA into the bud. The mMA enters anaphase while the dMA positions along the mother-bud axis. Entry of the dMA into anaphase leads to mitotic exit, resulting in the inheritance of one SPB by the bud.

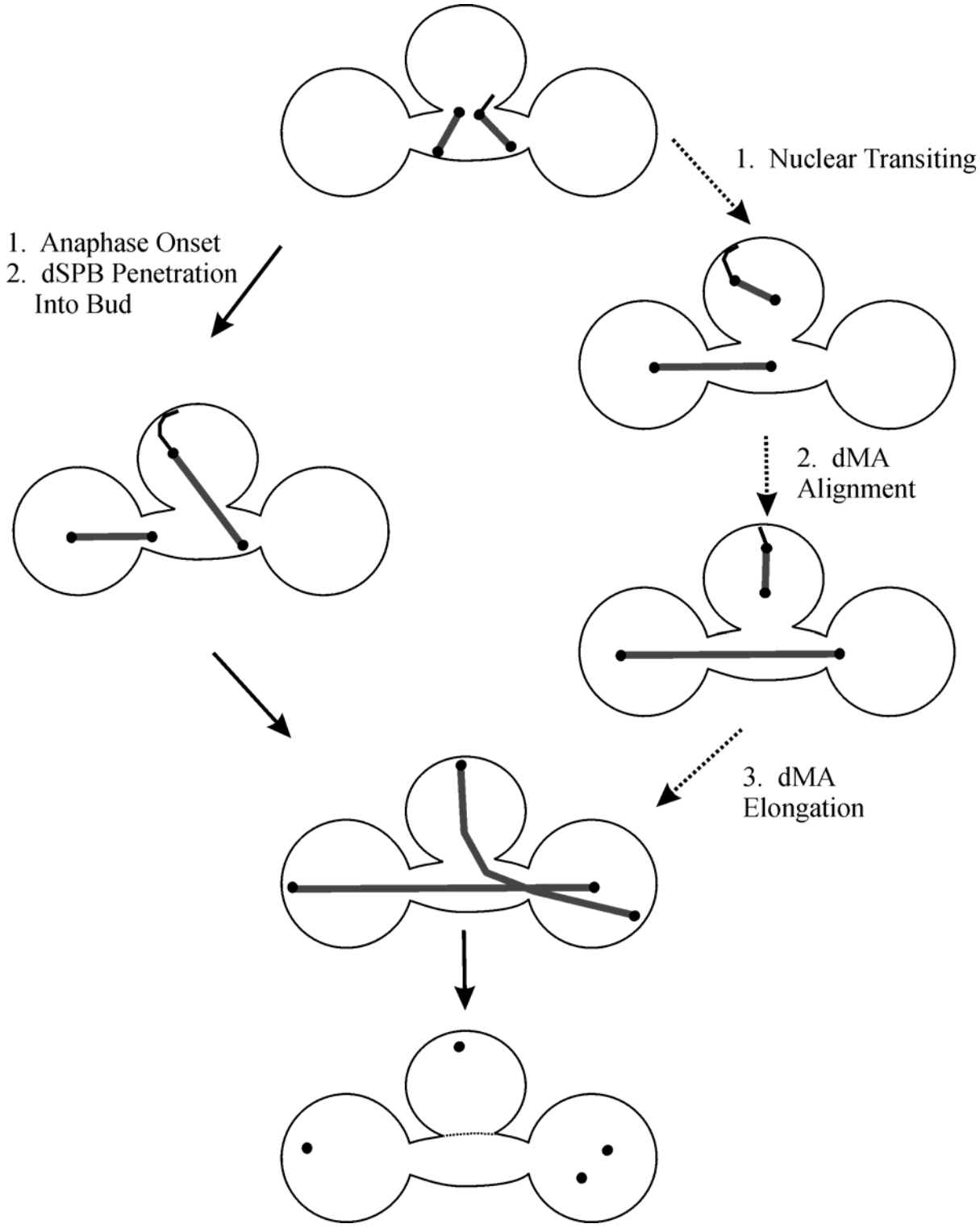
1. Nuclear Transiting
1. Anaphase Onset
2. dSPB Penetration
Into Bud
2. dMA
Alignment
3. dMA
Elongation

Figure 4.S1: Spindle dynamics in *kar9Δ* heterokaryons when the mMA elongates first.

Upper panel: Wide-field images of mitosis in *kar9Δ* heterokaryons. The mMA begins to elongate while the dMA is pulled into the bud (-2 min – 14 min). After the dMA rotates in the bud, spindle elongation begins (20 min – 48 min). Both spindles disassemble together (52 min). Bar, 2 μm, DIC image bottom right. *Lower panel*: Plot of spindle length over time. Black line – dMA; gray line – mMA; dashed black line – wild-type. Arrows denote anaphase onset of dMA (black) and mMA (gray). Note the long delay between anaphase onset of the dMA and the mMA.

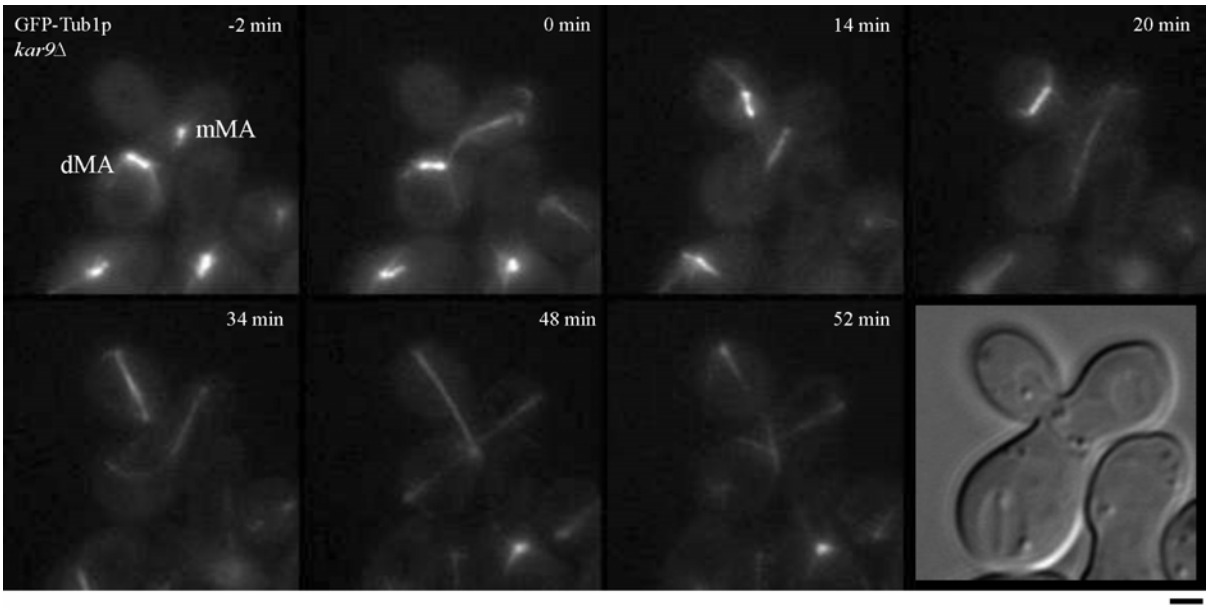
GFP-Tub1p
kar9Δ
-2 min
0 min
14 min
20 min
mMA
dMA
34 min
48 min
52 min

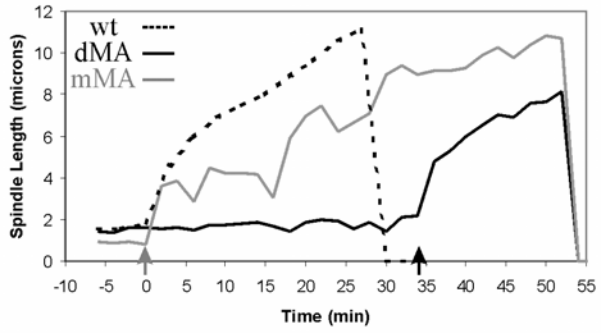
wt
dMA
mMA
Spindle Length (microns)
Time (min)
0
2
4
6
8
10
12
-10
-5
0
5
10
15
20
25
30
35
40
45
50
55

CHAPTER 5: PLUS END BINDING PROTEINS ARE REQUIRED TO RESIST MECHANICAL STRESS ON THE SPINDLE DURING MITOSIS

Contributing Authors: Jeffrey N. Molk, K. Mythreye, Melissa K. Gardner, Julian Haase, Ajit P. Joglekar, David J. Odde, E. D. Salmon, and Kerry Bloom

Abstract

During cell division, the mitotic apparatus must assemble while resisting mechanical stresses that promote spindle collapse. Models for spindle assembly propose that a balance of inward and outward forces from microtubule motor proteins result in a stable spindle length. In budding yeast, a major source of the inward force has been proposed to arise from the microtubule plus end binding protein Kar3p. Here we have tested if plus end binding proteins are required to resist mechanical stress on the spindle during mitosis. To introduce a mechanical stress on the spindle, we have used activated dicentric chromosomes that stretch between spindle poles in anaphase. When a conditional dicentric chromosome is activated, plus end binding proteins that function in the central spindle, including Kar3p, Bim1p, and Ase1p, are essential for cell viability. In the absence of plus end binding proteins, spindles break and dicentric chromosome mal-segregation is elevated. Mechanical stress is also present in preanaphase. We show Kar3p functions at interpolar microtubule plus ends to facilitate spindle pole separation in preanaphase. Together, our data supports a model for spindle assembly where Kar3p cross-links anti-parallel microtubules to resist inward forces from sister chromatid cohesion in metaphase and lagging chromosomes in anaphase.

Introduction

The mitotic spindle must assemble and function correctly in each cell division to prevent abnormal chromosome segregation events that lead to aneuploidy, a common feature of human solid tumors (Kops et al., 2005). In the bipolar spindle, microtubules (MTs) can interact to form interpolar MTs (ipMTs) or MT plus ends can attach to the kinetochore (kMTs) that forms on centromeric DNA sequences (Rieder and Salmon, 1998). MT associated proteins (MAPs), including motor proteins, establish and maintain dynamic MT-MT or kMT interactions (Kline-Smith et al., 2005). In *Saccharomyces cerevisiae*, MT dynamics are regulated at the plus end (Maddox et al., 2000; Tanaka et al., 2005). Thus, budding yeast is an ideal model system to examine how plus end binding proteins act on MTs to form spindles and segregate chromosomes.

A subset of MT motor proteins that bind plus ends have been implicated in spindle assembly and kinetochore function. Kar3p is a kinesin 14 motor protein with minus end motility that localizes to and depolymerizes MT plus ends (Chu et al., 2005; Endow et al., 1994; Maddox et al., 2003b; Sproul et al., 2005). Kar3p has been shown to genetically antagonize Cin8p and Kip1p, plus end directed kinesin 5 motors that slide anti-parallel MTs past one another (Kapitein et al., 2005; Roof et al., 1992; Saunders and Hoyt, 1992). Spindles collapse in *cin8 kip1* double mutants, consistent with a role in driving spindle poles apart (Roof et al., 1992; Saunders and Hoyt, 1992). Spindle collapse in *cin8 kip1* cells was suppressed by loss of Kar3p (Hoyt et al., 1993; Saunders and Hoyt, 1992). There are multiple hypotheses for the function of Kar3p during mitosis. The minus end motility of Kar3p could antagonize Cin8p and Kip1p on ipMTs by generating an inward force (Figure 5.1A). Alternatively, Kar3p depolymerase activity at kMT plus ends could pull the spindle

poles together to oppose Cin8p and Kip1p (Figure 5.1B) (Hildebrandt and Hoyt, 2000; Middleton and Carbon, 1994). In either case, loss of the Kar3p inward force is predicted to result in longer spindles. In fact, *kar3Δ* spindles are shorter than wild-type (Zeng et al., 1999). Similarly, spindles are shorter in the absence of Cik1p, an accessory factor required for Kar3p function at plus ends (Page and Snyder, 1992; Sproul et al., 2005). This suggests Kar3p may be required for spindle assembly and not exclusively as an inward force. Kar3p has been shown to cross-link cytoplasmic MT plus ends in the mating pathway (Chapter 3) (Meluh and Rose, 1990). Thus, an alternative hypothesis is that Kar3p cross-links MTs during spindle assembly (Figure 5.1C).

To examine how Kar3p and other plus end binding proteins function during mitosis, we have developed a method to introduce mechanical stress on the spindle. When cells enter anaphase, the cohesion between sister chromatids is dissolved, removing an inward force, or mechanical stress, on the spindle (Michaelis et al., 1997). The presence of a lagging dicentric chromosome can generate mechanical stress on the spindle in anaphase when cohesion is absent. Dicentric chromosomes are constructed by introducing a transcriptionally regulated centromere (*GAL-CEN*) at chromosome III (Chr III) (Hill and Bloom, 1989). Activation of the dicentric chromosome results in a midanaphase pause and a breakage-DNA repair cycle that generates monocentric rearrangement products (Brock and Bloom, 1994; Koshland et al., 1987; Yang et al., 1997). The viability of cells with an activated dicentric chromosome is reduced >1,000-fold in the absence of the DNA repair protein Rad52p (Brock and Bloom, 1994). Kinetochore mutants with activated dicentric chromosomes display a decrease in the frequency of DNA lesions, but cell viability is not compromised (Doheny et

al., 1993; Mythreye and Bloom, 2003). However, little is known about the behavior of cells with activated dicentric chromosomes in the absence of plus end binding proteins.

In this study, we have examined how plus end binding proteins resist mechanical stress during mitosis. Our results show Kar3p, Bim1p, and Ase1p are a subset of plus end binding proteins that are required for viability in the presence of an activated dicentric chromosome. Activation of the dicentric chromosome in *bim1Δ* cells resulted in elevated chromosome mal-segregation and broken spindles. A second mechanical stress occurs in preanaphase, when sister chromatids are attached to both spindle poles. We find that spindles are shorter and wider in *kar3Δ* and *bim1Δ* cells. Additionally, Kar3p localizes to ipMT plus ends and binds the anaphase spindle. Our data supports a model for spindle assembly in which Kar3p, Bim1p, and other plus end binding proteins are required to resist inward forces during mitosis that arise from sister chromatid cohesion. Further, we propose the ability of plus end binding proteins to resist mechanical stress on the spindle acts as a mechanism that prevents aneuploidy.

Materials and Methods

Media, growth conditions, and strain construction

Strains and plasmids used in this study are listed in Table 5.3. Media and strains, including gene deletions and GFP fusions, were prepared as described previously (Chapter 2) (Mythreye and Bloom, 2003). Deletions of *BIM1* were confirmed by PCR amplification and by sensitivity to 15 μg/mL of benomyl. Strains were maintained at 25°C except for some wild-type and *bim1Δ* cells carrying dicentric chromosomes that were grown at 32°C. *kar3Δ* cells expressing GFP fusion proteins were maintained at 25°C overnight and switched to 32°C for two to three hours prior to imaging. Cells with a conditional dicentric chromosome were grown in YCAT Galactose (monocentric) overnight at 25°C to mid-logarithmic phase and diluted into YPD (glucose – dicentric) to analyze dicentric chromosome behavior. Approximately 1000 cells were diluted in water and plated on YPG or YPD for viability assays. Plates were incubated at 25°C for up to 10 days before colonies were scored.

Dicentric chromosome breakage analysis – Southern blotting and PCR

Time course experiments on glucose and Southern blotting were performed as previously described (Brock and Bloom, 1994). Wild-type and cells with conditional dicentric chromosomes were grown overnight in 50 mLs of YCAT-Gal or YPG media and switched to fresh YPD at the start of the experiment. At time points, yeast were collected by centrifugation and genomic DNA was prepared. For Southern blotting, the genomic DNA was digested with *BamH1* and, after transfer of the DNA, the blot was probed with ^{32}P-*GAL-CEN* that was generated by PCR with Klenow polymerase. The blot was stripped and re-probed for ^{32}P-*MET14* as a control. Band intensity was measured using ImageQuant. For

PCR assays, 1 μL of genomic DNA was added to a 50 μL reaction (200 nM dNTP's, 4% DMSO, 400 nM primers), that was cycled as follows: 98°C, 1 min; (melting temperature 95°C, 1min – annealing temperature 60°C, 1 min – extension temperature 72°C, 2 min) for 27 cycles; final extension temperature 72°C, 5 min. 5 μL of each PCR reaction were loaded on a 1% agarose gel and stained for 15 min in 0.02% ethidium bromide before analysis.

Image acquisition, data analysis, and FRAP

Wide-field (Chapter 2) and confocal (Maddox et al., 2003a) images were obtained as previously detailed. Differential Interference Contrast (DIC) image exposure times were for 150 – 200 milliseconds (ms) and epi-fluorescence exposure times were 300 – 400 ms. LacI-GFP expression was induced as described previously (Thrower and Bloom, 2001). Images were processed as previously detailed (Chapter 2). To quantitate the dicentric Chr III mis-segregation events, cells were grown overnight in glucose media, induced for LacI-GFP expression for two hours, and five-plane Z-series of the population were acquired. The percentage of mitotic cells in the population were also recorded at this time. Spindle lengths were measured after calibration in MetaMorph (Molecular Devices Co., Sunnyvale, CA) with either the line or calipers tool from the compiled five-plane Z-series using the edges of the GFP-Tub1p fluorescence as the boundaries of the spindle. Spindle length measurements and GFP-Tub1p, Kar3p-GFP, and Nuf2p-GFP fluorescence intensity distribution analysis was performed as previously detailed (Gardner et al., 2005). All measurements were exported to Microsoft Excel (Microsoft Co., Seattle, WA) for further analysis. Photobleaching experiments and FRAP analysis was performed as previously detailed (Roumanie et al., 2005).

Results

Plus end binding protein mutants are sensitive to dicentric chromosome activation

To determine if plus end binding proteins are required for the cell to resist mechanical stress on the spindle, we constructed conditionally functional dicentric chromosomes. An ectopic centromere was constructed by introducing a *GAL1*-regulated *CEN3* cassette (*GAL-CEN3*) into Chr III. Regulation of the *GAL1* promoter allows the propagation of Chr III as a monocentric on galactose and as a dicentric on glucose (Hill and Bloom, 1987). In a wild-type cell with an activated dicentric chromosome, the attachment of both centromeres on a sister chromatid to opposite Spindle Pole Bodies (SPBs) results in Chr III breakage following anaphase onset (Figure 5.2A) (Brock and Bloom, 1994). The viability of cells carrying an activated dicentric chromosome is determined by the ratio of colony forming units on glucose relative to galactose (Brock and Bloom, 1994; Mythreye and Bloom, 2003). Wild-type cells show ~70% viability after activation of the dicentric chromosome (Figure 5.2B, Table 5.S1).

Dicentric cellular viability is greatly reduced in the absence of *RAD52* indicating that dicentric chromosome breaks are repaired by homologous recombination (Brock and Bloom, 1994). Dicentric strains lacking plus end binding proteins were reduced in viability by a factor of 5 – 300-fold (Figure 5.2B, Table 5.S1). The viability of cells with an activated dicentric chromosome was most severely compromised in *bim1Δ* and *kar3Δ* cells, followed by *cik1Δ*, *ase1Δ*, and *bik1Δ* cells. Importantly, Ase1p binds the central spindle after anaphase onset and has no known kinetochore functions (Pellman et al., 1995; Schuyler et al., 2003). The viability of cells with activated dicentric chromosomes was also severely compromised in *kar3-1* cells (Table 5.S1). However, deletions of the genes encoding the

cytoplasmic MT plus end binding proteins Kar9p, Dhc1p, and Kip3p caused only a three-fold reduction of viability in cells with activated dicentric chromosomes (data not shown). Sensitivity to the activated dicentric chromosome was not observed in *mcm21Δ* or *ndc10-2* cells where kinetochore function is compromised (Mythreye and Bloom, 2003). Therefore, mutations in MT plus end binding proteins reduce the viability of cells with an activated dicentric chromosome similarly to DNA repair mutants.

Dicentric chromosome breakage is suppressed in bim1Δ*,* kar3Δ*, and* ase1Δ *cells*

Reduced cellular viability following activation of the dicentric chromosome could result from a defect in DNA repair or elevated mis-segregation of the dicentric chromosome. We examined the mechanism that resulted in reduced cellular viability in *bim1Δ* cells. *bim1Δ* cells did not show sensitivity to 0.01% MMS suggesting Bim1p does not play a significant role in the repair of MMS mediated DNA lesions (data not shown). To test if dicentric chromosomes are broken in *bim1Δ* cells, we analyzed the conditional dicentric plasmid *pGAL-CEN*^{2}. Wild-type and *bim1Δ* cells were transformed with *pGAL-CEN*^{2} on galactose and single transformants were grown for eight to ten generations in either galactose or glucose before plasmid DNA was isolated and transformed into *E. coli*. Individual transformants containing the recovered plasmids were analyzed. Monocentric rearrangements occurred in all 50 of the dicentric plasmids recovered from wild-type cells grown on glucose (Figure 5.3A). In contrast, two in tact centromeres could be recovered from 54% of *bim1Δ* cells grown on glucose (Figure 5.3A; n = 50). Thus, deletion of *BIM1* suppresses dicentric plasmid rearrangements.

The reduction in dicentric plasmid rearrangements predicts that dicentric chromosomal rearrangements in *bim1Δ* cells would be reduced. Following a double strand DNA break in wild-type cells with an activated dicentric chromosome, recombination between *GAL-CEN3* and *CEN3* results in the appearance of a 1.1 Kb repair product (Brock and Bloom, 1994). Digestion of the genomic DNA with *BamHI* allows both *CEN3* fragments and the repair product to be visualized by Southern blotting. To determine if dicentric chromosomes exhibit reduced breakage in *bim1Δ* cells, we performed a time-course analysis. In wild-type cells, the repair product was observed within 2.5 to five hours after dicentric chromosome activation (Figure 5.3B). In contrast, *bim1Δ* cells do not show the appearance of a repair production until 12 to 24 hours after switching cells to glucose (Figure 5.3B). Further, quantitative analysis indicated 7.4% of *GAL-CEN3* was in tact after wild-type cells were switched to glucose for 30 hours while 36% of *GAL-CEN3* remained in tact in *bim1Δ* cells (Figure 5.3C). The five-fold increased *GAL-CEN3* in *bim1Δ* cells demonstrated a reduction in chromosome breaks had occurred. Similarly, measurements of *bim1Δ* cells showed an approximately four-fold reduction in the appearance of the 1.1 Kb repair product relative to wild-type (Figure 5.3D). Importantly, a decrease in the presence of the repair product was also observed in *ase1Δ* and *kar3Δ* cells (Figure 5.S1). Together, these data reveal dicentric chromosome breakage and repair is reduced in plus end binding protein mutants.

Dicentric chromosome mal-segregation occurs at a higher frequency in bim1Δ *cells*

A reduction in dicentric plasmid and chromosomal rearrangements predicts that mal-segregation of the dicentric chromosome leads to decreased viability. We used *bim1Δ* cells

to examine the segregation of the dicentric chromosome. To visualize dicentric chromosome segregation, the LacO coding sequence was integrated between the two centromeres on Chr III at *LEU2* and LacI fused to GFP was expressed to generate chromosome spots (Straight et al., 1997; Thrower and Bloom, 2001). Cells were grown in galactose or glucose for two to four generations before analysis. 98% of wild-type cells with an activated dicentric chromosome displayed one or two Chr III spots (Figure 5.4A). In contrast, 17.5% of *bim1Δ* cells had >2 Chr III spots after induction of the dicentric chromosome (Figure 5.4A). This suggests chromosome mal-segregation is elevated in *bim1Δ* cells. Defects in kMT attachments to both SPBs could increase mal-segregation of the dicentric chromosome. In wild-type cells, the dicentric chromosome is bioriented and found in between both SPBs (Figure 5.4B). However, in *bim1Δ* cells the dicentric chromosome is found proximal to one SPB in 48.5% of cells, a 7.5-fold increase over wild-type (Figure 5.4B). Therefore, dicentric chromosomes are mal-segregated in *bim1Δ* cells.

The defects in dicentric chromosome segregation in *bim1Δ* cells could arise from aberrant MT plus end interactions that weaken the anaphase spindle. To test this, we imaged the mitotic spindle using GFP-Tub1p in wild-type and *bim1Δ* cells with activated dicentric chromosomes. In >95% of wild-type cells, GFP-Tub1p was a single bar of fluorescence between SPBs (Figure 5.4C; n = 57 cells). However, in 38% of *bim1Δ* cells that had entered anaphase, the GFP-Tub1p fluorescence was discontinuous, often appearing as two foci (Figure 5.4C; n = 166 cells). This suggests that *bim1Δ* spindles are broken in the presence of activated dicentric chromosomes. Together, the reduced dicentric chromosome breakage, elevated dicentric chromosome mal-segregation, and defects in spindle structure suggest MT

plus end binding proteins are required to resist the mechanical stress induced by the dicentric chromosome.

Spindles are shorter and wider in kar3Δ *cells*

The activation of a dicentric chromosome introduces a mechanical stress on the anaphase spindle. As biorientation occurs in preanaphase, the tension at kinetochores is opposed by sister chromatid cohesion, resulting in mechanical stress on the spindle. *kar3Δ* mutants and *bim1Δ* cells exhibit similar behavior in the presence of activated dicentric chromosomes. To test whether these proteins also resist mechanical stress in preanaphase, we analyzed spindle structure in *kar3Δ* and *bim1Δ* cells.

kar3Δ and *bim1Δ* cells had shorter preanaphase mitotic spindles than wild-type cells (Figure 5.5A and Table 5.1) (Zeng et al., 1999). The reduced spindle length in *kar3Δ* cells was similar to spindles in *cin8Δ* cells (Table 5.1). This finding does not support the inward force model for spindle assembly. To examine if there is a difference in spindle morphology between *kar3Δ* and *cin8Δ* mutants, the distribution and density of MTs were analyzed by measuring the fluorescence intensity of GFP-Tub1p. Gardner and co-workers (2005) previously demonstrated the fluorescence intensity in the wild-type spindle peaked midway between the SPB and the equator at the quarter spindle where kMT plus ends are clustered. Using this method, we analyzed *bim1Δ* cells which have defects in spindle assembly (Tirnauer et al., 1999). Consistent with these results, we found spindles were almost two times as wide in *bim1Δ* cells when compared to wild-type cells (Figure 5.5B and Table 5.1). *kar3Δ* spindles were also wider than wild-type (Figure 5.5B). In contrast, the width of *cin8Δ* spindles was similar to wild-type (Figure 5.5B). The increased width of spindles in *kar3Δ*

cells could be due to defects in kMT or ipMT organization. Our analysis supports a defect in ipMT organization in *kar3Δ* and *bim1Δ* cells. Deletion of *KAR3*, *BIM1*, or *CIN8* reduced the fluorescence in the quarter spindle and resulted in a greater MT density near the spindle equator (Figure 5.5C). This suggests kMT plus ends are closer to the spindle equator, and not the SPBs, in *kar3Δ* cells. Therefore, the increase in spindle width is likely due to the disorganization of ipMTs.

The absence of a GFP-Tub1p fluorescence peak at the quarter spindle in *kar3Δ* cells suggests there may be a defect in kinetochore organization. To test this, we examined kinetochores marked with Nuf2p-GFP. Similar to previous studies (Pearson et al., 2001), we found kinetochores in wild-type cells formed two clusters in preanaphase (Figure 5.S2A). Since spindles are shorter in *kar3Δ* cells, the clusters are not well defined on either side of the spindle equator and the distribution of Nuf2p-GFP fluorescence was similar to a prometaphase configuration (Figure 5.S2A and 5.S2B). Time-lapse imaging demonstrated kinetochores in *kar3Δ* cells could transiently separate into two clusters and then re-associate (Figure 5.S2). However, the mean kMT length in *kar3Δ* cells was not different from wild-type (wt = 0.39 +/- 0.09 μm, n = 41; *kar3Δ* = 0.44 +/- 0.14 μm, n = 31; $p > 0.10$). This suggests the shorter spindles are not due to kMT defects. When *kar3Δ* cells entered anaphase, kinetochores separated into two clusters (data not shown). Therefore, the shorter and wider spindles in *kar3Δ* cells result from an inability to organize and slide ipMTs apart.

Dynamic Kar3p re-localizes from the SPBs to the central spindle during anaphase

Plus end binding proteins involved in spindle function often localize to ipMTs. Live cell imaging revealed Kar3p localized transiently inside the spindle as either one or two

clusters in preanaphase (Figure 5.6A, 0 min to 2.5 min; n = 6 cells). At anaphase onset, Kar3p-GFP localization to the central spindle was visible and appeared similar to GFP-Tub1p at the spindle midzone (Figure 5.6A, 4 min and 5 min, n = 10 cells; Figure 5.6B). By late anaphase, Kar3p-GFP was only visible at the SPBs (Figure 5.6A, 6.5 min to 22 min). Compared to the fluorescence of Nuf2p-GFP at kinetochores, Kar3p-GFP was closer to SPBs in preanaphase (Figure 5.6C). This suggests that Kar3p localizes to ipMT plus ends near the SPBs and not kinetochores in preanaphase.

Fluorescence intensity measurements of Kar3p-GFP demonstrated preanaphase SPBs were significantly brighter than late anaphase spindle poles (Figure 5.6D; p-value < 10^{-5} for each SPB). Thus, Kar3p could be released from the SPBs at anaphase onset to bind to the ipMTs. Interestingly, late anaphase spindles in *kar3Δ* cells disassembled if bent, occasionally leading to binucleate cells (see Figure 5.8). However, analysis of *kar3Δ* cells in anaphase demonstrated the kinetics of spindle elongation were similar to wild-type cells, though the initial phase of spindle elongation was elevated (Table 5.2; p-value > 0.03). This suggests Kar3p is required to maintain the integrity of the anaphase spindle in monocentric cells.

Kar3p could be released from the SPBs and bind ipMTs during anaphase. To test if a dynamic pool of Kar3p exists at the SPBs that could localize to the central spindle, photobleaching experiments were performed and Fluorescence Recovery After Photobleaching (FRAP) was measured. FRAP of Kar3p-GFP on preanaphase SPBs (Figure 5.7A, n = 6 cells) resulted in a half-recovery time of 57.3 +/- 15.5 sec (avg +/- SD). Fluorescence recovery to the SPB was best fit with a single exponential function (Figure 5.7B; R = 72.0 +/- 20.7%, n = 6 cells). Thus, Kar3p has a dynamic component at the SPB in

preanaphase. In contrast, four of seven cells photobleached in late anaphase displayed no recovery of fluorescence (Figure 5.7C). For the three cells where fluorescence redistributed after photobleaching, the half-recovery time was 60.5 +/- 30.3 sec, but the percent recovery was decreased relative to preanaphase (Figure 5.7D; R = 34.3 +/- 10.1). The percent recovery in late anaphase was significantly less than recovery measured in preanaphase (p-value < 0.001). Therefore, there is a dynamic fraction of Kar3p at the SPB in preanaphase that may bind the central spindle in early anaphase.

Nuclear transiting in kar3Δ *cells results in polyploidy*

kar3Δ cells display a preanaphase delay that resulted in nuclear transiting, or movement of the entire spindle between mother and bud, in 25% of time-lapse movies (Figure 5.8A; n = 16/64 cells). Nuclear transiting was not observed in wild-type cells (n = 29 cells). Penetration of the preanaphase spindle in the bud did not prevent anaphase onset (n = 5/16 cells) and mitotic exit defects occurred. 6% of *kar3Δ* cells displayed spindle elongation entirely in the mother or bud, leading to binucleate cells (Figure 5.8B; n = 4/64 cells). Unbudded cells with two SPBs, each associated with nuclear MTs, were visible in the population (Figure 5.8C). Together, we conclude that Kar3p cross-links ipMTs to resist mechanical stress during mitosis and is required to ensure one SPB is segregated to each daughter cell.

Discussion

The structural integrity of the mitotic spindle is critical for chromosome segregation. Here we show the central spindle is required to resist the introduction of mechanical stress that can lead to defects in chromosome segregation. MAPs such as Kar3p, Bim1p, and Ase1p are required for cells to recover from the inward force of an activated dicentric chromosome. Additionally, Kar3p is required to resist the mechanical stress generated during preanaphase spindle assembly. Our data supports a model where Kar3p cross-links ipMTs to allow spindle assembly and the separation of kinetochores into two clusters. As cells enter anaphase, Kar3p and other midzone components are required to resist mechanical stress to correct defects in chromosome segregation.

Preanaphase spindle assembly requires Kar3p

Bipolar spindle assembly requires Cin8p and Kip1p to move SPBs apart (Roof et al., 1992; Saunders and Hoyt, 1992), facilitating the proper separation of kinetochores. If Kar3p counterbalances Cin8p and Kip1p function, either at the kinetochore or along ipMTs, then removal of the inward force should allow spindles to become longer. In *kar3Δ* cells, spindles are shorter and wider (Figure 5.5) (Zeng et al., 1999). The simplest interpretation of this data is that Kar3p plays a structural role in preanaphase spindle assembly. Kar3p could function in the spindle similarly to its role in nuclear congression during mating. When haploid cells are mated, MT plus ends are cross-linked by Kar3p, leading to movement of two nuclei towards each other (Chapter 3). Kar3p requires Cik1p to function during mating (Page et al., 1994; Page and Snyder, 1992). Additionally, mutants in *BIM1* have a severe mating defect as well (Schwartz et al., 1997). We propose, similar to the complex that cross-links MT plus

ends during mating, that a complex minimally comprised of Kar3p, Cik1p, and Bim1p cross-links anti-parallel MT plus ends in budding yeast (Figure 5.9). This cross-linking provides the structural integrity to the mitotic spindle that allows Cin8p and Kip1p to slide MTs past one another. This was one of the original hypotheses for Kar3p function (Saunders and Hoyt, 1992) and does not rule out the possibility that Kar3p opposes Cin8p and Kip1p function after cross-linking has occurred. Metazoan cells have evolved multiple kinesin 14 molecules and one subset could be required for cross-linking while another provides an inward force during spindle assembly.

Midzone proteins localize in anaphase to resist mechanical stress on the spindle

As cells move into anaphase, Cin8p and Kip1p slide MTs apart during spindle elongation (Straight et al., 1998). However, late anaphase spindles lacking both Cin8p and Kip1p do not collapse (Saunders and Hoyt, 1992), suggesting other proteins provide the structural integrity at this time. In a wild-type spindle, inward forces are reduced after sister chromatid cohesion is lost. The introduction of a conditional centromere can result in a dicentric chromosome that attaches to opposite SPBs, introducing mechanical stress on the spindle. We find that central spindle integrity is required for the viability of cells with an activated dicentric chromosome (Figure 5.2, Table 5.S1). Activated dicentric chromosomes in *bim1Δ* cells resulted in broken spindles and chromosome mal-segregation (Figures 5.3 and 5.4). If spindle collapse results in kMT attachment defects, then the spindle assembly checkpoint would have to delay cell cycle progression until the errors are corrected. However, it is unknown if the spindle assembly checkpoint can be reactivated in the same cell cycle to correct these defects.

Model for spindle assembly and elongation

Plus end binding proteins accumulate on the ipMTs during mitosis to resist forces that cause spindle collapse. Based on this and our current data, we propose a new model for spindle assembly (Figure 5.9). Following duplication of the SPBs in S phase, Bim1p is required to facilitate the opposite orientation SPBs. The mechanism of Bim1p function during SPB migration remains unclear. As SPBs become opposed, Kar3p and Cik1p begin to cross-link ipMTs in G2/M. It is likely Cin8p and Kip1p assist in cross-linking ipMTs, though these proteins are not as effective as Kar3p/Cik1p. As cells move from prometaphase to metaphase, Cin8p and Kip1p slide anti-parallel MTs slide past one another. The inward force that opposes Cin8p/Kip1p arises from sister chromatid cohesion as centromeres are pulled apart. Supporting this hypothesis, loss of bipolar kMT attachments leads to longer mitotic spindles (Pearson et al., 2003), the phenotype predicted upon removal of the inward force. Kar3p could provide a secondary inward force. At anaphase onset, sister chromatid cohesion is dissolved and ipMTs polymerize to drive SPBs apart. The addition of Ase1p, Bik1p, and Slk19p to the central spindle at this time further strengthens the ipMTs which decrease from four to as low as one per SPB during anaphase (King and Hyams, 1983; Winey et al., 1995). Future studies on the roles of MT motors in spindle integrity and chromosome segregation will be critical to understand the molecular mechanisms that prevent aneuploidy.

Acknowledgements

We thank David Bouck, Jay Gatlin, Erin McCarthy, and members of the Bloom and Salmon laboratories for advice, assistance, and critical readings of the manuscript. This work was funded by the Human Frontier Science Program grant RGP29/2003 (E.D.S.), a National Science Foundation Career Award BES 9984955 (D.J.O.), and the National Institutes of Health grants GM-24364 (E.D.S.), GM-60678 (E.D.S.), and GM-32238 (K.B.).

Tables and Figures

	Spindle Length[A]	n
Wild-type	1.47 +/- 0.23	29
bim1Δ	1.29 +/- 0.25	33
cin8Δ	1.27 +/- 0.23	33
kar3Δ	1.25 +/- 0.17	25

[A]Length reported in μm (mean +/- SD)

Table 5.1: Spindle length measurements.

Wild-type and mutant cells expressing GFP-Tub1p were imaged using wide-field microscopy. Spindle lengths were measured according to previous methods (Gardner et al., 2005).

	Fast Phase[A]	Slow Phase[A]	Time to BD[B]	BD Length[C]	n
Wild-type	0.46 +/- 0.028	0.11 +/- 0.012	33 +/- 1.7	7.8 +/- 0.30	10
kar3Δ	0.62 +/- 0.098	0.16 +/- 0.017	30 +/- 2.4	8.3 +/- 0.30	19

[A]Rates reported as μm min^{-1}; see Straight et al. (1998) for *cin8Δ* and *kip1Δ* measurements
[B]BD – breakdown; time in min
[C]Length reported in μm

Table 5.2: Anaphase spindle elongation in *kar3Δ* cells.

Wild-type and *kar3Δ* cells expressing GFP-Tub1p were imaged from preanaphase to spindle breakdown. The fast and slow phase of spindle elongation was calculated as previously described (Straight et al., 1998). The image frame immediately before spindle elongation was visible (>2 μm), was scored as the time of anaphase onset. Spindle breakdown was recorded when the GFP-Tub1p fluorescence between SPBs became discontinuous.

Strain Name	Relevant Genotype	Source/Reference
YEF 473A	MAT**a** *trp1Δ63 leu2Δ1 ura3-52 his3Δ200 lys2-801*	(Bi and Pringle, 1996)
YEF 473B	MATα *trp1Δ63 leu2Δ1 ura3-52 his3Δ200 lys2-801*	(Bi and Pringle, 1996)
SFY 280-20A	MAT**a** *ade2-1 ade3 can1-100 his3-11,-15 leu2-3,-112 trp1-1 ura3-1 lys2Δ::HIS3 vik1Δ::KAN^r GFP-TUB1::URA3*	T. Davis[A]
MS 1119	MAT**a** *ura3-52 leu2-3, -112 ade2-101 kar3-1*	(Meluh and Rose, 1990)
GT1	MAT**a** *trp1Δ63 leu2Δ1 ura3-52 his3Δ200 lys2-801 GFP-TUB1::URA3*	P. Maddox[B]
DCB 131	MAT**a** *trp1Δ63 leu2Δ1 ura3-52 his3Δ200 lys2-801 NUF2::GFP-KAN^r SPC29::RFP-HB^r*	D. Bouck[B]
KBY 2275	MAT**a** *trp1Δ63 leu2Δ1 ura3-52 his3Δ200 lys2-801 GFP-TUB1::URA3 cin8Δ::LEU2*	C. Pearson[B]
KBY 5056	MAT**a** *trp1Δ63 leu2Δ1 ura3-52 his3Δ200 lys2-801 kar3Δ::TRP1 NUF2::GFP-URA3*	C. Pearson
KBY 9282	MATα *trp1Δ63 leu2Δ1 ura3-52 his3Δ200 lys2-801 KAR3::GFP-HB^r*	This Study
KBY 9293	MAT**a** *trp1Δ63 leu2Δ1 ura3-52 his3Δ200 lys2-801 kar3Δ::TRP1*	Chapter 3
KBY 9313	MAT**a** *trp1Δ63 leu2Δ1 ura3-52 his3Δ200 lys2-801 kar3Δ::TRP1 GFP-TUB1::URA3*	Chapter 3
KBY 9338	MAT**a** trp1Δ63 leu2Δ1 ura3-52 his3Δ200 lys2-801 kar3Δ::TRP1 *NUF2::GFP-URA3*	This Study
KBY 9340	MAT**a** *trp1Δ63 leu2Δ1 ura3-52 his3Δ200 lys2-801 kar3Δ::TRP1 GFP-TUB1::URA3 SPC29::RFP-HB^r*	This Study
KBY 9342	MAT**a** *trp1Δ63 leu2Δ1 ura3-52 his3Δ200 lys2-801 kar3Δ::TRP1 NUF2::GFP-URA3 SPC29::RFP-HB^r*	This Study
KBY 9344	MAT**a** *trp1Δ63 leu2Δ1 ura3-52 his3Δ200 lys2-801 pJB2#4*	This Study
KBY 9345	MAT**a** *trp1Δ63 leu2Δ1 ura3-52 his3Δ200 lys2-801 pJB2#7*	This Study
KBY 9346	MAT**a** *trp1Δ63 leu2Δ1 ura3-52 his3Δ200 lys2-801 kar3Δ::TRP1 pJB2#4*	This Study
KBY 9347	MAT**a** *trp1Δ63 leu2Δ1 ura3-52 his3Δ200 lys2-801 kar3Δ::TRP1 pJB2#7*	This Study
KBY 9348	MAT**a** *ura3-52 leu2-3, -112 ade2-101 kar3-1 pJB2#4*	This Study
KBY 9349	MAT**a** *trp1Δ63 leu2Δ1 ura3-52 his3Δ200 lys2-801 cik1Δ::KAN^r pJB2#4*	This Study
KBY 9350	MAT**a** *trp1Δ63 leu2Δ1 ura3-52 his3Δ200 lys2-801 cik1Δ::KAN^r pJB2#7*	This Study
KBY 9351	MAT**a** *ade2-1 ade3 can1-100 his3-11,-15 leu2-3,-112 trp1-1 ura3-1 lys2Δ::HIS3 vik1Δ::KAN^r GFP-TUB1::URA3 pJB2#4*	This Study
KBY 9352	MAT**a** *ade2-1 ade3 can1-100 his3-11,-15 leu2-3,-112 trp1-1 ura3-1 lys2Δ::HIS3 vik1Δ::KAN^r GFP-TUB1::URA3 pJB2#7*	This Study
KBY 9353	MAT**a** *trp1Δ63 leu2Δ1 ura3-52 his3Δ200 lys2-801 TEM1::GFP-KAN^r ase1Δ::HB^r pJB#4*	This Study
KBY 9354	MAT**a** *trp1Δ63 leu2Δ1 ura3-52 his3Δ200 lys2-801 TEM1::GFP-KAN^r ase1Δ::HB^r pJB#7*	This Study
KBY 9355	MAT**a** *trp1Δ63 leu2Δ1 ura3-52 his3Δ200 lys2-801 bik1Δ::KAN^r pJB2#4*	This Study

Strain Name	Relevant Genotype	Source/Reference
KBY 9356	MAT**a** *trp1Δ63 leu2Δ1 ura3-52 his3Δ200 lys2-801 bik1Δ::KAN^r pJB2#7*	This Study
KBY 9357	MAT**a** *trp1Δ63 leu2Δ1 ura3-52 his3Δ200 lys2-801 TEM1::GFP-KAN^r pJB2#4*	This Study
KBY 9358	MAT**a** *trp1Δ63 leu2Δ1 ura3-52 his3Δ200 lys2-801 TEM1::GFP-KAN^r pJB2#7*	This Study
KBY 9359	MAT**a** *ura3-52 leu2-3, -112 ade2-101 kar3-1 pJB2#7*	This Study
Plasmid Name	**Relevant Genotype**	**Source or Reference**
pJB2#4	*his4::URA3 GAL-CEN3* (inverted orientation)	(Brock and Bloom, 1994)
pJB2#7	*his4::URA3 GAL-CEN3* (direct orientation)	(Brock and Bloom, 1994)
pAFS125	*GFP-TUB1::URA3*	(Straight et al., 1997)

[A]University of Washington, Seattle, WA; [B]University of North Carolina, Chapel Hill, NC

Table 5.3: *S. cerevisiae* strains and plasmids used in this chapter (continued).

Table S1. Viability of cells carrying an activated dicentric chromosome

Relevant Genotype	Orientation	% Viability[A]	n
Wild-type	Inverted	77.6 +/- 8.3	8
	Direct	54.8 +/- 13	8
rad52Δ[B, C]	Inverted	2.0 +/- 0.2	6
ndc10-2 (33°C)[C]	Direct	74.5 +/- 1.0	6
bim1Δ	Direct	0.135	6
kar3Δ	Inverted	0.140 +/- 0.11	4
	Direct	0.150 +/- 0.070	4
kar3-1	Inverted	0.210 +/- 0.16	4
	Direct	5.84 +/- 1.0	3
cik1Δ	Inverted	1.08 +/- 0.58	4
	Direct	1.23 +/- 0.62	9
ase1Δ	Inverted	2.53 +/- 0.80	4
	Direct	2.24 +/- 1.4	4
bik1Δ	Inverted	2.08 +/- 2.2	4
	Direct	0.41 +/- 0.24	3
slk19Δ	Inverted	13.3 +/- 5.6	5
	Direct	11.4 +/- 5.7	3
vik1Δ	Inverted	39.9 +/- 2.6	3
	Direct	39.5 +/- 7.3	4

[A]Mean +/- Standard Deviation
[B](Brock and Bloom, 1994)
[C](Mythreye and Bloom, 2003)

Table 5.S1: Cellular viability in the presence of an activated dicentric chromosome.

Wild-type and mutant strains were scored for viability after plating on galactose (monocentric) or glucose (dicentric). The ratio of colony forming units on glucose/galactose is reported as the percent viability.

Figure 5.1: Models for Kar3p function during spindle assembly.

Hypothetical schematics for Kar3p function during preanaphase spindle assembly. (A) Inward force ipMT model for Kar3p function. Kar3p is proposed to act on ipMTs to generate an inward force that opposes Cin8p/Kip1p sliding of ipMTs away from the spindle equator. In the absence of Kar3p, Cin8p/Kip1p sliding be unopposed, resulting in longer preanaphase spindle lengths. (B) Inward force kMT model for Kar3p function. Note, this model and the inward force ipMT model are not mutually exclusive. Kar3p could depolymerize MT plus ends at the kinetochore, pulling the SPBs in toward the spindle equator. Cin8p/Kip1p function on ipMTs would oppose the depolymerase activity of Kar3p. In the absence of Kar3p, the inward force at the kinetochore would be reduced, generating longer kMTs and a longer preanaphase spindle. (C) Cross-linking model for Kar3p function. In this model, Kar3p acts to cross-linking anti-parallel ipMTs. After cross-linking, Cin8p/Kip1p can slide anti-parallel MTs relative to one another and, at this stage, Kar3p could act as an inward force as well. In the absence of Kar3p, the spindle would be *shorter*, and possibly wider, because ipMTs are not interacting properly.

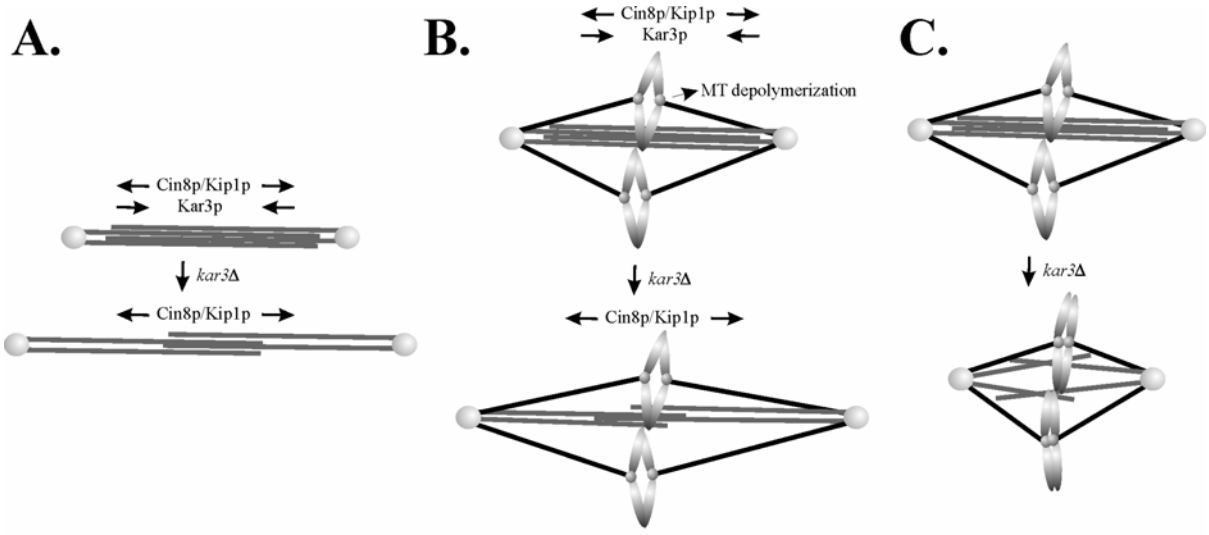

Inward force ipMT model

Inward force kMT model

Cross-linking model

Figure 5.2: Plus end binding proteins have reduced viability in the presence of an activated dicentric chromosome.

Dicentric chromosome activation results in decreased viability in MT plus end binding mutants. (A) Schematic of dicentric chromosome activation in wild-type cells. In approximately 50% of cells with an activated dicentric chromosome, the kinetochores will orient towards opposite SPBs. After anaphase onset, the bioriented dicentric chromosome will stretch between both SPBs, resulting in a midanaphase pause. To resume anaphase, the dicentric chromosome breaks and the DNA lesion is repaired generate a monocentric derivative. (B) Histogram of the viability of cells with an activated dicentric chromosome. Centromeres on the dicentric chromosome were in the direct orientation except for *rad52Δ* cells, which, along with *ndc10-2*, have been reported previously (Brock and Bloom, 1994; Mythreye and Bloom, 2003). Data for both orientations can be found Table 5.S1.

A.

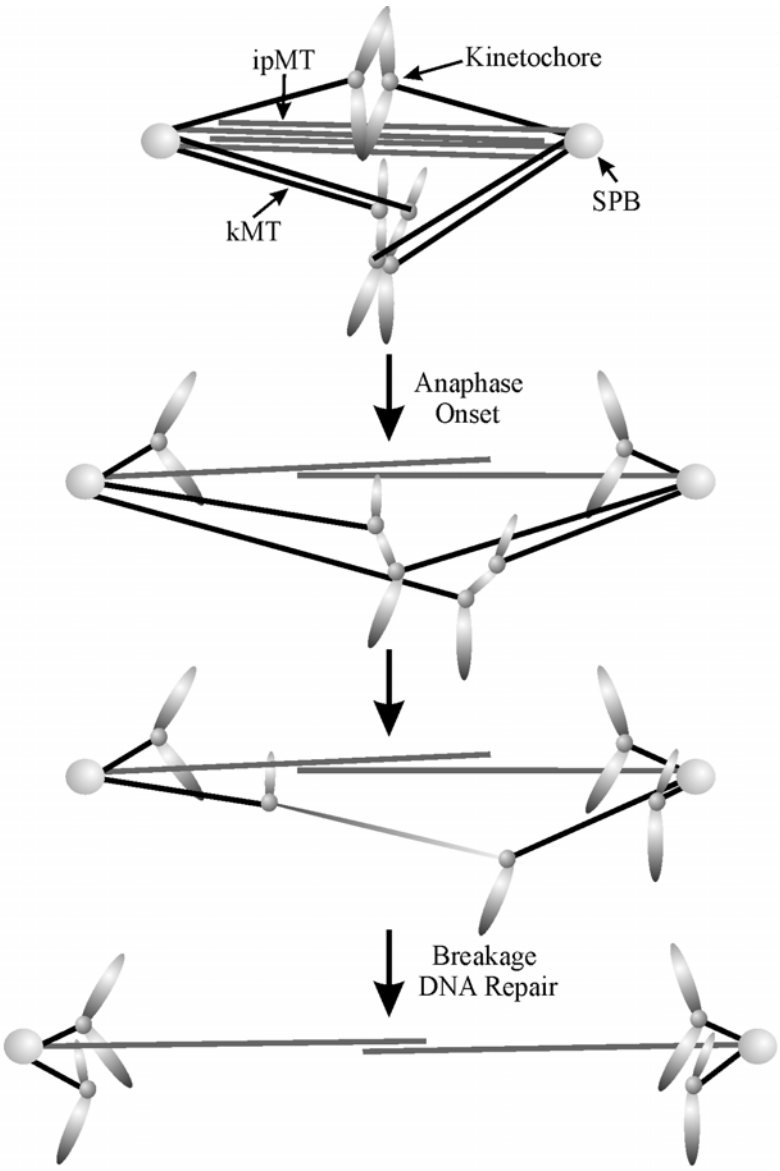
ipMT
Kinetochore
SPB
kMT
Anaphase
Onset
Breakage
DNA Repair

B.

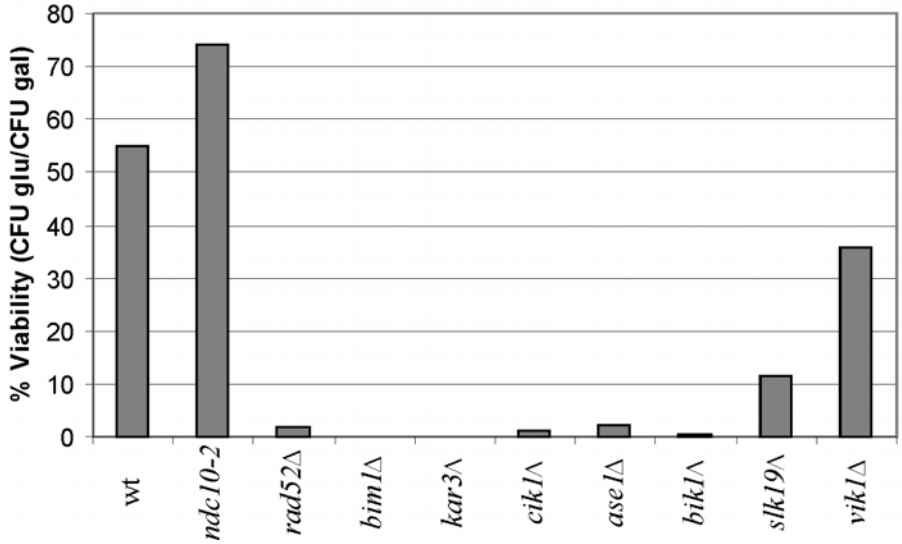
% Viability (CFU glu/CFU gal)
80
70
60
50
40
30
20
10
0
wt
ndc10-2
rad52Δ
bim1Δ
kar3Λ
cik1Λ
ase1Δ
bik1Λ
slk19Λ
vik1Δ

Figure 5.3: *bim1Δ* suppresses dicentric chromosome breakage.

(A) Restriction analysis of dicentric plasmid *pGAL-CEN*^{2} DNA (Hill and Bloom, 1989) recovered from wild-type or *bim1Δ* cells maintained on galactose or glucose. Plasmid DNA derived from wild-type and *bim1Δ* cells was restricted as previously described (Hill and Bloom, 1989). In wild-type cells, 0/50 cells had both centromeres in tact after plasmid recovery and analysis; 27/50 dicentric plasmids derived from *bim1Δ* cells had both centromeres in tact. (B) Time course for monocentric derivatives generated by recombination between the two centromeres on chromosome III. Wild-type and *bim1Δ* cells were cultured and the time course was performed as previously described (Brock and Bloom, 1994). Time (hours) indicates the time points after the switch to glucose that activated the dicentric chromosome. At each time point, the chromosomal DNA was prepared and analyzed by Southern analysis (see Methods). The Southern blot was also probed for *MET14* that served as a loading control. (C) Histogram of the percentage of radioactive *GAL-CEN3* relative to *MET14* over the time course for wild-type and *bim1Δ* cells determined by ImageQuant analysis. There was a 13.5-fold decrease in the *GAL-CEN3* band in wild-type cells but only a 2.8-fold decrease in *bim1Δ*. (D) Histogram of the percentage of radioactive 1.1 Kb rearrangement product relative to *MET14* over the time course for wild-type and *bim1Δ* cells determined by ImageQuant analysis. There was a 13.6-fold increase in the 1.1 Kb rearrangement product in wild-type cells but only a 3.8-fold increase in *bim1Δ* cells.

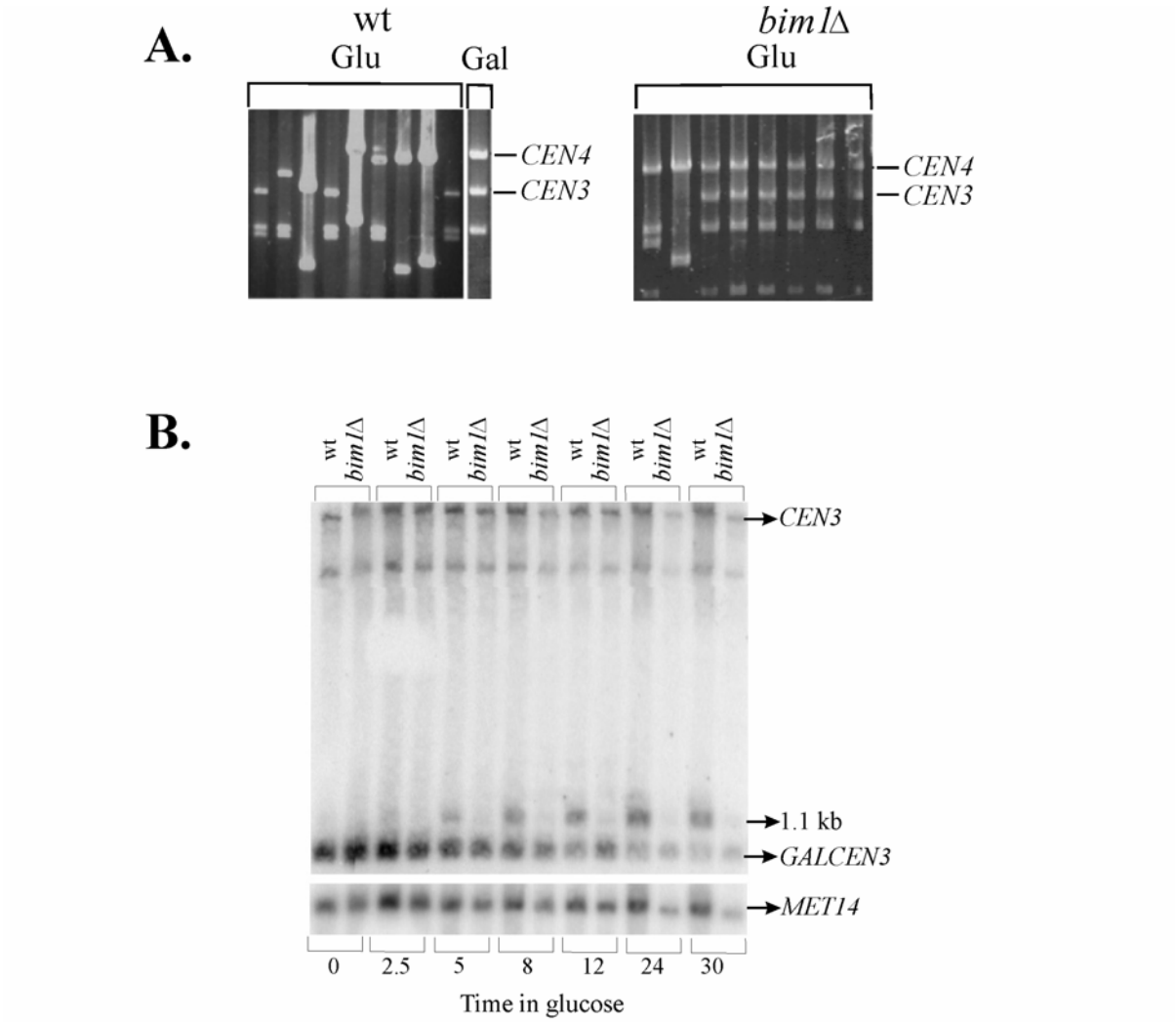
A.
wt
Glu
Gal
bim1Δ
Glu
CEN4
CEN3
CEN4
CEN3
B.
wt
bim1Δ
CEN3
1.1 kb
GALCEN3
MET14
0
2.5
5
8
12
24
30
Time in glucose
C.
wt
bim1Δ
GALCEN3
Fold relative to MET14 normalized to t = 0 hrs
Time (hrs)
D.
1.1 Kb rearrangement product
wt
bim1Δ
Fold relative to MET14 normalized to t = 0 hrs
Time (hrs)

Figure 5.4: The dicentric chromosome is mal-segregated in *bim1Δ* cells.

(A) Histogram of chromosome III segregation in wild-type, *bim1Δ* monocentrics, and *bim1Δ* dicentrics from cells expressing LacI-GFP with LacO integrated at Chr III. Bar, 2 μm. Unbudded or small budded cells were classified as G1/S. Medium to large budded cells were scored for one Chr III spot, two Chr III spots, two separated Chr III spots in anaphase, or >2 Chr III spots. Black bars – wild-type monocentrics (maintained on glucose; n = 91 cells); gray bars - *bim1Δ* monocentrics (grown on galactose; n = 139); white bars - *bim1Δ* dicentrics (cultured on glucose; n = 169). (B) Activated dicentric Chr III behavior relative to SPBs. Arrow marks the position of Chr III. Both cell types have LacO integrated at Chr III and express LacI-GFP. Wild-type cells SPBs marked with Spc72p-GFP. *bim1Δ* cells SPBs marked with Spc29p-RFP. Population images were taken three hours after switching cells to glucose. Dicentric Chr III position relative to the SPB was determined by measuring the distance of the Chr III spot from the SPB and the distance between the two SPBs. Wild-type cells (n = 97) have 94% of Chr III spots within the central one-third of the distance between SPBs. Only 51.5% of *bim1Δ* cells (n = 105) have the Chr III spot in the central one-third of the spindle. Bar, 2 μm. (C) Spindle morphology in wild-type and *bim1Δ* cells with activated dicentric chromosomes. Upper panels – GFP-Tub1p images; lower panels – overlay of GFP-Tub1p (green) with DIC image (red). In wild-type cells, spindles are in preanaphase or arrest in midanaphase with continuous GFP-Tub1p fluorescence. In 38% of *bim1Δ* cells with activated dicentric chromosomes that entered anaphase, the GFP-Tub1p fluorescence was not continuous, suggesting spindles had broken. Bar, 2 μm.

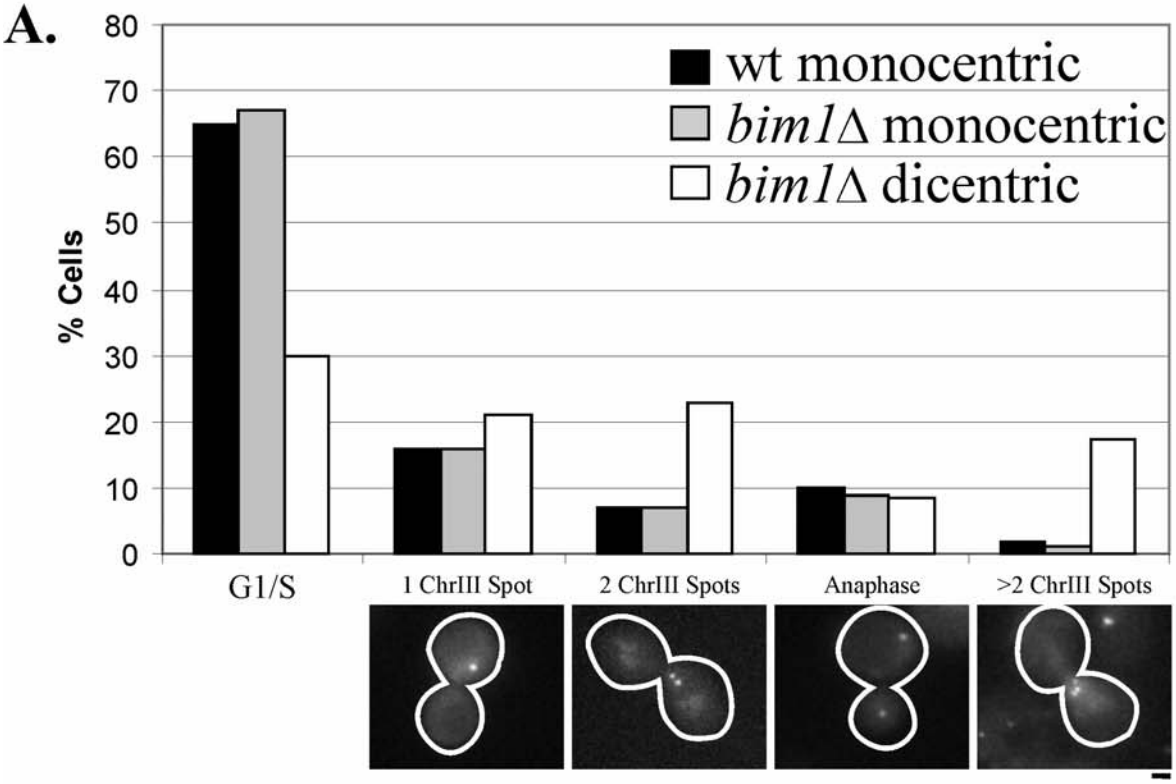
A.
80
70
60
50
40
30
20
10
0
% Cells
wt monocentric
bim1Δ monocentric
bim1Δ dicentric
G1/S
1 ChrIII Spot
2 ChrIII Spots
Anaphase
>2 ChrIII Spots

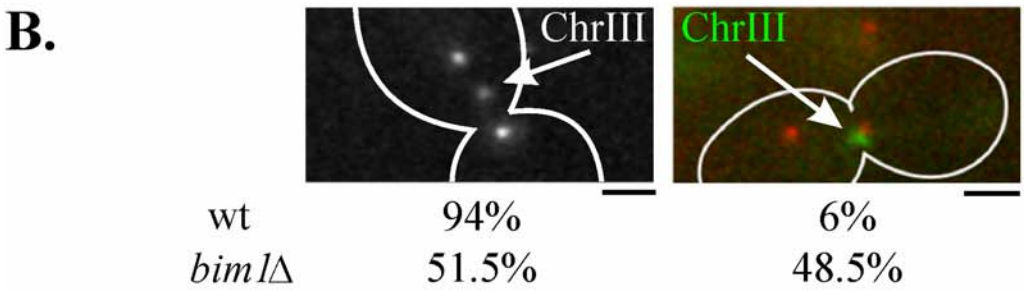
B.
ChrIII
ChrIII
wt
bim1Δ
94%
51.5%
6%
48.5%

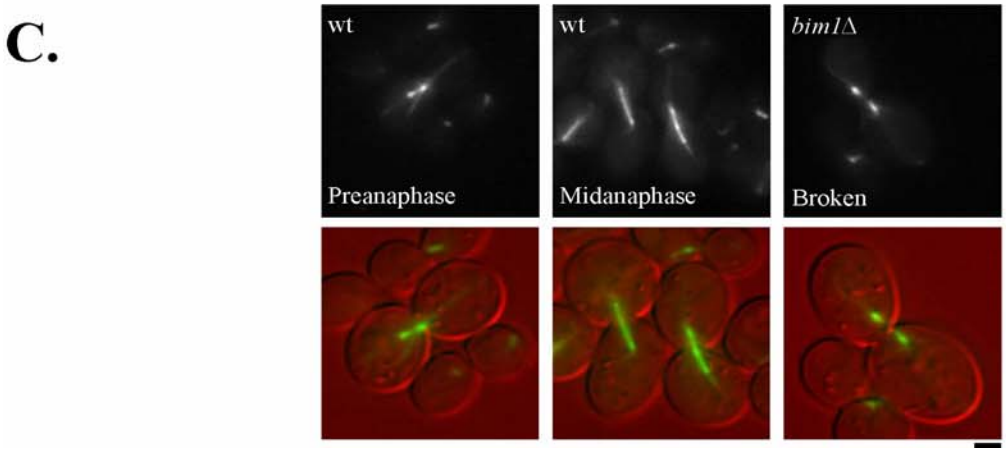
C.
wt
Preanaphase
wt
Midanaphase
bim1Δ
Broken

Figure 5.5: Spindles in *kar3Δ* cells are shorter and wider than wild-type.

(A) Images of wild-type and *kar3Δ* cells expressing GFP-Tub1p. Bar, 2 μm. (B) Spindle width measurements for wild-type, *bim1Δ*, *cin8Δ*, and *kar3Δ* cells. Spindles were wider in *kar3Δ* and *bim1Δ* cells but were not changed in *cin8Δ* cells. (C) GFP-Tub1p fluorescence density plots for wild-type, *bim1Δ*, *cin8Δ*, and *kar3Δ* cells. Wild-type cells show a peak of fluorescence at the quarter spindle where kMT plus-ends organize centromeres into a cluster. GFP-Tub1p fluorescence in *bim1Δ*, *cin8Δ*, and *kar3Δ* cells did not peak in the quarter spindle, suggesting a prometaphase distribution of kinetochores exists in each mutant. Wt – 29 cells; *kar3Δ* - 25 cells; *cin8Δ* - 33 cells; *bim1Δ* - 33 cells for both (B) and (C).

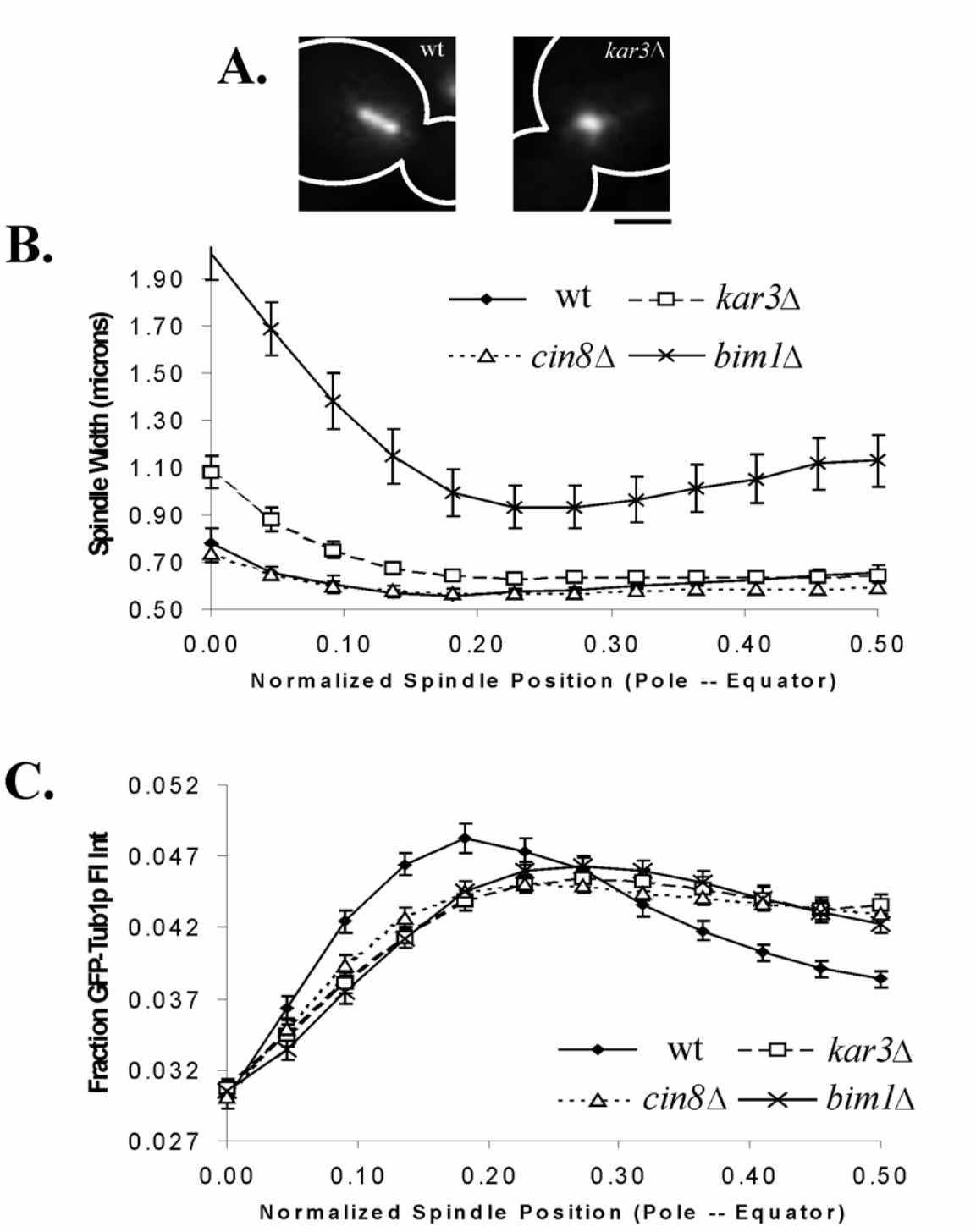
A.
wt
kar3Δ
B.
Spindle Width (microns)
1.90
1.70
1.50
1.30
1.10
0.90
0.70
0.50
wt
kar3Δ
cin8Δ
bim1Δ
0.00
0.10
0.20
0.30
0.40
0.50
Normalized Spindle Position (Pole -- Equator)
C.
Fraction GFP-Tub1p Fl Int
0.052
0.047
0.042
0.037
0.032
0.027
wt
kar3Δ
cin8Δ
bim1Δ
0.00
0.10
0.20
0.30
0.40
0.50
Normalized Spindle Position (Pole -- Equator)

Figure 5.6: Kar3p associates with ipMTs in preanaphase and anaphase.

Kar3p localizes to the central spindle during mitosis. Bar, 2 μm. (A) Kar3p-GFP localization during mitosis. (0 min - 2.5 min) Kar3p localized to the SPBs and transiently as two clusters interior to the SPBs (arrowheads) or to the middle of the spindle (arrow). (3.5 min - 5 min) Kar3p-GFP redistributed to the central spindle in early anaphase. (6.5 min - 22 min) Kar3p-GFP localized strongly to the SPBs with punctate distribution along the central spindle (arrows) in mid to late anaphase. (B) Comparison of Kar3p-GFP signal at the midzone (left panel, arrow) with GFP-Tub1p where there the overlap of MTs is visible (right panel, arrow). (C) The localization of Kar3p-GFP (n = 70 cells) relative to Nuf2p-GFP (n = 24 cells) plotted against normalized spindle position. Unlike Nuf2p-GFP, Kar3p-GFP is clustered close to the SPBs, suggesting localization to the ipMTs. (D) SPB fluorescence intensity of Kar3p-GFP during mitosis. dSPB is in dark gray, mSPB in light gray. Preanaphase spindles were categorized as unaligned (spindle was parallel to bud neck) or aligned (spindle was perpendicular to bud neck). Fluorescence intensity decreased as cells moved from preanaphase to anaphase.

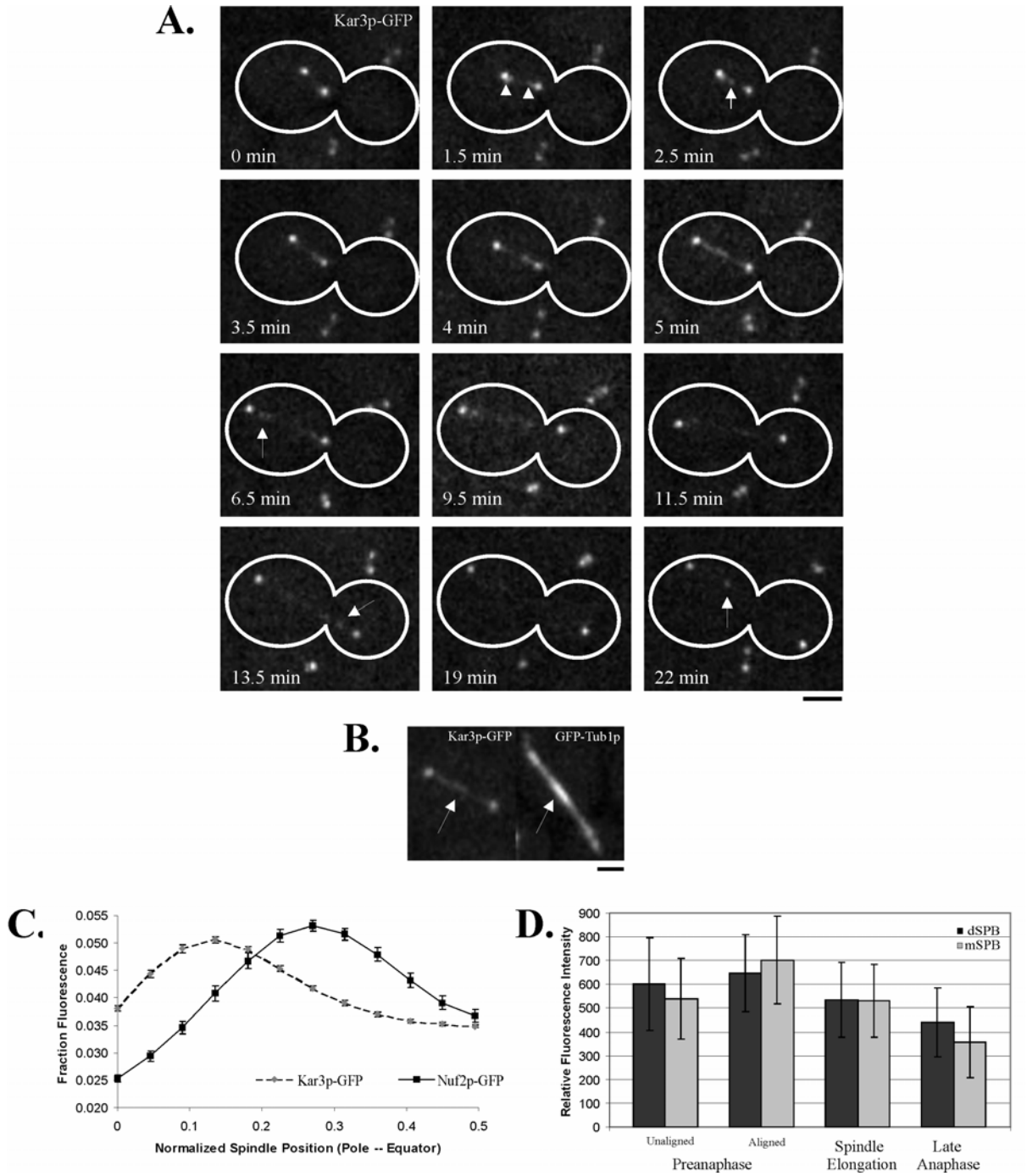
A.
Kar3p-GFP
0 min
1.5 min
2.5 min
3.5 min
4 min
5 min
6.5 min
9.5 min
11.5 min
13.5 min
19 min
22 min
B.
Kar3p-GFP
GFP-Tub1p
C.
Fraction Fluorescence
0.055
0.050
0.045
0.040
0.035
0.030
0.025
0.020
0
0.1
0.2
0.3
0.4
0.5
Kar3p-GFP
Nuf2p-GFP
Normalized Spindle Position (Pole -- Equator)
D.
Relative Fluorescence Intensity
900
800
700
600
500
400
300
200
100
0
dSPB
mSPB
Unaligned
Aligned
Preanaphase
Spindle Elongation
Late Anaphase

Figure 5.7: Photobleaching and FRAP analysis of Kar3p-GFP.

Photobleaching of Kar3p-GFP at the SPBs. Recovery was similar regardless of the SPB photobleached. Bar, 2 μm. (A) Representative photobleaching of Kar3p-GFP and recovery of fluorescence in preanaphase. (B) Fluorescence recovery after photobleaching measurements from preanaphase experiment in (A). Left panel displays measured recovery; right panel shows measured recovery (black squares) is best fit with a single exponential curve (gray triangles). (C) Late anaphase photobleaching experiment of Kar3p-GFP where recovery was observed. (D) Fluorescence recovery after photobleaching measurements from preanaphase experiment in (C). Left panel displays measured recovery; right panel shows measured recovery (black squares) is best fit with a single exponential curve (gray triangles). Note the decreased recovery relative to preanaphase.

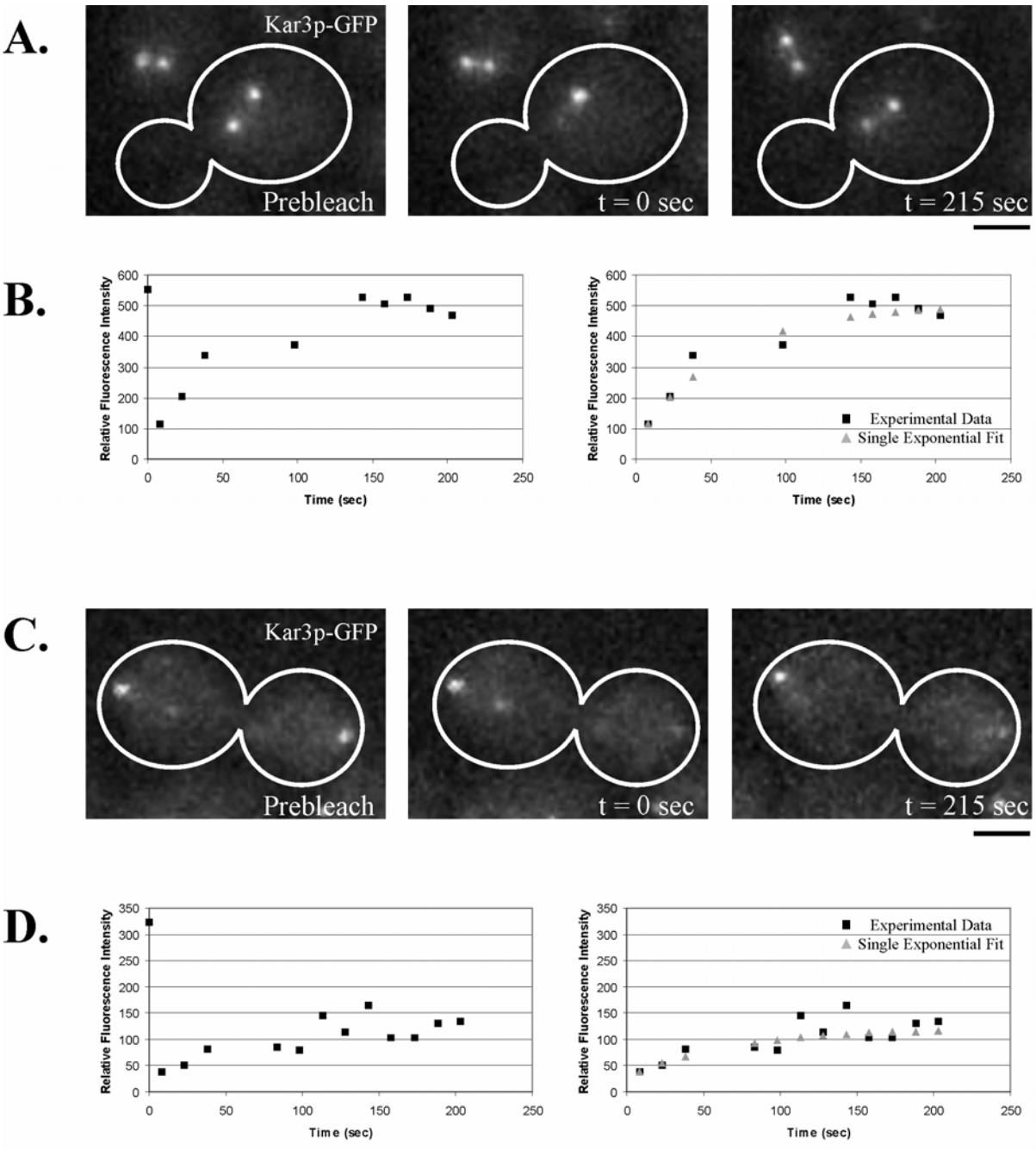
A.
Kar3p-GFP
Prebleach
t = 0 sec
t = 215 sec
B.
Relative Fluorescence Intensity
Time (sec)
Experimental Data
Single Exponential Fit
C.
Kar3p-GFP
Prebleach
t = 0 sec
t = 215 sec
D.
Relative Fluorescence Intensity
Time (sec)
Experimental Data
Single Exponential Fit

Figure 5.8: Mitotic exit is perturbed in *kar3Δ* cells.

kar3Δ cells were delayed in preanaphase and exited mitosis precociously. Bar, 2 μm. (A) *Upper panel*: Time-lapse images of spindle elongation in wild-type cells expressing GFP-Tub1p. 62% of mitotic spindles elongated within one hour (n = 29 cells). *Bottom panel*: Imaging of *kar3Δ* cells with a preanaphase delay where nuclear transiting, or rapid movement of the spindle between mother and bud, occurred. 36% of mitotic spindles in *kar3Δ* cells elongated within one hour (n = 64 cells). (B) Anaphase onset in *kar3Δ* spindles that were pulled into the bud resulted in inappropriate mitotic exit. DIC image is to right. (C) Polyploid *kar3Δ* cells were visible in the population. MTs were marked by GFP-Tub1p and SPBs were visualized with Spc29p-RFP. In unbudded cells, two SPBs with associated MTs were observed.

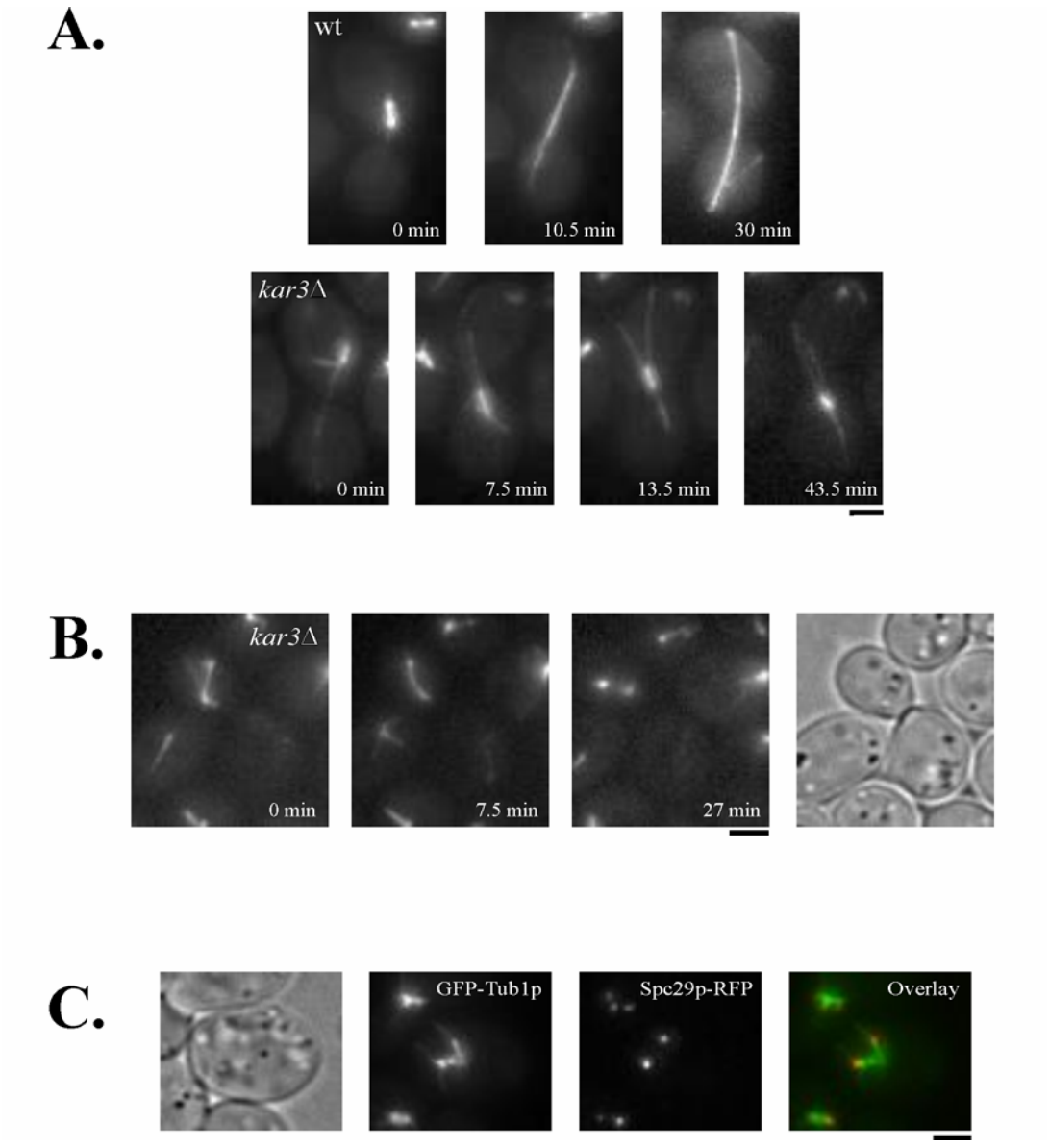
A.
wt
0 min
10.5 min
30 min
kar3Δ
0 min
7.5 min
13.5 min
43.5 min
B.
kar3Δ
0 min
7.5 min
27 min
C.
GFP-Tub1p
Spc29p-RFP
Overlay

Figure 5.9: Model for spindle assembly and elongation in budding yeast.

Additive model for mitotic spindle assembly and elongation in budding yeast. SPBs, gray circles; ipMTs, gray lines. Only two ipMTs are drawn in this schematic. After duplication of the spindle poles in S phase, Bim1p, either localized at or recruited to MT plus ends, enables SPBs to become oppositely oriented. Kar3p and Cik1p, associated preferentially with MT plus ends, cross-link anti-parallel MTs, further restricting the width of the spindle during prometaphase. Cin8p and Kip1p likely participate in cross-linking of ipMTs as well. Once ipMTs are sufficiently cross-linked, Cin8p and Kip1p slide anti-parallel MTs relative to one another to form the 1.5 μm metaphase spindle. The level of DNA compaction and the tension arising from the cohesion between sister chromatids after kinetochore biorientation is proposed to be the major inward force opposing Cin8p and Kip1p (not shown). Kar3p/Cik1p could also act as a second inward force. In anaphase, Ase1p, Bik1p, and Slk19p are recruited to the anaphase spindle to provide structural integrity. These plus end binding proteins are added during spindle assembly and elongation to prevent premature spindle collapse by resisting inward forces.

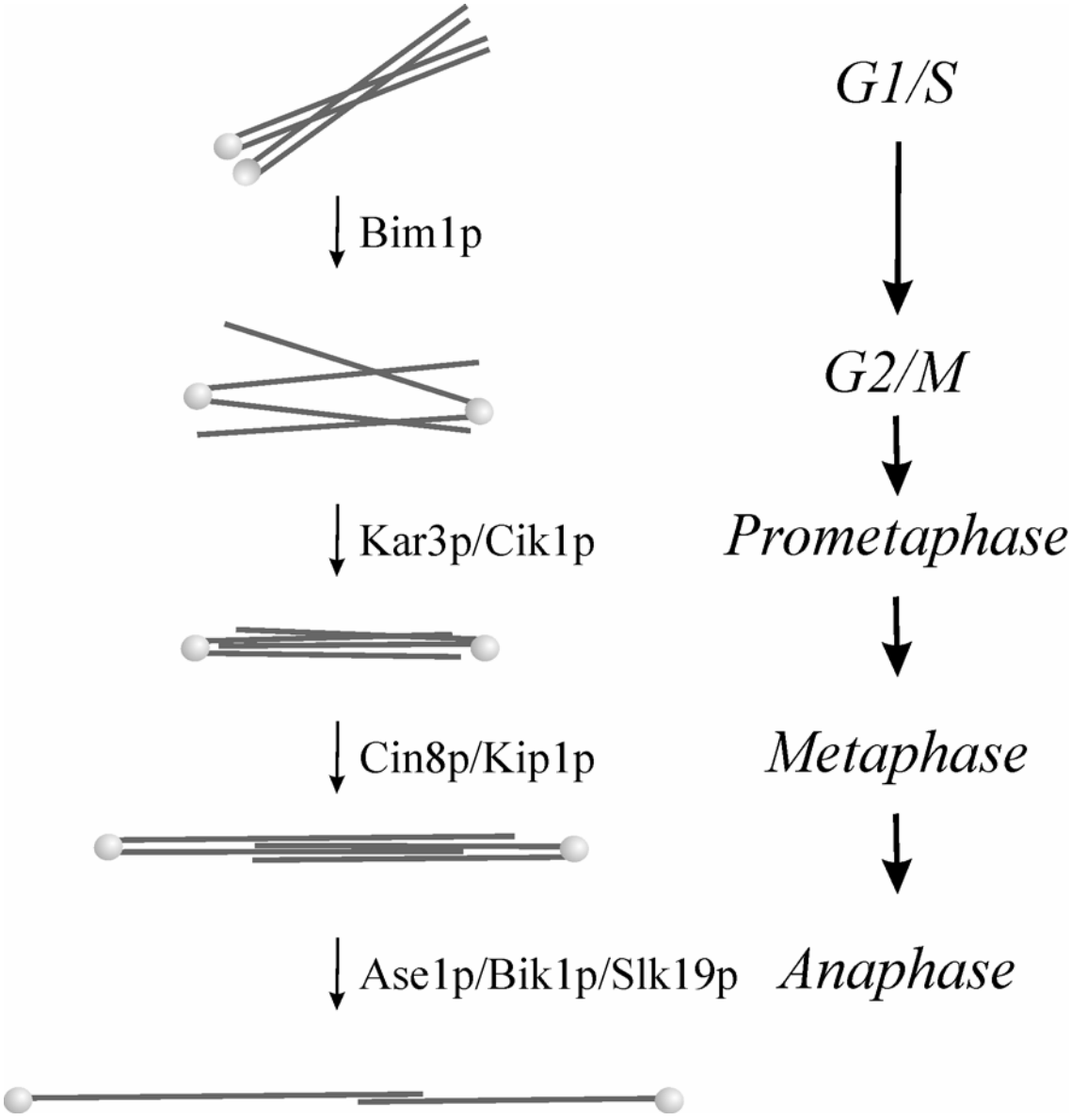
G1/S
Bim1p
G2/M
Kar3p/Cik1p
Prometaphase
Cin8p/Kip1p
Metaphase
Ase1p/Bik1p/Slk19p
Anaphase

Figure 5.S1: PCR based analysis of dicentric chromosome breaks.

Formation of repair products after activation of dicentric Chr III is suppressed in *ase1Δ* and *kar3Δ* cells. (A) Ethidium bromide stained agarose gel of PCR amplification experiments that probed for the repair product formed after dicentric breakage (left lanes) and the *MET14* locus (right lanes) that was used as a control. Images were captured using the Alpha Innotech AlphaImager 2200 system. (B) Quantification of PCR products in (A). Image files were processed in MetaMorph 6.1. Lines were drawn through each band and the integrated intensity was recorded in a linked Microsoft Excel spreadsheet. The background was determined by averaging the intensity of 15 pixels surrounding the band and multiplying this value by the width of the band. This background figure was subtracted from the band intensity, yielding the corrected intensity. To compare PCR reactions, the ratio of repair band to the *MET14* control band was plotted.

A.

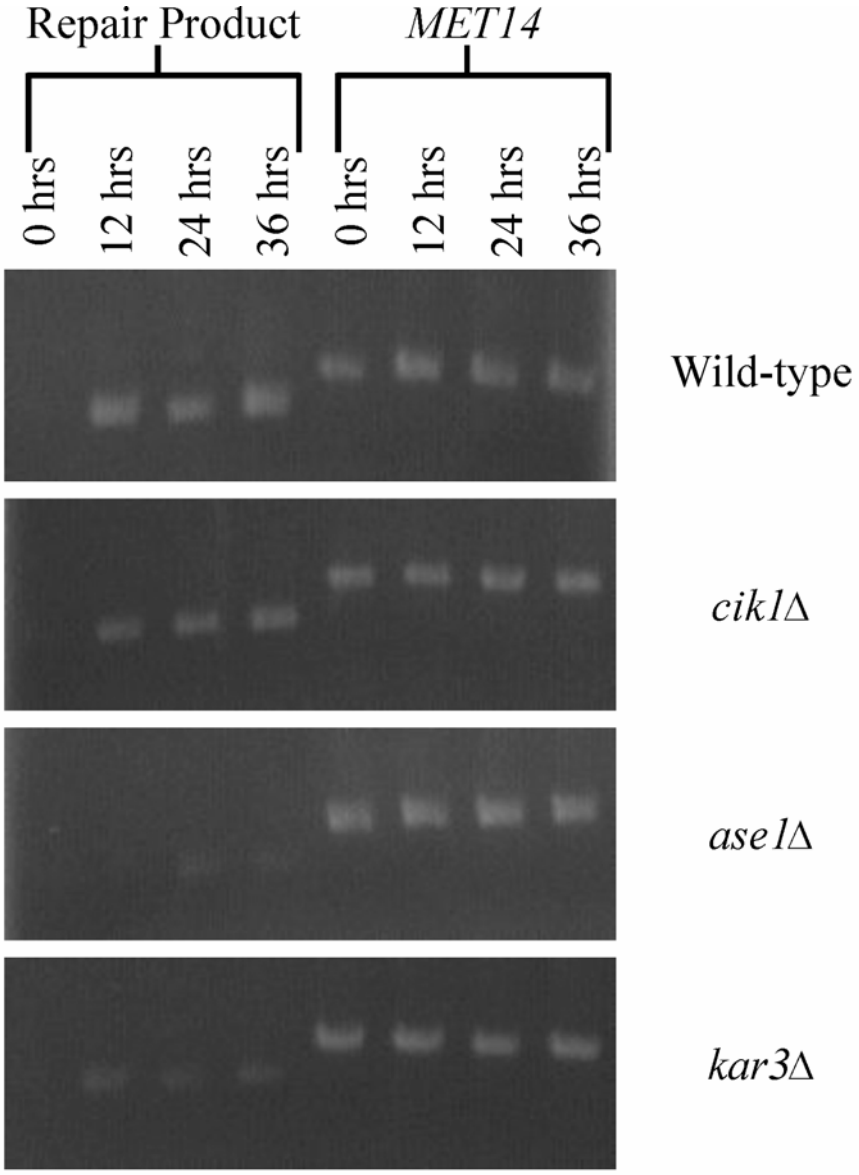
Repair Product
MET14
0 hrs
12 hrs
24 hrs
36 hrs
0 hrs
12 hrs
24 hrs
36 hrs
Wild-type
cik1Δ
ase1Δ
kar3Δ

B.

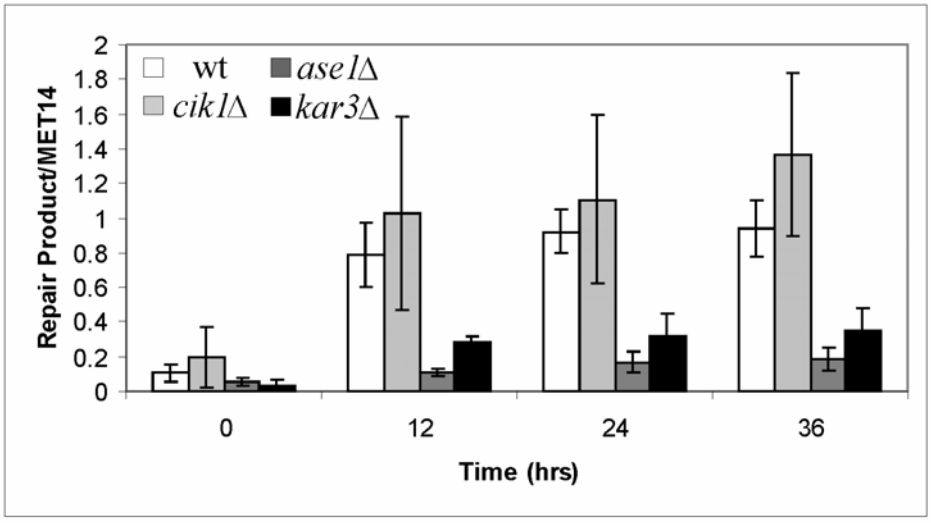
wt
ase1Δ
cik1Δ
kar3Δ
Repair Product/MET14
2
1.8
1.6
1.4
1.2
1
0.8
0.6
0.4
0.2
0
0
12
24
36
Time (hrs)

Figure 5.S2: Kinetochore distribution in the absence of Kar3p.

Kinetochores show a prometaphase distribution in *kar3Δ* cells during preanaphase. Bar, 2 μm. (A) Wild-type and *kar3Δ* cells expressing Nuf2p-GFP. In wild-type, kinetochores form two clusters while the shorter spindles in *kar3Δ* cells results in a single focus of fluorescence. (B) Nuf2p-GFP fluorescence intensity plot. Wild-type cells (n = 40) showed a peak of fluorescence in the quarter spindle whereas the Nuf2p-GFP signal was similar to a prometaphase distribution in *kar3Δ* cells (n = 30). (C) Kinetochores can transiently separate into two clusters during preanaphase in *kar3Δ* cells. (0 min - 13.5 min) Kinetochores are separated from a single focus into distinct clusters. (15 min - 19.5 min) Kinetochores reassociate into a single focus of fluorescence.

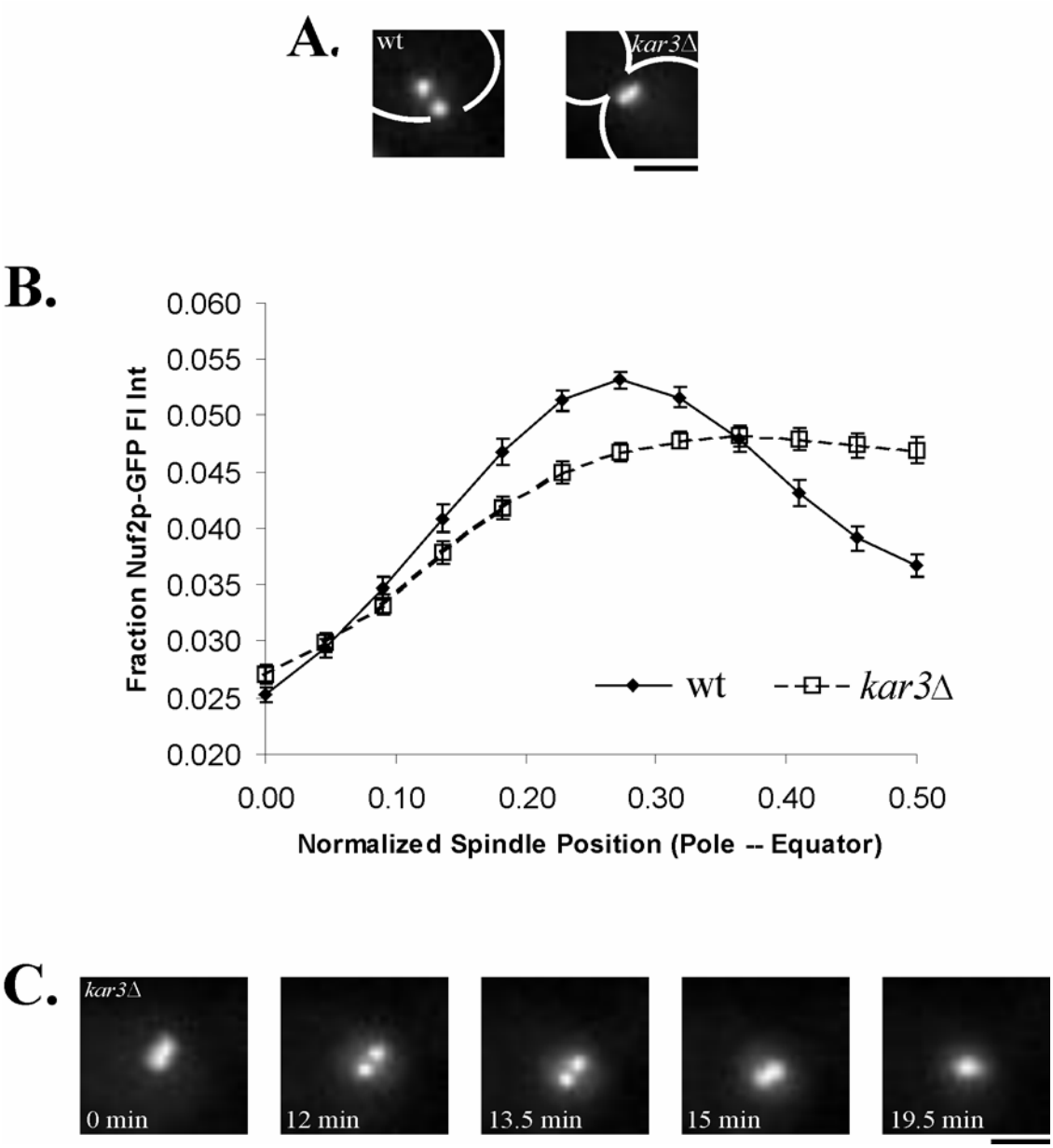
A.
wt
kar3Δ
B.
Fraction Nuf2p-GFP FI Int
0.060
0.055
0.050
0.045
0.040
0.035
0.030
0.025
0.020
0.00
0.10
0.20
0.30
0.40
0.50
Normalized Spindle Position (Pole -- Equator)
wt
kar3Δ
C.
kar3Δ
0 min
12 min
13.5 min
15 min
19.5 min

CHAPTER 6: SUMMARY AND CONCLUSIONS

MTs are required for nuclear migration and spindle assembly. This work has examined MTOC inheritance and plus end binding protein function during nuclear migration, nuclear congression, and spindle assembly. In each instance, proteins that interact with the ends of MTs are critical for cell propagation.

MTs are required to move the nucleus within the cell. In budding yeast, the failure to align the mitotic spindle along the mother-bud axis will result in chromosome segregation defects. The Mitotic Exit Network acts to ensure nuclear migration occurs properly. Mitotic exit is activated by the guanine nucleotide binding state of Tem1p that is controlled in part by the checkpoint protein Bub2p. Relief of Bub2p inhibition could trigger the switch of Tem1p from the GDP to GTP bound state; access to a protein, Lte1p that favors the GTP state; or other control mechanisms. By investigating Tem1p-GFP in living cells, it was shown that passage of the bud neck increased the abundance of Tem1p on the dSPB (Chapter 2). The increase in Tem1p-GFP upon penetration of the bud neck correlated with Cdc15p-GFP localization, indicating mitotic exit had been initiated (Chapter 2). If a critical concentration of Tem1p localized to the dSPB during anaphase to trigger mitotic exit, mutant analysis demonstrated this concentration is low (Chapter 2). Together, these data suggest Tem1p localizes in abundance to the dSPB to ensure mitotic exit occurs.

Models for MEN function propose that Tem1p is activated by accessing a chemical gradient of Lte1p or that the phosphorylation of Bub2p relieves Tem1p inhibition to

triggering mitotic exit (Bardin and Amon, 2001; Hu and Elledge, 2002). Tem1p-GFP appeared to localize in response to nuclear movements, enriching in the direction of nuclear motion (Chapter 2). These data suggest that Tem1p could respond to forces on the SPBs or nucleus during mitosis. In this model, MT interactions with the bud neck or bud cortex would result in transient forces on the dSPB and asymmetry in Tem1p-GFP localization. Alternatively, the asymmetry in Tem1p-GFP localization could correlate with post-translational modifications of Tem1p (Bardin et al., 2000; Liakopoulos et al., 2003), or by interactions between Tem1p and unknown SPB components. Upon activation of nuclear migration, dynein dependent forces pull the nucleus into the bud, placing large forces on the dSPB. These forces could increase Tem1p-GFP localization to the dSPB (Chapter 2). However, Lte1p does play a role in increasing Tem1p abundance on the dSPB (Chapter 2). Thus, budding yeast may have evolved a system to sense MT dependent forces on the nucleus. Tem1p could respond to both dSPB entry into the bud and forces on the spindle pole to ensure nuclear migration occurs before mitotic exit is activated.

A second type of nuclear migration occurs before karyogamy. In the mating pathway, oppositely oriented MTs interact during nuclear congression. Kar3p, Bik1p, and Kar9p are required for nuclear congression (Berlin et al., 1990; Kurihara et al., 1994; Meluh and Rose, 1990). Previous models for nuclear congression have suggested that overlapping MTs coupled to minus end depolymerization bring both nuclei together (Rose, 1996). However, imaging of Bik1p-3xGFP demonstrated MT plus ends interact to drive nuclear congression (Chapter 3). Plus end interactions were absent in *kar3Δ* cells and reduced in *bik1Δ* and *kar9Δ* cells (Chapter 3). These data support a model where Kar3p is required to initiate overlapping MT plus end interactions. Bik1p is also required for efficient plus end

interactions. In contrast, Kar9p acts solely as an orientation factor for MT plus ends before cell fusion. In this view, both Kar3p and Bik1p are required for the structural stability of overlapping MT arrays when forces are generated during mating.

In the absence of karyogamy, the cell is not inhibited from budding, resulting in the formation of two mitotic spindles (Demeter et al., 2000). Using these heterokaryons, anaphase onset was found to be autonomous between both spindles (Chapter 4). However, spindle disassembly was coordinated suggesting there is a pancellular signal for mitotic exit (Chapter 4). How does the cell coordinate spindle disassembly? One possible mechanism would be through MEN function. It is possible that after anaphase onset, cortical pulling forces are activated that result in the passage of one SPB into the bud. After SPB penetration into the bud, the release of Cdc14p could be maintained and the cell will exit mitosis.

As a second test of how overlapping MTs function during cell division, plus end binding proteins were analyzed during mitotic spindle assembly and elongation (Chapter 5). In some mutants, the spindle can disassemble prematurely in anaphase without resulting in lethality (Chapter 2) (Pellman et al., 1995). This suggests the central spindle is not required to perform chromosome segregation after the initial elongation stage. However, plus end binding proteins in the central spindle are required to resist the introduction of mechanical stress in anaphase (Chapter 5). Kar3p, Bim1p, and Ase1p are some of the plus end binding proteins required for the viability of cells with an activated dicentric chromosome. Kar3p localizes to ipMT plus ends and to the central spindle in anaphase (Chapter 5). These data suggest a new mechanism for spindle assembly where plus end binding proteins accumulate on the spindle to resist mechanical stress. The function of these plus end binding proteins is critical as a mechanism to avoid aneuploidy.

In what way can this work be extended to further the understanding of MTOC inheritance and plus end binding protein function? Concerning MTOC inheritance, it is still unclear what the role of astral forces on MEN activation is. Two components are required to answer this question. First, an understanding of the role astral forces play in spindle elongation is required. Does the central spindle restrain movement of the SPBs to the spindle poles as in other systems? Does dynein generate greater forces on the dSPB, enabling the nucleus to be pulled into the neck? The second component requires understanding if Tem1p can localize in response to forces. Directly severing a spindle in a cell that expresses Tem1p-GFP may result in increased Tem1p accumulation on the dSPB if the dSPB moves more quickly towards the cortex. However, the SPB did not touch the cortex more quickly, nor did Tem1p-GFP accumulate significantly, in *ase1Δ* cells (Chapter 2). This suggests the forces on the dSPB did not increase when spindle structure was perturbed. An alternative hypothesis is that an unknown protein is responsive to forces at the SPB and participates in the recruitment of Tem1p. Therefore, if the MEN includes a force response component, a complex set of protein-protein interactions may occur that have yet to be elucidated.

How do plus end binding proteins function to generate MT-MT interactions? Kar3p and Bik1p are required for nuclear congression but, unlike anaphase spindle elongation, Ase1p and Slk19p are not (our unpublished observations). Do Kar3p, Bik1p, and a small subset of other MAPs function in cross-linking oppositely oriented MTs? What other plus end binding proteins that are required for nuclear congression? Of particular interest is Bim1p. Bim1p is required for nuclear orientation to the shmoo tip but has a more severe karyogamy defect than cells lacking Kar9p (Chapter 3) (Kurihara et al., 1994; Miller and Rose, 1998; Schwartz et al., 1997). This suggests Bim1p may play a role in MT-MT

interactions during nuclear congression. Is the complex of proteins at the plus end conserved for ipMT function during mitosis? The addition of proteins such as Ase1p during spindle elongation could specifically resist mechanical stress from lagging chromosomes in anaphase. If so, how does a limited set of plus end binding proteins drive nuclear congression? Cytoplasmic MTs rarely survive the fixation for electron microscopy, though immunogold studies of Bik1p and Kar3p during nuclear congression could elucidate any cross-liking that may occur. How the MTs switch from dynamic instability before MT-MT interactions to persistent depolymerization after plus ends associate is also unknown.

Overlapping MT arrays are present in the mitotic spindle. What is the function of Kar3p during mitosis, particularly in anaphase spindle elongation? Kar3p is relied on during the life cycle of *S. cerevisiae*, making it one of the most critical proteins in the cell. Does Kar3p function at the kinetochore in anaphase to attach depolymerizing plus ends to the spindle poles during chromosome segregation? While this function is suggested by the requirement for Kar3p to attach shortening MTs to the shmoo tip (Maddox et al., 2003b), developing LacO assays to label centromeres or imaging kinetochores with Nuf2p-GFP or Cse4p-GFP would identify the presence of lagging chromosomes that could result from defects in kinetochore-MT attachments. Our preliminary results suggest lagging chromosomes are not increased in *kar3Δ* cells (Chapter 5). How does Kar3p interact with other central spindle proteins during spindle assembly? Does Kar3p form a complex with Ase1p, Bik1p, and other MAPs, to maintain MT plus end associations during persistent polymerization in the central spindle? Again, protein-protein interaction studies and a biochemical characterization of Kar3p function would illuminate this process.

In conclusion, these results have revealed new mechanisms for MTOC inheritance and MT-MT interactions. Budding yeast is viewed as a "simple" organism where, relative to metazoan cells, a few proteins are required to coordinate the behavior of a few MTs. However, despite the limited number of proteins required for each process, the idea that there is a simple mechanistic explanation is misleading. Rather, even this simple system displays complexities that require further examination. In recent years, the study of cell division has strived for universal mechanisms to explain biological phenomena across species. While this goal is logically appealing, realistically each organism has evolutionary distinctions that precludes the description of mitosis by a single set of steps. In budding yeast, the limited number of MTs likely reduces the proteins required for processes such as anaphase spindle elongation (Ase1p, Bik1p, Cik1p, Kar3p, and Slk19p) or nuclear congression (Bik1p, Cik1p, and Kar3p) but does not limit the complexity of the overall questions. How is one MTOC inherited by each daughter cell? How do a few MTs coordinately depolymerize to draw two entire nuclei through the cytoplasm prior to karyogamy? How does one or two MTs maintain the structural integrity of the mitotic spindle during anaphase? The mechanistic answers to these questions will require further studies into the behavior of MTs in budding yeast and other systems.

APPENDIX A: FRAP MEASUREMENTS

Introduction

Fluorescence Recovery After Photobleaching (FRAP) is a technique that measures the ability of a protein to exchange from one site in the cell with the cellular protein pool. This technique was pioneered with fluorescently labeled tubulin and it was demonstrated that tubulin is freely diffusible in the cytoplasm and could exchange between the cytoplasm and spindle (Salmon et al., 1984a; Salmon et al., 1984b). This finding was also demonstrated in budding yeast for GFP-Tub1p and other proteins such as Tem1p-GFP (Chapter 2) (Maddox et al., 2000). In this appendix, results are presented where a variety of proteins were photobleached in budding yeast to measure their exchange with the cytoplasmic pool during mitotic exit, polarity establishment, preanaphase and anaphase spindle function, and DNA damage response (Table A1). Additionally, FRAP measurements of *S. pombe* spindle assembly checkpoint proteins are recorded (Table A1).

Materials and Methods

Budding yeast were grown as detailed previously (Chapter 2). Fission yeast were propagated by standard methods (Tran et al., 2001). Photobleaching was performed as described previously (Chapter 2) (Roumanie et al., 2005). Image acquisition and FRAP analysis was varied as necessary (range 400 ms to 5 min intervals between each acquisition). Five plane Z-series or single plane images with a corresponding DIC image were acquired.

Table

Probe	Genetic Background	k	t1/2 (sec)	R (%)	n	Source
Mitotic Exit Network						
Tem1p-GFP (fast)	wt – late anaphase	0.203	4.50	62.1	6	Chapter 2
(slow)		0.0103	133	--	-	
Bub2p-GFP	wt – preanaphase	0.0190	40.7	44.9	6	
Cdc15p-GFP	wt – late anaphase	0.0241	29.3	61.9	2	
Lte1p-3xGFP	wt	0.0224	30.9	73.0	2	
Cell Polarity						
Bem1p-GFP	wt – MAT**a**	0.239	3.15	71.8	6	D. Lew[A]
	bem1Δ - MATα	0.295	2.74	63.0	6	D. Lew (DLY 6022)
	bud1Δ - MATα	0.249	2.84	80.2	6	D. Lew (DLY 6020)
CEN-Cdc24p-GFP	wt – MAT**a**/α	0.429	1.68	96.3	7	D. Lew
Spa2p-GFP	wt – MAT**a**	0.0435	16.7	61.0	6	D. Lew
	wt – MAT**a**/α	0.0493	16.7	76.5	5	D. Lew
	bud1Δ/ bud1Δ - MAT**a**/α	0.0514	14.8	78.9	6	D. Lew (DLY 6023)
GFP-Sec8p	wt	0.0543	16.8	81.7	11	P. Brennwald[B]
	rho3 Q74L	0.0568	15.4	77.4	8	P. Brennwald
	rho3 v51	0.0403	19.5	86.5	9	P. Brennwald
	sec3ΔNT	0.0725	12.4	77.7	7	P. Brennwald
	rho3 v51 sec3ΔNT	0.0575	13.8	69.0	6	P. Brennwald
Tubulin, Kinetochore, & SPB Proteins						
GFP-Tub1p	wt	0.0209	42.9	50.2	7	T. Davis[C]
	dam1-765	0.0226	34.7	63.2	7	T. Davis
	kar3Δ	0.0271	56.9	80.6	2	
	kar3-1	0.0122	83.6	54.1	2	
Nuf2p-GFP	wt	n/a	n/a	6.59	7[D]	
Kar3p-GFP	wt – preanaphase	0.0130	57.3	72.0	6	
	wt – late anaphase	0.0133	60.5	34.3	3[E]	
DNA Damage Response						
Rad52p-GFP	wt – glucose	0.750	1.16	50.4	2	
(fast)	Damage: GAL-HO	1.331	1.00	81.0	8	
(slow)		0.0293	62.4	--	-	
	Damage: MMS	0.735	1.17	44.7	8	
S. pombe *Spindle Assembly Checkpoint Proteins*						
Mad1p-GFP	wt	0.0691	33.7	86.3	4	K. Hardwick[F]
Mad3p-GFP	wt	0.0376	18.4	78.8	2	K. Hardwick

[A]Duke University, Durham, NC
[B]University of North Carolina, Chapel Hill, NC
[C]University of Washington, Seattle, WA
[D]Additionally, 7 cells were photobleached and did not recover (R < 5%)
[E]Additionally, 4 cells were photobleached and did not recover (R < 5%)
[F]University of Edinburgh, Edinburgh, Scotland

Table A1.1: FRAP measurements for GFP fusion proteins.

REFERENCES

Adames, N.R., and J.A. Cooper. 2000. Microtubule interactions with the cell cortex causing nuclear movements in Saccharomyces cerevisiae. *Journal of Cell Biology*. 149:863-74.

Adames, N.R., J.R. Oberle, and J.A. Cooper. 2001. The surveillance mechanism of the spindle position checkpoint in yeast. *Journal of Cell Biology*. 153:159-68.

Adams, A.E., and J.R. Pringle. 1984. Relationship of actin and tubulin distribution to bud growth in wild-type and morphogenetic-mutant Saccharomyces cerevisiae. *Journal of Cell Biology*. 98:934-45.

Akhmanova, A., and C.C. Hoogenraad. 2005. Microtubule plus-end-tracking proteins: mechanisms and functions. *Current Opinions in Cell Biology*. 17:47-54.

Alexander, S.P., and C.L. Rieder. 1991. Chromosome motion during attachment to the vertebrate spindle: initial saltatory-like behavior of chromosomes and quantitative analysis of force production by nascent kinetochore fibers. *Journal of Cell Biology*. 113:805-15.

Alexandru, G., W. Zachariae, A. Schleiffer, and K. Nasmyth. 1999. Sister chromatid separation and chromosome re-duplication are regulated by different mechanisms in response to spindle damage. *EMBO Journal*. 18:2707-21.

Allen, R.D., J. Metuzals, I. Tasaki, S.T. Brady, and S.P. Gilbert. 1982. Fast axonal transport in squid giant axon. *Science*. 218:1127-9.

Amos, L., and A. Klug. 1974. Arrangement of subunits in flagellar microtubules. *Journal of Cell Science*. 14:523-49.

Asakawa, K., S. Yoshida, F. Otake, and A. Toh-e. 2001. A novel functional domain of Cdc15 kinase is required for its interaction with Tem1 GTPase in Saccharomyces cerevisiae. *Genetics*. 157:1437-50.

Ayscough, K.R., J. Stryker, N. Pokala, M. Sanders, P. Crews, and D.G. Drubin. 1997. High rates of actin filament turnover in budding yeast and roles for actin in establishment and maintenance of cell polarity revealed using the actin inhibitor latrunculin-A. *Journal of Cell Biology*. 137:399-416.

Bajer, A.S. 1982. Functional autonomy of monopolar spindle and evidence for oscillatory movement in mitosis. *Journal of Cell Biology*. 93:33-48.

Bardin, A.J., and A. Amon. 2001. Men and sin: what's the difference? *Nature Reviews Molecular Cell Biology*. 2:815-26.

Bardin, A.J., R. Visintin, and A. Amon. 2000. A mechanism for coupling exit from mitosis to partitioning of the nucleus. *Cell*. 102:21-31.

Barrett, J.G., B.D. Manning, and M. Snyder. 2000. The Kar3p kinesin-related protein forms a novel heterodimeric structure with its associated protein Cik1p. *Molecular Biology of the Cell*. 11:2373-85.

Bergen, L.G., and G.G. Borisy. 1980. Head-to-tail polymerization of microtubules in vitro. Electron microscope analysis of seeded assembly. *Journal of Cell Biology*. 84:141-50.

Berlin, V., C.A. Styles, and G.R. Fink. 1990. BIK1, a protein required for microtubule function during mating and mitosis in Saccharomyces cerevisiae, colocalizes with tubulin. *Journal of Cell Biology*. 111:2573-86.

Bi, E., P. Maddox, D.J. Lew, E.D. Salmon, J.N. McMillan, E. Yeh, and J.R. Pringle. 1998. Involvement of an actomyosin contractile ring in Saccharomyces cerevisiae cytokinesis. *Journal of Cell Biology*. 142:1301-12.

Bi, E., and J.R. Pringle. 1996. ZDS1 and ZDS2, genes whose products may regulate Cdc42p in Saccharomyces cerevisiae. *Molecular and Cellular Biology*. 16:5264-75.

Binder, L.I., W.L. Dentler, and J.L. Rosenbaum. 1975. Assembly of chick brain tubulin onto flagellar microtubules from Chlamydomonas and sea urchin sperm. *Proceedings of the National Academy of Sciences U S A*. 72:1122-6.

Bloecher, A., G.M. Venturi, and K. Tatchell. 2000. Anaphase spindle position is monitored by the BUB2 checkpoint. *Nature Cell Biology*. 2:556-8.

Bosl, W.J., and R. Li. 2005. Mitotic-exit control as an evolved complex system. *Cell*. 121:325-33.

Boveri, T. 1902. On multipolar mitosis as a means of analysis of the cell nucleus. Hafner Press, New York, NY. 74-97 pp.

Brock, J.A., and K. Bloom. 1994. A chromosome breakage assay to monitor mitotic forces in budding yeast. *Journal of Cell Science*. 107:891-902.

Byers, B., and L. Goetsch. 1975. Behavior of spindles and spindle plaques in the cell cycle and conjugation of Saccharomyces cerevisiae. *Journal of Bacteriology*. 124:511-23.

Carminati, J.L., and T. Stearns. 1997. Microtubules orient the mitotic spindle in yeast through dynein-dependent interactions with the cell cortex. *Journal of Cell Biology*. 138:629-41.

Carvalho, P., M.L. Gupta, Jr., M.A. Hoyt, and D. Pellman. 2004. Cell cycle control of kinesin-mediated transport of Bik1 (CLIP-170) regulates microtubule stability and dynein activation. *Developmental Cell*. 6:815-29.

Cassimeris, L., N.K. Pryer, and E.D. Salmon. 1988. Real-time observations of microtubule dynamic instability in living cells. *Journal of Cell Biology*. 107:2223-31.

Castillon, G.A., N.R. Adames, C.H. Rosello, H.S. Seidel, M.S. Longtine, J.A. Cooper, and R.A. Heil-Chapdelaine. 2003. Septins have a dual role in controlling mitotic exit in budding yeast. *Current Biology*. 13:654-8.

Chalfie, M., and J.N. Thomson. 1982. Structural and functional diversity in the neuronal microtubules of Caenorhabditis elegans. *Journal of Cell Biology*. 93:15-23.

Chu, H.M., M. Yun, D.E. Anderson, H. Sage, H.W. Park, and S.A. Endow. 2005. Kar3 interaction with Cik1 alters motor structure and function. *EMBO Journal*. 24:3214-23.

Cimini, D., and F. Degrassi. 2005. Aneuploidy: a matter of bad connections. *Trends in Cell Biology*. 15:442-51.

Conde, J., and G.R. Fink. 1976a. A mutant of Saccharomyces cerevisiae defective for nuclear fusion. *Proc Natl Acad Sci U S A*. 73:3651-5.

Conde, J., and G.R. Fink. 1976b. A mutant of Saccharomyces cerevisiae defective for nuclear fusion. *Proceedings of the National Academy of Sciences U S A*. 73:3651-5.

Cottingham, F.R., L. Gheber, D.L. Miller, and M.A. Hoyt. 1999. Novel roles for saccharomyces cerevisiae mitotic spindle motors. *Journal of Cell Biology*. 147:335-50.

Cottingham, F.R., and M.A. Hoyt. 1997. Mitotic spindle positioning in Saccharomyces cerevisiae is accomplished by antagonistically acting microtubule motor proteins. *Journal of Cell Biology*. 138:1041-53.

Coue, M., V.A. Lombillo, and J.R. McIntosh. 1991. Microtubule depolymerization promotes particle and chromosome movement in vitro. *Journal of Cell Biology*. 112:1165-75.

Cross, F., L.H. Hartwell, C. Jackson, and J.B. Konopka. 1988. Conjugation in Saccharomyces cerevisiae. *Annual Review of Cell Biology*. 4:429-57.

D'Amours, D., and A. Amon. 2004. At the interface between signaling and executing anaphase--Cdc14 and the FEAR network. *Genes and Development*. 18:2581-95.

Daum, J.R., N. Gomez-Ospina, M. Winey, and D.J. Burke. 2000. The spindle checkpoint of Saccharomyces cerevisiae responds to separable microtubule-dependent events. *Current Biology*. 10:1375-8.

Demeter, J., S.E. Lee, J.E. Haber, and T. Stearns. 2000. The DNA damage checkpoint signal in budding yeast is nuclear limited. *Molecular Cell*. 6:487-92.

DeZwaan, T.M., E. Ellingson, D. Pellman, and D.M. Roof. 1997. Kinesin-related KIP3 of Saccharomyces cerevisiae is required for a distinct step in nuclear migration. *Journal of Cell Biology*. 138:1023-40.

Dogterom, M., J.W. Kerssemakers, G. Romet-Lemonne, and M.E. Janson. 2005. Force generation by dynamic microtubules. *Current Opinions in Cell Biology*. 17:67-74.

Doheny, K.F., P.K. Sorger, A.A. Hyman, S. Tugendreich, F. Spencer, and P. Hieter. 1993. Identification of essential components of the S. cerevisiae kinetochore. *Cell*. 73:761-74.

Drechsel, D.N., and M.W. Kirschner. 1994. The minimum GTP cap required to stabilize microtubules. *Current Biology*. 4:1053-61.

Endow, S.A., S.J. Kang, L.L. Satterwhite, M.D. Rose, V.P. Skeen, and E.D. Salmon. 1994. Yeast Kar3 is a minus-end microtubule motor protein that destabilizes microtubules preferentially at the minus ends. *EMBO Journal*. 13:2708-13.

Eshel, D., L.A. Urrestarazu, S. Vissers, J.C. Jauniaux, J.C. van Vliet-Reedijk, R.J. Planta, and I.R. Gibbons. 1993. Cytoplasmic dynein is required for normal nuclear segregation in yeast. *Proceedings of the National Academy of Sciences U S A*. 90:11172-6.

Euteneuer, U., and J.R. McIntosh. 1980. Polarity of midbody and phragmoplast microtubules. *Journal of Cell Biology*. 87:509-15.

Euteneuer, U., and J.R. McIntosh. 1981. Structural polarity of kinetochore microtubules in PtK1 cells. *Journal of Cell Biology*. 89:338-45.

Evans, L., T. Mitchison, and M. Kirschner. 1985. Influence of the centrosome on the structure of nucleated microtubules. *Journal Cell Biology*. 100:1185-91.

Fesquet, D., P.J. Fitzpatrick, A.L. Johnson, K.M. Kramer, J.H. Toyn, and L.H. Johnston. 1999. A Bub2p-dependent spindle checkpoint pathway regulates the Dbf2p kinase in budding yeast. *EMBO Journal*. 18:2424-34.

Fraschini, R., E. Formenti, G. Lucchini, and S. Piatti. 1999. Budding yeast Bub2 is localized at spindle pole bodies and activates the mitotic checkpoint via a different pathway from Mad2. *Journal of Cell Biology*. 145:979-91.

Gardner, M.K., C.G. Pearson, B.L. Sprague, T.R. Zarzar, K. Bloom, E.D. Salmon, and D.J. Odde. 2005. Tension-dependent regulation of microtubule dynamics at kinetochores can explain metaphase congression in yeast. *Molecular Biology of the Cell*. 16:3764-75.

Geymonat, M., A. Spanos, S.J. Smith, E. Wheatley, K. Rittinger, L.H. Johnston, and S.G. Sedgwick. 2002. Control of mitotic exit in budding yeast. In vitro regulation of Tem1 GTPase by Bub2 and Bfa1. *Journal of Biological Chemistry*. 277:28439-45.

Goldstein, A.L., and J.H. McCusker. 1999. Three new dominant drug resistance cassettes for gene disruption in Saccharomyces cerevisiae. *Yeast*. 15:1541-53.

Gonczy, P., S. Pichler, M. Kirkham, and A.A. Hyman. 1999. Cytoplasmic dynein is required for distinct aspects of MTOC positioning, including centrosome separation, in the one cell stage Caenorhabditis elegans embryo. *Journal of Cell Biology*. 147:135-50.

Gorbsky, G.J., P.J. Sammak, and G.G. Borisy. 1987. Chromosomes move poleward in anaphase along stationary microtubules that coordinately disassemble from their kinetochore ends. *Journal of Cell Biology*. 104:9-18.

Gorbsky, G.J., P.J. Sammak, and G.G. Borisy. 1988. Microtubule dynamics and chromosome motion visualized in living anaphase cells. *Journal of Cell Biology*. 106:1185-92.

Gould, R.R., and G.G. Borisy. 1977. The pericentriolar material in Chinese hamster ovary cells nucleates microtubule formation. *Journal of Cell Biology*. 73:601-15.

Gupta, M.L., Jr., C.J. Bode, D.A. Thrower, C.G. Pearson, K.A. Suprenant, K.S. Bloom, and R.H. Himes. 2002. beta-Tubulin C354 mutations that severely decrease microtubule dynamics do not prevent nuclear migration in yeast. *Molecular Biology of the Cell*. 13:2919-32.

Haber, J.E. 1998. Mating-type gene switching in Saccharomyces cerevisiae. *Annual Review of Genetics*. 32:561-99.

Harris, P. 1962. Some structural and functional aspects of the mitotic apparatus in sea urchin embryos. *Journal of Cell Biology*. 14:475-87.

Hartwell, L.H., and T.A. Weinert. 1989. Checkpoints: controls that ensure the order of cell cycle events. *Science*. 246:629-34.

Hasek, J., I. Rupes, J. Svobodova, and E. Streiblova. 1987. Tubulin and actin topology during zygote formation of Saccharomyces cerevisiae. *Journal of General Microbiology*. 133:3355-63.

Heidemann, S.R., and J.R. McIntosh. 1980. Visualization of the structural polarity of microtubules. *Nature*. 286:517-9.

Hildebrandt, E.R., and M.A. Hoyt. 2000. Mitotic motors in Saccharomyces cerevisiae. *Biochimica et Biophysica Acta*. 1496:99-116.

Hill, A., and K. Bloom. 1987. Genetic manipulation of centromere function. *Molecular and Cellular Biology*. 7:2397-405.

Hill, A., and K. Bloom. 1989. Acquisition and processing of a conditional dicentric chromosome in Saccharomyces cerevisiae. *Molecular and Cellular Biology*. 9:1368-70.

Hill, T.L. 1985. Theoretical problems related to the attachment of microtubules to kinetochores. *Proceedings of the National Academy of Sciences U S A*. 82:4404-8.

Hoepfner, D., F. Schaerer, A. Brachat, A. Wach, and P. Philippsen. 2002. Reorientation of mispositioned spindles in short astral microtubule mutant spc72Delta is dependent on spindle pole body outer plaque and Kar3 motor protein. *Molecular Biology of the Cell*. 13:1366-80.

Horio, T., and H. Hotani. 1986. Visualization of the dynamic instability of individual microtubules by dark-field microscopy. *Nature*. 321:605-7.

Howell, B.J., D.B. Hoffman, G. Fang, A.W. Murray, and E.D. Salmon. 2000. Visualization of Mad2 dynamics at kinetochores, along spindle fibers, and at spindle poles in living cells. *Journal of Cell Biology*. 150:1233-50.

Hoyt, M.A. 2000. Exit from mitosis: spindle pole power. *Cell*. 102:267-70.

Hoyt, M.A., L. He, L. Totis, and W.S. Saunders. 1993. Loss of function of Saccharomyces cerevisiae kinesin-related CIN8 and KIP1 is suppressed by KAR3 motor domain mutations. *Genetics*. 135:35-44.

Hoyt, M.A., L. Totis, and B.T. Roberts. 1991. S. cerevisiae genes required for cell cycle arrest in response to loss of microtubule function. *Cell*. 66:507-17.

Hu, F., and S.J. Elledge. 2002. Bub2 is a cell cycle regulated phospho-protein controlled by multiple checkpoints. *Cell Cycle*. 1:351-5.

Huffaker, T.C., J.H. Thomas, and D. Botstein. 1988. Diverse effects of beta-tubulin mutations on microtubule formation and function. *Journal of Cell Biology*. 106:1997-2010.

Huitorel, P., and M.W. Kirschner. 1988. The polarity and stability of microtubule capture by the kinetochore. *Journal of Cell Biology*. 106:151-9.

Huyett, A., J. Kahana, P. Silver, X. Zeng, and W.S. Saunders. 1998. The Kar3p and Kip2p motors function antagonistically at the spindle poles to influence cytoplasmic microtubule numbers. *Journal of Cell Science*. 111:295-301.

Hwang, E., J. Kusch, Y. Barral, and T.C. Huffaker. 2003. Spindle orientation in Saccharomyces cerevisiae depends on the transport of microtubule ends along polarized actin cables. *Journal of Cell Biology*. 161:483-8.

Hyman, A.A., and E. Karsenti. 1996. Morphogenetic properties of microtubules and mitotic spindle assembly. *Cell*. 84:401-10.

Hyman, A.A., and T.J. Mitchison. 1990. Modulation of microtubule stability by kinetochores in vitro. *Journal of Cell Biology*. 110:1607-16.

Inoue, S. 1953. Polarization optical studies of the mitotic spindle I: The demonstration of spindle fibers in living cells. *Chromosoma*. 5:487-500.

Inoue, S., and H. Sato. 1967. Cell motility by labile association of molecules. The nature of mitotic spindle fibers and their role in chromosome movement. *Journal of General Physiology*. 50:Suppl:259-92.

Jacobs, C.W., A.E. Adams, P.J. Szaniszlo, and J.R. Pringle. 1988. Functions of microtubules in the Saccharomyces cerevisiae cell cycle. *Journal of Cell Biology*. 107:1409-26.

Jaspersen, S.L., J.F. Charles, and D.O. Morgan. 1999. Inhibitory phosphorylation of the APC regulator Hct1 is controlled by the kinase Cdc28 and the phosphatase Cdc14. *Current Biology*. 9:227-36.

Johnson, R.T., and P.N. Rao. 1970. Mammalian cell fusion: induction of premature chromosome condensation in interphase nuclei. *Nature*. 226:717-22.

Jones, M.H., J.B. Bachant, A.R. Castillo, T.H. Giddings, Jr., and M. Winey. 1999. Yeast Dam1p is required to maintain spindle integrity during mitosis and interacts with the Mps1p kinase. *Molecular Biology of the Cell*. 10:2377-91.

Juang, Y.L., J. Huang, J.M. Peters, M.E. McLaughlin, C.Y. Tai, and D. Pellman. 1997. APC-mediated proteolysis of Ase1 and the morphogenesis of the mitotic spindle. *Science*. 275:1311-4.

Kahana, J.A., B.J. Schnapp, and P.A. Silver. 1995. Kinetics of spindle pole body separation in budding yeast. *Proceedings of the National Academy of Sciences U S A*. 92:9707-11.

Kapitein, L.C., E.J. Peterman, B.H. Kwok, J.H. Kim, T.M. Kapoor, and C.F. Schmidt. 2005. The bipolar mitotic kinesin Eg5 moves on both microtubules that it crosslinks. *Nature*. 435:114-8.

Kiehart, D.P. 1981. Studies on the in vivo sensitivity of spindle microtubules to calcium ions and evidence for a vesicular calcium-sequestering system. *Journal of Cell Biology*. 88:604-17.

Kilmartin, J.V., and A.E. Adams. 1984. Structural rearrangements of tubulin and actin during the cell cycle of the yeast Saccharomyces. *Journal of Cell Biology*. 98:922-33.

King, S.M., and J.S. Hyams. 1983. Analysis of anaphase B in saccharomyces cerevisiae using a monoclonal antibody against yeast tubulin. *European Journal of Cell Biology*. 29:121-5.

King, S.M., J.S. Hyams, and A. Luba. 1982. Ultrastructure of mitotic spindles isolated from a cell division cycle mutant of the yeast, Saccharomyces cerevisiae. *European Journal of Cell Biology*. 28:98-102.

Kirschner, M., and T. Mitchison. 1986. Beyond self-assembly: from microtubules to morphogenesis. *Cell*. 45:329-42.

Kirschner, M.W., R.C. Williams, M. Weingarten, and J.C. Gerhart. 1974. Microtubules from mammalian brain: some properties of their depolymerization products and a proposed mechanism of assembly and disassembly. *Proceedings of the National Academy of Sciences U S A*. 71:1159-63.

Kline-Smith, S.L., S. Sandall, and A. Desai. 2005. Kinetochore-spindle microtubule interactions during mitosis. *Current Opinions in Cell Biology*. 17:35-46.

Kops, G.J., B.A. Weaver, and D.W. Cleveland. 2005. On the road to cancer: aneuploidy and the mitotic checkpoint. *Nature Reviews Cancer*. 5:773-85.

Korinek, W.S., M.J. Copeland, A. Chaudhuri, and J. Chant. 2000. Molecular linkage underlying microtubule orientation toward cortical sites in yeast. *Science*. 287:2257-9.

Kosco, K.A., C.G. Pearson, P.S. Maddox, P.J. Wang, I.R. Adams, E.D. Salmon, K. Bloom, and T.C. Huffaker. 2001. Control of microtubule dynamics by Stu2p is essential for spindle orientation and metaphase chromosome alignment in yeast. *Molecular Biology of the Cell*. 12:2870-80.

Koshland, D., L. Rutledge, M. Fitzgerald-Hayes, and L.H. Hartwell. 1987. A genetic analysis of dicentric minichromosomes in Saccharomyces cerevisiae. *Cell*. 48:801-12.

Koshland, D.E., T.J. Mitchison, and M.W. Kirschner. 1988. Polewards chromosome movement driven by microtubule depolymerization in vitro. *Nature*. 331:499-504.

Kurihara, L.J., C.T. Beh, M. Latterich, R. Schekman, and M.D. Rose. 1994. Nuclear congression and membrane fusion: two distinct events in the yeast karyogamy pathway. *Journal of Cell Biology*. 126:911-23.

Ledbetter, M.C., and K.R. Porter. 1963. A "microtubule" in plant cell fine structure. *Journal of Cell Biology*. 19:239-50.

Lee, L., S.K. Klee, M. Evangelista, C. Boone, and D. Pellman. 1999. Control of mitotic spindle position by the Saccharomyces cerevisiae formin Bni1p. *Journal of Cell Biology*. 144:947-61.

Lee, L., J.S. Tirnauer, J. Li, S.C. Schuyler, J.Y. Liu, and D. Pellman. 2000. Positioning of the mitotic spindle by a cortical-microtubule capture mechanism. *Science*. 287:2260-2.

Lee, S.E., L.M. Frenz, N.J. Wells, A.L. Johnson, and L.H. Johnston. 2001. Order of function of the budding-yeast mitotic exit-network proteins Tem1, Cdc15, Mob1, Dbf2, and Cdc5. *Current Biology*. 11:784-8.

Lee, W.L., J.R. Oberle, and J.A. Cooper. 2003. The role of the lissencephaly protein Pac1 during nuclear migration in budding yeast. *Journal of Cell Biology*. 160:355-64.

Leslie, R.J., and J.D. Pickett-Heaps. 1983. Ultraviolet microbeam irradiations of mitotic diatoms: investigation of spindle elongation. *Journal of Cell Biology*. 96:548-61.

Li, R. 1999. Bifurcation of the mitotic checkpoint pathway in budding yeast. *Proceedings of the National Academy of Sciences U S A*. 96:4989-94.

Li, Y.Y., E. Yeh, T. Hays, and K. Bloom. 1993. Disruption of mitotic spindle orientation in a yeast dynein mutant. *Proceedings of the National Academy of Sciences U S A*. 90:10096-100.

Liakopoulos, D., J. Kusch, S. Grava, J. Vogel, and Y. Barral. 2003. Asymmetric loading of Kar9 onto spindle poles and microtubules ensures proper spindle alignment. *Cell*. 112:561-74.

Lin, H., P. de Carvalho, D. Kho, C.Y. Tai, P. Pierre, G.R. Fink, and D. Pellman. 2001. Polyploids require Bik1 for kinetochore-microtubule attachment. *Journal of Cell Biology*. 155:1173-84.

Lingle, W.L., S.L. Barrett, V.C. Negron, A.B. D'Assoro, K. Boeneman, W. Liu, C.M. Whitehead, C. Reynolds, and J.L. Salisbury. 2002. Centrosome amplification drives chromosomal instability in breast tumor development. *Proceedings of the National Academy of Sciences U S A*. 99:1978-83.

Longtine, M.S., A. McKenzie, 3rd, D.J. Demarini, N.G. Shah, A. Wach, A. Brachat, P. Philippsen, and J.R. Pringle. 1998. Additional modules for versatile and economical

PCR-based gene deletion and modification in Saccharomyces cerevisiae. *Yeast*. 14:953-61.

Maddox, P., E. Chin, A. Mallavarapu, E. Yeh, E.D. Salmon, and K. Bloom. 1999. Microtubule dynamics from mating through the first zygotic division in the budding yeast Saccharomyces cerevisiae. *Journal of Cell Biology*. 144:977-87.

Maddox, P.S., K.S. Bloom, and E.D. Salmon. 2000. The polarity and dynamics of microtubule assembly in the budding yeast Saccharomyces cerevisiae. *Nature Cell Biology*. 2:36-41.

Maddox, P.S., B. Moree, J.C. Canman, and E.D. Salmon. 2003a. Spinning disk confocal microscope system for rapid high-resolution, multimode, fluorescence speckle microscopy and green fluorescent protein imaging in living cells. *Methods in Enzymology*. 360:597-617.

Maddox, P.S., J.K. Stemple, L. Satterwhite, E.D. Salmon, and K. Bloom. 2003b. The minus end-directed motor Kar3 is required for coupling dynamic microtubule plus ends to the cortical shmoo tip in budding yeast. *Current Biology*. 13:1423-8.

Maekawa, H., T. Usui, M. Knop, and E. Schiebel. 2003. Yeast Cdk1 translocates to the plus end of cytoplasmic microtubules to regulate bud cortex interactions. *EMBO Journal*. 22:438-49.

Mandelkow, E.M., and E. Mandelkow. 1985. Unstained microtubules studied by cryo-electron microscopy. Substructure, supertwist and disassembly. *Journal of Molecular Biology*. 181:123-35.

Mandelkow, E.M., E. Mandelkow, and R.A. Milligan. 1991. Microtubule dynamics and microtubule caps: a time-resolved cryo-electron microscopy study. *Journal of Cell Biology*. 114:977-91.

Manning, B.D., J.G. Barrett, J.A. Wallace, H. Granok, and M. Snyder. 1999. Differential regulation of the Kar3p kinesin-related protein by two associated proteins, Cik1p and Vik1p. *Journal of Cell Biology*. 144:1219-33.

Masuda, H., and W.Z. Cande. 1987. The role of tubulin polymerization during spindle elongation in vitro. *Cell*. 49:193-202.

Mazia, D., and K. Dan. 1952. The isolation and biochemical characterization of the mitotic apparatus of dividing cells. *Proceedings of the National Academy of Sciences U S A*. 38:826-38.

McAinsh, A.D., J.D. Tytell, and P.K. Sorger. 2003. Structure, function, and regulation of budding yeast kinetochores. *Annuual Review of Cell and Developmental Biology*. 19:519-39.

McCollum, D., and K.L. Gould. 2001. Timing is everything: regulation of mitotic exit and cytokinesis by the MEN and SIN. *Trends in Cell Biology*. 11:89-95.

McDonald, K.L., E.T. O'Toole, D.N. Mastronarde, and J.R. McIntosh. 1992. Kinetochore microtubules in PTK cells. *Journal of Cell Biology*. 118:369-83.

McIntosh, J.R., U.P. Roos, B. Neighbors, and K.L. McDonald. 1985. Architecture of the microtubule component of mitotic spindles from Dictyostelium discoideum. *Journal of Cell Science*. 75:93-129.

McNeill, P.A., and M.W. Berns. 1981. Chromosome behavior after laser microirradiation of a single kinetochore in mitotic PtK2 cells. *Journal of Cell Biology*. 88:543-53.

Meluh, P.B., and M.D. Rose. 1990. KAR3, a kinesin-related gene required for yeast nuclear fusion. *Cell*. 60:1029-41.

Michaelis, C., R. Ciosk, and K. Nasmyth. 1997. Cohesins: chromosomal proteins that prevent premature separation of sister chromatids. *Cell*. 91:35-45.

Middleton, K., and J. Carbon. 1994. KAR3-encoded kinesin is a minus-end-directed motor that functions with centromere binding proteins (CBF3) on an in vitro yeast kinetochore. *Proceedings of the National Academy of Sciences U S A*. 91:7212-6.

Miller, R.K., K.K. Heller, L. Frisen, D.L. Wallack, D. Loayza, A.E. Gammie, and M.D. Rose. 1998. The kinesin-related proteins, Kip2p and Kip3p, function differently in nuclear migration in yeast. *Molecular Biology of the Cell*. 9:2051-68.

Miller, R.K., D. Matheos, and M.D. Rose. 1999. The cortical localization of the microtubule orientation protein, Kar9p, is dependent upon actin and proteins required for polarization. *Journal of Cell Biology*. 144:963-75.

Miller, R.K., and M.D. Rose. 1998. Kar9p is a novel cortical protein required for cytoplasmic microtubule orientation in yeast. *Journal of Cell Biology*. 140:377-90.

Mitchison, T., L. Evans, E. Schulze, and M. Kirschner. 1986. Sites of microtubule assembly and disassembly in the mitotic spindle. *Cell*. 45:515-27.

Mitchison, T., and M. Kirschner. 1984. Dynamic instability of microtubule growth. *Nature*. 312:237-42.

Mitchison, T.J. 1989. Polewards microtubule flux in the mitotic spindle: evidence from photoactivation of fluorescence. *Journal of Cell Biology*. 109:637-52.

Mitchison, T.J. 1993. Localization of an exchangeable GTP binding site at the plus end of microtubules. *Science*. 261:1044-7.

Mitchison, T.J., and M.W. Kirschner. 1985a. Properties of the kinetochore in vitro I: Microtubule nucleation and tubulin binding. *Journal of Cell Biology*. 101:755-65.

Mitchison, T.J., and M.W. Kirschner. 1985b. Properties of the kinetochore in vitro II: Microtubule capture and ATP-dependent translocation. *Journal of Cell Biology*. 101:766-77.

Mitchison, T.J., and E.D. Salmon. 1992. Poleward kinetochore fiber movement occurs during both metaphase and anaphase-A in newt lung cell mitosis. *Journal of Cell Biology*. 119:569-82.

Mohri, H. 1968. Amino-acid composition of "Tubulin" constituting microtubules of sperm flagella. *Nature*. 217:1053-4.

Murphy, D.B., and G.G. Borisy. 1975. Association of high-molecular-weight proteins with microtubules and their role in microtubule assembly in vitro. *Proceedings of the National Academy of Sciences U S A*. 72:2696-700.

Mythreye, K., and K.S. Bloom. 2003. Differential kinetochore protein requirements for establishment versus propagation of centromere activity in Saccharomyces cerevisiae. *Journal of Cell Biology*. 160:833-43.

Nicklas, R.B., B.R. Brinkley, D.A. Pepper, D.F. Kubai, and G.K. Rickards. 1979. Electron microscopy of spermatocytes previously studied in life: methods and some observations on micromanipulated chromosomes. *Journal of Cell Science*. 35:87-104.

Nigg, E.A. 2002. Centrosome aberrations: cause or consequence of cancer progression? *Nature Reviews Cancer*. 2:815-25.

O'Toole, E.T., M. Winey, and J.R. McIntosh. 1999. High-voltage electron tomography of spindle pole bodies and early mitotic spindles in the yeast Saccharomyces cerevisiae. *Molecular Biology of the Cell*. 10:2017-31.

Page, B.D., L.L. Satterwhite, M.D. Rose, and M. Snyder. 1994. Localization of the Kar3 kinesin heavy chain-related protein requires the Cik1 interacting protein. *Journal of Cell Biology*. 124:507-19.

Page, B.D., and M. Snyder. 1992. CIK1: a developmentally regulated spindle pole body-associated protein important for microtubule functions in Saccharomyces cerevisiae. *Genes and Development*. 6:1414-29.

Palmer, R.E., M. Koval, and D. Koshland. 1989. The dynamics of chromosome movement in the budding yeast Saccharomyces cerevisiae. *Journal of Cell Biology*. 109:3355-66.

Palmer, R.E., D.S. Sullivan, T. Huffaker, and D. Koshland. 1992. Role of astral microtubules and actin in spindle orientation and migration in the budding yeast, Saccharomyces cerevisiae. *Journal of Cell Biology*. 119:583-93.

Payne, C., V. Rawe, J. Ramalho-Santos, C. Simerly, and G. Schatten. 2003. Preferentially localized dynein and perinuclear dynactin associate with nuclear pore complex proteins to mediate genomic union during mammalian fertilization. *Journal of Cell Science*. 116:4727-38.

Pearson, C.G., P.S. Maddox, E.D. Salmon, and K. Bloom. 2001. Budding yeast chromosome structure and dynamics during mitosis. *Journal of Cell Biology*. 152:1255-66.

Pearson, C.G., P.S. Maddox, T.R. Zarzar, E.D. Salmon, and K. Bloom. 2003. Yeast kinetochores do not stabilize Stu2p-dependent spindle microtubule dynamics. *Molecular Biology of the Cell*. 14:4181-95.

Pellman, D., M. Bagget, Y.H. Tu, G.R. Fink, and H. Tu. 1995. Two microtubule-associated proteins required for anaphase spindle movement in Saccharomyces cerevisiae. *Journal of Cell Biology*. 130:1373-85.

Pereira, G., T. Hofken, J. Grindlay, C. Manson, and E. Schiebel. 2000. The Bub2p spindle checkpoint links nuclear migration with mitotic exit. *Molecular Cell*. 6:1-10.

Pereira, G., T.U. Tanaka, K. Nasmyth, and E. Schiebel. 2001. Modes of spindle pole body inheritance and segregation of the Bfa1p-Bub2p checkpoint protein complex. *EMBO Journal*. 20:6359-70.

Peterson, J.B., and H. Ris. 1976. Electron-microscopic study of the spindle and chromosome movement in the yeast Saccharomyces cerevisiae. *Journal of Cell Science*. 22:219-42.

Pickett-Heaps, J.D. 1969. The evolution of the mitotic apparatus: an attempt at comparative ultrastructural cytology in dividing plant cells. *Cytobios*. 3:257-80.

Pinsky, B.A., and S. Biggins. 2005. The spindle checkpoint: tension versus attachment. *Trends in Cell Biology*. 15:486-93.

Polaina, J., and J. Conde. 1982. Genes involved in the control of nuclear fusion during the sexual cycle of Saccharomyces cerevisiae. *Molecular and General Genetics*. 186:253-8.

Pryer, N.K., R.A. Walker, V.P. Skeen, B.D. Bourns, M.F. Soboeiro, and E.D. Salmon. 1992. Brain microtubule-associated proteins modulate microtubule dynamic instability in vitro. Real-time observations using video microscopy. *Journal of Cell Science*. 103:965-76.

Rao, P.N., and R.T. Johnson. 1970. Mammalian cell fusion: studies on the regulation of DNA synthesis and mitosis. *Nature*. 225:159-64.

Rieder, C.L., and S.P. Alexander. 1990. Kinetochores are transported poleward along a single astral microtubule during chromosome attachment to the spindle in newt lung cells. *Journal of Cell Biology*. 110:81-95.

Rieder, C.L., R.W. Cole, A. Khodjakov, and G. Sluder. 1995. The checkpoint delaying anaphase in response to chromosome monoorientation is mediated by an inhibitory signal produced by unattached kinetochores. *Journal of Cell Biology*. 130:941-8.

Rieder, C.L., E.A. Davison, L.C. Jensen, L. Cassimeris, and E.D. Salmon. 1986. Oscillatory movements of monooriented chromosomes and their position relative to the spindle pole result from the ejection properties of the aster and half-spindle. *Journal of Cell Biology*. 103:581-91.

Rieder, C.L., A. Khodjakov, L.V. Paliulis, T.M. Fortier, R.W. Cole, and G. Sluder. 1997. Mitosis in vertebrate somatic cells with two spindles: implications for the metaphase/anaphase transition checkpoint and cleavage. *Proceedings of the National Academy of Sciences U S A*. 94:5107-12.

Rieder, C.L., and E.D. Salmon. 1998. The vertebrate cell kinetochore and its roles during mitosis. *Trends in Cell Biology*. 8:310-8.

Rieder, C.L., A. Schultz, R. Cole, and G. Sluder. 1994. Anaphase onset in vertebrate somatic cells is controlled by a checkpoint that monitors sister kinetochore attachment to the spindle. *Journal of Cell Biology*. 127:1301-10.

Ro, H.S., S. Song, and K.S. Lee. 2002. Bfa1 can regulate Tem1 function independently of Bub2 in the mitotic exit network of Saccharomyces cerevisiae. *Proceedings of the National Academy of Sciences U S A*. 99:5436-41.

Robinow, C.F., and J. Marak. 1966. A fiber apparatus in the nucleus of the yeast cell. *Journal of Cell Biology*. 29:129-51.

Roof, D.M., P.B. Meluh, and M.D. Rose. 1992. Kinesin-related proteins required for assembly of the mitotic spindle. *Journal of Cell Biology*. 118:95-108.

Rose, A.B., and J.R. Broach. 1990. Propagation and expression of cloned genes in yeast: 2-microns circle-based vectors. *Methods in Enzymology*. 185:234-79.

Rose, M.D. 1991. Nuclear fusion in yeast. *Annual Review of Microbiology*. 45:539-67.

Rose, M.D. 1996. Nuclear fusion in the yeast Saccharomyces cerevisiae. *Annual Review of Cell and Developmental Biology*. 12:663-95.

Roumanie, O., H. Wu, J.N. Molk, G. Rossi, K. Bloom, and P. Brennwald. 2005. Rho GTPase regulation of exocytosis in yeast is independent of GTP hydrolysis and polarization of the exocyst complex. *Journal of Cell Biology*. 170:583-94.

Salmon, E.D. 1975. Pressure-induced depolymerization of spindle microtubules I: Changes in birefringence and spindle length. *Journal of Cell Biology*. 65:603-14.

Salmon, E.D., R.J. Leslie, W.M. Saxton, M.L. Karow, and J.R. McIntosh. 1984a. Spindle microtubule dynamics in sea urchin embryos: analysis using a fluorescein-labeled tubulin and measurements of fluorescence redistribution after laser photobleaching. *Journal of Cell Biology*. 99:2165-74.

Salmon, E.D., W.M. Saxton, R.J. Leslie, M.L. Karow, and J.R. McIntosh. 1984b. Diffusion coefficient of fluorescein-labeled tubulin in the cytoplasm of embryonic cells of a sea urchin: video image analysis of fluorescence redistribution after photobleaching. *Journal of Cell Biology*. 99:2157-64.

Salmon, E.D., and R.R. Segall. 1980. Calcium-labile mitotic spindles isolated from sea urchin eggs (Lytechinus variegatus). *Journal of Cell Biology*. 86:355-65.

Sammak, P.J., and G.G. Borisy. 1988. Direct observation of microtubule dynamics in living cells. *Nature*. 332:724-6.

Saunders, W., D. Hornack, V. Lengyel, and C. Deng. 1997a. The Saccharomyces cerevisiae kinesin-related motor Kar3p acts at preanaphase spindle poles to limit the number and length of cytoplasmic microtubules. *Journal of Cell Biology*. 137:417-31.

Saunders, W., V. Lengyel, and M.A. Hoyt. 1997b. Mitotic spindle function in Saccharomyces cerevisiae requires a balance between different types of kinesin-related motors. *Molecular Biology of the Cell*. 8:1025-33.

Saunders, W.S., and M.A. Hoyt. 1992. Kinesin-related proteins required for structural integrity of the mitotic spindle. *Cell*. 70:451-8.

Saxton, W.M., D.L. Stemple, R.J. Leslie, E.D. Salmon, M. Zavortink, and J.R. McIntosh. 1984. Tubulin dynamics in cultured mammalian cells. *Journal of Cell Biology*. 99:2175-86.

Scholey, J.M., M.E. Porter, P.M. Grissom, and J.R. McIntosh. 1985. Identification of kinesin in sea urchin eggs, and evidence for its localization in the mitotic spindle. *Nature*. 318:483-6.

Schuyler, S.C., J.Y. Liu, and D. Pellman. 2003. The molecular function of Ase1p: evidence for a MAP-dependent midzone-specific spindle matrix. *Journal of Cell Biology*. 160:517-28.

Schwartz, K., K. Richards, and D. Botstein. 1997. BIM1 encodes a microtubule-binding protein in yeast. *Molecular Biology of the Cell*. 8:2677-91.

Segal, M., K. Bloom, and S.I. Reed. 2002. Kar9p-independent microtubule capture at Bud6p cortical sites primes spindle polarity before bud emergence in Saccharomyces cerevisiae. *Molecular Biology of the Cell*. 13:4141-55.

Shaw, S.L., E. Yeh, K. Bloom, and E.D. Salmon. 1997a. Imaging green fluorescent protein fusion proteins in Saccharomyces cerevisiae. *Current Biology*. 7:701-4.

Shaw, S.L., E. Yeh, P. Maddox, E.D. Salmon, and K. Bloom. 1997b. Astral microtubule dynamics in yeast: a microtubule-based searching mechanism for spindle orientation and nuclear migration into the bud. *Journal of Cell Biology*. 139:985-94.

Sheeman, B., P. Carvalho, I. Sagot, J. Geiser, D. Kho, M.A. Hoyt, and D. Pellman. 2003. Determinants of S. cerevisiae dynein localization and activation: implications for the mechanism of spindle positioning. *Current Biology*. 13:364-72.

Shirayama, M., Y. Matsui, K. Tanaka, and A. Toh-e. 1994a. Isolation of a CDC25 family gene, MSI2/LTE1, as a multicopy suppressor of ira1. *Yeast*. 10:451-61.

Shirayama, M., Y. Matsui, and E.A. Toh. 1994b. The yeast TEM1 gene, which encodes a GTP-binding protein, is involved in termination of M phase. *Molecular and Cellular Biology*. 14:7476-82.

Sikorski, R.S., and P. Hieter. 1989. A system of shuttle vectors and yeast host strains designed for efficient manipulation of DNA in Saccharomyces cerevisiae. *Genetics*. 122:19-27.

Skibbens, R.V., V.P. Skeen, and E.D. Salmon. 1993. Directional instability of kinetochore motility during chromosome congression and segregation in mitotic newt lung cells: a push-pull mechanism. *Journal of Cell Biology*. 122:859-75.

Sluder, G., and J.J. Nordberg. 2004. The good, the bad and the ugly: the practical consequences of centrosome amplification. *Current Opinions in Cell Biology*. 16:49-54.

Snyder, J.A., and J.R. McIntosh. 1975. Initiation and growth of microtubules from mitotic centers in lysed mammalian cells. *Journal of Cell Biology*. 67:744-60.

Sorger, P.K., F.F. Severin, and A.A. Hyman. 1994. Factors required for the binding of reassembled yeast kinetochores to microtubules in vitro. *Journal of Cell Biology*. 127:995-1008.

Sproul, L.R., D.J. Anderson, A.T. Mackey, W.S. Saunders, and S.P. Gilbert. 2005. Cik1 targets the minus-end kinesin depolymerase kar3 to microtubule plus ends. *Current Biology*. 15:1420-7.

Straight, A.F., W.F. Marshall, J.W. Sedat, and A.W. Murray. 1997. Mitosis in living budding yeast: anaphase A but no metaphase plate. *Science*. 277:574-8.

Straight, A.F., J.W. Sedat, and A.W. Murray. 1998. Time-lapse microscopy reveals unique roles for kinesins during anaphase in budding yeast. *Journal of Cell Biology*. 143:687-94.

Sullivan, D.S., and T.C. Huffaker. 1992. Astral microtubules are not required for anaphase B in Saccharomyces cerevisiae. *Journal of Cell Biology*. 119:379-88.

Sullivan, M., C. Lehane, and F. Uhlmann. 2001. Orchestrating anaphase and mitotic exit: separase cleavage and localization of Slk19. *Nature Cell Biology*. 3:771-7.

Summers, K., and M.W. Kirschner. 1979. Characteristics of the polar assembly and disassembly of microtubules observed in vitro by darkfield light microscopy. *Journal of Cell Biology*. 83:205-17.

Tanaka, K., N. Mukae, H. Dewar, M. van Breugel, E.K. James, A.R. Prescott, C. Antony, and T.U. Tanaka. 2005. Molecular mechanisms of kinetochore capture by spindle microtubules. *Nature*. 434:987-94.

Theesfeld, C.L., J.E. Irazoqui, K. Bloom, and D.J. Lew. 1999. The role of actin in spindle orientation changes during the Saccharomyces cerevisiae cell cycle. *Journal of Cell Biology*. 146:1019-32.

Thrower, D.A., and K. Bloom. 2001. Dicentric chromosome stretching during anaphase reveals roles of Sir2/Ku in chromatin compaction in budding yeast. *Molecular Biology of the Cell*. 12:2800-12.

Tilney, L.G., J. Bryan, D.J. Bush, K. Fujiwara, M.S. Mooseker, D.B. Murphy, and D.H. Snyder. 1973. Microtubules: evidence for 13 protofilaments. *Journal of Cell Biology*. 59:267-75.

Tilney, L.G., and K.R. Porter. 1967. Studies on the microtubules in heliozoa. II. The effect of low temperature on these structures in the formation and maintenance of the axopodia. *Journal of Cell Biology*. 34:327-43.

Tirnauer, J.S., E. O'Toole, L. Berrueta, B.E. Bierer, and D. Pellman. 1999. Yeast Bim1p promotes the G1-specific dynamics of microtubules. *Journal of Cell Biology*. 145:993-1007.

Tran, P.T., L. Marsh, V. Doye, S. Inoue, and F. Chang. 2001. A mechanism for nuclear positioning in fission yeast based on microtubule pushing. *Journal of Cell Biology*. 153:397-411.

Vale, R.D., T.S. Reese, and M.P. Sheetz. 1985a. Identification of a novel force-generating protein, kinesin, involved in microtubule-based motility. *Cell*. 42:39-50.

Vale, R.D., B.J. Schnapp, T. Mitchison, E. Steuer, T.S. Reese, and M.P. Sheetz. 1985b. Different axoplasmic proteins generate movement in opposite directions along microtubules in vitro. *Cell*. 43:623-32.

Visintin, R., and A. Amon. 2001. Regulation of the mitotic exit protein kinases Cdc15 and Dbf2. *Molecular Biology of the Cell*. 12:2961-74.

Wach, A., A. Brachat, R. Pohlmann, and P. Philippsen. 1994. New heterologous modules for classical or PCR-based gene disruptions in Saccharomyces cerevisiae. *Yeast*. 10:1793-808.

Wadsworth, P., and E.D. Salmon. 1986a. Analysis of the treadmilling model during metaphase of mitosis using fluorescence redistribution after photobleaching. *Journal of Cell Biology*. 102:1032-8.

Wadsworth, P., and E.D. Salmon. 1986b. Microtubule dynamics in mitotic spindles of living cells. *Annals of the New York Academy of Sciences*. 466:580-92.

Walker, R.A., E.T. O'Brien, N.K. Pryer, M.F. Soboeiro, W.A. Voter, H.P. Erickson, and E.D. Salmon. 1988. Dynamic instability of individual microtubules analyzed by video light microscopy: rate constants and transition frequencies. *Journal of Cell Biology*. 107:1437-48.

Walker, R.A., N.K. Pryer, and E.D. Salmon. 1991. Dilution of individual microtubules observed in real time in vitro: evidence that cap size is small and independent of elongation rate. *Journal of Cell Biology*. 114:73-81.

Waterman-Storer, C.M., J. Gregory, S.F. Parsons, and E.D. Salmon. 1995. Membrane/microtubule tip attachment complexes (TACs) allow the assembly dynamics of plus ends to push and pull membranes into tubulovesicular networks in interphase Xenopus egg extracts. *Journal of Cell Biology*. 130:1161-9.

Weingarten, M.D., A.H. Lockwood, S.Y. Hwo, and M.W. Kirschner. 1975. A protein factor essential for microtubule assembly. *Proceedings of the National Academy of Sciences U S A*. 72:1858-62.

Weisenberg, R.C. 1972. Microtubule formation in vitro in solutions containing low calcium concentrations. *Science*. 177:1104-5.

Weisenberg, R.C., and W.J. Deery. 1976. Role of nucleotide hydrolysis in microtubule assembly. *Nature*. 263:792-3.

Weisenberg, R.C., and A.C. Rosenfeld. 1975. In vitro polymerization of microtubules into asters and spindles in homogenates of surf clam eggs. *Journal of Cell Biology*. 64:146-58.

Wilson, E.B. 1896. The Cell in Development and Inheritance. Macmillan, New York. 483 pp.

Winey, M., C.L. Mamay, E.T. O'Toole, D.N. Mastronarde, T.H. Giddings, Jr., K.L. McDonald, and J.R. McIntosh. 1995. Three-dimensional ultrastructural analysis of the Saccharomyces cerevisiae mitotic spindle. *Journal of Cell Biology*. 129:1601-15.

Yang, S.S., E. Yeh, E.D. Salmon, and K. Bloom. 1997. Identification of a mid-anaphase checkpoint in budding yeast. *Journal of Cell Biology*. 136:345-54.

Yeh, E., R.V. Skibbens, J.W. Cheng, E.D. Salmon, and K. Bloom. 1995. Spindle dynamics and cell cycle regulation of dynein in the budding yeast, Saccharomyces cerevisiae. *Journal of Cell Biology*. 130:687-700.

Yeh, E., C. Yang, E. Chin, P. Maddox, E.D. Salmon, D.J. Lew, and K. Bloom. 2000. Dynamic positioning of mitotic spindles in yeast: role of microtubule motors and cortical determinants. *Molecular Biology of the Cell*. 11:3949-61.

Yoshida, S., R. Ichihashi, and A. Toh-e. 2003. Ras recruits mitotic exit regulator Lte1 to the bud cortex in budding yeast. *Journal of Cell Biology*. 161:889-97.

Zeng, X., J.A. Kahana, P.A. Silver, M.K. Morphew, J.R. McIntosh, I.T. Fitch, J. Carbon, and W.S. Saunders. 1999. Slk19p is a centromere protein that functions to stabilize mitotic spindles. *Journal of Cell Biology*. 146:415-25.